Spinal muscular atrophy: Disease mechanisms and therapeutic approaches



Katharina Elisabeth Meijboom

Department of Physiology, Anatomy and Genetics

Green Templeton College, University of Oxford

Thesis for the degree of

Doctor of Philosophy

2018

Declaration

The work presented in this thesis was undertaken in Professor Matthew Wood's laboratory at the Department of Physiology, Anatomy and Genetics, University of Oxford, under the supervision of Dr. Melissa Bowerman and Professor Matthew Wood between 2014 and 2018. I, Katharina Elisabeth Meijboom, hereby declare that all work presented is my own with the following exceptions. The cell penetrating peptide-PMO conjugates utilized in Chapter 3 were produced by Dr. Frank Abendroth in the laboratory of Professor Mike Gait at the MRC Laboratory of Molecular Biology at the University of Cambridge. I received assistance with CMAP analyses and the analyses of the proteomic and transcriptomic data and in Chapters 3 and 4 from Dr. Jimena Monzón-Sandoval and Dr. Viola Volpato in the bioinformatics group of Professor Caleb Webber at the University of Oxford. The cardiotoxin injury experiment in Chapter 5 was performed by Benjamin Edwards of Professor the Kay Davies Group at the University of Oxford, and the sciatic nerve crush experiment was executed by Professor Daniel Anthony of the University of Oxford. Emily McFall, from the Professor Rashmi Kothary Group at the University of Ottawa, Canada conducted the initial qPCRs concerning the TWEAK/Fn14 pathway in *Smn*$^{2B/-}$ mice, as we did not have this mouse model in Oxford. After we received the *Smn*$^{2B/-}$ mouse model, I performed all further experiments myself. Sabrina Kubinski, a master's student in the Wood Group, executed part of the PCR arrays discussed in Chapter 5.

This work has not been submitted for any other degree at this university or any other institute of learning. This thesis includes text excerpts and figures of my first-author article published during the course of the DPhil.

Abstract

Spinal muscular atrophy (SMA) a neuromuscular disorder caused by loss of the survival motor neuron (SMN) protein and characterized by motor neuron loss and muscle atrophy. Recent clinical trials of SMN restoration therapies changed the SMA therapeutic landscape and led to the first approval of a treatment. SMN restoration clearly has a positive impact on SMA pathology but is not a cure; patients will now live longer with a less severe form of SMA, leading to a growth of the patient population with additional therapeutic needs. Novel second-generation therapies are therefore to alleviate SMA related muscle pathology that can be used in combination with SMN restoration treatments. In the first part of the thesis, an unbiased approach was applied in which proteomic and transcriptomic analyses of Smn-depleted and SMN-restored SMA skeletal muscle were used to investigate dysregulated pathways, presenting the opportunity to identify novel muscle-specific treatments. Proteomic and transcriptomic analyses performed on skeletal muscle from pre-symptomatic and symptomatic *Smn$^{-/-}$;SMN2$^{+/-}$* and WT mice firstly show that SMN restoration completely normalizes protein and transcript expression in *Smn$^{-/-}$;SMN2$^{+/-}$* mice. Next, Connectivity Map (CMap), a drug repositioning strategy using publicly available databases, was employed to analyze proteomic and transcriptomic data and identify treatments able to restore aberrant pathways in SMA muscle. CMap analyses on 'omics studies provided an extensive list of potential treatments for SMA, including some already tested in clinical and preclinical studies and new options, such as harmine. Reference genes produced by the CMap analysis for harmine shows certain genes to be upregulated and others downregulated in SMA mouse tissues and harmine treatment can reverse these expressions in various cell lines and *Smn$^{-/-}$;SMN2$^{+/-}$* mice. Importantly, harmine treatment significantly increases lifespan in severe *Smn$^{-/-}$;SMN2$^{+/-}$* and moderate *Smn$^{2B/-}$* mice, rescues myofiber size and prevents motor neuron death. In addition to validating CMap as a method for identifying new treatments for SMA, while using harmine as a proof-of-concept we also generated an extensive list of drugs that can similarly be evaluated. Next, a biased approach was applied in which the TWEAK/Fn14 pathway, critical to the regulation of denervation-induced muscle atrophy and muscle proliferation, differentiation and

metabolism, was investigated in SMA, since SMA is typified by neurodegeneration, muscle atrophy and metabolic perturbations. We investigated the expression profile of Tweak and Fn14 together with downstream metabolic effectors in SMA muscle and found significantly decreased levels during disease progression in *Smn*$^{-/-}$;*SMN2*$^{+/-}$ and *Smn*$^{2B/-}$ mice. Using C2C12 myoblasts and human myoblasts, we confirmed a regulated expression of the TWEAK/Fn14 pathway during differentiation, which is dysregulated in SMA fibroblasts. siRNA mediated knockdown in C2C12s suggests a role for SMN in the aberrant expression of the TWEAK/Fn14 pathway in SMA. Overlap in dysregulation of myopathy, myogenesis and glucose metabolism pathways in SMA mice and TWEAK and Fn14 KO mice reinforced this finding. Through pharmacological interventions that target TWEAK/Fn14 pathway signaling, SMA disease phenotypes were improved in two distinct SMA mouse models. Taken together, these findings show that both biased and unbiased approaches can be used in order to identify modulators of muscle pathology in SMA as well as demonstrates that new investigative approaches, such as CMap, can augment the progress made by SMN restoration therapies.

Acknowledgements

To begin, I would like to thank Doctor Melissa Bowerman for her daily supervision, mentorship and support throughout the years. Not only did she help to move my projects forward, but she is also a fantastic researcher and is my example of a successful woman in science. I would also like to extend my gratitude to Professor Matthew Wood for giving me the tremendous opportunity to work in his exceptional lab. I am enormously grateful to The SMA Trust and Muscular Dystrophy UK for their generous support of my doctoral research over the years. Furthermore, I remain thankful to Doctor Suzan Hammond, who first believed in me, wrote my grant application and has continued to provide advice on various aspects of SMA research.

Science is often best a collective endeavor. Therefore, I would like to express my sincere gratitude to our collaborators outside of the lab, notably Professor Caleb Webber, Doctor Jimena Monzón-Sandoval and Doctor Viola Volpato for their invaluable assistance with the 'omics studies, and Professor Daniel Anthony and Benjamin Edwards for performing skilled procedures required for this study and Emily McFall.

In addition, I am so, so grateful for the friendship, help and advice I received from the members of the Wood Group and for the supportive environment that they provided throughout my doctoral studies. In particular, I would like to thank the wonderful people in our office, 1.09, for our frequent discussions about science, weird science, life, love and the love for science. A special thanks to my science sister who started her doctoral studies at the same time as me, Tirsa van Westering, for our discussions and her advice and friendship and, of course, to Nina Ahlskog, whose knowledge knows no bounds, can handle any crisis, is a great friend and is the best baker in our lab. I would also like to thank Gareth Hazell, who kindly provided training on essential techniques and to whom I could always turn, as well as Sabrina Kubinski for her assistance with the qPCR arrays and Professor Carlo Rinaldi and Amarjit Bhomra for their help and advice.

My personal appreciation goes to those outside the lab, friends whose support made my DPhil experience so much better throughout, particularly Lorena and Marjolein. I would like to express my deep gratitude to my parents as well as my five siblings and their families for the love and support that has brought me to the exuberant end of this long road and aided my way towards obtaining the highest university degree possible. My parents, especially, believed in me no matter what, patiently enduring excited calls when I had good results and sympathetically listening when experiments did not work, or results were disappointing. My sister, Anja, and I spoke almost daily, and she picked me up many times after real and imaginary crises. I would additionally like to extend my genuine gratitude to Kaliopee Fiske, who, despite her illness, supported nonetheless. Finally, I would like to thank Peter Fiske. He has been an amazing partner and supported me in every aspect of my life, including my thesis, and is truly my rock.

Contents

Declaration i

Abstract ii

Acknowledgements iv

Contents vi

List of figures xii

List of tables xv

List of abbreviations xvii

1. Introduction 1

1.1 Spinal muscular atrophy 1

1.1.1 Disease and clinical information 1

1.1.2 Molecular mechanisms of SMA pathogenesis 2

1.1.3 SMN functions 4

1.1.4 Genetic modifiers 5

1.1.4.1 SMN-dependent modifiers 6

1.1.4.2 SMN-independent modifiers 8

1.2 SMA disease models 9

1.2.1 Cellular models 10

1.2.2 *Caenorhabditis elegans* – roundworm 12

1.2.3 *Drosophila melanogaster* – fruitfly 12

1.2.4 *Danio rerio* – zebrafish 13

1.2.5 *Mus musculus* – mouse 14

1.2.6 Other mammalian models 18

1.3 Tissue and cell type specific pathology in SMA 18

1.3.1 Motor neuron pathology 19

1.3.2 Neuromuscular junction pathology 23

1.3.3 Muscle pathology 25
1.3.4 Peripheral pathology 27
1.3.4.1 Heart and cardiovascular system 27
1.3.4.2 Pancreas and metabolism 28
1.3.4.3 Liver 29
1.4 Therapeutic development for the treatment SMA 29
1.4.1 Overview 29
1.4.2 Oligonucleotide-based approaches 30
1.4.3 Spinraza® 33
1.4.4 The use of cell-penetrating peptides to promote peripheral and CNS treatment 34
1.4.5 Gene therapies 36
1.4.6 HDAC inhibitors 37
1.4.7 Neuroprotection strategies 38
1.4.8 Therapies targeting muscle pathology 39
1.4.9 Therapeutic window 41
1.4.10 Combinational treatment 43
1.5 Thesis aims and hypotheses 44
1.5.1 Result I. Hypothesis and objectives 44
1.5.2 Result II. Hypothesis and objectives 45
1.5.3 Result III. Hypothesis and objectives 45

2. General materials and methods 47

2.1 Animals 47
2.2 Harvest of animal tissues in preparation for further experiments 47
2.3 Histology 48
2.3.1 Laminin staining of skeletal muscle 48
2.3.2 Hematoxylin and eosin staining of skeletal muscle 48
2.3.3 Immunohistochemistry of spinal cord sections 48
2.4 RT-qPCR for mRNA quantification 49
2.5 Cell culture – maintenance and differentiation 51
2.6 Cloning of a stable and inducible construct overexpressing MyoD in human fibroblasts 52
2.7 Western blot 57
2.8 Statistical Analysis 58

3. Results I Coupled transcriptomic and proteomic analyses to identify potential new SMN-independent treatments for SMA muscle pathology 59

3.1 Introduction 59

3.2 Materials and methods 64

3.2.1 Animals and animal procedures 64

3.2.2 Proteomic analysis 64

3.2.3 Transcriptomic analysis 64

3.2.4 Synthesis of Pip6a peptide-PMO conjugates 65

3.2.5 Programs used for transcriptomic analyses, and statistics 65

3.2.5.1 Microarray processing 65

3.2.5.2 Differential expression 66

3.2.5.3 Gene Ontology 66

3.2.5.4 Principal component analysis and clustering 66

3.2.6 Programs used for proteomic analyses, and statistics 67

3.2.6.1 Differential expression 67

3.2.6.2 Gene ontology 67

3.2.6.3 Principal component analysis 67

3.3 Results 68

3.3.1 Restoration of full-length SMN in Pip6a-PMO treated skeletal muscle 68

3.3.2 Proteomic analyses 69

3.3.3 Transcriptomic analyses 70

3.3.4 Correlation of proteomic and transcriptomic data 71

3.3.5 Analyses of differently expressed proteins and transcripts 74

3.3.6 Gene ontology terms 76

3.4 Discussion 80

3.4.1 Low correlation between proteomic and transcriptomic data 80

3.4.2 Proteins dysregulated in treatment group compared to WT 82

3.4.3 GO terms 83

3.4.4 Conclusion and future directions 84

4. Results II Using CMap for the development of combinatorial therapies for SMA: Harmine shows promising effects *in vivo* and *in vitro* 86

4.1 Introduction 86

4.2 Material and methods 90

4.2.1 Animals and procedures 90
4.2.2 Cell culture 90
4.2.3 CMap analysis 91
4.2.4 RNA-Sequencing 91
4.2.5 Programs used for pathway analyses, and statistics 92
4.2.5.1 Differential expression 92
4.2.5.2 Gene ontology 92
4.2.5.3 Network pathway analysis 92
4.3 Results 93
4.3.1 CMap analysis provides therapeutic options for the treatment of SMA 93
4.3.2 Identification of harmine as a proof-of-concept compound of the use of CMap analyses to find muscle treatments for SMA 96
4.3.3 Doses up to 25 µM concentration harmine did not affect cell viability and proliferation 100
4.3.4 Validation of CMap results through rescue of genes and proteins via harmine treatment *in vitro* and *in vivo* 101
4.3.5 Harmine treatment increases SMN mRNA expression but not SMN protein expression 105
4.3.6 Harmine treatment improves disease phenotype and survival 106
4.3.7 Harmine treatment increases myofiber size in the severe SMA mouse model 108
4.3.8 Harmine displays neuroprotective properties in the CNS of severe SMA mice 109
4.3.9 Pathway analysis after RNA sequencing reveals full rescue of 20% of dysregulated genes in the severe SMA mouse model after harmine treatment 111
4.4 Discussion 116
4.4.1 Capability of CMap analysis to find therapeutic options for SMA 116
4.4.2 Harmine 117
4.4.3 Effects of harmine on SMN expression 120
4.4.4 Pathway analysis demonstrates pathways rescued by harmine treatment 121
4.4.5 The effect of harmine treatment on skeletal muscle in SMA 122
4.4.6 Conclusion and future directions 123
5. Results III Defining a role for the TWEAK/Fn14 pathway in muscle pathology in SMA 124
5.1 Introduction 124

5.2 Materials and methods 130
5.2.1 Animals and animal procedures 130
5.2.2 Nerve crush 131
5.2.3 Cardiotoxin 131
5.2.4 Human skeletal muscle 131
5.2.5 Small interfering RNA 132
5.2.6 PCR array 133
5.3 Results 134
5.3.1 Dysregulation of the TWEAK/Fn14 pathway expression in SMA 134
5.3.2 Altered NF-κB activity in severe SMA mice 142
5.3.3 Dysregulation of the TWEAK/Fn14 pathway is not denervation dependent 143
5.3.4 Cardiotoxin-induced myofiber necrosis activates the TWEAK/Fn14 cascade 145
5.3.5 Relationship between Smn, Tweak and Fn14 *in vivo* 147
5.3.6 Smn depletion presents a role behind muscle pathology in SMA via the TWEAK/Fn14 pathway during myogenic differentiation 148
5.3.7 Overlap between dysregulation of myopathy and myogenesis genes in *Smn$^{-/-}$;SMN2$^{+/-}$*, *Fn14$^{-/-}$* and *TWEAK$^{-/-}$* mice 151
5.3.8 Overlap between dysregulation of glucose metabolism pathways in *Smn$^{-/-}$;SMN2$^{+/-}$*, *Fn14$^{-/-}$* and *TWEAK$^{-/-}$* mice 154
5.3.9 Modulating TWEAK levels by Fc-TWEAK treatment improves phenotype of moderate SMA mouse model 159
5.3.10 Fc-TWEAK treatment improves muscle phenotype in the severe and moderate SMA mouse models 161
5.4 Discussion 165
5.4.1 Dysregulation of TWEAK/Fn14 in SMA 165
5.4.2 Unanticipated findings 166
5.4.3 Metabolic perturbations in SMA and connections to the TWEAK/Fn14 pathway 167
5.4.4 Differences of TWEAK/Fn14 pathway dysregulation in distinct skeletal muscle demonstrates unequal vulnerabilities in SMA skeletal muscle 169
5.4.5 Modulation of the pathway – treatment options 170
5.4.6 Conclusion and future directions 170

6. Discussion 172
6.1 Overview of results 172
6.2 Application to other fields 176

6.2.1 Connectivity map analysis 176
6.2.2 TWEAK/Fn14 pathway 176
6.3 SMA research: the way forward 177
6.4 Importance of considering heterogeneity among SMA patients in the investigation of therapeutic avenues 178
6.5 Differences in dysregulation of muscle-related pathways in SMA compared to other muscle conditions 181
6.6 Concluding remarks 182

References 183

Supplementary data 218

List of figures

Figure 1.1 Schematic of SMN1 and SMN2 genes. 3

Figure 1.2. Schematic of splice-switching strategy to redirect alternative splicing pattern in the *SMN2* gene. 31

Figure 2.1. The overexpression vector pInducer20-eGFP plasmid used for MyoD overexpression. 53

Figure 3.1. Ratio full-length *SMN2* significantly increased in Pip6a-PMO treated *Smn*$^{-/-}$;*SMN2*$^{+/-}$ mice. 69

Figure 3.2. Coefficient of variation in proteomic samples replicates within the six experimental groups. 70

Figure 3.3 Clustering of groups in proteomic samples after PCA. 71

Figure 3.4. Clustering of groups in transcriptomic samples after PCA. 72

Figure 3.5 Pearson's correlation between proteomic and transcriptomic data and clustering of data. 73

Figure 3.6. Overlap among differentially expressed genes. 76

Figure 3.7. Top enriched terms among dysregulated genes and proteins in SMA with a reversed effect of Pip6a-PMO treatment. 79

Figure 4.1. The Connectivity Map Concept. 87

Figure 4.2. Defining the differently expressed genes and proteins in TA from SMA mice vs. WT. 94

Figure 4.3. Chemical structure of harmine. 97

Figure 4.4. Dose-dependent toxicity of harmine treatment *in vitro*, assessed by MTS assays. 101

Figure 4.5. Validation by qPCR of proteomic and transcriptomic data comparing symptomatic P7 SMA muscle with age-matched WT controls. 103

Figure 4.6. mRNA expression levels of validation genes of harmine treated and untreated SMA mice and healthy control TA muscle. 104

Figure 4.7. Effects of harmine treatment on *Smn* and *SMN* transcripts. 106

Figure 4.8. Effects of daily oral 10 mg/kg treatment on weight and survival in severe and moderate SMA mice. 108

Figure 4.9. Treatment of *Smn$^{-/-}$;SMN2$^{+/-}$* mice with harmine (10 mg/kg) increases fiber diameter in *tibialis anterior* muscle..... 109

Figure 4.10. Harmine increases GLT-1 expression *in vivo* in *Smn$^{-/-}$;SMN2$^{+/-}$* mice..... 110

Figure 4.11. Treatment of harmine (10 mg/kg) results in rescue of motor neuron death in *Smn$^{-/-}$;SMN2$^{+/-}$* mice. 111

Figure 4.12. Differential gene expression analysis based on the negative binomial distribution (DESeq2)..... 113

Figure 4.13. Gene Ontology (GO)/Molecular function for genes fully rescued (Table 4.5: 1038 genes) and partly rescued (Figure 4.12a: 574 genes) by harmine treatment in skeletal muscle. 114

Figure 4.14. Network pathway analysis using a Phenotypic-Linkage Network. 115

Figure 5.1. The TWEAK/Fn14 signaling cascade. 126

Figure 5.2. Proposed mechanisms of dysregulation of the TWEAK/Fn14 pathway in skeletal muscle leading to muscle pathology and metabolic dysfunction in SMA..... 128

Figure 5.3. *Parvalbumin* mRNA expression in vulnerable and resistant skeletal muscle in SMA..... 136

Figure 5.4. Aberrant mRNA expression of the TWEAK/Fn14 pathway in *Smn$^{-/-}$;SMN2* mice. 138

Figure 5.5. Effects of Tweak and Fn14 on Pgc-1α expression displayed in correlation..... 139

Figure 5.6. Aberrant mRNA expression of the TWEAK/Fn14 pathway in *Smn$^{2B/-}$* mice..... 139

Figure 5.7. mRNA expression of the TWEAK/Fn14 pathway in SMA Type 1 skeletal muscle..... 140

Figure 5.8. The canonical and non-canonical NF-κB pathways are dysregulated in TA of symptomatic P7 *Smn$^{-/-}$;SMN2$^{+/-}$* mice. 143

Figure 5.9. Hematoxylin-eosin staining and cross-sectional area analyses of TA muscle fibers after nerve crush. 144

Figure 5.10. Cardiotoxin and saline treatment of *tibialis anterior* muscle in 10-day-old mice. 146

Figure 5.11. TWEAK/Fn14 pathway mRNA expression in *Smn*$^{-/-}$;*SMN2*$^{+/-}$, *Fn14*$^{-/-}$ and *TWEAK*$^{-/-}$ mouse skeletal muscle. 148

Figure 5.12. siRNA mediated knockdown of *Tweak*, *Fn14* and *Smn* in C2C12 cells during differentiation. 150

Figure 5.13. Overview of effects of siRNA mediated knockdown of *Tweak*, *Fn14* and *Smn* in C2C12 cells during differentiation 151

Figure 5.14. Overlap between dysregulated genes involved in myogenesis and myopathy, in P7 *Smn*$^{-/-}$;*SMN2*$^{+/-}$, *Fn14*$^{-/-}$ and *TWEAK*$^{-/-}$ mice. 153

Figure 5.15. Overlap between dysregulated genes involved in glucose metabolism in P7 *Smn*$^{-/-}$;*SMN2*$^{+/-}$, *Fn14*$^{-/-}$ and *TWEAK*$^{-/-}$ mice. 156

Figure 5.16. Fc-TWEAK treatment improves disease phenotypes in severe and moderate SMA mice. 160

Figure 5.17. mRNA expression of Tweak/Fn14 pathway and muscle markers after Fc-TWEAK treatment in *triceps* from *Smn*$^{-/-}$;*SMN2*$^{+/-}$ and *Smn*$^{2B/-}$ mice and healthy littermates, compared to untreated animals. 163

Figure 5.18. Fc-TWEAK treatment in *Smn*$^{-/-}$;*SMN2*$^{+/-}$ mice increases fiber diameter in *tibialis anterior* muscle. 164

List of tables

Table 1.1. Relationship of *SMN2* copy number to disease classification, age of onset, typical symptoms and life expectancy [7]. 1

Table 1.2. Mouse models of SMA. 1

Table 2.1. Primers used for quantitative real-time PCR. 50

Table 2.2. Primers for the restrictions sites around the MyoD gene. 54

Table 2.3. PCR protocol. 54

Table 2.4. PCR temperature conditions. Calculated with NEB Tm calculator. 54

Table 2.5. Ligation reaction with and without MyoD insert. 55

Table 3.1. Groups used for proteomic and transcriptomic analyses. 68

Table 3.2. Up- and down regulated genes at transcript and protein level. 74

Table 3.3. Proteins downregulated in Pip6a-PMO treated SMA mice compared to WT mice. 75

Table 4.1. Biological processes of SMA disease consistency, disease progression and reversed by SMN restoration treatment by Pip6a-PMO. 95

Table 4.2. CMap analysis of integrated transcriptomic and proteomic ''treatment'' genes and proteins. 96

Table 4.3. CMap analysis results of transcriptomic data and proteomic data. 98

Table 4.4. Summary of *in vitro* studies investigating effects of harmine on various cell types. 103

Table 4.5. Differential gene expression analysis based on DESeq2 showing DEG between various groups of harmine treated and untreated SMA and WT skeletal muscle. 113

Table 5.2. Age of patients/control humans when skeletal muscles were collected. 132

Table 5.3. Skeletal muscles were harvested from $Smn^{-/-};SMN2^{+/-}$ and $Smn^{2B/-}$ mice at various timepoints during disease progression. 134

Table 5.4. Number of dysregulated genes compared to WT mice, $p < 0.05$. 153

Table 5.5. Myogenesis and myopathy genes significantly dysregulated in the same direction in P7 *Smn*$^{-/-}$;*SMN2*$^{+/-}$, *Fn14*$^{-/-}$ and *TWEAK*$^{-/-}$ mouse *triceps* and *quadriceps*, when compared to P7 WT *triceps* and *quadriceps*. 154

Table 5.6. Number of dysregulated genes compared to WT. 156

Table 5.7. Glucose metabolism genes significantly dysregulated in the same direction in P7 *Smn*$^{-/-}$;*SMN2*$^{+/-}$, *Fn14*$^{-/-}$ and *TWEAK*$^{-/-}$ mice *triceps* and *quadriceps*, when compared to P7 WT *triceps* and *quadriceps*. 157

Table 5.8. KEGG pathways of glucose metabolism genes. 158

List of abbreviations

2'OMePS	2'-O-methyl phosphorothioate
AAV	adeno-associated virus
ActRIIB	Activin Receptor Type IIB
ActRIIB-Fc	a soluble activin receptor IIB
ALS	amyotrophic lateral sclerosis
ANOVA	analysis of variance
ARE	AU-rich elements
ASO	Antisense Oligonucleotides
bp	base pair
BSA	Bovine Serum Albumin
cDNA	complementary deoxyribonucleic acid
CHOP-INTEND	Children's Hospital of Philadelphia Infant Test of Neuromuscular Disorders
CMAP	compound motor action potential amplitude
CMap	connectivity map analysis
CNS	central nervous system
CPP	cell-penetrating peptides
CRE	cAMP-responsive element
CRISPR-Cas9	Clustered Regularly Interspaced Short Palindromic Repeats associated protein 9
DE	Differently expressed
DEG	differently expressed genes
DM1	Myotonic dystrophy type 1
DMD	Duchenne muscular dystrophy
DMEM	Dulbecco's Modified Eagle's Media
DMSO	dimethyl sulfoxide
DNA	deoxyribonucleic acid
dNTP	Deoxynucleotide
eGFP	Enhanced green fluorescent protein
ER	endoplasmic reticulum

ESC	embryonic stem cell-like cells
ESE	exon splicing enhancer
ESS	exon splicing silencer
FBS	fetal bovine serum
FDA	Food and Drug Administration
FDR	false discovery rate
GO	gene ontology
h	hours
H&E	hematoxylin-and-eosin
HDAC	histone deacetylase
HEK293	human embryonic kidney cells 293
HFMSE	Hammersmith Functional Motor Scale Examination
HiRIEF	high-resolution isoelectric focusing
HPLC	high-performance liquid chromatography
HS	horse serum
ICV	intracerebroventricular
iPSC	induced pluripotent stem cell
ISE	intronic splicing enhancer
ISS	intronic splicing silencer
IV	intravenous
kb	kilobase
kDa	kilodalton
KEGG	Kyoto Encyclopedia of Genes and Genomes
KO	knockout
LC-MS	liquid chromatography–mass spectrometry
lncRNA	long non-coding RNA
MAO	monoamine oxidase
mRNA	messenger RNA
miRNA	microRNA
MS	mass spectrometry

MUNE	motor unit number estimation
NCALD	neurocalcin-Δ
NF-κB	nuclear factor kappa-light-chain-enhancer of activated B cells
NMJ	neuromuscular junctions
ns	not significant
P	postnatal day
p	probability value
PBS	phosphate buffered saline
PCA	principal component analysis
PCR	polymerase chain reaction
PEI	Polyethylenimine
PFA	Paraformaldehyde
PMO	phosphorodiamidate morpholino oligomer
PVDF	polyvinylidene fluoride
PCR	polymerase chain reaction
qPCR	quantitative polymerase chain reaction
RIPA	radioimmunoprecipitation
RNA	ribonucleic acid
RNAi	RNA interference
ROS	reactive oxygen species
RT	reverse transcription
RT-qPCR	reverse transcriptase-quantitative PCR
SD	standard deviation
siRNA	small interfering RNA
SMA	spinal muscular atrophy
SMARD	spinal muscular atrophy with respiratory distress
SMAX2	X-linked SMA
snRNP	small nuclear ribonucleoproteins
SSO	splice-switching oligonucleotides
STRING	Search Tool for the Retrieval of Interacting Genes/Proteins

SVZ	subventricular zone
TA	*tibialis anterior*
TALEN	transcription activator-like effector nuclease
UPS	ubiquitin-proteasome system
UTR	untranslated region
VPA	valproic acid
WB	Western blot
WT	wild type

1. Introduction

1.1 Spinal muscular atrophy

1.1.1 Disease and clinical information

Spinal muscular atrophy (SMA) is an autosomal recessive disorder that occurs in 1:6,000–1:10,000 newborns [1] and is the leading genetic cause of infant mortality [2]. The major pathological component of the disease is the selective loss of lower alpha motor neurons in the ventral horn of the spinal cord, resulting in progressive muscle denervation [3], skeletal muscle atrophy and eventually, paralysis and death [4]. The first descriptions of SMA were by Guido Werdnig [5] in Austria in 1891 and Johann Hoffmann [6] in Germany in 1893. SMA can be classified into five types, which are based on severity of clinical symptoms and age of onset (Table 1.1) [7].

Table 1.1. Relationship of *SMN2* copy number to disease classification, age of onset, typical symptoms and life expectancy [7].

TYPE	AGE OF ONSET	SYMPTOMS	LIFE EXPECTANCY	SMN2 COPY
0	Prenatal	Less active fetus	< birth, days after birth	1
1	0–6 months	Cannot sit, respiratory muscle weakness	< 2 years	1, 2, 3
2	6–18 months	Cannot walk	< 40 years	2, 3, 4
3	18 months–5 years	Needs support to walk	Adult	3, 4
4	> 5 years	Restricted mobility	Adult	4, 5

Type 0 is the most severe form in which there are reduced fetal movements *in utero,* and pregnancies often result in death *in utero* or stillbirth. Type 0 babies who are born alive only survive for a few days and have profound weakness, hypotonia at birth and are ventilator-dependent until death [8–10]. Type 1 is the most common type and is further known under the name of Werdnig-Hoffmann disease. These patients are very severely affected and are normally diagnosed before six months of age. They are

never able to sit unsupported, and life expectancy is less than two years [11]. Type 2 patients are diagnosed between six and 18 months, and children can normally sit unsupported [12]. They are unable to walk and have a reduced life expectancy (adulthood, < 40 years). This is mainly caused by respiratory complications [13,14]. In Type 3, also called Kugelberg-Welander disease, symptoms normally occur between 1.5 and 5 years [12,15]. These patients are able to walk (after disease progression with support) and have a normal life expectancy. Patients experience considerable neuromuscular weakness. The adult-onset Type 4 is the mildest form of SMA and is characterized by normal life expectancy and modest disability [16].

1.1.2 Molecular mechanisms of SMA pathogenesis

In 1990, two research groups found the location of the gene causing SMA [17,18]. In 1995, it was identified as the *survival motor neuron (SMN)* gene on chromosome 5q [19]. The *SMN* gene region has a large duplication of a 500 kb element. In humans the *SMN1* gene is found on the telomeric area while there is a near-identical centromeric copy of the *SMN1* gene, termed *SMN2*. This duplication is quite recent in evolutionary terms as most species have only one copy [20]. One critical difference between *SMN2* and *SMN1* is a single nucleotide change (C to T) of six base pairs into exon 7 [21]. The C to T transition does not alter an amino acid, but results in the exclusion of exon 7 from ~90% of the mature transcript [22] (Figure 1.1). This protein, termed SMNΔ7, does not efficiently oligomerize, is unstable and gets rapidly degraded by the ubiquitin/proteasome pathway [23].

Exon 7 of the *SMN1* and *SMN2* genes is characterized as having weak 3' and 5' splice sites [20], and its inclusion into the mature transcript is determined by cis-acting elements such as intronic splicing silencers (ISSs), intronic splicing enhancers (ISEs), exonic splicing silencers (ESSs) and exonic splicing enhancers (ESEs) [24]. Alternate hypotheses have been proposed as to how the cytosine to thymine/uracil transition causes exclusion of exon 7 in 90% of mature transcripts. For example, some models explain that this transition would abrogate an essential ESE [21] or create new ESSs [25,26] or could strengthen the inhibitory context of the sequence [27].

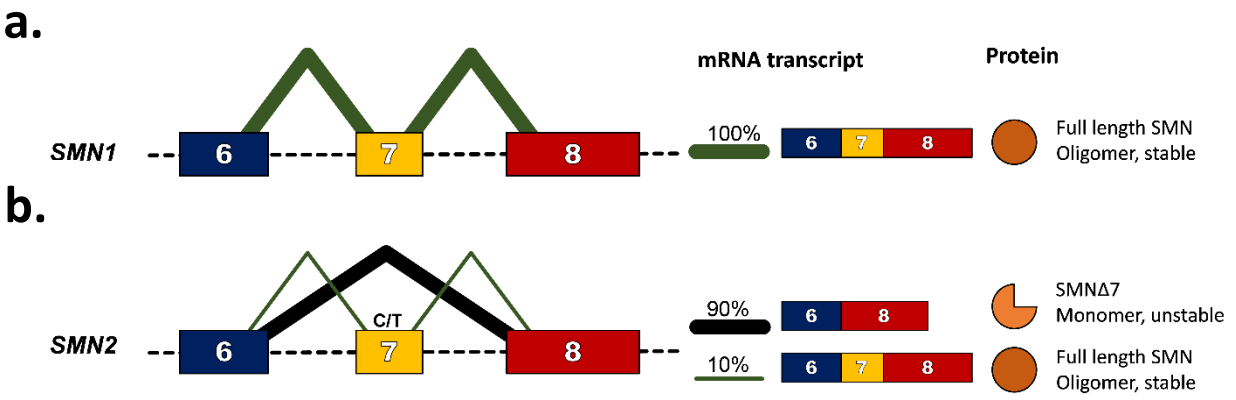


Figure 1.1 Schematic of SMN1 and SMN2 genes. a. The *SMN1* gene produces a full-length SMN protein, a stable oligomer. **b.** C>T transition at position 6 of exon 7 of the *SMN2* gene disrupts an exon splicing enhancer region resulting in exclusion of exon 7 from 90% of the mature *SMN* transcript which produces SMNΔ7 protein and is an unstable monomer.

More than 95% of patients have homozygous deletions involving exon 7 of the *SMN1* gene and subsequent loss of functional SMN protein [28–30]. *De novo* mutation rate in patients is about 2%, which is relatively high [31]. This is because the region of the *SMN* genes on chromosome 5 is unstable and contains various low copy number repeats. This causes a high rate of unequal crossing over and *de novo* mutations. Mildly affected patients often undergo conversion of *SMN1* to *SMN2* instead of deletion of *SMN1* [32].

The pan-ethnicity of SMA carrier frequency of zero copies of *SMN1* is 1:54 [33], but differs among ethnicities: Egyptian and Saudi Arabian population 1:20 [34], Moroccan population 1:25 [35], Caucasian population 1:46 [36], Asian population 1:48 [36], Hispanic population 1:76 [36], Black (Sub-Saharan ancestry) population 1:100 [36] and Malian population 1:209 [37]. In small groups with a high inbreed rate, the carrier frequency tends to be higher, such as in the Hutterite population 1:8 [38] and a Muslim Arab village population in Israel 1:8 [39]. These carrier frequencies are relatively high, despite the mortality rate of severe forms of SMA. This could be explained by the high rate of *de novo* mutations in the *SMN* genes [31].

Complete loss of SMN is lethal [24]. Significantly for affected individuals, ~10% of *SMN2* transcripts will include exon 7 in the mature transcript and thus produce some functional SMN protein that confers survival beyond birth. Furthermore, as the *SMN2* gene is subject to gene duplication, the number of copies, and hence the total level of functional SMN protein, is the main determinant in the clinical outcome for patients with SMA, as outlined in Table 1. Healthy carriers with one functional *SMN1* copy and zero *SMN2* copies have 50% functional full-length SMN protein, which is sufficient not to develop SMA [15,28]. Most SMA patients have 2–3 *SMN2* copies and are classified within Type 1, Type 2 and occasionally Type 3 patient groups. Milder Type 3 and Type 4 patients have < 4 copies, which would be about 40% SMN, still below the 50% SMN level seen in healthy carriers with zero *SMN2* copies. Some individuals have five or more copies of *SMN2* and zero copies of *SMN1*, but do not exhibit any signs of SMA pathology [40–42]. In the unaffected population with two *SMN1* copies, the number of *SMN2* copies varies as well; 15% have no copies of *SMN2*, 33% have one copy of *SMN2*, and 50% carry two copies of *SMN2* [15].

1.1.3 SMN functions

The human SMN protein consists of 294 amino acids with a molecular mass of approximately 32 kDa [19] and is uniformly located in the cytoplasm and nucleus, where it is concentrated in nuclear bodies, named Geminis [43]. As is noted in Section 1.1.4.2, many cellular pathways are affected by SMN depletion, such as ubiquitin homeostasis, cytoskeleton and endocytosis pathways. The dysregulation in all these pathways contributes to SMA pathology. However, SMN is proven to play a role in many other processes. The main established role of the SMN protein is its housekeeping role in RNA metabolism by the formation of, or interaction with ribonucleoprotein (RNP) complexes. SMN plays a canonical role in the assembly of small nuclear RNPs (snRNPs). snRNPs are part of the spliceosome of the nucleus and are required for the catalysis of intron removal during pre-mRNA splicing [44]. snRNP complexes are comprised of one small nuclear RNA and seven Sm core proteins. SMN assembles snRNPs by a large multiprotein SMN complex that consists of SMN, Gem-associated proteins (Gemin2-

8) and serine-threonine kinase receptor-associated protein (UNRIP) [45–47]. The SMN complex assembles a heptameric ring of Sm proteins around all U1, U2, U4, U4atac, U5, U11 or U12 small nuclear RNAs to form the mature snRNP [47]. These newly assembled snRNPs are then translocated to the nucleus where they catalyze splicing. Consistent with its role in snRNP assembly, SMN downregulation causes widespread defects in splicing [48–51], particularly splicing of minor introns [52,53]. However, one study found that splicing abnormalities only occurred in late-symptomatic *SMNΔ7* SMA mice, which might be caused by secondary effect of cell injury [49].

Various studies have tried to induce SMA-like phenotypes by disturbing snRNP assembly, but failed to do so [54–56]. Furthermore, other evidence suggests that some effects on alternative splicing are indirect, as other splicing factors could also be affected by downregulation of SMN [57]. Taking this information together, it has been postulated that aberrant splicing, because of SMN depletion, might contribute to SMA pathology, but is not centrally causative. This does not rule out the chance of significant early changes in a small number of transcripts that are crucial to motor neuron survival or other early SMA pathology (further explained in Section 1.3.1). SMN also regulates other functions than snRNP assembly, such as small nucleolar RNPs which post-transcriptionally modify non-coding RNAs [58,59], the 3' end of histone mRNA processing [60,61], transport of newly synthesized proteins by the biogenesis and regulating steady state level of signal recognition particles [62,63] and telomerase activity [64,65]. Knowledge about the functions and the system-wide network of SMN interactions are crucial to understand motor neuron and peripheral pathology in SMA.

1.1.4 Genetic modifiers

Although a general correlation between *SMN2* copy number and disease severity exists, there are other factors affecting SMN levels and disease severity, such as genetic modifiers influencing splicing, transcription, translation and the stability and integrity of the *SMN2* gene, RNA and protein. Multiple cases have revealed intrafamilial variation of phenotype, whereby family members with the same

number of *SMN* copies can display different disease severity caused by genetic modulators. Genetic modifiers in SMA can be divided into SMN-dependent modifiers and SMN-independent modifiers.

1.1.4.1 SMN-dependent modifiers

Various genetic modifiers can modify the *SMN* mRNA transcript and/or protein, thereby modifying disease severity. Exon 7 of the *SMN* genes encodes a protein domain that is indispensable for oligomerization and function of the SMN protein [66]. Exon 7 and introns 6 and 7 are packed with *cis*-regulatory splicing elements that act as enhancers or silencers. Various splicing factors bind either directly or indirectly on the *cis*-regulatory splicing elements and can facilitate the integration or skipping of exon 7 [67–70], which, as mentioned in paragraph 1.2 have weak 3' and 5' splice sites [20]. Between 3–4 % of SMA patients exhibit pathogenic variants that affect splicing of *SMN* mRNA or SMN protein function [30]. These pathogenic variants can reduce or even abrogate SMN protein function [71]. Variant c.863G >T, for example, can disrupt an ESE site for TRA2-β1 and cause exon 7 skipping in both *SMN1* and *SMN2* [71]. However, other variants can strongly modulate disease severity. *SMN2* exon 7 splicing can as well be inhibited by binding of heterogeneous nuclear ribonucleoprotein A1 (hnRNPA1). Patients in which hnRNP Q is elevated have milder symptoms [72]. Furthermore, the variant c.859G >C, a single base substitution in exon 7 of the *SMN2* gene creates a new exonic splicing enhancer-binding site for SF2/ASF (SRSF1) that enhances exon 7 inclusion by about 20%. The phenotype in patients with this variant is less severe and does not correlate with *SMN2* copy numbers, even if patients have only one *SMN2* copy [73].

Although SMN is ubiquitously expressed, it displays higher expression in the spinal cord and during embryonic development [74,75]. Transcription is regulated by various factors. Upregulation of SMN can be achieved by activating interferon-stimulated response element (ISRE) that overlaps with an interferon-regulatory factor-binding motif (IRF-E) in the SMN promoter. Activated by interferon-β and interferon-γ, the transcription factor IRF-1 binds to the ISRE/IRF-E sequence of SMN, which leads to SMN upregulation [76]. The SMN promoter also has, among others, two cAMP-responsive element (CRE)

sites. cAMP response element binding protein 1 (CREB1) binds to the CRE-II site and increases *SMN* transcription two to four fold [77]. Activation of *signal transducer and activator of transcription 5* (STAT5) causes interaction with a binding site of the *SMN2* promoter, which increases SMN expression [78,79]. FL-*SMN2* transcription is also regulated by epigenetic factors, such as histone acetylation and CpG methylation in the *SMN2* promoter [80].

Genetic modifiers can also target mRNA stability of SMN mRNA. In the 3'-UTR of SMN mRNA, AU-rich elements (ARE) are found, a binding motif that regulates the mRNA degradation. The ARE-binding protein *Hu antigen R* (HuR) stabilizes SMN mRNA after activation of the p38 pathway, resulting in increased SMN protein expression [81]. Furthermore, U1a protein is a key regulator of SMN expression. U1A, a component of the U1 small nuclear ribonucleoprotein (U1 snRNP) complex, inhibits polyadenylation upon direct binding to mRNA. When the amount of U1A exceeds U1 snRNP, it inhibits SMN polyadenylation and decreases SMN protein levels [82].

Post-translational processes can also regulate and/or degrade SMN protein. SMN is phosphorylated by *glycogen synthase kinase 3* (GSK3), which influences SMN turnover. When GSK3 is inactivated, phosphorylation of SMN decreases and SMN stability increases [83,84]. Phosphorylation of SMN by *protein kinase alpha* inhibits SMN degradation [85,86]. To maintain cellular homeostasis, correct protein degradation is required. This is regulated by, among others, the ubiquitin-proteasome system (UPS). Ubiquitin plays an extensive role in SMN degradation. The proteasome can be inhibited in various ways, thereby increasing SMN levels [87,88]. Interestingly, the closely SMA-related disease, X-linked SMA (SMAX2), is caused by mutations in the ubiquitin-like modifier-activating enzyme 1 (UBA1) [89]. Disruptions in ubiquitin homeostasis have been reported across a range of SMA animal models [90–92] and in SMA patient iPSC -derived motor neurons [92]. Research demonstrates that upregulation of UBA1 in *Smn*$^{-/-}$; *SMN2*$^{+/-}$ SMA mice results in increased SMN protein levels [92].

SMN has many genetic modifiers, working on different levels. Other factors, such as hypoxia, starvation and oxidative stress, can have a strong impact on full-length SMN splicing. Both hypoxia

and starvation abolish correct *SMN2* splicing [93]. Effects of starvation were observed in disease end-stage SMA mice (*Smn*$^{-/-}$*SMN2*$^{+/-}$), which were underfed and extremely weak [94]. This might be induced by the lack of nutrients that downregulates anabolic processes. Extra/different nutrition increased survival of SMA mice [95,96]. Respiratory intervention in SMA patients [97] and mice [93] revealed significant improvement. Finally, oxidative stress can also trigger skipping of multiple exons of SMN in *Smn*$^{+/-}$;*SMN2*$^{+/+}$ SMA mice [98].

1.1.4.2 SMN-independent modifiers

Other genetic modifiers do not modify SMN, but are pathways affected by reduced SMN levels, or they modify SMA disease pathology independently from SMN.

SMN depletion causes changes in the endocytosis and cytoskeleton pathways downstream of SMN. Cytoskeleton pathways play important roles in many cellular functions such as axonal growth, morphology maintenance, axonal transport, synaptic vesicle trafficking and neurotransmission, neuronal differentiation and maturation of the neuromuscular junctions (NMJ) [99,100]. These processes have proven to be affected in SMA patients. The importance of cytoskeletal and actin properties in SMA is further demonstrated by findings in SMA-patient family members with no *SMN1* who have an upregulation of the actin-binding protein plastin 3 (PLS3), which protects them from developing SMA [101–103]. All asymptomatic *SMN1*-deleted family members were women [102]. This might be explained by the location of PLS3, which is on the X-chromosome. Overexpression of PLS3 in various SMA models was able to correct SMA pathology in various SMA animal models [104–106]. PLS3 is dysregulated in the *Smn*$^{2B/-}$ mouse model and in Smn-depleted PC12 cells (neuronal-like cell line) [107,108]. Other actin-related proteins, such as Cdc42, cofilin and profilin IIa were also dysregulated in the *Smn*$^{2B/-}$ mouse model [107–109]. All these proteins are downstream of the RhoA/Rho kinase (ROCK) pathway. The role of the RhoA/ROCK pathway in neuronal cells is modulation of the cytoskeleton. Dysregulation of this pathway affects through perturbation of the actin cytoskeleton, neuronal development, neuronal survival and neurodegeneration [110]. Knockdown of Smn in neuronal-like PC12 cells caused an

upregulation in the RhoA/ROCK pathway [107]. This upregulation of the RhoA/ROCK pathway was also found in the spinal cords of *Smn* $^{2B/-}$ mice compared to WT mice [111]. Inhibition of the RhoA/ROCK pathway led to a significant increase in survival of *Smn* $^{2B/-}$ mice and improved NMJ maturation and size [111,112]. Furthermore, muscle myofiber size was increased after RhoA/Rock inhibition [111,112]. Although the RhoA/ROCK pathway seems to be affected by SMN depletion, manipulation of the RhoA/ROCK pathway did not alter SMN levels [111,112].

The actin cytoskeleton is also involved in endocytic processes, such as in the transport of synaptic vesicles, release of cargo and recycling of synaptic vesicles [113]. Defects in vesicular transport are associated with neurodegenerative disease pathogenesis [114]. Impaired synaptic vesicle release was found at the NMJ of *SMNΔ7* mice in different studies [115–117]. Further, accumulation of autophagic vesicles was found in patient fibroblasts and murine SMA mouse motor neurons [118,119]. These findings point toward defects in the synaptic vesicle cycle and perturbated intracellular trafficking and cargo delivery in SMA. Overexpression of PLS3 could restore endocytic and exonal pathology in various SMN-depleted cell lines in Smn-depleted zebrafish [106]. The relevance of the cytoskeleton as an SMA genetic modifier is further illustrated by the finding of various asymptomatic *SMN1*-deleted family members in which neurocalcin-Δ (NCALD) was downregulated, compared to SMA affected family members [120]. NCALD is a Ca^{2+}-dependent negative regulator of endocytosis, and NCALD knockdown improved endocytosis and NMJ function in various SMA models (mouse, zebrafish, *C. elegans*) [120].

The main SMA genetic modifier is without a doubt *SMN2*. However, different genes and pathways can modify SMA pathology, either by influencing *SMN2* or by modulating other molecular and cellular pathways affected in SMA, which could be targeted as a therapy for SMA (see Section 1.4.8).

1.2 SMA disease models

Discovery of the *SMN* gene in 1995 [19] and understanding of the molecular basis of SMA allowed for the creation of both cellular and animal models of the disease. In 2000, the first SMA animal model

was created [121,122]. The use of SMA models, both cellular and animal, has rapidly facilitated our understanding of the SMN protein and SMA pathogenesis.

1.2.1 Cellular models

As SMA is characterized by early death of motor neurons, these cells are an obvious choice as a cellular model for SMA. However, patient neuronal cell types are inaccessible during life, and postmortem analyses of tissues often result in poor survival of cells, which limit their potential use as a cellular model for drug screening and disease modeling. There are different ways to overcome these problems, and there are currently a number of motor neuron cellular models. Advances in induced pluripotent stem cell (iPSC) technology have made it possible to dedifferentiate any cell type back to an embryonic-like cell that retains self-renewal properties and multilineage differentiation [123]. iPSCs can be generated from different types of cells, but skin fibroblasts, blood cells or cells extracted from urine are normally used. By ectopically expressing various reprogramming factors, the cells dedifferentiate into embryonic stem cell-like (ESC) cells [123]. ESCs can also be directly isolated from the inner cell mass of a preimplantation blastocyst [124]. Both iPSCs and ESCs are pluripotent and can give rise to all somatic cell types, such as motor neurons. The limitation with ESCs for SMA research is the rare supply of preimplantation genetically diagnosed cells from donated SMA embryos. A way to work around this issue is to knockdown or deplete the *SMN1* gene from healthy ESCs using RNA interference. Motor neurons derived from *SMN1* depleted ESCs revealed SMA phenotypes, such as specific motor neuron degeneration, defects in axonal outgrowth and increased oxidative stress [125].

An easier way is to use iPSC technology to differentiate SMA patient cells into iPSCs and subsequently motor neurons. The first SMA iPSC line was created in 2009, whereby dermal fibroblasts from a Type 1 SMA patient and his healthy mother were reprogrammed into iPSCs. This study demonstrated that the SMA iPSCs had indeed lower SMN protein compared to control iPSCs, due to *SMN1* loss [126]. These iPSCs were differentiated into motor neurons. At first, SMA motor neurons revealed no differences in morphology or differentiation efficacy compared to control motor neurons, but they later started to

reveal similar SMA phenotypes that were observed in other *in vitro* models, such as selective motor neuron death and reduced soma size [126]. After this success, many different groups have reprogrammed SMA patient cells into iPSCs to study different pathologies [127–130].

Before the use of iPSCs and to avoid the difficulty to maintain as well as manipulate primary neurons, immortalized mouse motor neuron-like hybrid NSC-34 [131,132], embryonic carcinoma p19 [133,134] and rat pheochromocytoma PC12 [107] cells were frequently used *in vitro* models of developing motor neurons in SMA research.

Many studies investigating splicing of *SMN2* and the effects of SMN depletion on splicing, have used non-neuronal cell lines, such as human embryonic kidney cells 293 (HEK293) cells [135–137] and human HeLa cells which originated from a cancerous cervical tumor [138,139]. A particular useful non-neuronal cell type to study *SMN2* splicing is SMA patient-derived fibroblasts, which can be isolated from skin samples from SMA patients and unaffected family members as controls. These patient fibroblasts naturally have the same mutations and *SMN2* copies as the patient, but the skin is pathophysiologically spared in patients, resulting in healthy cells with low SMN levels [140]. There are many studies that used patient fibroblasts to study *SMN2* splicing and SMN protein levels after treatment of splice-switching oligonucleotides, small molecules and other compounds targeting SMN [141–143]. Different SMA patient fibroblast cell lines with different number of *SMN2* copies are commercially available.

As described in Section 1.3.3, skeletal muscle weakness and atrophy are also characteristics of SMA. To study the muscle intrinsic effects of SMN, stable myoblast-like cell lines have been created, knocking down SMN levels using short hairpin RNAs [144]. These studies demonstrated intrinsic defects in proliferation, myoblast fusion and myotube morphology after SMN knockdown [144]. All of these defects were also shown in primary myoblasts from $Smn^{2B/-}$ mice [145] and defects in myoblast fusion in SMA patient skeletal muscle cells from muscle biopsies [146].

In summary, SMA cell culture models remain an accurate, cost-effective and convenient way of providing insights into and modeling of disease pathogenesis. Particularly, the use of patient-derived iPSCs have proven to be very useful when studying different cell types and pathologies, but other cell models have made it possible to answer questions of SMA pathology.

1.2.2 *Caenorhabditis elegans* – roundworm

The roundworm *C. elegans* has been used as a model organism since 1963 and allows for rapid investigation of molecular pathways [147]. Genetic mutations can be induced by exposing/feeding worms mutagens or RNA interference (RNAi) [148]. *C. elegans* has only one copy of *Smn* and knockdown of this gene using RNAi causes larval lethality [149]. A null mutation of *Smn* that deletes most of the *Smn* coding region results in developmental arrest, a reduced lifespan and progressive motor function loss [150]. Muscle-specific expression of SMN does not rescue pathology while neuronal-specific-induced *Smn* expression was partially able to rescue developmental arrest and motor defects [150]. As the null mutation induced a very severe pathology, a *C. elegans* model was created with a point mutation in *Smn*, which caused weak motor defects and a slightly reduced lifespan [151]. *C. elegans* models are an efficient discovery tool for large-scale screening of SMN modifiers.

1.2.3 *Drosophila melanogaster* – fruitfly

The fruitfly *Drosophila melanogaster* was first used in research in 1901 and has been a useful laboratory tool ever since [152]. The first *Drosophila* model for SMA was published in 2000 and had point mutations in the *Smn* gene [153]. Zygotic mutant *Drosophila* demonstrated abnormal motor behavior and neuromuscular junction defects. SMN has to be restored in both muscles and neurons to alleviate this phenotype [154]. *Drosophila* is one of the best animal models for systemically researching gene function and its relation to neuromuscular junction formation as many molecules that are involved in synaptic transmission are conserved between humans and *Drosophila* [155]. Homozygous null SMN *Drosophila* survive beyond embryogenesis due to the mother's contribution of SMN protein [156,157]. The

maternally supplied SMN runs out during the larval state, and animals start to exhibit progressively decreased motility, coordination and growth and die before or at the pupal state [153,158]. As is described in Sections 1.1.3 and 1.2.5, SMN has proven to affect splicing in various SMA mouse models. However, in *Drosophila,* both the major [156] and minor intron small nuclear RNA [158] were not obviously affected after SMN depletion. This suggests that the effects of SMN on small nuclear RNAs could be species specific. *Drosophila* Smn knockout mutants are especially useful in genetic screens for genes that interact with SMN.

1.2.4 *Danio rerio* – zebrafish

In the 1960s, zebrafish were developed as a model to study vertebrate genetics [159]. The zebrafish is a useful model to study SMA, as its motor neuron circuit is well-characterized, and it has a relatively simple neuromuscular organization [160–162]. Zebrafish are transparent, which enables *in vivo* imaging, electrophysiology and motor studies. A wide range of techniques can be used to manipulate gene expression, by using CRISPR-Cas [163], transcription activator-like effector nucleases (TALENs) [164] and morpholino antisense oligos [162]. An experiment in which Smn protein was downregulated ~60%, using *smn*-targeted morpholino injections into one-to-four cell stages of embryos, has recapitulated many aspects of motor neuron defects in SMA, such as truncation and ectopic branching of axons [162]. Motor neuron defects were ameliorated using wild type smn expression, but not *Δ7smn.* An interesting finding was that motor axon development defects preceded motor neuron death in smn-depleted animals [162]. Various genetic screens in zebrafish found promising Smn mutants corresponding to human mutations [165], which enabled the creation of new zebrafish SMA models carrying endogenous *smn* mutations that closely resemble the genetic characteristics of human SMA [166]. This revealed that *SMN2* is similarly spliced in zebrafish as in humans, and splicing can be corrected using antisense oligonucleotides [166]. Overall, the zebrafish SMA model can help better understand disease pathologies and is an excellent model for quick and easy testing of drugs.

1.2.5 *Mus musculus* – mouse

Early attempts, to create a mouse model for SMA by homozygous disruption of *Smn* resulted in early embryonic death [24]. In 2000 two groups were successful by creating an SMA mouse model that survived multiple days after birth [121,122]. Since then, many other SMA mouse models have been created. This section will provide an overview of the most used SMA mouse models and will categorize, according to its severity: prenatal lethal, severe, intermediate and mild SMA mouse models.

In both of the first mouse models that were created and survived after birth, the murine *Smn* gene was homozygously knocked out, and the human *SMN2* transgene was introduced: $Smn^{-/-};SMN2^{+/+}$. In the Burghes group, the homozygous murine Smn knockout mice had two *SMN2* copies and resulted in a severe SMA mouse model. The mice were born with normal numbers of motor neurons, but after five days, these animals died with only 60% of motor neurons left [121]. The Hung Li group, originally created SMA mice with different severities within the same litter. The severity of the pups in the litter (severe, moderate and mild) was based on the number of *SMN2* copies per pup. The most severe pups died before P10 (1 SMN copy), the intermediate pups died at approximately two-four weeks (2 SMN copies) and mild pups did not have a reduced lifespan but had short and enlarged tails (3 SMN copies) [122].

The most widely used severe SMA mouse models are the $Smn1^{-/-};SMN2^{+/+};SMN\Delta7^{+/+}$ (in this thesis called *SMNΔ7*) and the Taiwanese $Smn1^{hung\ -/-};SMN2Hung^{+/-}$ (in this thesis called $Smn^{-/-};SMN2^{+/-}$). The *SMNΔ7* mouse model is based on the $Smn^{-/-};SMN2^{+/+}$ from the Burghes laboratory and was an attempt to create a SMA mouse model that was slightly less severe by adding an extra transgene, *SMNΔ7*: $Smn^{-/-};SMN2^{+/+}:SMN\Delta7$ [167] (termed *SMNΔ7*). The *SMNΔ7* mice die around day 13 after birth and lose about 50% of motor neurons [168,169]. The severe $Smn^{-/-};SMN2^{+/-}$ have two tandem *SMN2* copies per allele and have a similar phenotype as the *SMNΔ7* mice [170]. This mouse model is sometimes preferred over the

Table 1.2. Mouse models of SMA.

Name	Genotype	Severity	Mortality	Description
Smn1 targeted mutation	*Smn*$^{-/-}$	Embryonic lethal	Embryonic lethal	Mice with homozygous SMN disruption display massive cell death during early embryonic development [24].
Burghes' severe model	*Smn*$^{-/-}$;*SMN2*$^{+/+}$	Severe	4–6 days	The mice are born with normal numbers of motor neurons, but after five days, these animals died with only 60% of motor neurons left [121].
Hung Li mouse model	*Smn*$^{-/-}$;*SMN2*	Severe, moderate and mild	10 days, 2–4 weeks, normal lifespan	SMA mice with different severities within the same litter (severe, moderate and mild) which is based on the number of *SMN2* copies per pup [122].
SMNΔ7	*Smn*$^{-/-}$;*SMN2*$^{+/+}$;*SMNΔ7*$^{+/+}$	Severe	13 days	The *SMNΔ7* mouse model is based on the *Smn*$^{-/-}$;*SMN2*$^{+/+}$ from the Burghes laboratory and is slightly less severe by addition of an extra transgene, *SMNΔ7* [167].
Taiwanese mouse model	*Smn*$^{-/-}$;*SMN2*$^{+/-}$	Severe	8–12 days	The severe *Smn*$^{-/-}$;*SMN2*$^{+/-}$ mouse model has two tandem *SMN2* copies per allele [170].
Smn$^{2B/-}$	*Smn*$^{2B/-}$	Moderate	18–30 days	These mice have a mutation that consists of a substitution of three nucleotides in an exon-splicing enhancer of exon 7 that binds to Tra2beta (2B) which causes large amounts of skipping of exon 7 [171,172]. This mutation on one allele, in combination with a knockout allele, results in a moderate SMA mouse model.
A2G	*A2G*$^{+/-}$; *Smn*$^{-/-}$;*SMN2*$^{+/+}$	Mild	227 days	The *A2G* mouse model has a transgene carrying a missense mutation in exon 1 of the *Smn* gene which was introduced in the Burghes *Smn*$^{-/-}$;*SMN2*$^{+/+}$ severe model [121,174]. Heterozygous A2G *Smn*$^{-/-}$;*SMN2*$^{+/+}$ mice have a 29% decrease of motor neurons at 3.5 months, a 25% motor neuron loss and skeletal muscle atrophy at five months [174].
Smn C>T	*Smn*$^{C-T/-}$	Mild	Normal lifespan	Adult onset muscle weakness, decreased activity and alterations of muscle fiber size [175].

SMNΔ7 model, as it has only two genetically modified alleles, which makes it easier to cross this model with other mouse models.

Since severe SMA mouse models die at a very young age (5–13 days, depending on which model), they more so reflect Type 1 patients. In order to identify therapeutic compounds for milder Type 2, 3 and 4 patients, it is beneficial to have an SMA mouse model that manifests phenotype at a later age and has a longer disease time course. More moderate SMA mouse models were created to meet this need. The $Smn^{2B/-}$ mouse model has a mutation that consists of a substitution of three nucleotides in an exon-splicing enhancer of exon 7 that binds to Tra2beta (2B). This causes large amounts of skipping of exon 7, even in the absence of the C>T transition that is found in human *SMN2* [171,172]. This mutation on one allele, in combination with a knockout allele, results in an SMA mouse model that survives approximately 20–30 days as cited in the literature [111,173], and 18–20 days as research for this paper revealed and is described in Chapters 4 and 5. The discrepancy is due to the original mouse model being on a mixed genetic background. The mice we use now have been backcrossed on a pure C57BL/6 background. $Smn^{2B/-}$ mice have ~15% functional SMN protein and are characterized by motor neuron loss, neuromuscular defects and immature neuromuscular junctions. $Smn^{2B/2B}$ mice have ~30% full-length SMN protein and are phenotypically normal [173].

Milder SMA mouse models have also been generated. The A2G mouse model has a transgene carrying a missense mutation in exon 1 of the *Smn* gene which was introduced in the $Smn^{-/-};SMN2^{+/+}$ severe model [121,174]. Heterozygous A2G $Smn^{-/-};SMN2^{+/+}$ mice have a 29% decrease of motor neurons at 3.5 months of age, a 25% motor neuron loss and skeletal muscle atrophy at five months, and die around 227 days [174]. In order to investigate *SMN2* splicing, an SMA mouse model was created that has a C>T mutation in the murine *Smn* gene, which causes exon 7 skipping. *Smn C>T* mice have a normal lifespan, but develop adult onset muscle weakness, decreased activity and alterations of muscle fiber size [175] .

There are various factors that determine the severity of SMA mouse models. The main factor influencing disease severity is the amount of full-length SMN. However, phenotypic analysis also

revealed that the genetic background of the mice plays a role in severity. For example, *SMNΔ7* mice exhibit a more severe phenotype when on a complete congenic C57BL/6J background than on an FVB/N background (11 days); however, *SMNΔ7* mice with a mixed genetic background lived longest (13–14 days) [167]. As mentioned earlier, mouse strain also influences severity in the $Smn^{2B/-}$ mouse model. $Smn^{2B/-}$ on an FVB/N background had a shorter lifespan than on a C57BL/6 background [176]. The location of the *SMN2* transgene also plays a role in the severity of the mouse model [177]. The *SMN2* gene can be randomly inserted or specifically inserted into the murine *Smn* locus. Different insertion sites can result in different SMN levels and variable expression between tissues. Lastly, differences in severity in the same mouse model at different animal facilities can arise, which might be explained by inbreeding and diet [96].

In addition to genetic mouse models with systemic SMN depletion, there are also tissue-specific models. These models examine the specific effects of SMN depletion on a certain tissue or cell type. Such mouse lines can be generated by crossing mice with a Cre-recombinase gene downstream of a tissue-specific promoter with mice containing an *Smn* allele with two loxP sites flanking exon 7 (SmnF7). A combination of both results in mice that have an exclusion of exon 7 and a corresponding depletion of SMN protein in a specific tissue or cell type. This technique has been applied in several tissues and cell types, such as pan-neuronal cells [178], motor neurons [178,179], skeletal muscle [178,180] and hepatocytes [181]. To evaluate the developmental requirements for SMN, the cre-recombinase system can also be used to restore expression of full-length *SMN2* at various timepoints by tamoxifen administration [182].

Taken together, although the mouse model has limitations, the development of SMA mice has enabled the study of disease mechanisms in a tremendous way and increased the potential for pharmacological studies.

1.2.6 Other mammalian models

In 2015, a porcine model of SMA was developed, using intrathecal delivery of scAAV9-mediated *Smn* mRNA knockdown [183]. This model is characterized by motor neuron loss and axon degeneration, and the pigs develop a clear SMA-like phenotype with the first signs of muscle weakness occurring around day 25. The weakness starts in the hind limbs, then progresses to the front legs. Between 46–69 days, these animals reach their humane endpoint. This phenotype is rescued by introduction of human *SMN1* via self-complimentary adeno-associated virus 9-SMN (scAAV9-SMN) [183]. As pigs lack the intron-splicing silencer in exon 7 and have a modified splicing of *SMN1*, they are not a model for splicing modulation studies [184]. However, this model is useful for pre-clinical testing of gene therapy approaches.

Other large animals, such as non-human primates, have also been used in SMA research, but as they lack the *SMN2* gene, they are not used for *SMN2* exon 7 splicing studies. They are, however, used for safety and bioavailability studies for gene replacement [185,186] and antisense oligonucleotide studies [187].

1.3 Tissue and cell type specific pathology in SMA

The key feature of SMA is the selective death of motor neurons, which causes denervation followed by skeletal muscle atrophy. Since SMN has housekeeping functions (e.g., RNA metabolism, see previous Section 1.1.3) and is ubiquitously expressed, it is no surprise that, in addition to motor neurons, NMJs and muscles, other organs and tissues in the body (Section 1.3.4) are also affected [188]. There is presently no direct answer to the question about what makes some cell types more vulnerable to SMN depletion than other cell types and tissues. There is evidence that SMN depletion affects splicing in a tissue specific manner [48]. Another option to consider is that there might be distinctive roles, other than housekeeping, for SMN in different tissues and cell types. This could explain why some cell types and tissues are affected earlier and more severely than others.

It is important to acknowledge that motor neuron pathology and other pathologies interrelate with one another, and, therefore, are sometimes hard to divide into distinct entities. Nevertheless, they will be discussed herein individually.

1.3.1 Motor neuron pathology

The key feature of SMA is the selective death of motor neurons, but the reasons and mechanistics behind this selective cell death are still poorly understood. What makes it harder is that motor neurons are not uniformly susceptible to SMA. Different populations of motor neurons are vulnerable whereas others are more resistant to SMN depletion. Natural history of SMA patients demonstrates that the disease is characterized by an acute phase of motor neuron death and dysfunction, followed by a chronic phase due to a more resistant subset of motor neurons [189]. A study using *Smn*$^{-/-}$*;SMN2* mice demonstrated that even motor neurons with similar characteristics can exhibit a very different vulnerability. Interestingly, the morphological characteristics, position of the innervated muscle in the body or muscle fiber type innervated, did not necessarily determine or modulate the susceptibility of the motor neurons [190]. A transcriptional analysis of vulnerable and more resistant motor neurons from *Smn*$^{2B/-}$ mice at a pre-symptomatic timepoint demonstrated that vulnerable motor neurons and Smn levels correlate with a decrease in transcripts implicated in ribosome, rRNA binding, ubiquitin and oxidative phosphorylation [191].

Furthermore, SMN has proven to fulfill a neuroprotective function in motor neurons. Indeed, a study that used SMA patient-derived iPSC motor neurons demonstrated that motor neurons expressing high levels of SMN and treated with cytotoxic compounds were less prone to cell death than motor neurons expressing low levels of SMN [192]. WT motor neurons in which SMN is downregulated using a siRNA are more prone to die than motor neurons expressing normal levels of SMN. However, upregulation of SMN in both SMA and amyotrofic lateral sclerosis (ALS) patient-derived motor neurons, increased viability [192]. ALS is a motor neuron disease characterized by upper and lower motor neuron death.

There are a number of intrinsic and extrinsic factors that influence motor neuron health in SMA. To start with, intrinsic factors are related to SMN's role in splicing, as described in Section 1.1.3. Recent research revealed that SMN affects the major and minor spliceosome differently. The minor spliceosome has a pronounced role in neuronal homeostasis, which suggests its implications for the pathogenesis of motor neurons in motor neuron diseases [193]. Several studies have found that the minor spliceosome components are significantly downregulated in the spinal cord of late symptomatic SMA mice while the major spliceosome pathway remains normal [48,194]. This suggests that cell types expressing a higher proportion of genes that mainly use this minor splicing pathway are more selectively affected by SMN depletion than other cell types, thereby contributing to selective motor neuron vulnerability. Minor spliceosome component levels were also found to be reduced in ALS [195]. Indeed, RNA-seq analyses of various cell types in SMA identified genes whose splicing is selectivity dysregulated in motor neurons, but not in other neuronal cell types [196]. This research was executed in cell populations from the spinal cord in pre-symptomatic P0 *SMNΔ7* mice. One of these incorrectly spliced genes is agrin [196], a stimulator of acetyl choline receptor clustering and accountable for NMJ maturation [197]. Another misspliced gene is *Gria4* [196], which encodes the AMPA-type glutamate receptor 4 and might be responsible for the altered electrophysiological properties found in SMA motor neurons [168,179]. A similar study in Smn-depleted zebrafish identified neurexin2a to be misspliced using a transcriptomic microarray. This mis-splicing of neurexin2a was confirmed in motor neurons from $Smn^{-/-};SMN2^{+/+}$ mice [198]. Knockout of neurexin2a in mice revealed neuromuscular junction defects, similar to those demonstrated in SMA and other motor neuron diseases [199,200]. These studies together demonstrate that SMN likely has a role in splicing in the CNS which is disturbed after SMN depletion and therefore leads to motor neuron death. a

Neurons have a high requirement for energy, which is supplied by mitochondria, whose role it is to supply cells with ATP. Various studies have demonstrated abnormal mitochondrial transport and morphology in neuronal SMA cells. In the motor neuron-like NSC-34 cell type, mitochondrial defects were reported after SMN knockdown using RNAi [201]. As motor neurons are large cells with a high-

energy demand, impaired mitochondrial function affects motor neuron viability and axonal transport. This is supported by a study showing significant reduction in mitochondrial transport as well as in axonal number and size in axons of motor neurons derived from SMN-knockdown hESCs and SMA iPSCs [202]. A further study in *Smn*$^{-/-}$;*SMN2*$^{+/-}$ mice crossed with *Hb9:GFP* transgenic mice, which specifically label motor neurons with GFP, revealed functional impairment and fragmentation of mitochondria in motor neurons. Mitochondria had reduced respiration, decreased ATP synthesis, defective retrograde transport, decreased membrane potential and increased oxidative stress level [203] (see Section 1.1.4.1 about oxidative stress in SMA). Altogether, this reveals a potential role of SMN in mitochondria and motor neuron death.

There is also evidence pointing toward a non-splicing function of SMN in motor neurons. SMN is mainly found in the nucleus, but small portions are in the axon in granular forms [204–207]. This axonal SMN is not part of the SMN complex and does not include Sm proteins [204]. A time-lapse image of SMN protein has demonstrated that the protein is transported along the axon [204]. Various studies have illustrated that axonal SMN localizes with RNA-binding proteins and mRNAs [205,208–210], which suggests a role for SMN in the transport, stability or the local translation of axonal mRNAs. This is supported by evidence that SMN reduction leads to a decline in levels of several hundreds of mRNAs in axons [211–213]. This disruption in axonal localization of mRNAs might be partly responsible for the selective vulnerability of motor neurons. Further studies in NSC-34 cells and in Smn-depleted primary mouse motor neurons uncovered approximately 1,000 dysregulated genes in neurites. Among these were multiple genes involved in neurogenesis, axonal outgrowth, synaptogenesis and neurotransmitter release [211,212].

Cytoskeleton stability also plays a role in motor neuron vulnerability. As discussed in Section 1.1.4 about genetic modifiers, the cytoskeleton has a tremendous role in axonal growth, morphology maintenance, axonal transport, synaptic vesicle trafficking and neurotransmission, neuronal differentiation and maturation of the NMJ [99,100]. MicroRNAs, which are small non-coding RNA molecules, may also play a role in motor neuron vulnerability. MicroRNAs regulate axonal outgrowth

by regulating local translation. For example, miR-183, which targets inhibition of mTOR translation, is upregulated in rat, human and mouse cells after Smn depletion. Knockdown of miR-183 in *SMNΔ7* mouse neurons resulted in improvement of axonal length [214]. Similarly, miR-431 is upregulated in SMN-knockdown primary mouse motor neurons, and knockdown causes neurite length to increase in these cells [215].

Motor neurons are not only influenced by intrinsic factors, but also by extrinsic factors, which may play a crucial role in motor neuron health in SMA, one example being surrounding non-neuronal cells like glia. The various types of glia cells are astrocytes, oligodendrocytes and microglia, which regulate myelination, homeostasis and the immune response [216]. Various studies report astrocytic defects in pre-symptomatic *SMNΔ7* mice [217] and SMA iPSC-derived and primary murine astrocytes [218]. Astrocytes have, among others, been implicated in synapse formation and electrophysiological properties of motor neurons [219]. Specifically restoration of SMN in astrocytes of *SMNΔ7* and *SMN*$^{2B/-}$ mice, resulted in improvement in motor functions, NMJ occupancy ratio and lifespan [218,220]. However, SMN restoration in SMA astrocytes did not rescue motor neuron soma death [218,220]. Further, Schwann cells, which are myelinating glial cells of lower motor neurons in the periphery, are affected in SMA. Defective secretion of myelination was found in different SMA mouse models, which are required for motor axon transmission [221]. Overexpressing SMN in myelinating Schwann cells in *Smn*$^{-/-}$*;SMN2* mice reversed myelination defects and significantly improved neuromuscular function and decreased neuromuscular junction pathology [222]. However, in studies in which SMN was upregulated in astrocytes of SMA mice, restoration of SMN in Schwann cells had no impact on motor neuron death in *Smn*$^{-/-}$*;SMN2* mice [222].

There are also interactions between sensory and motor neurons, which may influence motor neuron viability in SMA. Furthermore, there is evidence of an impaired sensory system in SMA, as was studied in the *SMNΔ7* mouse model, that demonstrated that deafferentation from sensory inputs onto motor neurons resulted in lower input from presynaptic activity and could account for the impaired motor

activity of SMA [168]. Furthermore, SMN depletion can cause overlapping defects in both sensory and motor neurons, such as growth cone size [223].

Finally, there is bi-directional communication at the neuromuscular junction between the axon terminal and innervated muscle, which might modulate motor neuron health in SMA. In an older study, spinal neurons isolated from neonatal chickens were treated with muscle extracts from SMA patients and aged-matched controls. The muscle extracts from SMA patients, but not aged-matched controls, resulted in inhibition of neurite outgrowth [224]. Other studies have failed to reveal a negative influence of muscle on motor neurons. Indeed, studies in which SMN was depleted only in muscle, the NMJ and motor neurons were spared [180], whereas increased muscle-specific SMN expression in SMA mice did not restore NMJ and motor neuron pathology [225,226].

1.3.2 Neuromuscular junction pathology

Neuromuscular junction (NMJ) dysfunction in SMA has been hypothesized to be caused by motor neuron death. Intriguing, however, is the fact that NMJ pathology starts before motor neuron death [168,169]. NMJs in SMA demonstrate three main pathological features, which have also been demonstrated in SMA mouse models: immaturity, neurofilament accumulation and denervation.

Various groups have demonstrated dramatic abnormalities in NMJ morphology in SMA mouse models, as the NMJs are immature, significantly smaller and (sometimes) fragmented, compared to WT mice [227]. At P14, 50% of NMJs in the *SMNΔ7* SMA mouse models were immature, compared to 10% of NMJs in WT mice [228]. This delayed maturation is also associated with impaired synaptic function of motor terminals. This is confirmed by a study in *SMNΔ7* mice, which demonstrated slowed postsynaptic potentials and ~55% reduced evoked neurotransmitter release [117]. Neurofilament accumulation in motor nerve terminals is reported in both SMA patients and SMA mouse models [115,228,229] and increases over time [228]. Moreover, neurofilament accumulation is only found at the endplate and not in the motor neuron cell body, motor root and nerve [230,231]. A study using *SMNΔ7* SMA mice reveals that

neurofilament accumulation develops before the onset of denervation. Furthermore, NMJs in proximal muscles are affected earlier by neurofilament accumulation than those in distal muscles [169]. It has been hypothesized that neurofilament accumulation is associated with slow and delayed transport of components important for NMJ maturation and maintenance, thereby contributing to NMJ dysfunction in SMA [232]. NMJ denervation is a canonical characteristic of SMA and the extent of denervation in patients can be tested by using the motor unit number estimation (MUNE) and the maximum compound motor action potential amplitude (CMAP) techniques, both of which apply electromyography to estimate the number of motor units (MUNE) and action potentials (CMAP) in a muscle. Denervation in SMA patients is correlated with disease severity [189]. A study using *Smn$^{-/-}$;SMN2* mice demonstrated very early denervation at embryonic day 18.5 [233].

Some, if not all, of NMJ pathologies are directly or indirectly affected by low levels of SMN. Indeed, SMN knockdown in neonatal *SMN2;CreER;Smn$^{F7/-}$* mice-induced severe neuromuscular pathology; whereas SMN depletion after full NMJ maturation in P17 *SMN2;CreER;Smn$^{F7/-}$* mice had a relatively low effect [234]. This highlights the temporal requirements for SMN in NMJ maturation and maintenance during development. Also, as discussed in Section, 1.3.1, SMN depletion in motor neurons downregulates certain mRNAs that are important for NMJ maturation and formation [196,199,200]. This might explain the fact that there is NMJ dysfunction before actual motor neuron death.

Another phenomenon that may contribute to NMJ pathology in SMA is neuronal dying-back pathology, by which the motor nerve terminal progressively retracts from the target muscle fiber. This was observed in various SMA studies [229,230], demonstrating morphological pathology of motor endplates. For example, a study in *Smn$^{-/-}$;SMN2* mice revealed that motor nerve terminals were only partly overlying acetylcholine receptors, supporting the dying-back neuropathy hypothesis in SMA [229].

In conclusion, NMJ pathology is an early event in SMA pathogenesis, which may be directly and indirectly caused by SMN depletion and is followed by motor neuron dysfunction.

1.3.3 Muscle pathology

Muscle pathology in SMA patients starts at a prenatal age. Histological analyses of skeletal muscle in Type 1 SMA fetuses at 12–15 weeks gestational age revealed smaller myotubes than in skeletal muscle from healthy control fetuses [235]. In another study, comparing 14-weeks' gestation SMA muscle to healthy control muscle demonstrated abnormalities in muscle markers, where SMA samples had a higher percentage of myotubes expressing fast myosin and a lower percentage of myotubes expressing slow myosin compared to control samples [236]. There were no differences in the number of satellite cells, as measured by Pax7-positive nuclei, in SMA compared to control samples at this age. Satellite cells are precursors to skeletal muscle cells. Postnatally (ages 1–13 months after birth) however, the numbers of satellite cells in SMA were increased, compared to the control group, suggesting an abnormal myogenic process [236]. A study investigating regulation of myogenesis in Type 1 and Type 3 patients revealed elevated expression of myoblast determination gene MyoD, myogenin and muscle-specific myogenic factor 5 (Myf5). This was also found in primary myoblast from *Smn*$^{2B/-}$ mice [145]. These results point toward the notion that skeletal muscle pathology starts with impaired muscle maturation and is one of the primary pathologies in SMA.

However, it is hard to determine if muscle pathology is primarily caused by motor neuron death and denervation (Sections 1.3.1 and 1.3.2), or if there are also intrinsic abnormalities caused by SMN deficiency either directly or indirectly. There are some indications for muscle-specific functions of SMN. Indeed, SMN forms a complex with α-actinin in myofibers of *Drosophila melanogaster* [156]. Supporting this are the results found in a study knocking down *Smn* in C2C12 myoblasts, which caused defects in myoblast fusion and myotube morphology [144]. To gain insight in the role of SMN in skeletal muscle pathology and to circumvent early lethality and denervation-induced atrophy, *Smn* exon 7 can be deleted using the Cre-LoxP system specifically in skeletal muscle. Smn exon 7 deletion in skeletal muscle was carried out in WT mice and led to severe muscular dystrophy after three weeks of age and death at an average of 33 days [180]. Selective restoration of Smn by 50% in satellite cells in these mice

improved phenotype and extended survival to 8 months [237]. This, and other research [238], led to the hypothesis that muscle pathology in SMA is caused, at least partly, by SMN deficiency in satellite cells. A study in primary myoblast from *Smn*$^{2B/-}$ mice demonstrated decreased levels of myogenic regulatory factors (Pax7, MyoD, myogenin and MRF4), and found in *Smn*$^{2B/-}$ mice skeletal muscle a decrease in myofiber size and an increase in immature myofibers. SMN upregulation in *Smn*$^{2B/-}$ mice increased myofiber size, myofiber maturity and attenuated the disruption of the myogenic program in these mice [145]. Similar to motor neurons, skeletal muscle also has a high demand for energy, which is supplied by mitochondria. A study in *quadriceps* muscle samples from 24 SMA Type 1–3 patients demonstrated impaired muscle mitochondrial biogenesis which most likely contributed to pathologic change in the skeletal muscle of the patients [239]. A change in mitochondrial function, integrity and content promotes muscle wasting [240].

Interestingly, not all skeletal muscles are equally affected in SMA patients [241]. SMA patients have proximal muscle weakness, which affects the lower limbs more than the upper limbs. The *diaphragm* is relatively spared. Initially, distal muscles are spared, but they become severely affected later in the disease [242]. An explanation for this uneven muscle pathology could be that different muscles undergo denervation at different times, developmental delay and compensation of hypertrophy in remaining myofibers. The different vulnerabilities of different muscles in SMA were confirmed by a study in *SMNΔ7* mice [169].

Furthermore, genetic modifiers (Section 1.1.4) such as plastin 3, profilin and the RhoA/ ROCK pathway that influence actin might have effects on muscle pathology. Downregulation of ROCK using ROCK inhibitors results in improvement of skeletal muscle mass and an increase in lifespan, while it does not change the motor neuron viability or increase expression of the SMN protein [111,112].

1.3.4 Peripheral pathology

SMA is a neurodegenerative condition and is often referred to as a motor neuron disease. However, there are many clinical reports of additional peripheral organ pathology contributing to the disease. Also, as discussed in Sections 1.3.1 and 1.3.2, non-neuronal cells in the CNS and muscle are affected, not all of which are caused by motor neuron death and denervation but can be caused by a SMN-specific role in these cells and tissues. A very interesting study supporting a role of SMN in the periphery reveals that systemic restoration of SMN in *Smn*$^{-/-}$*;SMN2* mice was much more effective than CNS restoration alone [243]. Furthermore, organs and cell pathology, other than in the CNS and skeletal muscle, have been reported in a number of SMA patients, mainly in most severely affected Type 1 and 2 patients. The effects of SMN depletion-causing pathology in organs in the periphery may have an impact on SMA disease progression and motor neuron vulnerability and are important to consider. In the following sections, there will be an overview of the most common peripheral pathologies in SMA. However, pathology has also been found in other organs and cell types, such as bones and testis.

1.3.4.1 Heart and cardiovascular system

A subgroup of severe SMA patients present cardiac defects defined by structural and functional defects. Structural abnormalities such as atrial septal defects [29,244–246], atrioventricular septal defects [29,246], valvular aortic stenosis [244], severe coarctation of the aorta [29], hypoplastic aortic arch [247], univentricular heart [29], partial atrioventricular canal [29], tricuspid atresia [29], and several characteristics of hypoplastic left heart syndrome [248,249], are mainly found in Type 1 patients, whereas disturbances of cardiac rhythm were found in both severe Type 1 [250] and in more mildly affected SMA Type 2 and 3 patients [251–253]. In addition, autonomic nervous system dysfunctions such as digital necrosis and vascular thrombosis, potentially as a consequence of cardiac pathology, have been reported in Type 1 patients [254]. Some SMA patients also exhibit bradycardia [250,255]. Cardiac pathology has been demonstrated in several SMA mouse models. Structural defects reflected by decreased heart size

were found in *Smn*$^{-/-}$;*SMN2* [243,256,257] , *SMNΔ7* [258–260], *Smn*$^{\Delta 7/\Delta 7}$; *SMN2*$^{+/-}$[261] mice, which can partially be explained by reduced weight and body size in SMA mouse models. Functional heart defects were found in *Smn*$^{-/-}$;*SMN2* [256,257], *SMNΔ7* [258,260,262], *Smn*$^{-/-}$;*SMN2*$^{+/+}$ [259], *Smn*$^{\Delta 7/\Delta 7}$; *SMN2*$^{+/-}$ [261] mice and consisted mainly of bradyarrhythmia and other murine cardiac rhythm problems. These findings suggest that SMN is relevant for normal cardiogenesis.

1.3.4.2 Pancreas and metabolism

SMN has also been implicated in the modulation of metabolism and pancreas morphology. Diabetes and alterations in glucose metabolism have been reported in SMA Type 1, 2 and 3 patients [263–266]. The most common metabolic defect in SMA patients is alterations in fatty acid metabolism [265,266]. Metabolic defects have been also demonstrated in SMA mouse models. Metabolism is, among other things, dependent on circadian rhythm. Circadian regulation is critical for many biological processes, disruption of which causes diverse metabolic disorders [267]. Circadian rhythm genes were dysregulated in various metabolic tissues of *Smn*$^{-/-}$*;SMN2* [268]. Other metabolic defects found in SMA mouse models were fasting hyperglycemia, hyperglucagonemia, glucose intolerance and hypersensitivity to insulin, which was demonstrated in *Smn*$^{2B/-}$ mice [263]. These animals also had a decrease in *β* cells and an increase in *α* cells within pancreatic islets, which corresponded to a functional inability to metabolize glucose [263]. This shift in pancreatic cell composition was also found in the pancreas from diseased Type 1 patients [263]. The authors found that these metabolic defects started at a pre-symptomatic timepoint, revealing that metabolic and pancreatic defects are independent of late-stage SMA pathology caused by motor neuron death. This was strengthened by the finding of metabolic defects in Smn (+/−) heterozygous mice with 50% Smn, which lack the SMA neuromuscular pathology and overt phenotype [269]. This suggests that a decrease of SMN levels (in this case, of only 50%) might have a negative impact on SMA patients, when their SMN levels are increased and live longer.

Another factor that influences metabolism in SMA is skeletal muscle pathology. One of the key roles of skeletal muscle is in the maintenance of metabolic homeostasis. Indeed, skeletal muscle is the

largest insulin-sensitive tissue in the body and is involved in glucose utilization [270]. Therefore, it is not surprising that muscle metabolism is affected in SMA, which is characterized by muscle atrophy. A study in *Smn$^{-/-}$;SMN2* mice revealed dysregulation of krüppel-like factor 15 (KLF15) in skeletal muscle [271]. This was also demonstrated in skeletal muscle from Type 1, 2 and 3 patients [271]. KLF15 is a transcription factor, which among others, is expressed in skeletal muscle and is involved in regulation of amino acid, glucose and lipid metabolism [272]. Modulation of KLF15 in both *Smn$^{-/-}$;SMN2* and *Smn$^{2B/-}$* mice significantly increased lifespan and weight [271].

1.3.4.3 Liver

As mentioned in the previous section, fatty acid metabolism is often altered in SMA patients. The liver, alongside skeletal muscle and adipose tissue, is heavily involved in fatty acid metabolism [273]. Type 1, 2 and 3 patients have demonstrated abnormal levels of liver proteins [265,266,274]. Furthermore, fatty acid-filled vacuoles are found in livers from deceased SMA Type 1 patients [266]. Thus, SMN is proposed to have a specific function in the liver [275]. Interestingly, the liver expresses high levels of SMN in humans, even higher than in the spinal cord [276]. As such, targeted deletion of Smn in embryonic mouse liver results in atrophy and severe dysfunction, failure to regenerate, iron overload and late embryonic death [181].

1.4 Therapeutic development for the treatment SMA

1.4.1 Overview

Whilst Spinraza® is the first approved treatment for SMA, other strategies are being investigated, primarily to upregulate expression of SMN protein. These strategies involve using viral-mediated delivery of the *SMN1* gene or change SMN2 splicing using HDAC inhibitors or small molecules that modulate SMN expression. Other strategies are SMN independent, and focus on neuroprotection or to enhance muscle strength, which could be used in concordance with SMN upregulation therapies.

One of the strategies to develop treatments for SMA is through repurpose of FDA approved drugs for other conditions and diseases. In the sections below, I will describe various treatments that have been tested for other diseases, such as ALS, Duchenne muscular dystrophy, Becker's disease and epilepsy. Repurposing of FDA-approved drugs presents several advantages, such as shorter development and approval times, higher success rates compared to standard developing new compounds (which can take up to 16 years) and reduced costs. A downside of the use of repurposed drugs is that these were less pre-clinically researched and repurposed drugs are often originally not developed for diseases which requires CNS penetration, and might therefore be less useful in SMA. Drugs might also present non-specific mechanism causing side effects, which are overlooked because of less pre-clinical research.

Overall, the development of new therapies for the treatment of SMA is making fast advances. Translational research is resulting in therapeutic strategies tested in clinical trials, which are demonstrated to be safe and efficient. However, challenges remain. One should keep in mind that there is a therapeutic window for treatment, which might be different in each SMA Type. Also, no cure has been developed for SMA yet. A promising strategy is to combine various drugs, to deliver a longer-lasting and more effective treatment for SMA.

1.4.2 Oligonucleotide-based approaches

Modulation of splicing patterns to overcome genetic mutations has been demonstrated in numerous diseases, most notably in Duchenne muscular dystrophy (DMD) [277]. To facilitate this in DMD, splice-switching oligonucleotides (SSO) are designed to bind to pre-mRNA through Watson-Crick base-pairing, either to consensus splice sites or to splicing enhancer regions, in order to prevent recognition of an exon, thereby inducing subsequent removal of the exon from the mature transcript and restoring the reading frame altered by out-of-frame deletion mutations. For SMA however, the challenge is to enhance inclusion, rather than exclusion of exon 7 from the mature transcript. The first such successful

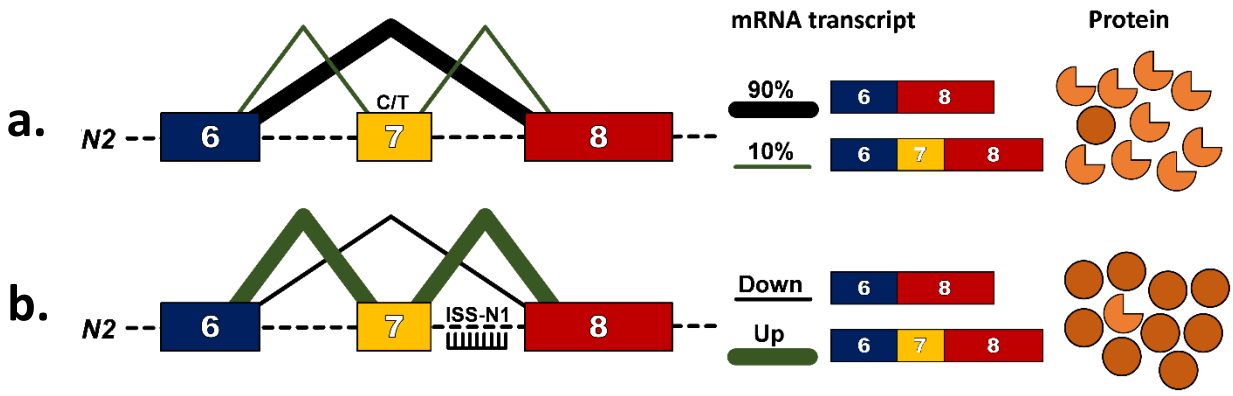


Figure 1.2. Schematic of splice-switching strategy to redirect alternative splicing pattern in the *SMN2* gene. a. C>T transition at position 6 of exon 7 of the *SMN2* gene disrupts an exon splicing enhancer region resulting in exclusion of exon 7 from 90% of the mature *SMN* transcript. **b.** Splice-switching oligonucleotides targeting the intronic splice suppressor N1 downstream of exon 7, promotes inclusion of exon 7 and production of a functional SMN protein. : Truncated SMNΔ7 protein; : full-length SMN protein.

attempt targeted the 3' splice site of exon 8, which resulted in an increase in the use of the 3' splice site of exon 7 and the subsequent increase in full-length protein [278]. The decisive breakthrough in this field came with the identification of a 15 nucleotide splicing silencer element sequence in intron 7, termed intronic splicing silencer-N1 (ISS-N1) [68]. The ISS-N1 sequence is recognized by heterogeneous nuclear ribonucleoprotein A1/A2 (hnRNPA1/A2), a splicing repressor protein. Through specific targeting of this site with SSOs, recognition by hnRNPA1/A2 is blocked, removing the repressor signal and promoting exon 7 inclusion into the mature *SMN2* transcript [279] (Figure 2).

A large body of pre-clinical studies has been performed in mouse models of SMA to investigate the use of SSOs to target ISS-N1 as a potential therapeutic avenue. Numerous SSO chemistries targeting ISS-N1 have been tested *in vivo*, including 2'-O-methyl phosphorothioate (2'OMePS) [280], phosphorodiamidate morpholino oligomer (PMO) [143,281,282] and 2'-O-methoxyethoxy (2'-MOE) [283]. One of the earliest successes was with a 2'MOE chemistry against ISS-N1, named ASO-10-27. Systemic administration to the *Smn*$^{-/-}$;*SMN2*$^{+/-}$ mice at P0 and P3 of a 160 µg/g/injection of ASO-10-27 resulted in a life extension from < 12 days to a median survival of 248 days [243]. One crucial aspect of this study

demonstrated that systemic treatment by subcutaneous administration, in combination with intracerebroventricular (ICV) administration, was much more effective than ICV administration alone (extending the median lifespan by 25-fold), suggesting a synergistic benefit of body-wide SMN restoration. Although significant, this study was performed in PND0/3 mice, thus the potential for SSOs to cross an immature blood brain barrier and contributing to efficacy cannot be ruled out. Indeed, in an earlier study, while tail vein administration of ASO-10-27 into a mildly affected adult SMA model (*Smn*$^{+/-}$;*SMN2*$^{+/-}$) demonstrated enhanced exon 7 inclusion body-wide, no activity was observed in the spinal cord [279], suggesting that direct administration to the CNS would be necessary for therapeutic efficacy for this chemistry. Having demonstrated proof-of-principle in mouse models, the feasibility and practicality of ICV infusion delivery of ASO-10-27 was studied in adult cynomolgus monkeys [284]. No full-length *SMN* transcript was measured after treatment, as cynomolgus monkeys lack the *SMN2* gene. The study in monkeys was to test feasibility and practicality of delivering ASO-10-27 to the spinal cord of adult cynomolgus monkeys, histological examination of brain and spinal cord tissue sections did not reveal overt pathology attributable to the drug, further demonstrating that ASO-10-27 was well tolerated [284]. The functionality and safety of ASO-10-27 have been validated in both SMA mice and cynomolgus monkeys [243,283–285].

It should be noted that while targeting of ISS-N1 by SSOs has been the most successful strategy to date, other oligonucleotide-based approaches have also been studied. Bi-functional oligonucleotides have been developed that consist of an exon 7 targeting element coupled to a serine-arginine rich protein to enhance recognition and thus promote inclusion by cellular splicing machinery into the mature transcript [286]. This approach was used successfully to demonstrate increased *SMN2* exon 7 inclusion in SMA fibroblasts [287] and ICV injection elicited a robust induction of full-length SMN protein in the brain and spinal cord of neonatal *SMNΔ7* mice, resulting in increased lifespan, motor neuron survival and weight gain [288]. An alternate approach to *SMN* exon 7 inclusion has been to target a recently identified, long non-coding RNA (lncRNA) that is found on the antisense strand of *SMN* (SMN-AS1) [289]. This lncRNA is enriched in neurons and transcriptionally represses SMN expression by

recruiting Polycomb repressive complex-2. Combining administration of a 2'MOE gapmer to down-regulate SMN-AS1 with an *SMN2* targeting SSO, increased median survival from 25 days (*SMN2* SSO alone) to 37 days.

1.4.3 Spinraza®

The pre-clinical success of ASO-10-27 in severe mouse models of SMA led to IONIS Pharmaceuticals, in conjunction with Biogen, to develop this approach for treatment of SMA patients. Specifically, this drug, known under the names ISIS-SMNRx, Nusinersen and Spinraza, is an 18mer SSO comprising 2'-MOE chemistry on a fully modified phosphorothioate backbone. The first clinical trial [290] was initiated in 2011 in a Phase I open-label, single-ascending dose study to assess safety, tolerability, pharmacokinetics and clinical effects of intrathecal administration in 28 patients with Type 2 and 3 SMA (ages 2–14 years). Both the SSO drug and the lumbar puncture procedure were well tolerated with no adverse effects when treated up to the highest tested single dose of 9 mg. Furthermore, the 9 mg dosing group demonstrated improvement on the Hammersmith Functional Motor Scale Examination (HFMSE) of 17.6% by day 85. Through a further open-label extension study, the majority of children with SMA Type 2 and 3 receiving the two tested highest doses of 6 and 9 mg, continued to demonstrate improvement in motor function tests with the amelioration of symptoms being dose-dependent and stable [290]. A Phase II, open-label, dose-escalation study assessed the safety, tolerability, pharmacokinetics and clinical efficacy of 6 or 12 mg repeat loading-dose of three times over three months followed by four monthly administrations through intrathecal administration in twenty Type 1 patients where treatment was initiated between three weeks and six months upon identification of SMA symptoms. Significantly, in this study, repeat intrathecal administration of the drug was well tolerated with no safety concerns identified. Promising improvements in motor milestones and motor functions, survival or permanent ventilation independence and improvements in neuromuscular electrophysiology were observed in most, but not all treated infants [291]. Additionally, analysis of post-mortem tissue indicated that nusinersen was broadly distributed

throughout the spinal cord and brain including the target motor neurons [291,292]. As no safety concerns were identified in this study, a large Phase III randomized, double-blind, sham-controlled was initiated in 2014, incorporating 122 SMA Type 1 patients (ENDEAR), and 126 non-ambulatory Type 2 patients (CHERISH) who were administered 12 mg intrathecal dosing. In August 2016, ENDEAR met its primary endpoints, which were improvements in the event-free survival of Type 1 patients and an increase in the proportion of motor milestone responders in the Hammersmith Infant Neurological Examination. In November 2016, CHERISH met its primary endpoint, which was a significant positive change in HFMSE scores. Following 15 months of treatment, patients in the CHERISH study had achieved an improvement of 4 points in the HFMSE scale compared to a decline of 1.9 points in the sham placebo arm. A similar trend was observed in the ENDEAR study, with infants demonstrating a significant improvement in the achievements of motor milestones compared to natural history. The treatment again revealed a favorable safety profile, and most adverse events were either related to the disease, common events in the general public or because of the lumbar puncture procedure [293]. The evidence from the ENDEAR trial showed that some of the Type 1 SMA infants treated for three years were surviving without ventilation and some patients even learned to walk [294]. This is unprecedented for Type 1 SMA patients, since they live normally less than two years and often never achieve the ability to sit, let alone walk (see Section 1.1.1). Based on the positive data from this Phase III trial, in December 2016, the U.S. Food and Drug Administration (FDA) and in May 2017, the European Medicines Agency (EMA) approved Spinraza (nusinersen) as the first and only genetic treatment to date for SMA [295].

1.4.4 The use of cell-penetrating peptides to promote peripheral and CNS treatment

Cell-penetrating peptides (CPPs) were first discovered in 1994 by Derossi and colleagues [296]. CPPs contain natural or non-natural amino acids and are usually between 5–40 amino acids in length. CPPs carry a net positive charge, which enables them to transport conjugated bioactive cargoes through the cell membrane [297]. Different strategies are used to deliver oligonucleotides using CPPs such as co-

incubation approaches, non-covalent complexes, CPP-functionalized nanoparticles and CPP-oligonucleotide conjugates. All these approaches have proven successful *in vitro*, but accomplishing *in vivo* delivery has proven more challenging.

A common strategy is the conjugation of the CPP to an SSO with a covalent bond. This method is very promising although there are a few constraints with the use of CPP/SSO conjugates. Firstly, this approach is only relevant to neutral charge SSO chemistries, such as PMO and PNA [298]. Negative-charged oligonucleotides conjugated to a CPP result in lower or no delivery into cells due to the lack of electrostatic interactions [299]. Secondly, SSOs are used to change pre-mRNA splicing. Hence, in order to prevent degradation, it is important that CPP-SSO conjugates avoid activation of Ribonuclease H after binding to the target pre-mRNA. When using SSOs for splice switching, it is crucial to use a chemistry that confers a steric block mechanism, since RNase H cleavage would otherwise destroy the pre-mRNA [300].

As discussed in Section 1.3.1, although the main pathological feature of SMA is motor neuron death, SMN depletion affects most tissues and cell types in the human body. Therefore, in order to treat SMA, both periphery and CNS should be targeted. This makes the use of CPPs in combination with SSOs a particular promising method of treatment. The delivery of oligonucleotides by CPPs has been demonstrated in a wide variety of tissues, such as muscle, liver, lungs, kidney, spleen, intestine, lymph nodes, *diaphragm* and the heart [143,298,301–305]. Several studies have demonstrated CPP-SSO delivery in the central nervous system. Caille and colleagues CPPs to deliver ASOs in the subventricular zone (SVZ) of the CNS in adult mice [306]. In a study by Du and colleagues, systemic IV delivery of an arginine-rich, CPP conjugated to an antisense morpholino oligonucleotide, resulted in uptake in all areas of the brain in mice [305]. A promising CPP that crosses the blood-brain barrier is the ApoE peptide that could be conjugated to SSOs such as PMOs [307].

Our laboratory was the first to publish a study describing CPP-SSO delivery for the treatment of SMA [143]. The CPP, called Pip6a, was conjugated to a PMO that targets the ISS-N1 site in *SMN2*, to achieve

systemic delivery. This study demonstrates the potent efficacy of delivering Pip6a-PMO to both CNS and peripheral tissues in *Smn*$^{-/-}$;*SMN2*$^{+/-}$ mice following systemic intravenous injection. Full-length upregulation of SMN after Pip6a-PMO treatment resulted in phenotypic correction and improvement in neuromuscular junction morphology and reduced programmed cell death in the spinal cord. Survival of *Smn*$^{-/-}$;*SMN2*$^{+/-}$ mice treated at P0 and P2 with 10 µg/g was extended from 12 days to a median survival of 457 days. This is a higher survival than the earlier described ASO-10-27 SSO from the Krainer group [243], in which SMA animals survived from 12 days to a median survival of 248 days, and where a rather higher dose was used (twice 160 µg/g). To date, this study displays the most extensive increase in survival of SMA mice following SSO treatment [282,308] [281]. Despite the highly extended survival of the Pip6a-PMO treated SMA mice [143], the animals still developed tail and ear necrosis after several weeks and had a lower weight than unaffected animals at all times. The SMA mice treated with a naked PMO were comparable to untreated SMA mice. The potency of the Pip6a CPP conjugated to a PMO was further supported *in vitro* using the neuroblastoma cell line SH-SY5Y. Treatment with a naked PMO failed to increase full-length *SMN2* expression, whereas treatment with the Pip6a-PMO resulted in a significant dose-dependent increase of full-length *SMN2* expression [143]. CPPs have also been studied to systemically deliver the SMN protein, rather than the *SMN2* SSOs, but were not successful with this approach [309].

1.4.5 Gene therapies

The use of viral-mediated delivery of the *SMN1* gene has demonstrated extension of lifespan in SMA mice [186,258,310–312] and porcine [183] models. In 2014, AveXis initiated a Phase I open-label, dose-escalation trial, testing the safety and efficacy of intravenous delivery of AAV9-SMN (AVXS-101) in SMA Type 1 patients. Interim Phase I data from a group of 12 patients receiving the proposed therapeutic dose demonstrated that AVXS-101 was generally well tolerated. All patients reached 13.6 months of age event-free as defined by death or requiring ventilation at least 16 hours per day, whereas the event-free survival rate based on natural history is 25%. A mean increase in the baseline of The Children's

Hospital of Philadelphia Infant Test of Neuromuscular Disorders (CHOP-INTEND) test of 24.7 points was also observed in this group, reflecting improvements in motor function with 2/12 patients achieving scores considered in the range of normal with 5/12 patients able to sit unassisted for more than 30 seconds [313,314]. An open-label Phase III study is currently being conducted in pre-symptomatic infants with SMA Types 1, 2 and 3, testing relevant clinical goals, safety and survival after a one dose treatment of AAV9-SMN [315]. Despite the successes of AAV9-SMN treatment, a major limitation of systemic viral delivery of an *SMN1* transgene is the activation of the immune system, which will limit the possibility of multiple treatments. However, considering the importance of SMN protein in development, it may be that significant restoration of SMN protein at an early stage through viral delivery could have a significant benefit to clinical prognosis. Another limitation is possible motor neuron toxicity of viral vectors. A study of three rhesus macaques and three pigs with AAVhu68-SMN, which is closely related to AAV9-SMN and at a dose similar to that employed in the spinal muscular atrophy clinical trial, resulted in severe toxicity in both rhesus macaques and pigs. All rhesus macaques exhibited marked transaminase elevations, and one developed acute liver failure and had to be euthanized four days after injection. They further developed all degeneration of dorsal root ganglia sensory neurons. All piglets exhibited proprioceptive deficits and ataxia within 14 days, which impaired ambulation and necessitated euthanasia [185].

1.4.6 HDAC inhibitors

Histone deacetylase (HDAC) inhibitors have also been used to promote *SMN2* transcription to increase levels of full-length SMN protein. Valproic acid (VPA), which has been used in the clinic to treat epilepsy, showed an induction of SMN protein levels in SMA fibroblasts [316,317]. Treatment with VPA in Phase II open-label studies demonstrated increased muscle strength and motor function in Type 2 [318] and Type 3 and 4 patients [319]. However, in later clinical trials with SMA Type 3 and 4 patients receiving similar doses, no beneficial effect was demonstrated after 12 months of treatment [320–322]. It has been suggested that inconsistency in these clinical results is due to responders and non-responders to the

drug, again implicating that pre-selection of potential responders could improve the potential for this approach [323]. Another drawback of using VPA for the treatment of SMA patients is its increased risk of causing pancreatitis. As described in Section 1.3.4.2, pancreatic defects are found in severe SMA patients [324].

Treatment with Sodium Phenylbutyrate also increases full-length *SMN2* mRNA and protein in SMA patient fibroblasts. It has also been used in the clinic to treat urea cycle disorder. An uncontrolled, open-label pilot study investigated the use of Sodium Phenylbutyrate in Type 2 SMA patients and resulted in a two-fold increase in SMN mRNA and improved Hammersmith Motor Function Scale scores [325]. Two other Phase II/III clinical trials were terminated early due to slow enrollment [326].

Other HDAC inhibitors such as Trichostatin A [95] and suberoylanilide hydroxamic acid (Vorinostat) [327,328] were all proven to increase *SMN2* expression in animal models and patient-derived cells. A general drawback of using HDAC inhibitors for the treatment of SMA is that HDAC inhibitors are not SMN specific, therefore there are potential side effects and a need for dose limitations.

1.4.7 Neuroprotection strategies

In addition to SMN directed therapies, several other strategies are moving towards clinical development. As motor neuron death is the key feature of SMA, neuroprotection therapies have been proposed to prevent motor neuron death and stabilize motor neuron function. As discussed in Section 1.3.1, mitochondrial dysfunction occurs in SMA motor neurons, which can cause motor neuron death. Olesoxime is an orally administered cholesterol-like small molecule, which can preserve mitochondrial function and prevent apoptosis by reducing release of pro-apoptotic factors and permeability of the membrane when under stress [329]. Olesoxime was identified in a cell-based screen as a neuroprotective for ALS [330], which is a condition also characterized by motor neuron death. In a first Phase II clinical trial, 165 SMA Type 2 and 3 patients were treated with Olesoxime for 24 months. Olesoxime did not significantly improve motor neuron function, although it maintained motor function and prevented

functional decline for two years. A Phase III clinical trial was halfway halted because of disappointing results, patients showed deterioration of motor function after 18 months [331]. Another neuroprotective strategy considered for treatment of SMA is the antibiotic Ceftriaxone, which increases glutamate reuptake by upregulation of glutamate transporter Glt-1 and has been proven to be effective in ALS mice [332]. However, Ceftriaxone treatment was unsuccessful to stop functional decline in a Phase III clinical trial in ALS patients [333]. Ceftriaxone treatment in *SMNΔ7* mice increased survival by 31.6% and ameliorated motor dysfunction [334]. Another treatment targeting glutamate levels in motor neurons is Riluzole, which was evaluated in a Phase I clinical trial. However, the clinical trial could not be completed after support from the pharmaceutical company was withdrawn. Riluzole seemed to increase survival of SMA Type 1 patients but did not change motor function [335].

Another approach for neuroprotection in SMA is to replace or support dying motor neurons using transplantation of stem-cell derived motor neurons into the CNS. Surprisingly, a study in an ALS rat model found that functional improvement can occur without functional integration of motor neurons [336]. An explanation for this is that human neural stem cells secrete neurotrophic factors, which positively modulate the microenvironment of motor neurons [337,338]. Two studies in *SMNΔ7* mice demonstrated an improvement of both neuromuscular function and motor unit pathology and an increase in survival after intrathecal transplantation of embryonic stem cell-derived neural stem cells [339,340]. In a controversial clinical trial that was discontinued by Italian authorities, three Type 1 children underwent multiple intrathecal and intravenous infusions of mesenchymal stem cells and showed an impressive improvement in motor function and general health, which declined after 7 months after the treatment was discontinued [341]. However, a letter from the researchers conducting the study denied these positive results and declared there was no improvement after treatment [342].

1.4.8 Therapies targeting muscle pathology

As discussed in Section 1.3.3, SMN is proposed to also have muscle specific functions, and SMN restoration in skeletal muscle in SMA can ameliorate muscle pathology and even increase survival [237].

In addition to SMN restoration strategies there are other ways to treat muscle in SMA, for example by enhancing muscle strength. One strategy is by inhibiting myostatin. Myostatin is a member of the TGF-beta super-family and an endogenous negative regulator of muscle size. Myostatin can be counterbalanced by follistatin, which binds myostatin to neutralize it. In 1997, a study in mice where myostatin was knocked-out revealed that their muscles were 2–3 times larger than WT mice, which was a result of muscle cell hyperplasia and hypertrophy [343]. Furthermore, a case study is published about a child with a mutation in the myostatin gene. This child was very muscular, caused by muscle hypertrophy [344]. Myostatin signaling can be decreased in various ways, such as using an antagonist such as follistatin or antibodies against myostatin or against its receptor Activin Receptor Type IIB (ActRIIB). A study in *SMNΔ7* mice demonstrated increased muscle mass, gross motor function improvement and increase of 30% in lifespan after recombinant follistatin treatment [345]. However, another study could not replicate these findings in the same mouse model, in which myostatin was downregulated by recombinant follistatin treatment and in another experiment by post-natal administration of a soluble activin receptor IIB (ActRIIB-Fc) [346]. A myostatin knockout *SMNΔ7* mouse model was subsequently created, which showed no improvement in muscle function or survival. It was therefore suggested that the amelioration of SMA symptoms in the initial study with recombinant follistatin could be caused by another unknown function of follistatin, a multifaceted protein involved in various cellular pathways [347]. However, a study in the mild $SMA^{C/C}$ mouse model demonstrated improved muscle phenotype and function after myostatin was inhibited by ActRIIB [348]. The discrepancy in results from these studies could be explained by the different mouse models. $SMA^{C/C}$ mice have a normal lifespan and show mild impairment of motor unit activation, whereas the *SMNΔ7* mouse model is very severe and dies around day 13 after birth because of cardiac problems (see Section 1.2.5) and therefore might die before the treatment has time to become effective. To overcome the severity and early death in *SMNΔ7* mice, the mice were treated in another study with a suboptimal dose of *SMN2* splicing modifiers until adulthood and myostatin was inhibited by an intramuscular injection of AAV1-follistatin, which ameliorated muscle atrophy and improved muscle function [349]. It

may be that myostatin inhibition would not be beneficial for severe Type 1 patients but might ameliorate symptoms in less severely affected Type 2, 3 and 4 patients. However, a recent and pivotal study shows that SMA patients already exhibit decreased myostatin expression [350]. It thus remains unclear if inhibition of something that is already low would be beneficial as a treatment. Recently, a Phase I trial was started in later-onset SMA patients in which myostatin is inhibited by the antibody SRK-015 (ScholarRock) [351]. Efficacy and safety results have not been reported yet.

Another muscle strength enhancing strategy currently in clinical trials is the small molecule CK-2127107 (2-aminoalkyl-5-N-heteroarylpyrimidine) which is a skeletal muscle troponin activator that slows the rate of calcium release from the regulatory troponin complex of fast skeletal muscle fibers, which results in a decrease of the energy required to pump calcium back to the sarcoplasmic reticulum, which may improve muscle contractility and reduce activity-related fatigability [352]. CK-2127107 was evaluated in three separate Phase I trials in healthy humans to test safety and efficacy to enhance muscle force. CK-2127107 proved to increase skeletal muscle contractility which enhances physical performance [353]. CK-2127107 is currently being evaluated in a Phase II trial in ambulant and nonambulant SMA Type 2, 3 and 4 patients to determine the pharmacodynamic effect on skeletal muscle function and fatigability. No results have been published yet [354]. Additional compounds influence SMA genetic modifiers (Section 1.1.4.2), which improve muscle function (Section 1.3.3). One of these are inhibitors of the RhoA/ROCK pathway, Y-27632 and Fasudil, which increased muscle fiber and postsynaptic endplate size in *Smn*$^{2B/-}$ mice [112,355]. Stabilization of SMN, resulting in muscle improvement, could also be achieved by targeting the genetic modifier p38 (Section 1.1.4.1) with BAY 55–9837, an agonist of the vasoactive intestinal peptide receptor 2 (VPAC2) [356].

1.4.9 Therapeutic window

There are various parameters to consider while trying to determine the therapeutic window for SMA treatment. First, not all affected cell types and tissues will have the same therapeutic window. Motor neurons do not regenerate, so treatment should start before denervation events, whereas other cell

types such as myofibers, have the ability to regenerate, which increases the therapeutic window. However, some, if not most, treatment strategies require at least some degree of functionality (for example, therapies that target muscle pathology as described in Section 1.4.8).

Second, SMA is a heterogenous disease with different severities. The therapeutic window is different for all 4 Types of SMA. As is demonstrated in Table 1.1, age of onset of symptoms in Type 1 SMA patients is within the first six months of life and life expectancy is less than two years. The median age at symptom onset among Type 1 patients was 1.2 months, and the median survival of SMA patients with one or two SMN2 copies was only 8 months, as was demonstrated in a recent natural history of SMA studies [357,358]. As discussed in Section 1.3.1, natural history of SMA patients demonstrates an acute phase of motor neuron death and dysfunction, which is followed by a chronic phase which is due to a more resistant subset of motor neurons [189]. Typically, SMA Type 1 patients undergo a rapid loss of motor function in the first three months of life and have lost 95% of motor units at six months [357]. Autopsy studies describe between 50% and 73% of motor neurons are lost at death in Type 1 patients aged 4 to 22 months [359,360]. Therefore, the therapeutic window for SMA Type 1 patients is short and treatment should be administered as soon as possible. Based on mentioned neurophysiological and autoptic data, treatment should be started in the first 3 months, whereas treatment between 3 and 6 months appears to be suboptimal [361]. Ideally, therapies targeting SMN restoration or neuroprotection should start about a month before motor neuron death and pathology. Results from current therapeutic trials suggest that Type 1 patients benefit from early treatment [362], preferably within a week after birth, which is an argument for newborn genetic screening [363]. Another benefit of treating at a young age is that younger patients have a lower immune response against viral vectors than older patients [364]. It is also important to consider the temporal requirements of SMN in various tissues [365] (which is described in the various Sections in 1.3). SMN restoration should therefore be achieved by the earliest treatment possible. Motor neurons are particularly affected early in SMA. One way of expanding the therapeutic window for SMN restoration, is by neuroprotection of motor neurons.

The natural history of Type 2 and 3 patients demonstrate an active motor unit loss in a preclinical phase of the disease, followed by a chronic phase with relative stability and a slow disease progression [189]. Information about the correlation between pre-symptomatic and post symptomatic motor function data and postmortem data in Type 2 and 3 patients are scarce, hence it is difficult to define a therapeutic window. More natural history data of Type 2, 3 and 4 patients are needed. In addition, the use of mild animal models might help to form an answer about a therapeutic window. Various studies have generated milder SMA models by treating severe SMA mouse models with low doses of splice-switching oligonucleotides or small molecule splice modifiers, to study the therapeutic window and effectiveness of SMN restoration during disease progression [308,349]. However, most SMA model research is focused on Type 1 patients with severe pathology. These animal models support results from natural history studies in patients. SMN restoration by gene therapy or antisense oligonucleotide therapy demonstrated greatest effects when delivered within birth–3 days in mice and were less effective beyond p5. Nevertheless, scAAV9-SMN treatment in the SMA porcine model at the time of onset of symptoms showed remarkable improvements [183], which implies that the therapeutic window might be longer in larger animals/humans, than in mice.

1.4.10 Combinational treatment

Because SMA is caused by an insufficiency of SMN, this represents an attractive target for therapeutic restoration. As discussed previously, Spinraza has been approved as a therapy for SMA and other approaches are also currently being explored in clinical trials such as gene therapy (e.g. AveXis's AAV9-SMN) and small molecules (e.g. HDAC inhibitors) to restore SMN levels. These new treatments have changed the therapeutic landscape for SMA, as SMN restoration therapy can clearly have a positive impact on many aspects of disease in the patient population. Nevertheless, the fact that SMN restoration strategies fall short from representing a 'cure' means that these clinical successes will most likely lead to SMA patients living longer with the condition (albeit in a less severe form) and to a significant enlargement of the patient population. Further, as previously mentioned, there is a clear

therapeutic window for SMN-enhancing strategies. Many patients are diagnosed after symptoms have already arisen, which means that for these patients, the treatment will be suboptimal. For these reasons, additional SMN-independent therapies could be used in combination with SMN restoration therapies. This will provide further protection and stability to the neuromuscular system to deliver a longer-lasting and more effective treatment. Secondary combinatorial treatments could be used to prevent further pathology (e.g. neuroprotective therapies like Olesoxime) to widen the therapeutic window, or it could be used in the chronic phase of SMA. Muscle-specific therapies could give patients more strength and increase quality of life. However, further research is necessary to evaluate which treatments and which disease stages would be most optimal. As SMA is a heterogenous disease, different combinations might be useful for the distinct Types of SMA.

1.5 Thesis aims and hypotheses

This thesis addresses the following hypotheses and aims:

1.5.1 Result I. Hypothesis and objectives

Hypothesis

Analyses of differential protein and transcript expression between Smn-depleted and SMN-restored SMA skeletal muscle may reveal pathways that are not rescued in SMN restoration therapy, presenting the opportunity to identify muscle-specific treatments that can be used in combination with SMN restoration therapy.

Objectives

1. Perform a proteomic and transcriptomic analysis on the same muscle (*tibialis anterior*) of *Smn$^{-/-}$;SMN2$^{+/-}$* and control WT mice.
2. Confirm SMN restoration after Pip6a-PMO treatment in *tibialis anterior*.
3. Compare proteomic and transcriptomic data and investigate their overlap.

4. Identify differentially expressed proteins, transcripts and gene ontology pathways in Smn-depleted and SMN-restored SMA skeletal muscle.

1.5.2 Result II. Hypothesis and objectives

Hypothesis

Connectivity map analysis can predict pharmacological compounds that alleviate skeletal muscle pathology in SMA by making connections between SMA disease genes and compounds that influence expression of these genes.

Objectives

1. Perform CMap analyses over the proteomic and transcriptomic data obtained from skeletal muscle (*tibialis anterior*) of *Smn$^{-/-}$;SMN2$^{+/-}$* and control WT (Chapter 3).
2. Choose a compound for proof of concept.
3. Evaluate toxicity and effects on proliferation of selected drug *in vitro*.
4. Validate the genes and proteins identified as differentially expressed by the proteomic and transcriptomic data and predicted to be affected by selected drug.
5. Study the effects of the selected drug treatment on survival and weight in the severe *Smn$^{-/-}$;SMN2$^{+/-}$* and the moderate *Smn$^{2B/-}$* SMA mouse.
6. Examine the effects of the selected drug on skeletal muscle myofiber size, neuromuscular junctions and motor neuron number.
7. Study the effects of selected drug on gene expression in skeletal muscle to determine prediction power of CMap.

1.5.3 Result III. Hypothesis and objectives

Hypothesis

Aberrant expression of the TWEAK/Fn14 pathway in SMA muscle promotes and exacerbates muscle atrophy and modulation of this pathway may ameliorate disease pathology.

Objectives

1. Characterize the expression profile of the TWEAK/Fn14 pathway and its downstream effectors in SMA mouse and patient muscle.
2. Investigate if dysregulation of the TWEAK/Fn14 pathway is dependent on denervation, muscle atrophy, developmental stage and/or the presence of *SMN*.
3. Define the role of the TWEAK/Fn14 signaling cascade during myoblast differentiation.
4. Determine the therapeutic potential for modulating the TWEAK/Fn14 pathway as a muscle specific pathway.
5. Investigate similarities of dysregulation in glucose metabolism as well as myopathy and myogenesis pathways between SMA *Smn*$^{-/-}$;*SMN2*$^{+/-}$, *Fn14*$^{-/-}$ and *TWEAK*$^{-/-}$ mouse skeletal muscle.

2. General materials and methods

2.1 Animals

Wild-type mice (FVB/N [366] and C57BL/6J [367]) were obtained from Jackson Laboratories. Two SMA mouse models were used, the severe *Smn*$^{-/-}$;*SMN2*$^{+/-}$ mouse model [122] which has a median lifespan ranging between 8–11 days (FVB.Cg-Smn1tm1Hung Tg(SMN2)2Hung/J, from Jackson Laboratories) and the moderate *Smn*$^{2B/-}$ mouse model [172] which has a median lifespan ranging between 18–20 days (generously provided by Dr. Lyndsay M Murray, University of Edinburgh). Fn14 KO [368] and TWEAK KO [369] mouse models (generously provided by Dr. Linda C Burkly, Biogen) do not exhibit an overt phenotype.

All experiments with live animals were performed at the Biomedical Services Building, University of Oxford. Experimental procedures were authorized and approved by the University of Oxford ethics committee and UK Home Office (current project license PDFEDC6F0, previous project license 30/2907) in accordance with the Animals (Scientific Procedures) Act 1986.

2.2 Harvest of animal tissues in preparation for further experiments

Mice aged post-natal day (P) 0–10 were sacrificed by decapitation. Cervical dislocation was used to sacrifice mice older than P10. Both males and females were randomly used. Muscle and spinal cord, used for histology, were either directly placed in PBS, or fixed in 4% Paraformaldehyde (PFA) overnight, or embedded in paraffin. Tissues for RNA and protein isolation were placed in cryovials and snap-frozen in liquid nitrogen.

2.3 Histology

2.3.1 Laminin staining of skeletal muscle

Tibialis anterior (TA) muscles were fixed in 4% PFA overnight. Tissues were sectioned (13 µm) and incubated in blocking buffer for 2 hours (0.3% Triton-X, 20% FBS and 20% normal goat serum in PBS). After blocking, tissues were stained overnight at 4 °C with rat anti-laminin (Sigma) in blocking buffer. The next day tissues were washed in PBS and probed using goat-anti-rat IgG 488 secondary antibodies (Invitrogen) for one hour. PBS washed tissues were mounted in Fluoromount-G (Southern Biotech). Images were taken with a DM IRB microscope (Leica) with a 20× objective. Quantitative assays were performed on 3–5 mice for each group and five sections per mouse. The area of muscle fiber within designated regions of the TA muscle sections was measured using Fiji (ImageJ) [370].

2.3.2 Hematoxylin and eosin staining of skeletal muscle

TA muscle sections were first deparaffinized in xylene and then fixed in 100% ethanol. Following a rinse in water, samples were stained in hematoxylin (Fisher) for 3 min, rinsed in water, dipped 40 times in a solution of 0.02% HCl in 70% ethanol and rinsed in water again. The sections were next stained in a 1% eosin solution (BDH) for 1 min, dehydrated in ethanol, cleared in xylene and mounted with Fluoromount-G (Southern Biotech). Images were taken with a Leitz DM RBE microscope (Leica) with a 20× objective. Quantitative assays were performed on 3–5 mice for each group and five sections per mouse. The area of muscle fiber within designated regions of the TA muscle sections was measured using Fiji (ImageJ) [370].

2.3.3 Immunohistochemistry of spinal cord sections

Spinal cords were removed and post-fixed in 4% PFA, followed by 30% sucrose in PBS. The lumbar area of the spinal cord was removed and flash-frozen in Optimal cutting temperature compound (OCT) and cut at 20 µm thick frozen sections. For immunohistochemical analysis of motor neuron number,

sections were first rehydrated 40 min in PBS followed by 10 min permeabilization in 0.1% Triton X. Sections were washed in PBS and stained with Neurotrace 500/525 green fluorescent Nissl (1 in 500; Invitrogen). Sections were then washed in PBS, counterstained with DAPI and mounted in Fluoromount-G (Southern Biotech). Images were taken with a DM IRB microscope (Leica) with a 20× objective. Quantitative assays were performed on 3–5 mice for each group and five sections per mouse using Fiji (ImageJ) [370].

2.4 RT-qPCR for mRNA quantification

RNA was extracted from tissues and cells by either an RNeasy kit® from Qiagen or by guanidinium thiocyantate-acid-phenol-chloroform extraction using TRIzol Reagent (Life Technologies) as per manufacturer's instructions. The same RNA extraction method was employed for similar experiments. A Precellys tissue lyser (Bertin Technologies, Paris, France) was used to homogenize tissues prior to extraction. RNA was re-suspended in a suitable amount of nuclease-free water (30–50 µL, Life Technologies). Samples were purity-assessed and quantified through the use of a NanoDrop ND 1,000 spectrophotometer (Thermo Scientific, Loughborough, UK). Protein and phenol contamination of the sample was assessed by the $\frac{A_{260}}{A_{280}}$ ratio, as phenol absorbs at 270 nm and Tyrosine and Tryptophan at 280 nm. This ratio is expected to be 1.8–2 for pure RNA. The $\frac{A_{260}}{A_{230}}$ was used to measure salt and organic contaminations, which is expected to be >1.8 for pure RNA. Samples that largely failed to meet these criteria were purified or re-extracted.

350 ng–1 µg of RNA was converted to cDNA, by the High Capacity cDNA Kit (Life Technologies) according to manufacturer's instructions. The cDNA template was amplified on a StepOnePlus™ Real-Time PCR Thermocycler (Life Technologies) with SYBR Green mastermix® from Applied Biosystems. qPCR data was analyzed using the StepOne Software v2.3 (Applied Biosystems). Primers used for qPCR were obtained from IDT and sequences for primers were either self-designed, from the literature or ready-made (Table 2.1). For all new primers, a standard curve was ran to test efficacy of the primers.

The qPCR data was analyzed using delta delta Ct analysis. We normalized relative expression level of all tested genes in mouse tissue and cells to *PolJ*. This reference/housekeeping primer was picked based on previous research showing this gene is stably expressed in different tissues in various conditions [371]. For human cells and tissues, we ran a GeNorm kit (Primer Design), which resulted in the identification of *RPL13A* as a reference/housekeeping gene. RPL13A was ordered from IDT (209604333).

Table 2.1. Primers used for quantitative real-time PCR. a. Mouse primers.

Mouse	Forward	Reverse
Aspm	5′-TTCTATGACGAACGCTGGAAG-3'	5′-CTTTCCGCTCCCAAAACAAG-3'
Cdkn1a	5′-CAGATCCACAGCGATATCCAG-3'	5′-AGAGACAACGGCACACTTTG-3'
Clpx	5′-ACAAATACTGACCGAGCCAC-3'	5′-TTCTTTCCAGGGCCAATCTC-3'
Fn14	5′-TCGTGTTGGGATTCGGCTTGGT-3'	5′-ACTTTTCTCTCCGGCGGCATCT-3'
Gls	5′-GTGGTTTCTGCCCAATTACTG-3'	5′-CCCAGCAACTCCAGATTTTG-3'
Glut4	5′-GACGGACACTCCATCTGTTG-3'	5′-CATAGCTCATGGCTGGAACC-3'
HkII	5′-GAAGGGGCTAGGAGCTACCA-3'	5′-CTCGGAGCACACGGAAGTT-3'
Klf15	5′-TGCGTCGGCACACAGGCGAGAA-3'	5′-CCGGTGCCTTGACAACTCATCT-3'
MCM2	5′-AAAGCATCTCCATCTCCAAGG-3'	5′-GGCTCTGTGAGGTCTACATTC-3'
Mef2D	5′-GCTCCATGCAGTTCAGCAATCCAA-3'	5′-AGGCTCCATTAGCACTGTTGAGGT-3'
MuRF-1	5′-AGGACTCCTGCCGAGTGAC-3'	5′-TTGTGGCTCAGTTCCTCCTT-3'
MyoD	5′-TACAGTGGCGACTCAGATGC-3'	5′-GAGATGGCGTCCACTATGCT-3'
Myogenin	5′-CTACAGGCCTTGCTCAGCTC-3'	5′-ACGATGGACGTAAGGGAGTG-3'
Parvalbumin	5′-GCAAGATTGGGGTTGAAGAA-3'	5′-GTGTCCGATTGGTACAGCCT-3'
PGC1α	5′-TGGAGTGACATAGAGTGTGCTGC-3'	5′-CTCAAATATGTTCGCAGGCTCA-3'
PolJ	5′-ACCACACTCTGGGGAACATC-3'	5′-CTCGCTGATGAGGTCTGTGA-3'
Ppm1b	5′-CTTTCTACCTTCGCCCCAG-3'	5′-ATCTTCCATTTCTACTCTCCATCC-3'
Smn	5′-TGCTCCGTGGACCTCATTTCTT-3'	5′-TGGCTTTCCTGGTCCTAATCCTGA-3'
SnrnP27	5′-CTGGAGGGTAAAACAGAGGAAG-3'	5′-AGACACGTTGATGGCATAGG-3'
Tob2	5′-CCTCAGCTACAACCTGAATACC-3'	5′-TCTTTCCCTCTTGCGTTTGG-3'
Tweak	5′-AAGTTCACTGAGGGGCCTTGCT-3'	5′-TGTGAACAAGCTCTGGCTGCCT-3'

b. Human primers

Human	Forward	Reverse
ASPM	5’-GGACAAAACCCATTATCGCTG-3'	5’-CCCTGTTCCTGCTTTTCCTTC-3'
CDKN1a	5’-TGTCACTGTCTTGTACCCTTG-3'	5’-GGCGTTTGGAGTGGTAGAA-3'
CLPX	5’-GTGCTTTCAGTTGCTGTGTAC-3'	5’-TCATCCTCCCGTCTTCTTATTTC-3'
Fn14	5'-GCGCTCTGAGCCTGACCTTC-3'	5'-GGTGGTGAACTTCTCTCTCCTGC-3'
GLS	5’-TTCCAGAAGGCACAGACATG-3'	5’-GGCTCAGTACTCTTTCACCAG-3'
Glut-4	5’-ACTGGACGAGCAACTTCATC-3'	5’-GAGGACCGCAAATAGAAGGAA-3'
HKII	5’-GATTGTCCGTAACATTCTCATCGA-3'	5’-TGTCTTGAGCCGCTCTGAGAT-3’
KLF-15	5’-ATGCACAAATGTACTTTCCCT-3'	5’-TCAGTTCACGGAGCGCACGGA-3’
MCM2	5’-ATTTCGTCCTGGGTCCTTTC-3'	5’-CGCTGGTAGTTCTGATAGATGG-3'
Mef2D	5’-GTGTAAGGTGTGCCGAGAC-3'	5’-CAAACTTCCGCTTGGTGAAAG-3'
MyoD	5’- CGAACCCCAACCCGATATAC-3'	5’-GGGCATTTAAGTTCAATCTTTTGG-3'
Myogenin	5’-ATCGTGGACAGCATCACAG-3'	5’-CCGGCTTGGAAGACAATCTC-3'
Parvalbumin	5’-CTACCGACTCCTTCGACCA-3’	5'-CGAGATTGGGTGTTCAGGG-3'
PGC1α	5'-AAACAGCAGCAGAGACAAATGC-3'	5'-TTGGTTTGGCTTGTAAGTGTTGTG-3'
Ppm1b	5’-CCCTTGCCTCAGATTTATTGC-3'	5’-TTCCATTTCCACTCTCCATCC-3'
SMN, delta 7	5’-ACTTACTATCATGCTGGCTG-3'	5’-CCAGCATTTCCATATAATAGCC-3'
SMN, full-length	5’-GCTTTGGGAAGTATGTTAATTTCA-3'	5’-CTATGCCAGCATTTCTCCTTAATT-3'
SMN, total	5’-GCGATGATTCTGACATTTGG-3'	5’-GGAAGCTGCAGTATTCTTCT-3'
SnrnP27	5’-AGAAACAAAGAGCAAAGAACGG-3'	5’-TTTACAGAGCCATCCACCTTC-3'
Tob2	5’-AGCTACAACCTGAACACCATG-3'	5’-TCTCTTTTCTGTGGTCTTGGG-3'
TWEAK	5'-CTGTCAGGTGCACTTTGATGAG-3'	5'-AGCAAGTCCAGCTTCAGGTAGA-3'

2.5 Cell culture – maintenance and differentiation

Two murine cell lines were used, C2C12s [372], which is a murine myoblast cell line originally generated from a thigh muscle of a C3H mouse, and NSC-34s [373], a motor neuron-like cell line, which was produced by fusion of motor neuron enriched, embryonic mouse spinal cord cells with mouse neuroblastomas. Both cell lines were maintained in growth media, which consisted of Dulbecco’s Modified Eagle’s Media (DMEM) supplemented with 10% fetal bovine serum (FBS) and 1% Penicillin/Streptomycin (all Life Technologies). The cells were cultured at 37˚C with 5% CO_2. C2C12

myoblasts were differentiated in DMEM containing 2% horse serum (HS) for 7 days to form multinucleated myotubes.

Human SMA patient (GM03813, Coriell Institute) and control (AG02261, Coriell Institute) fibroblast cell lines were converted into myoblast cell lines (described in Section 2.6). The patient fibroblasts were obtained from a 3-year-old male with Type 2 SMA. The donor had a homozygous deletion of exons 7 and 8 in the *SMN1* gene and had 3 copies of the *SMN2* gene. The biopsy source was skin cells from the arm (Coriell Institute). Both fibroblast and myoblast cells were cultured in DMEM, supplemented with 1% antibiotics/antimycotics, and 20% FBS to promote growth, as these cells were slow growers. For induction of myoblast differentiation, serum concentrations were lowered to 2% horse serum for 10 days. Cell lysates were collected during proliferation and differentiation for qPCR and Western analyses.

2.6 Cloning of a stable and inducible construct overexpressing MyoD in human fibroblasts

MyoD was cloned into pInducer20 to generate an inducible fibroblast cell line which overexpresses MyoD to induce it into a myoblast cell line. This process was also executed with an eGFP sequence for control. We used the overexpression vector pInducer20-eGFP plasmid (Figure 2.1) and the human myogenic differentiation 1 (MYOD1) plasmid (Origene, SC125952).

eGFP was cut out and removed from the vector by restriction enzymes BsmBI (between TRE-promotor and eGFP) and AscI (right after eGFP). To ligate MyoD into the restricted vector, a BsmBI restriction site was added at the start of the MyoD sequence, and an AscI site at the end of the MyoD sequence, using PCR (primers in Table 2.1). The PCR product was digested with BsmBI and AscI to generate the right overhangs and then it was ligated into the BsmBI and AscI-digested vector.

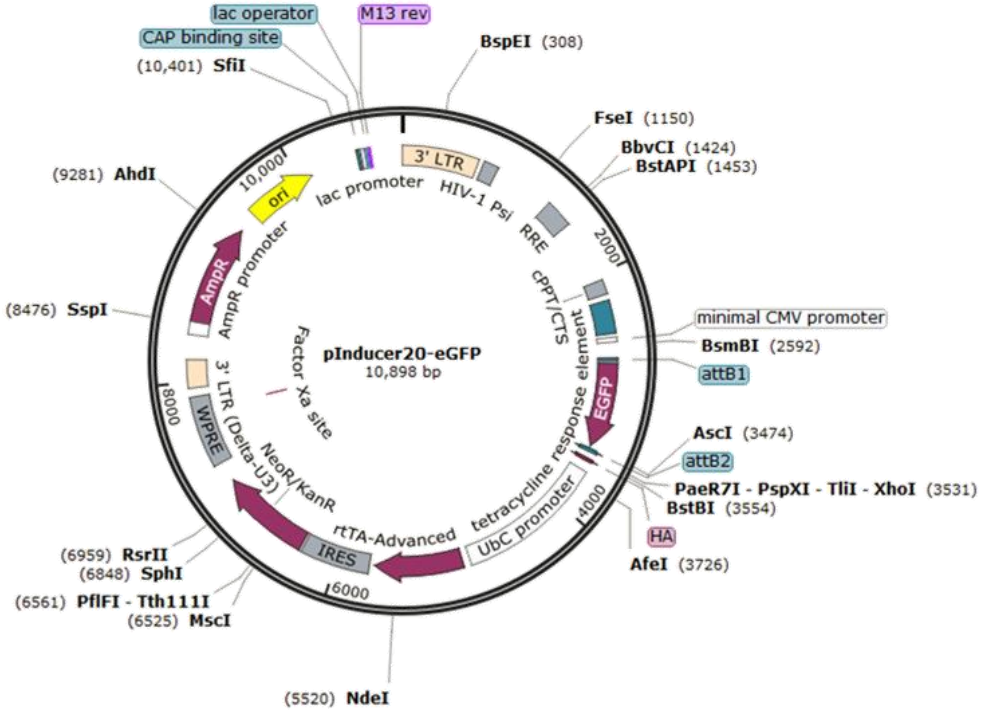


Figure 2.1. The overexpression vector pInducer20-eGFP plasmid used for MyoD overexpression.

MyoD was first extracted from the MYOD1 plasmid from Origene (Table 2.2), using Phusion High-Fidelity DNA Polymerase (Thermofisher), to avoid unwanted mutation (this polymerase has an extremely low error rate). PCR temperature conditions were calculated with the NEB Tm calculator (Table 2.3).

To remove the original template (Origene MyoD plasmid) and remove potential additional incorrect products, the PCR product was mixed with DNA loading dye and loaded onto a 1% TAE-agarose gel. The PCR product was cut out at the expected size, 996 base pairs. QiaGen Gel Extraction Kit was used to isolate DNA from the piece of gel. The DNA was eluted in 50 µL nuclease free water.

Both the MyoD PCR product and pInducer20-eGFP were restricted with AscI and BsmbI. The PCR products were purified using a QiaGen PCR Purification Kit and eluted in nuclease free water.

Table 2.2. Primers for the restrictions sites around the MyoD gene.

MyoD BsmBI Fw primer	5'-ATATATCGCCTGGAGACGCATGGAGCTACTGTCGCCA-3'
MyoD AscI Rv primer	5'-ATATATGGCGCGCCTCAGAGCACCTGGTATAT-3'

Table 2.3. PCR protocol.

5x Phusion GC buffer	10 µl
10 mM dNTPs	1 µl
10 µMFw primer	2.5 µl
10 µMRv primer	2.5 µl
DMSO	1.5 µl
Phusion DNA polymerase	0.5 µl
Plasmid pCMV6-XL5-MyoD1 (1 ng/µl)	1 µl
Nuclease Free Water	31 µl

Table 2.4. PCR temperature conditions. Calculated with NEB Tm calculator.

98 °C	30 sec
98 °C	10 sec
53 °C	30 sec
72 °C	30 sec
72 °C	5 min
4 °C	Hold

To isolate the pInducer20 vector and dispose of the eGFP insert, the digested pInducer20-eGFP was loaded onto a gel, and the PCR product was cut out (exp. size = 10.000 bp) and DNA isolated by a QiaGen Gel Extraction Kit. The 880 bp eGFP band was discarded.

MyoD was ligated into the pInducer20 vector, using NEB Quick Ligase (Table 2.4). Ligation reaction was also performed without the MyoD insert, as a control.

Table 2.5. Ligation reaction with and without MyoD insert.

2x NEB Quick lig. buffer	10 µl
pInducer20 vector	2 µl
MyoD insert	6 µl/0 µl
ddH2O	2 µl
NEB Quick Ligase	1 µl

E. coli was transformed with the ligation mixes and plated out on LB-Agar-Ampicillin plates to select for ligation mixes with the insert and incubated at 37 ^{o}C overnight. We performed minipreps utilizing QiaGen miniprep kit, on 7 colonies, to check for the insert. The MyoD insert contains a restriction site for MluI, whereas eGFP does not, therefore the plasmids isolated by miniprep were restricted using MIuI and BamHI (BamHI is present at 2 other locations in the pInducer20 plasmid). The samples were ran on a 1% TAE gel and I took UV pictures of the gel. Plasmids with the right insert: pInducer20-MyoD + MluI + BamHI had three fragments, at 980 bp, 2600 bp, and 7400 bp. Plasmids without the insert had 3500 bp and 7400 bp fragments. All seven selected colonies had the insert. 0.5 mL bacteria was cultured from one of the selected colonies with the MyoD insert overnight in 100 mL LB medium and 100 µL ampicillin (100mg/ml) overnight. A midiprep was used on 95 mL of the bacterial culture, using the Sigma GenElute HP Plasmid Midiprep Kit. Glycerol stocks were made to store the remaining bacterial culture at a -80 ^{o}C freezer.

To select for cells expressing the plasmid, the pInducer20 plasmid contains a Neomycin resistance gene. Cells expressing this gene can survive in the presence of the antibiotic G418. The toxicity of G418 for cells that do not express this resistance gene strongly differs per cell line / type. Therefore, we performed a “kill-curve” on the SMA patient and control human fibroblast. A range of concentrations ranging from 250–2500 µg/mL G418 was used to determine the lowest concentration that kills all the cells after 3–5 days. After 5 days, the lowest concentration that killed all the cells was determined: 1000 µg/ml. Cells were treated with this concentration for 1 week, starting 24 h after transfection, for

selection after lentiviral transfection. Half of this concentration was used to culture cells after selection, to keep selecting for cells that retained the construct.

To generate a lentiviral stock, HEK293T cells were passaged in a T75 flask to a 50% confluency. The next day, 5 µg PSPAX2 plasmid, 5 µg pVSV-G plasmid, 10 µg lentiviral plasmid (pInducer20-MyoD) were mixed in 1.5 mL OptiMEM and combined and incubated with 40 µG PEI in 1.5 mL OptiMEM. Culture medium was removed from Hek293T and OptiMEM/DNA/PEI mixture was added overnight. The next day, this mixture was replaced with 10 mL culture medium (10 mL DMEM + 1% Penicillin/Streptomycin + 10% FCS) and cells were cultured for 48 hours. Conditioned medium from the HEK293T cells was collected and span down to isolate supernatant. The supernatant was filtered using a 20 mL syringe and a 0.45 µm filter. 1 mL of supernatant was immediately used for infection of fibroblasts, and the remaining lentiviral supernatant was stored in 1 mL aliquots in cryovials at -80 ^{o}C.

Lentiviral infection of pInducer20-MyoD lentivirus was executed in 50–60% confluency SMA patient and control fibroblasts in a T25 flask overnight. The lentiviral stock was used undiluted, since pInducer20 is a large plasmid which causes lentiviral particle production and plasmid integration efficiency to be relatively low. Viral particles and cells have the same charge, and therefore slightly repulse each other. Therefore, Polybrene was used, which binds to the viral particles and neutralizes their charge, resulting in increased infection of the virus (final concentration: 8 µg/ml). The next day, lentiviral supernatant was replaced with culture medium. After 24 h, G418 was added to the cells (1000 µg/ml). After a week, we cultured cells with a G418 500 µg/ml concentration.

To induce overexpression of MyoD or the control eGFP, cells were cultured with 500 ng/mL doxycycline for 24 hours (continuing using this concentration during experiments, changing medium every other day). The cell lines were characterized by qPCR or western blot for MyoD upregulation. Percentage of cells expressing GFP were quantified using FACS sorting of eGFP positive cells.

2.7 Western blot

Freshly prepared radioimmunoprecipitation (RIPA) buffer was used to homogenize tissue and cells, consisting of 50 mM Tris pH 8.8, 150mM NaCl, 1% NP-40, 0.5% Sodium Deoxycholate, 0.1% SDS and with complete mini-proteinase inhibitors (1 tablet per 10 ml extraction solution, Roche). Western blotting was performed by loading equal amounts of total protein, measured by Bradford Assay. The Bradford assay works as follows. The absorbance maximum for an acidic solution of Coomassie Brilliant Blue G-250 shifts from 465 nm to 595 nm when proteins are added and the binding to proteins occur. Both hydrophobic and ionic interactions stabilize the anionic form of the dye, causing a visible color change. Protein extract samples were diluted 1:50 in ddH2O. 5 µl of both protein samples and BSA standards (0, 0.125, 0.25, 0.5, 1.0 µg/µl) were placed per well of a microplate in triplicates. 250 µl Bradford reagent was added per well and incubated for 5 ml at room temperature. Absorbance was measured at 595 nm. Using the absorbance of BSA standards, protein concentrations were calculated.

For the Western blot, protein samples were first diluted 1:1 with Laemmli sample buffer (Bio-Rad, Hemel Hempstead, UK) containing 5% β-mercaptoethanol (Sigma) and heated at 100°C for 10 minutes. Next, samples were loaded on freshly made 1.5 mm 12% polyacrylamide separating and 5% stacking gel and electrophoresis was performed at 120 V for ~1.5h in running buffer. Subsequently, proteins were transferred from the gel onto to a polyvinylidene fluoride (PVDF) membrane (Merck Millipore) via electroblotting at 120 V for 60 minutes in transfer buffer containing 20% methanol. To prevent non-specific antibody binding, membranes were then incubated for 2h in Odyssey Blocking Buffer (Licor) on a rocker with speed 35–40 (gentle shaking). The membrane was then probed overnight at 4°C with primary antibodies in Odyssey Blocking Buffer and 0.1% Tween-20. The next day, after three 10-minute washing steps with PBS, the membrane was incubated for 1 hour at room temperature with secondary antibodies conjugated to infrared dyes. Lastly, the membrane was washed again three times 10 minutes in PBS and visualized by scanning 700 nm and 800 nm channels on the LI-COR Odyssey CLx infrared imaging system (LI-COR) for 2.5 minutes per channel. The background was

subtracted and signal of protein of interest was divided by signal of the housekeeping protein, per sample.

2.8 Statistical Analysis

Statistical analyses were carried out using GraphPad Prism 7, Excel or SPSS. Comparisons between two groups were made using a two-sided *t-test*. One-way analysis of variance (ANOVA) and Bonferroni correction post hoc test were performed for comparisons of one variable in more than two groups and two-way ANOVA performed for comparisons with more than 1 variable. A *p*-value below 0.05 was considered as statistically significant for all experiments and in graphs is demonstrated by *, $p < 0.01$ as **, $p < 0.001$ as *** and $p < 0.0001$ as ****.

All other statistical analyses are explained in the relevant research chapters.

3. Results I

Coupled transcriptomic and proteomic analyses to identify potential new SMN-independent treatments for SMA muscle pathology

3.1 Introduction

As described in Chapter 1, SMA is caused by mutations or deletions in the *SMN1* gene, whose protein product plays several important cellular functions. The SMN protein is essential for the survival of all organisms [24,374]. The SMN protein is a multifunction protein, which controls amongst other functions, various aspects of RNA metabolism through the assembly of snRNPs [47,375–377], which are part of the spliceosome. The spliceosome ensures correct splicing of mRNA exons and introns. Several transcriptomic studies have been conducted in SMA models to evaluate SMN's role in RNA processing pathways, however, as can be read in Sections 1.1.3 and 1.3.1, whether defects in these pathways directly contribute to disease pathogenesis or if impairment of a motor neuron specific SMN function causes SMA remains unclear. SMN also plays a role in transcription and histone mRNA processing [65,378,379], DNA repair [53,380], translation [57,381], stress granule formation [382], cytoskeleton maintenance and signaling [107,109,383]. All these different functions of SMN make it difficult to study SMA.

To better understand the role of SMN, transcriptomic and proteomic analyses are useful tools, facilitating unbiased quantitive comparisons of the transcriptome and proteome of SMA tissues and cells and allowing the investigation of downstream molecular consequences of SMN depletion.

Transcriptomic studies in particular revealed evidence of splicing defects in SMA and of the housekeeping function of SMN in splicing (Section 1.1.3). Transcriptomic analysis of motor neurons isolated by laser capture microdissection from *Smn*$^{-/-}$;*SMN2*$^{+/-}$ and healthy heterozygous mice

(*Smn*$^{-/-}$;*SMN2*$^{+/-}$) at an early symptomatic stage revealed that splicing and mRNA dysregulations appear to be more strongly affected in motor neurons than in whole spinal cord and heart samples [384]. An RNA-seq study in motor neurons from pre-symptomatic P1 *SMNΔ7* mice found cell-specific selective mRNA dysregulations, such as agrin Z exon skipping (critical for NMJ maintenance) and upregulation of complement factor C1q (role in synaptic pruning) [196]. Another study demonstrated that splicing defects were widespread and found in the spinal cord, brain, heart and kidney of P6 *SMNΔ7* mice. However, splicing defects were tissue-specific, whereby distinct splicing defects emerged in different tissues [48]. Splicing defects were also found to be increased during disease progression when comparing spinal cords from pre-symptomatic, symptomatic and late symptomatic *SMNΔ7* mice [49]. RNA-seq in the spinal cord, brain, liver, and skeletal muscle of symptomatic *Smn*$^{-/-}$;*SMN2* mice revealed changes in splicing of U12-dependent introns, which, as discussed in Section 1.1.3, is part of the SMN complex and therefore plays a major role in splicing [139]. These changes in U12 were also found in SMN-deficient HeLa [139] cells and in the spinal cord of mice 30 days after SMA induction [53] by ASO 20-37, which mediates skipping of exon 7 from the human *SMN2* transgene. In addition to splicing defects, transcriptomic studies have also demonstrated effects of SMN deficiency in SMA on: ribosome biology and translation in brains and spinal cord tissues from *Smn*$^{-/-}$;*SMN2*$^{+/-}$ mice [385]; mis-splicing of various Ca^{2+} channel genes, which might explain disrupted Ca^{2+} homeostasis in SMA [139]; DNA damage [53]; selective endoplasmic reticulum (ER) stress activation in SMA patient-derived induced pluripotent stem cells (iPSCs) [386]; neuronal development and activity in *Smn*$^{-/-}$;*SMN2*$^{+/+}$ mouse embryonic stem cell-derived motor neurons [387]. These transcriptomic studies provided insights in the effects of SMN deprivation on splicing and other SMA pathologies, in a plethora of SMA animal models and cell models.

Only recently have proteomic studies in SMA been performed in a variety of cell types and tissues such as Schwann cells [91], the hippocampus [388], embryonic stem cells-derived motor neurons [389], Smn-depleted NSC34 cells [131], Type 1 SMA patient fibroblast [390] and iPSC-derived motor neurons [140]. All these studies found various proteins dysregulated in SMA. Indeed, a proteomic study conducted on

synapses isolated from the hippocampus of pre-symptomatic *Smn*$^{-/-}$*;SMN2* SMA mice highlighted significant dysregulation of protein ubiquitination pathways in SMA mice compared to littermate controls [90]. As discussed in Section 1.1.4, ubiquitin pathways are involved in axonal and synaptic stability [391] as well as stability and degradation of the SMN protein [23,85,390]. The dysregulation of ubiquitin pathways was also found in proteomic studies in Schwann cells isolated from the peripheral nerve of *Smn*$^{-/-}$*;SMN2* SMA mice [91] and SMA iPSC-derived motor neurons [140]. The same study found that many proteins associated with neurodevelopment and differentiation such as UBA1, beta III-tubulin and UCHL1 were decreased in SMA motor neurons [140]. This study is further supported by the results of a proteomic study on hippocampus from *Smn*$^{-/-}$*;SMN2* SMA mice [388]. Proteomics are also a valuable tool for biomarker discovery for SMA disease status. Mutsaers and colleagues [392] used label-free proteomics to identify proteins in muscle from SMA mice that correlate with the status of the disease and found that Calreticulin and GRP75/Mortalin are indicators of disease progression. SMA-MAP, a plasma protein panel for SMA patients found a set of SMA biomarkers significantly associated with motor function and other measures of SMA symptoms [393]. Despite these extensive studies, there is no definitive answer to how depletion of SMN causes SMA and whether defects in these pathways, directly contribute to disease pathogenesis.

As described in Chapter 1, Sections 1.4.2, 1.4.3, 1.4.5 and 1.4.6, SMN restoration therapy is a successful treatment approach that has recently reached the clinic. SMN restoration conducted in our lab demonstrates significant rescue in lifespan and neuromuscular phenotype with survival increasing from P12 to a mean of 456 days [143] after SMN restoration therapy in *Smn*$^{-/-}$*;SMN2*$^{+/-}$ mice. The treatment consisted of a PMO targeting the N1 (ISS-N1) site [68], covalently conjugated to a to cell penetrating peptide Pip6a. The mice were treated by a facial intravenous (IV) injection at P0 and P2 with a 10 mg/kg dose of the SSO Pip6a-PMO. The dramatic increase of survival after treatment is combined with an increase of SMN expression in the CNS and peripheral tissues; reduced NMJ denervation, a rescue of levels of circulating insulin-like growth factor 1 (IGF1), which is a neurotrophic

factor reduced in severe SMA models [286,394]; and a downregulation of apoptotic markers in the spinal cord [143].

Although SMN restoration undoubtedly has positive effects on SMA patients, it is not a cure and it might be of less benefit for older patients (described in Chapter 1, Section 1.4.9). One way to provide a longer-lasting and more effective treatment for SMA is the use of combinatorial treatments consisting of SMN and non-SMN targeting pharmacological compounds (Section 1.4.10). As skeletal muscle pathology plays a major role in SMA and alleviating muscle defects improves disease phenotypes (Section 1.3.3.), combinatorial therapies targeting skeletal muscle in combination with SMN restoration therapy are an attractive strategy.

In the current study, we opted to use an in-depth approach by combining proteomic and transcriptomic techniques, thus investigating dysregulations of both transcripts and proteins in Smn-depleted skeletal muscle, while also studying effects of SMN restoration in skeletal muscle, enabling us to identify SMN-independent and -dependent changes in muscle to develop novel muscle-specific therapies that can be used in combination with SMN restoration therapy. In order to do so, we investigated the molecular changes occurring in skeletal muscle of *Smn*$^{-/-}$;*SMN2*$^{+/-}$ SMA mice treated with the SMN enhancing Pip6a-PMO while at the same time, evaluating these changes against the specific pathways and proteins that are inherently different between SMA and wild type mice. We performed a proteomic and transcriptomic analysis on the same muscle to achieve a thorough assessment of total changes observed in SMA in skeletal muscle and to determine which changes are restored or unchanged following SMN restoration therapy with Pip6a-PMO.

Hypothesis

Analyses of differential protein and transcript expression between Smn-depleted and SMN-restored SMA skeletal muscle may reveal pathways that are not rescued in SMN restoration therapy, presenting the opportunity to identify muscle-specific treatments that can be used in combination with SMN restoration therapy.

Objectives

1. Perform a proteomic and transcriptomic analysis on the same muscle (*tibialis anterior*) of *Smn$^{-/-}$;SMN2$^{+/-}$* and control WT mice.
2. Confirm SMN restoration after Pip6a-PMO treatment in *tibialis anterior*.
3. Compare proteomic and transcriptomic data and investigate their overlap.
4. Identify differentially expressed proteins, transcripts and gene ontology pathways in Smn-depleted and SMN-restored SMA skeletal muscle.

3.2 Materials and methods

3.2.1 Animals and animal procedures

Proteomics and transcriptomic analyses were performed on the *tibialis anterior* (TA) of the severe *Smn$^{-/-}$;SMN2$^{+/-}$* SMA mouse model and FVB/N WT mice [366]. We used 6 groups with an *n* = 3 as is demonstrated in Table 3.1: pre-symptomatic stage *Smn$^{-/-}$;SMN2$^{+/-}$* postnatal day (P) 2, control P2 WT, symptomatic stage *Smn$^{-/-}$;SMN2$^{+/-}$* P7, control P7 WT, Pip6a-PMO treated *Smn$^{-/-}$;SMN2$^{+/-}$* P7, Pip6a-scrambled treated *Smn$^{-/-}$;SMN2$^{+/-}$* P7. The Pip6a-PMO and Pip6a-scrambled conjugates were both separately prepared in 0.9% saline solution and administered at a dose of 10 µg/g via an intravenous facial vein injection at P0 and P2. Half of the TA was used for proteomic analysis and the other half for transcriptomic analysis. Tissues were flash frozen in liquid nitrogen immediately after harvest at P2 and P7.

3.2.2 Proteomic analysis

Proteomic analyses were performed on half of the TAs by the Lehtiö group at the Karolinska Institute, using a liquid chromatography–mass spectrometry (LC-MS)-based method. This method applies unbiased genome-discovery, which permits unbiased genome-wide discovery of protein-coding loci. High-resolution isoelectric focusing (HiRIEF) was used at the peptide level in the 3.7–5.0 pH range. Two tandem mass tags (TMTs, chemical labels) were used for mass spectrometry (MS)-based quantification and identification of proteins. The data was median normalized based on peptide ratio. This accounted for differences in the amount of proteins added during sample preparation (accuracy of protein measurements and pipetting).

3.2.3 Transcriptomic analysis

RNA of half of the TAs was extracted by guanidinium thiocyantate-acid-phenol-chloroform extraction using TRIzol Reagent (Life Technologies) as per manufacturer's instructions. GeneChip® Mouse

Transcriptome Assay 1.0 arrays were used (Affymetrix core facility, Karolinska Institute) for 100 ng of RNA per sample. This assay has four probes per exon and approximately 40 probes per gene to analyze expression at both exon and gene levels. The remaining RNA was used for evaluation of full-length *SMN2* exon 7 inclusion using qPCR after generation of cDNA.

3.2.4 Synthesis of Pip6a peptide-PMO conjugates

The PMO sequence targeting ISS-N1 intron 7 (-10-27) (5'-ATTCACTTTCATAATGCTGG-3') and scrambled PMO (5'-TAC GTT ATA TCT CGT GAT AC-3') were purchased from Gene Tools LLC (Corvallis).

The Pip6a-PMO peptide conjugates were produced by Doctor Frank Abendroth in the laboratory of Professor Mike Gait at the MRC Laboratory of Molecular Biology in Cambridge, UK. The Pip6a Ac-(RXRRBRRXRYQFLIRXRBRXRB)-COOH peptide was manufactured by standard 9-fluorenylmethoxy carbonyl chemistry, purified to >90% purity by reverse-phase high-performance liquid chromatography (HPLC) and conjugated to the 3' end of the PMO through an amide linkage. The conjugate was purified by cation exchange HPLC, desalted and analyzed by mass spectrometry. Pip6a peptide-PMO conjugates were dissolved in sterile water and filtered through a 0.22 µm cellulose acetate membrane before use.

3.2.5 Programs used for transcriptomic analyses, and statistics

3.2.5.1 Microarray processing

Annotations for the Mouse Transcript Array 1.0 at the transcript level were obtained from the Affymetrix website (http://www.affymetrix.com/products_services/arrays/specific/mo_trans_assay.affx#1_4). We performed background correction and RMA normalization at the probe level (n = 72688) using oligo R package. We summarized the data in ensemble transcript IDs using the average.

3.2.5.2 Differential expression

For differential expression analysis, we used limma R package at the transcript level. We considered a transcript differentially expressed if their FDR < 0.05. We considered a gene differentially expressed if at least one of the associated transcripts was differentially expressed.

3.2.5.3 Gene Ontology

For Gene Ontology enrichment analysis of transcriptomic data, we used an ad hoc script in R. We downloaded Gene Ontology annotations from Ensembl through BiomaRt. We only used Gene Ontology terms that had at least 50 genes present in our background population (all the genes detected in the microarray). To test for enrichment in a particular gene list, we counted the number of annotated genes in each term and compare it with 10000 random samples of genes of the same size. From the randomizations, we obtained the expected number of annotations for each GO term, along with an expected standard error of the mean value. Using these values, we calculated a Z-score to estimate a *p* value. We adjusted the *p* values for multiple testing following a Benjamini-Hochberg correction.

3.2.5.4 Principal component analysis and clustering

For principal component analysis of transcriptomic data, we used the prcomp R function on the RMA normalized gene expression data at the transcript level, or the genes level (for comparison with proteomic data). To measure the similarity between gene expression profiles, we used the Ward hierarchical clustering on the Euclidean distance of 1–r, where r is the correlation between the expression profiles.

3.2.6 Programs used for proteomic analyses, and statistics

3.2.6.1 Differential expression

For differential expression analysis of protein data, we used limma R package at the protein level. We considered a protein differentially expressed if their FDR < 0.05.

3.2.6.2 Gene ontology

For Gene Ontology enrichment analysis of proteomic data, we used topGO R function and adjusted *p* values for multiple testing following a Benjamini-Hochberg correction.

3.2.6.3 Principal component analysis

For principal component analysis of proteomic data, we used the prcomp R function on the normalized expression data at the protein level. To measure the similarity between gene expression profiles, we used the Ward hierarchical clustering on the Euclidean distance of 1–r, where r is the correlation between the expression profiles.

3.3 Results

3.3.1 Restoration of full-length SMN in Pip6a-PMO treated skeletal muscle

In order to isolate and identify protein and transcript changes occurring in SMA skeletal muscle, it is important to work with a muscle that is affected early during disease progression and investigated at a symptomatic timepoint. The *tibialis anterior* (TA) is a skeletal muscle that is affected early in SMA [395,396]. To investigate the effects of SMN restoration, *Smn*$^{-/-}$;*SMN2*$^{+/-}$ mice were treated at birth and P2 with 10 mg/kg of Pip6a-PMO and TAs were harvested at P7. These animals were compared to 7-day old untreated *Smn*$^{-/-}$;*SMN2*$^{+/-}$, Pip6a-scrambled treated (10 mg/kg) and WT mice. To evaluate disease progression over time, we compared symptomatic P7 *Smn*$^{-/-}$;*SMN2*$^{+/-}$ mice to pre-symptomatic P2 *Smn*$^{-/-}$;*SMN2*$^{+/-}$ mice. Half of the TAs were used for proteomic analyses and RNA was isolated from the other half. This RNA was used for transcriptomic analyses and qPCR analyses investigating levels of *SMN*.

Table 3.1. Groups used for proteomic and transcriptomic analyses. All groups existed of *n* = 3 animals.

Age	Group	Treatment	Label
P2	*Smn*$^{-/-}$;*SMN2*$^{+/-}$	Untreated	**P2 SMA**
P2	Wild type	Untreated	**P2 WT**
P7	*Smn*$^{-/-}$;*SMN2*$^{+/-}$	Pip6a-PMO (ISS-N1)	**P7 Pip6a**
P7	*Smn*$^{-/-}$;*SMN2*$^{+/-}$	Pip6a-PMO (scrambled)	**P7 Scrambled**
P7	*Smn*$^{-/-}$;*SMN2*$^{+/-}$	Untreated	**P7 SMA**
P7	Wild type	Untreated	**P7 WT**

qPCR analysis of full-length *SMN2* mRNA in the muscle demonstrates as expected a significant upregulation of full-length *SMN2* in Pip6a-PMO treated *Smn*$^{-/-}$;*SMN2*$^{+/-}$ mice compared to untreated and Pip6a-scrambled treated mice (Figure 3.1). Interestingly, Figure 3.1b illustrates downregulation of

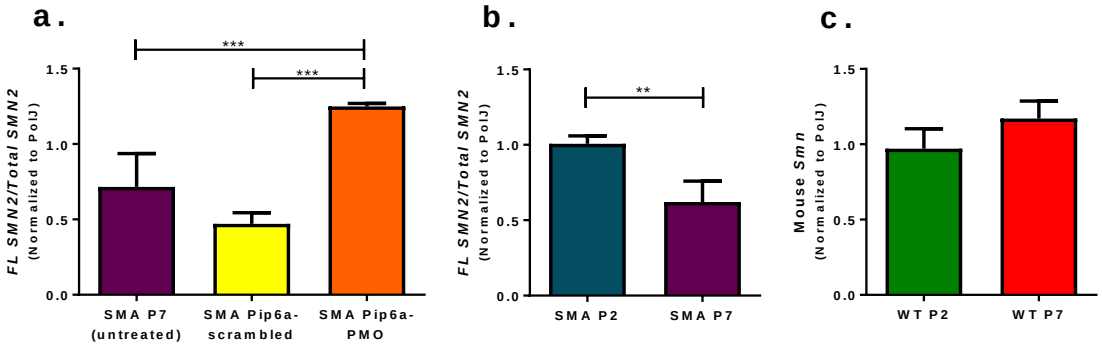


Figure 3.1. Ratio full-length *SMN2* significantly increased in Pip6a-PMO treated *Smn*$^{-/-}$;*SMN2*$^{+/-}$ mice. RNA expression of full-length *SMN* transcript analyzed by quantitative RT-PCR related to total *SMN* transcripts, represented by exon 2a and 2b amplicons. **a.** Pip6a-PMO treatment in *Smn*$^{-/-}$;*SMN2*$^{+/-}$ mice significantly increased the ratio full-length *SMN*/total *SMN* compared to untreated mice. The Pip6a-scrambled treatment had no effect on full-length SMN levels in *Smn*$^{-/-}$;*SMN2*$^{+/-}$ mice ($p < 0.001$ and $p < 0.0001$, one-way ANOVA, Bonferroni). **b.** The ratio full-length *SMN*/total *SMN* significantly decreased over time in P7 *Smn*$^{-/-}$;*SMN2*$^{+/-}$ mice compared to P2 *Smn*$^{-/-}$;*SMN2*$^{+/-}$ mice ($p < 0.001$, Student's *t* test). **c.** This decrease of mouse Smn is not found in aged-matched WT control, comparing P7 WT with P2 WT ($p = 0.0924$, Student's *t* test).

full-length *SMN2* in SMA untreated P7 animals compared to SMA untreated P2 animals. No decrease of mouse *Smn* was found in P7 WT animals versus P2 WT. These results confirm increase of full-length *SMN* after Pip6a-PMO restoration therapy in *Smn*$^{-/-}$;*SMN2*$^{+/-}$.

3.3.2 Proteomic analyses

After validating SMN's expression in the TAs of the six experimental groups, we did a proteomic analysis of the same muscle sample. The coefficient of variation was calculated between replicates in protein samples. Figure 3.2 demonstrates a small variation amongst replicates within all groups, reflecting the high quality of the material and techniques used and similarity between animals in the same group. Among a total of 9798 proteins detected, most proteins (8152) were detected in all samples in all groups.

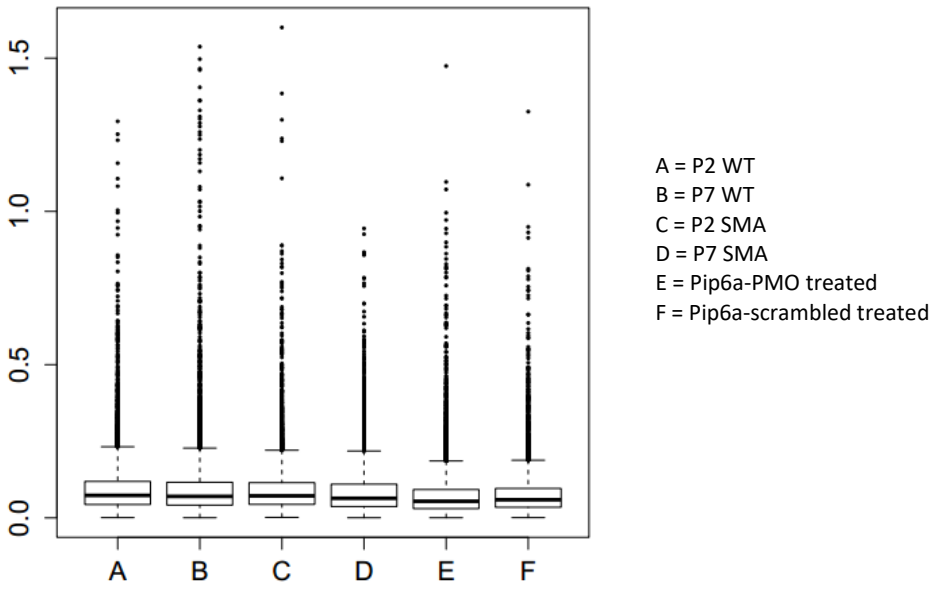


Figure 3.2. Coefficient of variation in proteomic samples replicates within the six experimental groups.

A principal component analysis (PCA) was conducted for both subsets of proteomic data. Subset 1 concerns treatment and includes only P7 data (WT, SMA, Pip6a-PMO and Pip6a-scrambled, Figure 3.3a) while subset 2 focusses on development and includes data for untreated WT and SMA at both P2 pre-symptomatic and P7 symptomatic stages (Figure 3.3b). The clean clustering of data reveals a low variance within distinct groups. Remarkably, Pip6a-PMO treated symptomatic SMA samples and WT samples cluster together, demonstrating low differences between these two groups (Figure 3.3a). Also, pre-symptomatic SMA and WT samples cluster together, confirming that *Smn*$^{-/-}$*;SMN2*$^{+/-}$ SMA animals are truly in a pre-symptomatic stage at P2 (Figure 3.3b).

3.3.3 Transcriptomic analyses

For the transcriptomic analyses we used GeneChip® Mouse Transcriptome Assay 1.0 arrays on the same TA muscle tissue used for proteomics. The total number of transcripts identified was 93,594 (ensemble transcript IDs) corresponding to 37,450 genes (ensemble gene IDs). A PCA was also

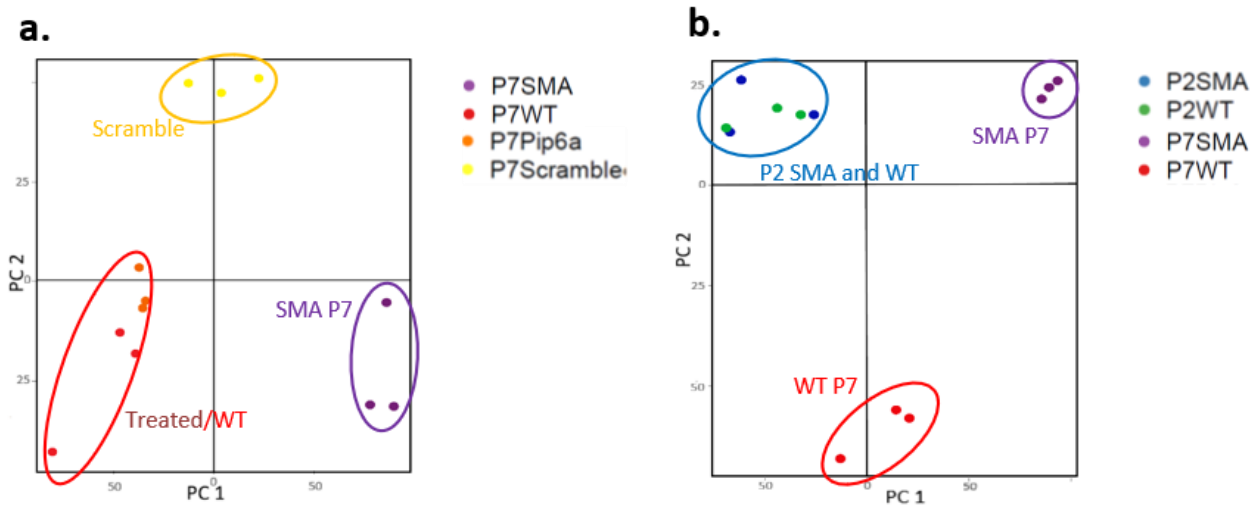


Figure 3.3 Clustering of groups in proteomic samples after PCA. a. Subset 1, PCA on protein data for P7 (WT, SMA, Pip6a-PMO and Pip6a-scrambled), **b.** Subset 2, PCA on protein data for untreated WT and SMA at both P2 and P7.

conducted for both subsets 1 and 2, as described above in section 3.3.2 (Figure 3.4). Strong similarities in clustering was found between proteomic (Figure 3.3a and b) and transcriptomic data (Figure 3.4a and b) such as Pip6a-PMO treated symptomatic SMA samples and WT samples cluster together, demonstrating small differences between these two groups and pre-symptomatic SMA and WT samples cluster together.

3.3.4 Correlation of proteomic and transcriptomic data

To investigate similarities between proteomic and transcriptomic datasets, we did a Pearson's correlation, which demonstrated a low correlation between proteomic and transcriptomic data (Figure 3.5a). In order to make both distributions comparable, proteomic and transcriptomic data was first scaled (transformed to z-score values), and a PCA analysis was conducted, demonstrating that PC1 divides the data at the transcript and protein level (Figure 3.5b). A new expression matrix was formed (in which the rows are genes and columns samples), where the variance given by PC1 was removed. The Pearson's correlations are represented in the heatmap in Figure 3.5c. Figure 3.5c

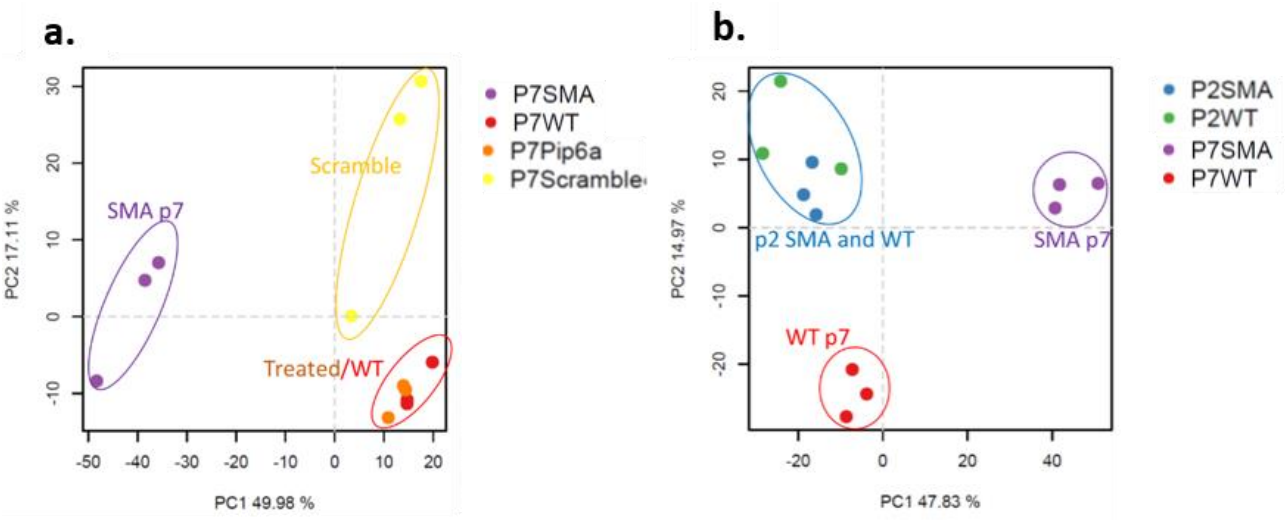
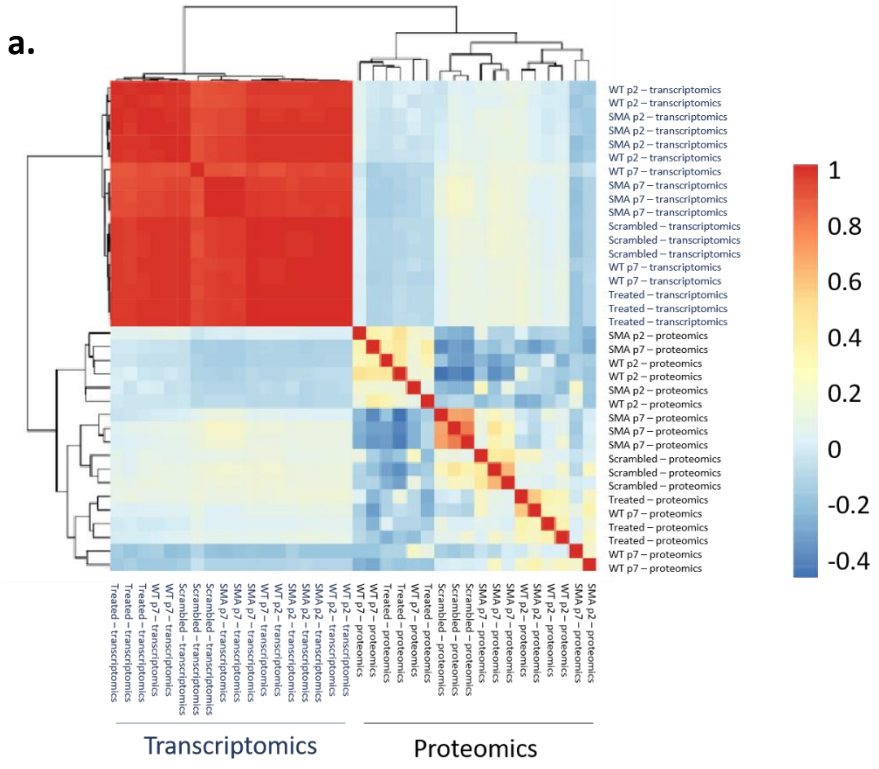


Figure 3.4. Clustering of groups in transcriptomic samples after PCA. a. Subset 1, PCA on transcript data for P7 (WT, SMA, Pip6a-PMO and Pip6a-scrambled), **b.** Subset 2, PCA on transcript data for untreated WT and SMA at both P2 and P7.

demonstrates a clustering of the different groups, based on correlation of proteomic and transcriptomic data after PC1 is removed. The clean clustering reveals low variances within distinct groups.



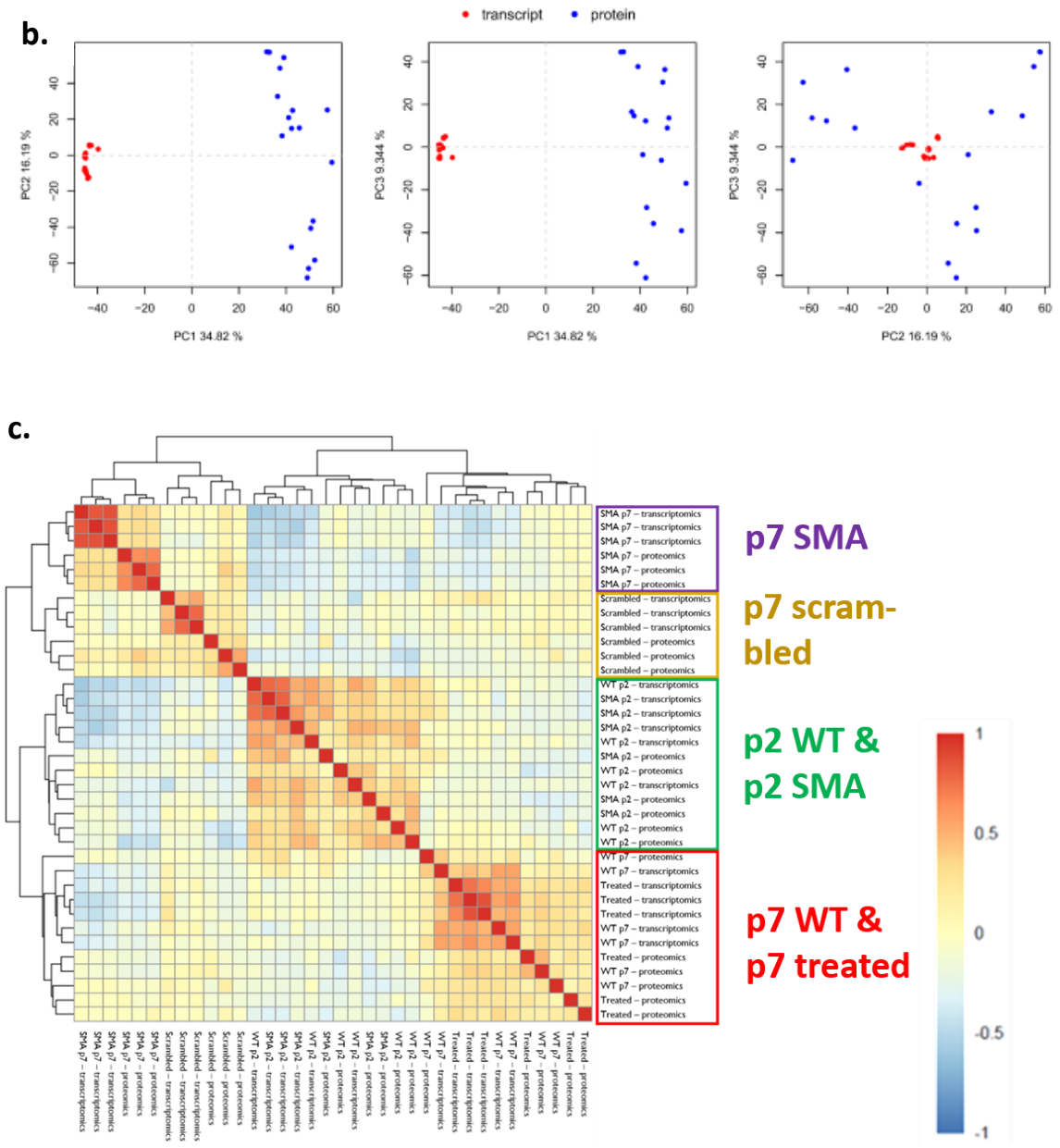


Figure 3.5 Pearson's correlation between proteomic and transcriptomic data and clustering of data. **a.** Pearson's correlation between proteomic and transcriptomic data demonstrates a low correlation between proteomic and transcriptomic data and high correlation within transcriptomic samples and a low correlation within proteomic samples. Pearson's correlations between samples are represented in a heatmap (red higher correlation and blue lower correlation). **b.** PCA analysis illustrates PC1 divides the data at the transcript and protein level, red dots represent transcript samples and blue dots protein data. **c.** Correlation between transcript and protein data demonstrates samples from the different groups (as described in Table 3.1) cluster, once PC1 has been removed. Pearson's correlations between samples are represented in the heatmap (red higher correlation and blue lower correlation, the range of these correlations is from -0.58 to 1).

3.3.5 Analyses of differently expressed proteins and transcripts

Next, proteomic and transcriptomic data were analyzed for differentially expressed proteins and transcripts. As expected, greatest differences were found on both transcript and protein level between symptomatic SMA mice and WT mice (Table 3.2). However, after Pip6a-PMO treatment in SMA mice, all transcripts were rescued as well as most proteins (except for 11). This demonstrates SMN restoration at an early timepoint (P7) and rescue of dysregulated transcripts and proteins on a molecular level. This is in accordance our recent work that illustrates a significant rescue in lifespan and neuromuscular phenotype with survival increasing from P12 to over 400 days in Pip6a-PMO treated *Smn*$^{-/-}$;*SMN2*$^{+/-}$ SMA mice [143]. The 11 proteins that were significantly downregulated in the Pip6a-PMO treated SMA mice compared to the WT group were also downregulated in untreated and Pip6a-scrambled-treated SMA mice. One of these proteins is the SMN protein, which shows that despite the impressive rescue of symptoms and survival, Smn protein levels are still lower than in WT animals. The remainder proteins are immunoglobulins subunits (8) and a TAP binding protein and a Tap1 transporter 1 (Table 3.3).

Table 3.2. Up- and down regulated genes at transcript and protein level. A false discovery rate (FDR) of < 0.05 was used for both protein and transcript data. Genes were considered differentially expressed if at least one of their corresponding transcripts had an FDR < 0.05. The percentages are relative to the total of both transcripts and proteins differentially expressed per condition.

UP regulated	P7WT vs. P7SMA	P7SMA vs. P7Pip6a	P7SMA vs. P7Scrambled	P7WT vs. P7Scrambled	P7WT vs. P7Pip6a	P7Scrambled vs. P7Pip6a	P2SMA vs. P7SMA	P2WT vs. P7WT	P2 SMA vs. P2 WT
Transcripts	5698	4959	4539	1225	0	702	4986	2473	0
Proteins	715	2694	1606	258	0	430	902	367	0
Intersect	253	1213	653	87	0	137	397	214	0
Jaccard-Index	4.11%	18.84%	11.89%	6.23%	0	13.77%	7.2%	8.15%	0%
DE-Transcript-only	88.39%	58.17%	70.76%	81.52%	0	56.78%	83.6%	86.02%	0%
DE-Protein-only	7.50%	23.00%	17.35%	12.25%	0	29.45%	9.2%	5.83%	0

DOWN regulated	P7WT vs. P7SMA	P7SMA vs. P7Pip6a	P7SMA vs. P7Scrambled	P7WT vs. P7Scrambled	P7WT vs. P7Pip6a	P7Scrambled vs. P7Pip6a	P2SMA vs. P7SMA	P2WT vs. P7WT	P2 SMA vs. P2 WT
Transcripts	5343	4755	3627	787	0	1166	4956	1688	0
Proteins	2659	640	402	509	11	178	4400	883	0
Intersect	1302	247	144	155	0	60	1604	252	0
Jaccard-Index	19.43%	4.80%	3.71%	13.58%	0%	4.67%	20.7%	10.87%	0%
DE-Transcript-only	60.31%	87.57%	89.65%	55.39%	0%	86.14%	43.2%	61.92%	0%
DE-Protein-only	20.25%	7.63%	6.64%	31.03%	0%	9.19%	36.1%	27.21%	0%

Table 3.3. Proteins downregulated in Pip6a-PMO treated SMA mice compared to WT mice. Proteins were considered downregulated if FDR < 0.05.

Proteins downregulated in Pip6a-PMO treated SMA mice vs. WT mice
Immunoglobulin kappa variable 4-53
Immunoglobulin kappa variable 10-95
Immunoglobulin kappa variable 8-28
Immunoglobulin kappa variable 8-19
Immunoglobulin kappa constant
Immunoglobulin heavy constant gamma 1
Immunoglobulin heavy variable 3-5
Immunoglobulin heavy variable 1-81
TAP binding protein
Tap1 transporter 1, ATP-binding cassette, sub-family B
Survival Motor Neuron

Figure 3.6a reveals the overlap among differentially expressed genes in the P7 untreated, Pip6a-PMO treated and Pip6a-scrambled treated SMA mice. Figure 3.6b demonstrates upregulated genes in untreated P7 SMA and downregulated in Pip6a-PMO and Pip6a-scrambled treated SMA mice, while Figure3.6c illustrates overlap between downregulated genes in untreated P7 SMA mice and upregulated in Pip6a-PMO and Pip6a-scrambled treated SMA mice. Especially interesting are the genes that are up- or downregulated in the P7 SMA mice and the other way around in the Pip6a-PMO

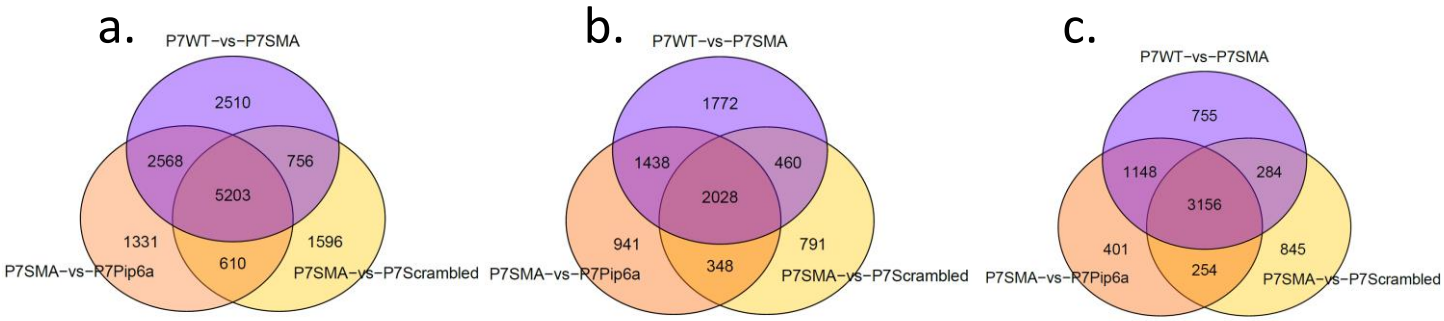


Figure 3.6. Overlap among differentially expressed genes. a. Overlap in differentially expressed genes in P7 untreated, Pip6a-PMO treated and Pip6a-scrambled groups. **b.** Overlap in upregulated genes in untreated P7 SMA group and downregulated genes in Pip6a-PMO and Pip6a-scrambled treated groups. **c.** Overlap in downregulated genes in the untreated P7 SMA group and upregulated in Pip6a-PMO and Pip6a-scrambled groups.

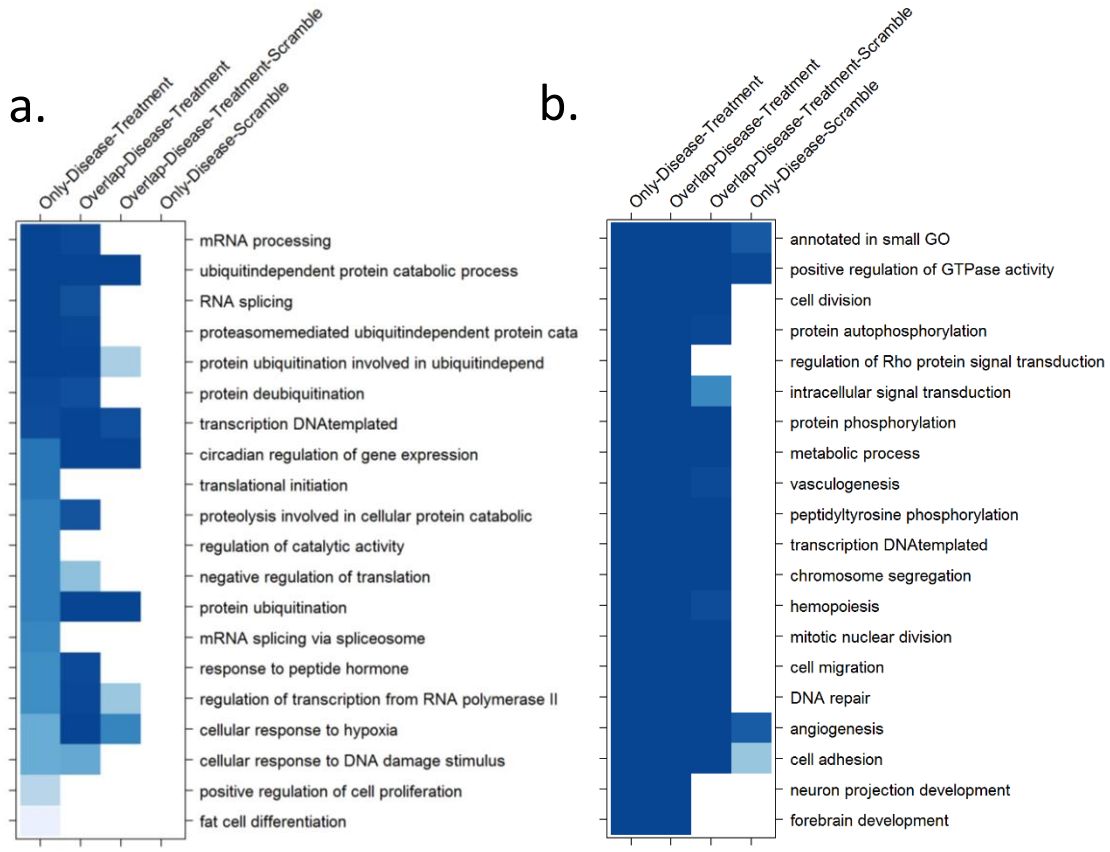
treated group, but not in the Pip6a-scrambled control group. Table 3.2 illustrates that a considerable amount of proteins and transcripts were restored in the Pip6a-scrambled treated group. This was most likely due to the scrambled sequence and/or the chemistry, as a foreign chemistry enters the cell, it can disrupt processes in cells and therefore change transcript and protein levels. It is unlikely that the transcripts that were restored in the Pip6a-scrambled group were induced by targeting *SMN2* exon 7 (as in Pip6a-PMO), as Figure 3.1 reveals no difference in full-length SMN in untreated P7 SMA mice and Pip6a-scrambled treated P7 SMA mice.

3.3.6 Gene ontology terms

We next performed GO analyses on genes and proteins differently expressed in the distinct groups. Figure 3.7a demonstrates enriched gene ontology (GO) terms among upregulated genes in the SMA mice P7 and downregulated in the Pip6a-PMO treated group, but not in the Pip6a-scrambled group. This table provides useful information about which pathways to target with new SMN-independent therapeutic targets to treat SMA. The same is true for Figure 3.7b, which illustrates the GO terms among downregulated genes in the SMA mice P7 and upregulated in the Pip6a-PMO treated group, but not in the Pip6a-scrambled group. Figure 3.7c demonstrates GO and Kyoto Encyclopedia of Genes

and Genomes (KEGG) pathway enrichment and biological processes of proteins dysregulated in SMA and reversed by Pip6a-PMO treatment, but not by Pip6a-scrambled treatment. Analysis is based on 1240 proteins that were differently expressed in SMA vs. WT and were reversed by Pip6a-PMO, but not Pip6a-scrambled, treatment.

The GO and KEGG analyses reveal that many molecular functions that are dysregulated in SMA mice compared to WT mice and recovered by Pip6a-PMO SMN restoration are involved in RNA metabolism and splicing. This is not surprising, due to SMN's housekeeping function in splicing (Section 1.1.3). Interestingly, SMN restoration also restored circadian regulation of gene expression (Figure 3.7a). We have recently reported dysregulated expression of the core clock genes (clock, ARNTL/Bmal1, Cry1/2, Per1/2) and clock output genes (Nr1d1 and Dbp) in *Smn*$^{-/-}$;*SMN2*$^{+/-}$ mouse tissues during disease progression [268]. SMN restoration also improved dysregulated ubiquitin pathways (Figure 3.7a, c), the regulation of Rho protein signal transduction (Figure 3.7b) and actin binding pathways (Figure 3.7c) which are all dysregulated in SMA and are genetic modifiers of SMA (Section 1.1.4). Together these results show GO analyses on protein and transcript data provide useful information about which pathways and biological processes are rescued by SMN restoration treatment.


a.
Only-Disease-Treatment
Overlap-Disease-Treatment
Overlap-Disease-Treatment-Scramble
Only-Disease-Scramble
mRNA processing
ubiquitindependent protein catabolic process
RNA splicing
proteasomemediated ubiquitindependent protein cata
protein ubiquitination involved in ubiquitindepend
protein deubiquitination
transcription DNAtemplated
circadian regulation of gene expression
translational initiation
proteolysis involved in cellular protein catabolic
regulation of catalytic activity
negative regulation of translation
protein ubiquitination
mRNA splicing via spliceosome
response to peptide hormone
regulation of transcription from RNA polymerase II
cellular response to hypoxia
cellular response to DNA damage stimulus
positive regulation of cell proliferation
fat cell differentiation
b.
Only-Disease-Treatment
Overlap-Disease-Treatment
Overlap-Disease-Treatment-Scramble
Only-Disease-Scramble
annotated in small GO
positive regulation of GTPase activity
cell division
protein autophosphorylation
regulation of Rho protein signal transduction
intracellular signal transduction
protein phosphorylation
metabolic process
vasculogenesis
peptidyltyrosine phosphorylation
transcription DNAtemplated
chromosome segregation
hemopoiesis
mitotic nuclear division
cell migration
DNA repair
angiogenesis
cell adhesion
neuron projection development
forebrain development

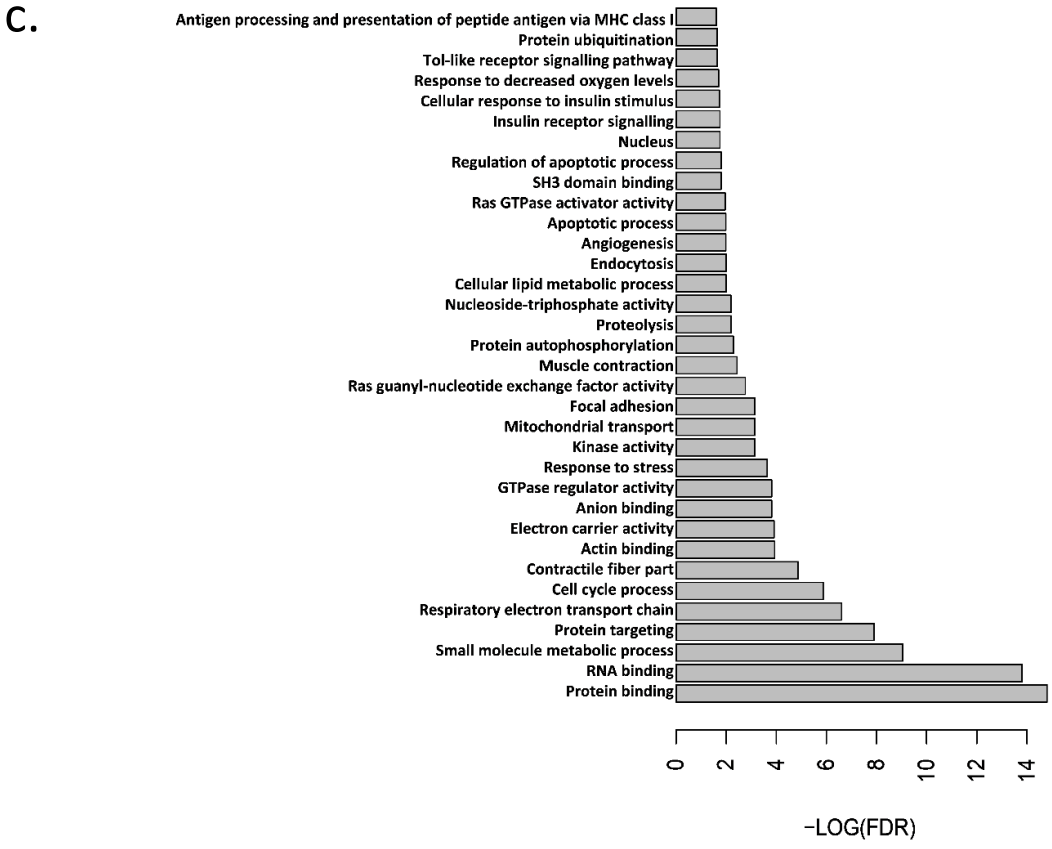

c.
Antigen processing and presentation of peptide antigen via MHC class I
Protein ubiquitination
Tol-like receptor signalling pathway
Response to decreased oxygen levels
Cellular response to insulin stimulus
Insulin receptor signalling
Nucleus
Regulation of apoptotic process
SH3 domain binding
Ras GTPase activator activity
Apoptotic process
Angiogenesis
Endocytosis
Cellular lipid metabolic process
Nucleoside-triphosphate activity
Proteolysis
Protein autophosphorylation
Muscle contraction
Ras guanyl-nucleotide exchange factor activity
Focal adhesion
Mitochondrial transport
Kinase activity
Response to stress
GTPase regulator activity
Anion binding
Electron carrier activity
Actin binding
Contractile fiber part
Cell cycle process
Respiratory electron transport chain
Protein targeting
Small molecule metabolic process
RNA binding
Protein binding
0
2
4
6
8
10
12
14
−LOG(FDR)

Figure 3.7. Top enriched terms among dysregulated genes and proteins in SMA with a reversed effect of Pip6a-PMO treatment. a. Heatmap with the top 20 enriched GO terms among significantly upregulated genes in the SMA mice P7 and downregulated in the Pip6a-PMO treated group, but not in the scrambled group. **b.** GO terms for downregulated genes in the SMA mice P7 and upregulated in the Pip6a-PMO treated group, but not in the scrambled group. For simplicity the heat maps only display the top 20 GO terms (with smaller FDRs for each of the comparisons). Darker blue represents smaller FDRs. **c.** Gene ontology and Kyoto Encyclopedia of Genes and Genomes pathway enrichment and biological processes of proteins dysregulated in SMA and reversed by Pip6a-PMO treatment, but not by Pip6a-scrambled treatment. Analysis is based on 1240 proteins that were differently expressed in SMA vs. WT and were reversed by Pip6a-PMO, but not Pip6a-scrambled, treatment. Larger values of –log(FDR) represent smaller FDRs.

3.4 Discussion

The approval of the first ever treatment of SMA, Spinraza, and other SMN restoration therapies currently in clinical trials, represent an important milestone for SMA research and treatment. However, as described in Chapter 1, Section 1.4.9, a number of challenges remain, including Spinraza not being a cure and older patients benefiting less from SMN restoration [362]. Therefore, in this study, we investigated which genes, proteins and in general, pathways, are restored or unchanged after SMN restoration therapy. To induce Smn expression, we used Pip6a-PMO [143], which targets the *SMN2* ISS-N1 site and is delivered to the CNS and periphery.

3.4.1 Low correlation between proteomic and transcriptomic data

We found a low correlation between protein and transcript data. At first, this seemed surprising, as biology links RNA and protein. However, systematic studies quantifying transcripts and proteins at a genomic scale from the same cells/tissues under similar conditions often reveal a similar low correlation between transcript and protein (e.g. [397–399]).

Multiple methodological and biological factors may cause this disparity. Firstly, there are intrinsic differences between proteomic and transcriptomic techniques. This is a problem encountered by most studies, however, some techniques are more comparable than others. RNA-seq is expected to have a larger correlation with protein data than DNA microarrays, because RNA-seq allows the investigation of a broader range of differential expressions (such as isoforms, differential exon usage, insertions, deletions and SNPs), whereas microarrays are normally limited to the detection of transcripts that correspond to already existing genomic sequence information. To overcome part of this problem, we used DNA microarray assays that evaluate alternative splicing, enabling for identification of multiple isoforms. For proteomic investigation, we used LC-MS-based analyses. MS-based proteomics is particularly suitable for protein identification and quantification and supports both relative and absolute protein measurements. This makes this method adequate for mRNA/protein correlations [400]. Secondly, transcript to protein quantitative correlations depend strongly on the quality of the data, as

data with a high variability would make an inherently perfect correlation appear less significant [400]. Our data suggests a higher variability within protein samples and groups than in RNA samples, which could partly explain why the correlation between the proteomic and transcriptomic data in the current data is low.

There are multiple biological processes beyond transcript concentration that contribute to protein expression, potentially causing a lower correlation between transcript and protein data. Translation rates can be influenced by the mRNA sequence, for example through the gene's codon composition. Different codons can be used to translate the same amino acid. This is referred to as the 'codon-bias' [401]. Also, upstream open reading frames [402] or internal ribosomal entry sites [403] influence translation rates. Translation rates can be modulated through binding of proteins to regulatory elements on the mRNA, by the binding of non-coding RNAs, for example by the relative availability of transcript and ribosomes or by micro RNAs [404]. Further, the half-lives of mRNA and protein are different, for mRNA it is 9 hours whereas the median half-life of proteins is 46 hours [405]. Half-life can also be modulated by the complex ubiquitin-proteasome pathway [406], and autophagy can influence protein concentrations independent of transcript concentrations [400]. In addition, protein synthesis takes time, therefore transcript changes will affect protein levels only after a certain delay. And proteins may be transported away from the transcript after synthesis, therefore, a direct comparison between transcript and protein abundances from the same cell type or location might not be appropriate [400]. Because of the factors that influence translation rates, genes with high RNA levels may have low protein level and vice versa, thereby causing a low correlation between protein and transcript data.

Multiple solutions have been proposed to overcome these problems such as union of transcriptomic and proteomic data in which a reference data set is created [407,408], extraction of common functional context of transcriptomic and proteomic features [409], merging datasets in individual domains [410] or multiple regression analysis to predict contribution of sequence features in mRNA-protein correlation

[411,412] (more solutions reviewed in [413]). However, we decided to do the main analyses individually in parallel of each other, converging the data after analyses.

3.4.2 Proteins dysregulated in treatment group compared to WT

One of the original research questions of this project was to identify pathways that were not restored after SMN restoration therapy, to find complementary treatments. However, to our surprise, as can be seen in table 3.2, while in untreated SMA mice vs. WT mice, a total of 11041 transcripts and 3374 proteins were dysregulated, in Pip6a-PMO treated mice compared to WT mice, all transcripts were restored to normal expression levels, and only 11 proteins were downregulated following treatment with Pip6a-PMO.

One of these proteins is SMN, which is still downregulated after SMN restoration therapy. Various studies have demonstrated that less than 100% SMN protein allows for survival and absence of symptoms [173,414]. Bowerman and colleagues [173] illustrate in the $Smn^{2B/-}$ SMA mouse model, that 15% normal level of Smn protein will result in motor neuron loss, motor defects and decreased survival. However, the *$Smn^{2B/2B}$* mice have only 36.24% SMN protein in the spinal cord, but still have a normal lifespan and are indistinguishable from their WT littermates. This research suggests that increasing SMN protein levels only slightly could have a significant positive effect on survival and SMA symptoms [173].

Eight of the proteins that remained downregulated after Pip6a-PMO treatment are immunoglobulins. Interestingly, mutations in genes coding immunoglobulins cause spinal muscular atrophy with respiratory distress (SMARD), which is a rare type of SMA not caused by SMN depletion [415]. Another protein downregulated in Pip6a-PMO treated SMA mice is the TAP binding protein, which is a transmembrane glycoprotein that mediates interaction between newly assembled major histocompatibility complex (MHC) class I molecules and the transporter associated with antigen processing (TAP). This is required for the transport of antigenic peptides across the endoplasmic

reticulum membrane. A study demonstrated MHC class I genes were upregulated after Smn knockdown in motor neurons [211]. This upregulation of MHC class I genes was also found in SOD1^{G93A} mice [416,417], a model for ALS. This might point towards a potential neuroprotective function of MHC class I up-regulation [211]. MHC class I overexpression also promotes axonal regeneration and stability of NMJs after axonal damage [418,419]. The downregulation of the TAP binding protein in the current study might be indirect a result of SMN restoration. Furthermore, the TAP binding protein is known to interact with Tap1 transporter 1, ATP-binding cassette sub-family B, another protein in Table 3.3 [420,421]. This protein transports various molecules across extra- and intra-cellular membranes and is predicted to be affected at splicing level in SMA brain, spinal cord and kidney (supplementary data of [48]).

Although there are indirect interactions between downregulated proteins in the Pip6a-PMO treated group and SMA pathogenesis, it remains unclear if these 10 differentially expressed proteins are meaningful and play a direct role in SMA, or if they are the result of a statistical Type I error. 9798 proteins were identified in this study, which means that with an FDR of < 0.05, errors are likely to occur.

3.4.3 GO terms

As this study and many others have demonstrated, depletion of SMN causes dysregulation of many transcripts and proteins that can be related to each other on a higher level. In order to get a deeper understanding of the molecular functions, biological processes and cellular components of these differently expressed genes and proteins in SMN-depleted muscle, we conducted gene ontology analyses. We found that many of the dysregulated genes and proteins in SMA muscle are involved in RNA metabolism and splicing, supporting SMN's major role in splicing [48–53]. In addition to the canonical function of the SMN protein, SMN is also involved in other processes. We found that SMN restoration also restored circadian regulation of gene expression. Interestingly, we have recently shown the dysregulated expression of the core clock genes and clock output genes [268]. Metabolic perturbations

and abnormal sleep have also been reported in SMA patients [422–424], which could point toward a perturbed circadian phenotype in SMA [268]. Thus, we demonstrate that previously identified dysregulated biological processes are rescued by SMN restoration therapy. This gives an indication of the importance of SMN restoration therapy. In conclusion, the gene ontology analyses revealed biological processes that are dysregulated in SMA that could be targeted in future research.

3.4.4 Conclusion and future directions

This is, to the best of our knowledge, the first elaborate study investigating protein and transcript changes after SMN restoration therapy in SMA muscle. This study has demonstrated that the expression levels of thousands of dysregulated proteins and transcripts in the TA of *Smn*$^{-/-}$;*SMN2*$^{+/-}$ SMA mice can be restored by SMA restoration therapy using Pip6a-PMO. This study also demonstrates how the Pip6a-PMO successfully treats the periphery.

However, as to answering the original research question, we could not identify pathways that remained unchanged after SMN restoration therapy for the development of complementary treatments. Although this rescue is a highly encouraging result, SMN restoration strategies until now have fallen short of representing a 'cure', which means that these clinical successes may lead to SMA patients living longer with the condition (albeit in a less severe form) as well as the existence of a significantly enlarged patient population. Second-generation therapies that can be used in concordance with SMN restoration therapy are also useful when considering the discrete therapeutic window in which treatment of SMA is effective. Despite the encouraging recovery of dysregulated genes in SMA after SMN restoration treatment found in this study, it is more than ever important to not only rely on SMN restoration therapy to treat SMA, but to investigate therapies that can be used in combination with SMN restoration therapy. These therapies could be adapted to the patient's need, e.g. the severity of SMA pathology and when the patient was diagnosed.

This study has generated a great deal of data comparing not only symptomatic SMA mice to WT mice and Pip6a-PMO treated SMA mice to WT mice, but also data comparing untreated pre-symptomatic mice to untreated symptomatic mice, which allows us to see the evolution of pathological pathways over time in the muscle of WT and SMA mice. This data presents us with the opportunity to systematically analyze the proteomic and transcriptomic data using Connectivity Map (CMap) analysis [425]. CMap is a database in which the molecular effects of 10,000 approved drugs and bioactive compounds have been tested on various human cell lines. For future studies, instead of focusing on a particular pathway or gene to find treatments, I will use a non-biased approach to study the data produced in this study. I will use the list of differentially expressed genes in SMA during disease progression to identify novel drugs to restore muscle-specific pathologies in SMA. This pharmacological compound will not be dependent on SMN restoration and can be used in concordance with SMN restoration therapy. As proven in this study, SMN restoration provided an incredible rescue of dysregulated genes and protein after SMN restoration. Together with the combinatorial treatment it will result in a longer-lasting and more effective treatment for SMA.

4. Results II

Using CMap for the development of combinatorial therapies for SMA: Harmine shows promising effects *in vivo* and *in vitro*

4.1 Introduction

As discussed in Chapter 1, recent clinical trials of SMN restoration therapies have changed the SMA therapeutic landscape and led to the first approval of a treatment, Spinraza. SMN restoration clearly has a positive impact on SMA pathology but is not a cure. Patients will most likely be living longer with a less severe form of SMA, meaning a growth of the patient population with potential additional needs. Therefore, second-generation therapies are required in combination with SMN restoration to protect motor neurons and/or alleviate muscle pathology (Section 1.4.10). Skeletal muscle is highly affected in SMA, which is caused by both denervation following motor neuron death and intrinsic SMN-related pathologies [144,145,235] (Section 1.3.3). As muscle composes a large part of the body, muscle pathology plays a highly influential role in disease prognosis in SMA and therefore, improvement in muscle health could have beneficial effects in SMA. This was demonstrated by a study in which selective restoration of Smn in satellite cells improved phenotype and extended survival in an SMA mouse model [237]. Furthermore, rescuing muscle pathology in a non-Smn-dependent way in SMA mouse models increased survival [111,112]. Therefore, the aim of our study is to identify novel muscle-specific treatments that could eventually be used in combination with SMN restoration therapies.

In recent years, extensive proteomic and transcriptomic studies in various SMA cells and tissues have generated a great deal of data, of which normally only a small part was used to study a certain pathway or compound in depth. A technique to further analyze and utilize extensive datasets to discover pharmacological compounds that can potentially have a reversed effect on genetic conditions is

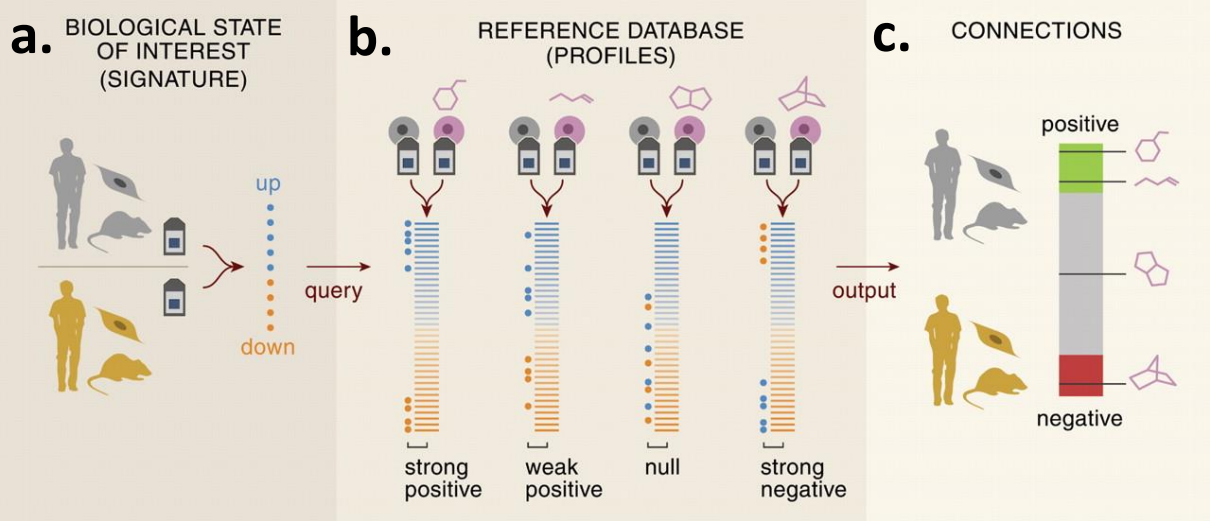


Figure 4.1. The Connectivity Map Concept. Gene-expression profiles derived from the treatment of cultured human cells with a large number of perturbagens populate a reference database. **a.** Gene-expression signatures represent any induced or organic cell state of interest. **b.** Pattern-matching algorithms score each reference profile for the direction and strength of enrichment with the query signature. **c.** Perturbagens are ranked by this "connectivity score"; those at the top ("positive") and bottom ("negative") are functionally connected with the query state (panel a) through the transitory feature of common gene-expression changes. Figure adopted from: Lamb, J. et al. (2006). Science; 313:1929–1935 [425].

Connectivity Map (CMap) analysis [425,426]. The purpose of CMap is to identify associations between gene expression profiles for a disease state and a drug treatment state. CMap links gene expression patterns associated with the disease state (Figure 4.1a) with corresponding patterns derived from drug-treated cell lines (Figure 4.1b). To do so, a publicly available database is used, which contains over 1.5 million gene expression profiles from ~5.000 small molecule compounds and ~3.000 genetic compounds. Many of these compounds have already received FDA and EMA approval, making them attractive therapeutic candidates (repurposing of drugs: Section 1.4.1). The compounds have been tested in 4 different cell lines: breast cancer epithelial cell line MCF7, prostate cancer epithelial cell line PC3 and the nonepithelial lines HL60 (leukemia) and SKMEL5 (melanoma) [425]. All compounds were used at a 10 mM concentration and some across a range of other concentrations to explore dose-response curves. The cells were treated for 6 and 12 hours [425]. CMap analysis has previously been used to identify new

potential therapeutics for a range of different diseases and conditions such as skeletal muscle atrophy [427], osteoarthritic pain [428], osteoporosis [429], gliomas [430], lung adenocarcinoma [431], hepatoblastoma [432], acute myeloid leukemia [433] and kidney disease [434]. CMap was also used to establish prediction models for different adverse drug reactions and to evaluate drug safety [435]. These studies show encouraging results, illustrating the benefits of CMap.

In the previous chapter, we firstly studied pathways, genes and proteins that were unchanged after Pip6a-PMO SMN restoration therapy in *Smn*$^{-/-}$;*SMN2*$^{+/-}$ mice. Proteomic and transcriptomic analyses performed on the *tibialis anterior* (TA) of P7 *Smn*$^{-/-}$;*SMN2*$^{+/-}$ and WT mice revealed that all genes and all, but 11 proteins were rescued after SMN restoration. In this chapter, we took the opportunity to systematically analyze the proteomic and transcriptomic data using Connectivity Map (CMap) analysis, to find novel muscle-specific treatments for SMA. Based on CMap analysis we identified harmine as a possible treatment for muscle pathology in SMA. We showed that analysis of gene expression signatures may represent an emerging approach to discover therapeutic agents for SMA.

Hypothesis

Connectivity map analysis can predict pharmacological compounds that alleviate skeletal muscle pathology in SMA by making connections between SMA disease genes and compounds that influence expression of these genes.

Objectives

1. Perform CMap analyses over the proteomic and transcriptomic data obtained from skeletal muscle (*tibialis anterior*) of *Smn*$^{-/-}$;*SMN2*$^{+/-}$ and control WT (Chapter 3).
2. Choose a compound for proof of concept.
3. Evaluate toxicity and effects on proliferation of selected drug *in vitro*.
4. Validate the genes and proteins identified as differentially expressed by the proteomic and transcriptomic data and predicted to be affected by selected drug.

5. Study the effects of the selected drug treatment on survival and weight in the severe *Smn*$^{-/-}$;*SMN2*$^{+/-}$ and the moderate *Smn*$^{2B/-}$ SMA mouse.
6. Examine the effects of the selected drug on skeletal muscle myofiber size, neuromuscular junctions and motor neuron number.
7. Study the effects of selected drug on gene expression in skeletal muscle to determine prediction power of CMap.

4.2 Material and methods

4.2.1 Animals and procedures

The CMap analyses were conducted on the proteomic and transcriptomic data described in Chapter 3 and information about animal procedures can be found in Section 3.2.1. Effects of harmine treatment on weight and survival were tested in the severe *Smn*$^{-/-}$;*SMN2*$^{+/-}$ and intermediate *Smn*$^{2B/-}$ SMA mouse models. Heterozygous littermates (*Smn*$^{+/-}$;*SMN2*$^{+/-}$ and *Smn*$^{2B/+}$) were used as healthy controls. Animals were weighed and monitored daily and culled upon reaching their defined humane endpoint. To investigate molecular and histological changes after harmine treatment, *Smn*$^{-/-}$;*SMN2*$^{+/-}$ and healthy littermates were treated daily for seven days and skeletal muscle and spinal cord were harvested at P7. All treated animals were gavaged daily with 10 mg/kg of harmine hydrochloride (sc-295136, Insight Biotechnology Ltd, Sante Cruz) dissolved in 0.9% saline. To reduce the total number of mice used, the fast-twitch *tibialis anterior* and *triceps* muscles from the same mice were used interchangeably for respective molecular and histological analyses.

For RNA sequencing experiments after harmine treatment, *Smn*$^{-/-}$;*SMN2*$^{+/-}$ (n = 3) and WT FVB/N (n = 3) were treated daily with 10 mg/kg harmine and the *tibialis anterior* was harvested at P7, tissues were flash frozen in liquid nitrogen immediately after harvest.

4.2.2 Cell culture

Four cell lines were used to investigate effects of harmine on gene expression: C2C12, NSC-34, SMA patient myoblasts and control human myoblasts. Cells were seeded in a 6-well plate and treated for 48 hours. Cells were then lysed, and RNA extracted using TRIzol Reagent (Life Technologies) as per manufacturer's instructions. Cell viability and proliferation after harmine treatment were evaluated with a 3-(4,5-dimethylthiazol-2-yl)-5-(3-carboxymethoxyphenyl)-2-(4-sulfophenyl)-2H-tetrazolium (MTS) assay kit (Colorimetric). C2C12 and NSC-34 cells were seeded in a 6-well plate with a 50% confluency and treated with a 1, 10, 25 or 50 nM concentration of harmine (sc-202644, Insight

Biotechnology Ltd, Sante Cruz) dissolved in DMSO (final concentration was 0.03%) for either 24, 48 or 72 hours with no further changes of media or re-addition of compounds. The measurements were made according to manufacturer's instructions. Briefly, 10 µl of MTS reagent was added directly to the wells and cell plates were incubated at 37°C for a minimum of 1 hour. Absorbance was measured at 490 nm on a CLARIOstar® plate reader (BMG LABTECH). Background absorbance was first subtracted using a set of wells containing medium only, then normalized to and expressed as a relative percentage of the plate-averaged untreated control. To chemically induce apoptosis, cells were treated with 10 µM Staurosporine (Abcam, Cambridge, UK).

4.2.3 CMap analysis

Proteomic and transcriptomic expression data is described in Chapter 3 and information about material and methods can be found in Section 3.2. CMap was used to obtain candidate drugs for SMA using proteomic and transcriptomic data separately. The Ensembl transcript ids were mapped to HG-U133A ids using biomaRt (Ensembl transcript id *mus musculus* → Ensembl gene id *mus musculus* → ortholog_one2one → Ensembl gene id *homo sapiens* → HG-U133A id. We entered these signatures into the latest dataset of CMap (Build 02, http://www.broadinstitute.org/cmap) and compared it to so-called instances. An instance is defined as the basic unit of data and metadata in CMap and has information about which compound is tested, the concentration of the compound and the cell line the compound was tested in.

4.2.4 RNA-Sequencing

Total RNA was extracted from P7 *tibialis anterior* using an RNeasy Microarray Tissue Mini Kit. Lysis and homogenization are performed using QIAzol Lysis Reagent, a phenol-guanidine-based lysis reagent. The aqueous phase is then directly applied to an RNeasy spin column for further RNA cleanup. The remaining genomic DNA was removed with the treatment of DNase I. 3 µG RNA was provided per sample dissolved in 30 µl RNAse free water. cDNA synthesis and RNA-seq library construction were

performed at the Oxford Genomics Centre (Oxford, United Kingdom) using poly(A) enrichment of the mRNA (mRNA-Seq) to remove ribosomal RNA and HiSeq 4000 Systems for sequencing. All samples passed quality control.

4.2.5 Programs used for pathway analyses, and statistics

4.2.5.1 Differential expression

For differential expression analysis, we used DESeq2 on gene counts expressed across all samples (15523 genes) after removal of one outlier (Harmine treated SMA sample 1). We considered a gene differentially expressed if their FDR < 0.05.

4.2.5.2 Gene ontology

For Gene Ontology enrichment analysis of proteomic data, we used topGO R function and adjusted *p* values for multiple testing following a Benjamini-Hochberg correction.

4.2.5.3 Network pathway analysis

To generate the network pathway analysis of DEG genes in SMA and genes rescued by harmine treatment and to investigate functional clustering of gene variants in an unbiased way, we used Phenotypic-Linkage Network [436]. We used the 500 genes that were most differently expressed to construct a network.

4.3 Results

4.3.1 CMap analysis provides therapeutic options for the treatment of SMA

To identify new treatment options for muscle pathology in SMA, we used the Connectivity Map (CMap), which is a bioinformatics tool that shows functional connections between drugs and gene expression signatures of diseases [425]. We built three expression signatures from proteomic data and three from transcriptomic data, described in Chapter 3. All signatures contained 500 upregulated and 500 downregulated genes and proteins that best discriminated the groups, which were as follow:

1. Differently expressed genes (DEG) between untreated P7 *Smn$^{-/-}$;SMN2$^{+/-}$* mice vs. age-matched WT controls
2. DEG between untreated P7 *Smn$^{-/-}$;SMN2$^{+/-}$* mice vs. Pip6a-PMO treatment
3. Overlap of DEG:
    a. Genes upregulated in untreated P7 *Smn$^{-/-}$;SMN2$^{+/-}$* mice and downregulated in Pip6a-PMO treated P7 *Smn$^{-/-}$;SMN2$^{+/-}$* mice
    b. Genes downregulated in untreated P7 *Smn$^{-/-}$;SMN2$^{+/-}$* mice and upregulated in Pip6a-PMO treated P7 *Smn$^{-/-}$;SMN2$^{+/-}$* mice

We entered these signatures into CMap and compared it to so-called instances, which are defined by expression profiles of the four cell lines (MCF7, PC3, HL60 and SKMEL5) treated with ~5.000 small molecule compounds and ~3.000 genetic compounds at different concentrations. Each instance received a connectivity score, ranging from −1 to 1. These connectivity scores represent the relative association of the respective instance with the specific query. A positive connectivity score indicates that a drug will induce the input signature in human cell lines, while a negative connectivity score indicates that a drug will reverse the input signature. As we were looking for a treatment that will reverse differently expressed genes and proteins in the SMA disease condition, we were interested in

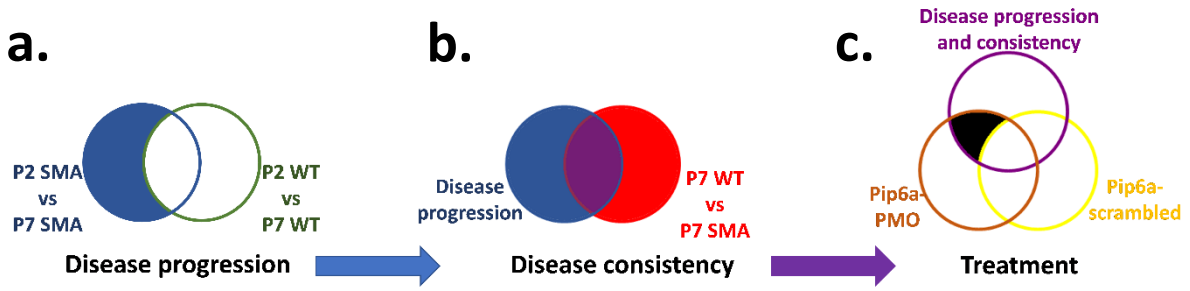


Figure 4.2. Defining the differently expressed genes and proteins in TA from SMA mice vs. WT. a. Disease progression is displayed in the first panel: DEG between pre-symptomatic P2 SMA vs. symptomatic P7 SMA, extracting DEG between P2 WT vs. P7 WT, as these DEG are part of normal development. **b.** To account for disease consistency, overlap between disease progression and genes/proteins differentially expressed between symptomatic P7 SMA and age-matched WT controls was evaluated. **c.** In the third panel is the overlap in DEGs of disease progression and consistency with DEG after Pip6a-PMO treatment in the opposite way, while extracting DEG in Pip6a-scrambled.

negative connectivity scores, which indicate a potential therapeutic value. Only the top 20 results were ranked and used, which all had $p < 0.05$. Out of the compounds identified by CMap, five drugs already considered for treatment of SMA in preclinical and clinical studies, namely salbutamol [437], alsterpaullone [83], trichostatin A [95], Valproic acid [318–322], Vorinostat [327,328] and sodium phenylbutyrate [325], were highly ranked, thereby underscoring the capability of CMap in identifying relevant therapeutic options.

Furthermore, we integrated transcriptomic and proteomic changes during disease progression (Figure 4.2), in which we first evaluated “disease progression”, identifying DEG between pre-symptomatic P2 SMA vs. symptomatic P7 SMA that follow significantly different expression patterns than in normal WT development. Then we assessed “disease consistency”, where we looked at the overlap between “disease progression” genes and proteins and genes and proteins differentially expressed in symptomatic P7 SMA mice compared to age-matched WT controls. Lastly, we obtained the overlap between the defined “disease consistency” genes and proteins with differently expressed genes and proteins in Pip6a-PMO samples (in the opposite direction) but not with the Pip6a-scrambled samples

(Figure 4.2c, black part), termed “treatment” genes and proteins. This resulted in a list of biological processes consistent with disease progression and reversed by treatment, displayed in Table 4.1. Using the expression signature based on SMA disease progression, consistency and reversed by SMN restoration treatment resulted in a list of drugs that are proposed to have a similar effect to Pip6a-PMO SMN restoration treatment and reverse disease progression and consistency. Two of these are HDAC inhibitors already considered for the treatment of SMA: trichostatin A [95] (Table 4.2) and Vorinostat [327,328], which are known to increase SMN protein levels by influencing *SMN2* splicing.

Table 4.1. Biological processes of SMA disease consistency, disease progression and reversed by SMN restoration treatment by Pip6a-PMO. This table is based on the “treatment” genes and proteins.

UP regulated in disease	DOWN regulated in disease
Positive regulation of tumor necrosis factor production	Regulation of translation
mRNA splicing via spliceosome	Chromatin modification
Regulation of transcript DNA templated	Positive regulation of peptidyl serine phosphorylation
mRNA processing	Protein ubiquitination involved in ubiquitin-dependent protein catabolic process
Translational initiation	Proteasome-mediated ubiquitin-dependent protein catabolic process
RNA splicing	Protein polyubiquitination
Response to toxic substance	Axonogenesis
Cellular response to drug	Forebrain development
Protein deubiquitination	Regulation of Rho protein signal transduction
ER-associated ubiquitin dependent protein catabolic process	Regulation of mitotic cell cycle
Proteasome mediated ubiquitin dependent protein catabolic process	Regulation of catalytic activity
Positive regulation of tumor necrosis factor production	Positive regulation of protein targeting to mitochondrion
Activation of MAPK activity	Mitophagy in response to mitochondrial depolarization
Proteolysis involved in cellular protein catabolic process	Smoothened signaling pathway
Chemokine mediated signaling pathway	Intracellular signal transduction
Cellular response to interferon gamma	Calcium ion transport
	Potassium ion transport

Table 4.2. CMap analysis of integrated transcriptomic and proteomic ''treatment'' genes and proteins. CMap results are based on ''treatment'' genes and proteins as explained in Figure 4.2, showing the 10 compounds with the lowest scores.

CMap name	Dose	Cell type	Score	Function
0198306-0000	10 µM	MCF7	-1	Small molecule
Isocorydine	12 µM	MCF7	-0.974	Alkaloid from Peumus boldus
Glycocholic acid	9 µM	MCF7	-0.967	Crystalline bile acid
Cyclopenthiazide	11 µM	MCF7	-0.958	Thiazide diuretic
Alimemazine	5 µM	PC3	-0.941	Antihistamine
Wortmannin	10 nM	MCF7	-0.936	Steroid metabolite of the fungi Penicillium funiculosum
Amantadine	10 µM	MCF7	-0.917	Dopamine agonist
Trichostatin A	100 nM	PC3	-0.908	HDAC inhibitor, already evaluated for SMA
Fenoterol	10 µM	HL60	-0.907	Adrenoreceptor agonist, asthma medication
Mitoxantrone	8 µM	MCF7	-0.906	Chemotherapy

4.3.2 Identification of harmine as a proof-of-concept compound of the use of CMap analyses to find muscle treatments for SMA

For clarity, we decided to show only the top 10 Connectivity Map with the most significant negative correlations to the three defined signatures in both transcriptomic and proteomic data in Table 4.3: 1. from DEG SMA vs. WT, 2. from DEG SMA vs. treated, and 3. overlap of DEG between signature 1 and 2. However, more information can be found in the Supplementary data, including scores for perturbagens per signature (instead of instances). Instances are defined as a basic unit of data originating from a certain compound tested, the concentration of the compound and the cell line the compound was tested in, and a perturbagen represents the overall effect of multiple instances from the same compound.

Not all compounds scoring low are suitable candidates for an SMA treatment. Several options for example, are chemotherapies, which is not a feasible therapeutic approach considering the weak

condition many patients are in and the many side effects these treatments present. And, as discussed in the previous section, other options have already been considered and evaluated for the treatment of SMA. Based on the expression signatures from proteomic and transcriptomic data, we identified the pharmacological compound harmine, which demonstrated large negative scores in various instances in transcriptomic (Table 4.3a–c) and proteomic (Table 4.3d) data. Other compounds closely related to harmine, originating from the same plant Peganum Harmala, showed large negative correlations as well in the various signatures such as harmol (Table 4.3b, d) and harmalol (see Supplementary Table 6).

Harmine (Figure 4.3) is an alkaloid that was originally isolated from seeds of Peganum harmala but is also found in other plants and in the human body. It has been traditionally used for ritual and medicinal preparations in the Middle East, Central Asia and South America [438,439].

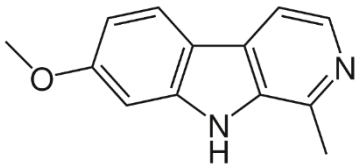


Figure 4.3. Chemical structure of harmine.

Harmine has various therapeutic effects [440], such as vasorelaxant [441], anti-inflammatory [442,443], antimicrobial [444,445], analgesic [443], antioxidative [446,447], antimutagenic [447], antitumor [448–450], antidepressive [451–453], antiaddictive [454,455], and neuroprotective [456–459] properties. The pharmacological mechanisms involve several molecular targets, including monoamine oxidase (MAO) [460–462], serotonin 5-$HT_{2A/C}$ receptors [463–465], imidazoline $I_{1/2}$ receptors [466], reactive oxygen species (ROS) [446,448], dual specificity tyrosine-phosphorylation-regulated kinase (DYRK1A) [467], glutamate transporter 1 (GLT-1) [456,458], and neurotrophic factors [452,468]. Interestingly, harmine has positive effects in studies on the motor neuron disease ALS [469], the muscular dystrophy disease myotonic dystrophy type 1 (DM1) [470] and neurological conditions, showing neuroprotective properties [456–459,469]. As SMA is characterized by motor neuron death (like ALS) and muscle pathology (like DM1) and would benefit of neuromuscular protection, we decided to validate our combined ‘omics and drug repositioning strategy with harmine.

Table 4.3. CMap analysis results of transcriptomic data and proteomic data. The CMap analyses were based on three expression signatures: untreated P7 *Smn*$^{-/-}$;*SMN2*$^{+/-}$ vs. age-matched WT controls (**a., d.**), untreated P7 *Smn*$^{-/-}$;*SMN2*$^{+/-}$ vs. Pip6a-PMO treatment (**b., e.**), and the overlap of differently expressed genes between these two signatures (**c., f.**). Only the 10 most negative correlation scores are displayed per CMap analysis. Tables **a.–c.** represents CMap analysis results from transcriptomic data and tables **d.–f.** represents CMap analysis results from proteomic data.

a.

From DE between SMA and WT

CMap name	Dose	Cell type	Score
Monocrotaline	12 µM	HL60	-1
Salbutamol	17 µM	HL60	-0.991
Disulfiram	13 µM	HL60	-0.937
Indoprofen	14 µM	MCF7	-0.911
Zardaverine	15 µM	MCF7	-0.901
Oxamniquine	14 µM	PC3	-0.9
Harmine	**16 µM**	**HL60**	**-0.897**
Guanabenz	14 µM	PC3	-0.896
Hydrochlorothiazide	13 µM	HL60	-0.894
Aciclovir	18 µM	PC3	-0.883

b.

From DE between SMA and treatment

CMap name	Dose	Cell type	Score
Troglitazone	10 µM	HL60	-1
Harmine	**16 µM**	**HL60**	**-0.99**
Sulfamethizole	15 µM	HL60	-0.975
Netilmicin	3 µM	HL60	-0.93
Pha-00846566e	10 µM	PC3	-0.909
Harmol	**16 µM**	**HL60**	**-0.906**
Zaprinast	15 µM	HL60	-0.887
Zardaverine	15 µM	MCF7	-0.88
Sb-203580	1 µM	MCF7	-0.876
Vinpocetine	11 µM	HL60	-0.875

c.

From DE overlap SMA vs. WT and SMA vs. treatment

CMap name	Dose	Cell type	Score
Disulfiram	13 µM	HL60	-1
Sulfamethizole	15 µM	HL60	-0.921
Zaprinast	15 µM	HL60	-0.92
Harmine	**16 µM**	**HL60**	**-0.919**
Oxamniquine	14 µM	PC3	-0.906
Sb-203580	1 µM	MCF7	-0.893
Cinchonine	14 µM	HL60	-0.886
Ciprofibrate	14 µM	HL60	-0.885
Cyclic adenosine monophosphate	12 µM	HL60	-0.883
Salbutamol	17 µM	HL60	-0.873

d.

From DE between SMA and WT

CMap name	Dose	Cell type	Score
Harmol	**16 µM**	**PC3**	**-1**
Irinotecan	100 µM	MCF7	-0.919
Digitoxigenin	11 µM	MCF7	-0.911
Harmol	**16 µM**	**MCF7**	**-0.888**
Oxybenzone	18 µM	PC3	-0.878
Harmine	**16 µM**	**PC3**	**-0.867**
Meropenem	10 µM	MCF7	-0.861
Tanespimycin	1 µM	PC3	-0.858
Monorden	100 nM	PC3	-0.852
Digitoxigenin	11 µM	MCF7	-0.845

e.

From DE between SMA and treatment

CMap name	Dose	Cell type	Score
Acacetin	14 µM	PC3	-1
Estriol	14 µM	MCF7	-0.98
Methylprednisolone	11 µM	MCF7	-0.956
Etamsylate	15 µM	PC3	-0.952
Alsterpaullone	10 µM	PC3	-0.952
Luteolin	14 µM	MCF7	-0.942
Fluorocurarine	12 µM	MCF7	-0.94
Dexpanthenol	19 µM	MCF7	-0.938
5213008	18 µM	MCF7	-0.932
Pirenzepine	9 µM	MCF7	-0.929

f.

From DE overlap SMA vs. WT and SMA vs. treatment

CMap name	Dose	Cell type	Score
Camptothecin	11 µM	PC3	-1
Irinotecan	100 µM	PC3	-0.94
0175029-0000	10 µM	MCF7	-0.93
Mitoxantrone	8 µM	MCF7	-0.925
Alsterpaullone	10 µM	PC3	-0.912
Irinotecan	100 µM	MCF7	-0.849
Doxorubicin	7 µM	MCF7	-0.823
Gw-8510	10 µM	PC3	-0.812
0175029-0000	1 µM	MCF7	-0.811
Daunorubicin	7 µM	MCF7	-0.796

4.3.3 Doses up to 25 μM concentration harmine did not affect cell viability and proliferation

We first performed an MTS assay to investigate the possible effect of harmine treatment on the proliferation and viability on two murine cell lines, the motor neuron hybrid cell line NSC-34 and the myoblast cell line C2C12. These cell lines represent the two cell types particularly affected in SMA: motor neurons and skeletal muscle. As shown in Figure 4.4a, harmine dose-dependently inhibited proliferation and viability at 50 μM in C2C12 cells, with effects becoming more severe over time. Harmine treatment at 1 μM, 10 μM and 25 μM concentrations did not induce apoptosis compared to untreated C2C12 cells. 50 μM harmine treatment in NSC-34 caused severe toxicity, with proliferation/viability levels as low as the negative control Staurosporine (Figure 4.4b). 1 μM, 10 μM and 25 μM harmine treatment in NSC-34 did not cause a change of proliferation and viability compared to untreated NSC-34 cells. The vehicle in which harmine was dissolved, DMSO (final concentration 0.03%), caused a significant toxicity in C2C12 cells after 72h treatment. While high doses of harmine are toxic in cells, we found that doses up to 25 μM concentration harmine did not impact cell viability and proliferation.

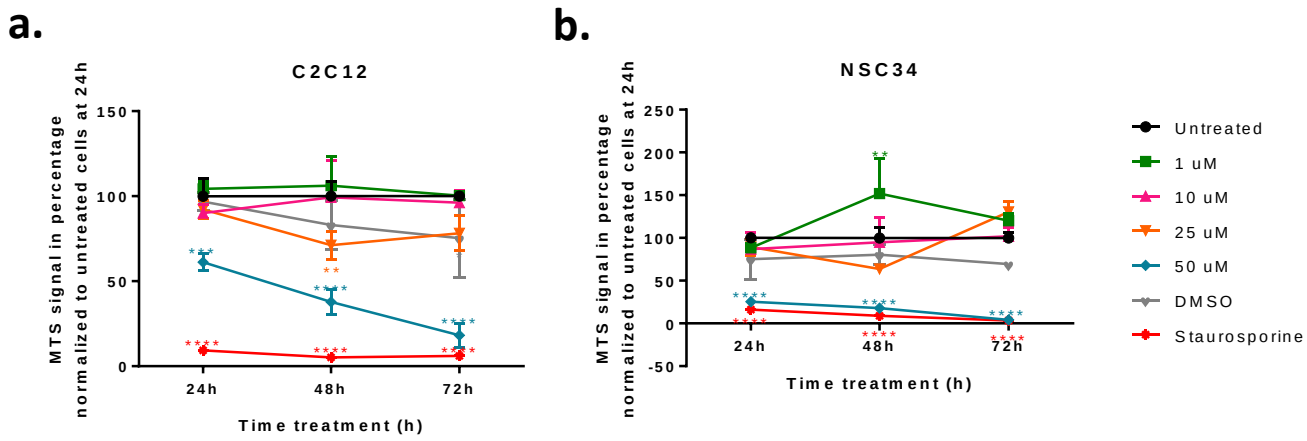


Figure 4.4. Dose-dependent toxicity of harmine treatment *in vitro*, assessed by MTS assays. Harmine treatment at different concentrations was assessed at three timepoints 24h, 48h and 72h. All groups are normalized to untreated cells at 24h (100%). Harmine vehicle was DMSO and the negative control is Staurosporine. **a.** MTS scores from 1 µM, 10 µM, 25 µM and 50 µM concentration harmine treated in C2C12 cells. **b.** MTS scores from 1 µM, 10 µM, 25 µM and 50 µM concentration harmine treated in NSC-34 cells. Two-way ANOVA (*post hoc*: Bonferroni) was conducted comparing all groups to the untreated group (black line) at the same timepoint, ** $p < 0.01$, *** $p < 0.001$, **** $p < 0.0001$, $n = 3$ per group.

4.3.4 Validation of CMap results through rescue of genes and proteins via harmine treatment *in vitro* and *in vivo*

To confirm independently the transcriptomic, proteomic and CMap results associated with harmine, we performed quantitative RT-PCR analysis of 2 genes (*Tob2* and *Cdkn1a*) and 2 proteins (*Ppm1b* and *Clpx*) that are upregulated and 2 genes (*Aspm* and *Mcm2*) and 2 proteins (*Snrnp27* and *Gls*) that are downregulated in P7 SMA muscle compared to WT and predicted to be reversed by harmine treatment. We used RNA from the same TA samples on which proteomic and transcriptomic studies were performed. We validated the proteomic and transcriptomic results and found that genes and proteins that were downregulated in SMA in the proteomic and transcriptomic data, were indeed significantly downregulated in the qPCR analyses on skeletal muscle (Figure 4.5). The same was true for upregulated genes. All validation genes and proteins were chosen purely based on CMap prediction, meaning that all these genes and proteins were dysregulated in our SMA samples and

significantly reversed by harmine treatment in all CMap instances (i.e. at every dose and cell type tested). Interestingly, one of the proteins strongly downregulated in SMA is Snrnp27 (Figure 4.5a), which is a small nuclear RNPs (snRNPs). snRNPs are part of the spliceosome of the nucleus and are required for the catalysis of intron removal during pre-mRNA splicing [44]. As discussed in Section 1.1.3, SMN plays a canonical role in the assembly of snRNPs. Another interesting validation gene, based on transcriptomic data (Figure 4.5d), is *cyclin dependent kinase inhibitor 1A* (*Cdkn1a* or *p21*), which is a mediator of cell cycle arrest downstream of p53 and is a regulator of cell cycle and DNA repair. This gene is reported to be upregulated in various SMA models [27,48,49,53,471].

Furthermore, we tested if harmine treatment, as predicted by CMap analyses, has indeed an opposite effect on *Tob2*, *Cdkn1a, Aspm*, *Mcm2, Snrnp27* and *Gls in vitro*. C2C12, NSC-34, SMA patient myoblasts and control myoblasts were treated with 25, 35 and 50 µM levels of harmine for 48 hours and were compared to untreated cells to investigate if harmine treatment influenced the expression of the genes in the predicted direction. Results are summarized in Table 4.4 (individual graphs can be found in supplementary data Figure 1). All results labelled 'significant' were in the right direction ($p < 0.05$, downregulated in SMA and upregulated by harmine treatment and *vice versa*). *Snrnp27* was upregulated after harmine treatment in all tested cell types, whereas *Gls* was only upregulated after harmine treatment in NSC-34 and *Ppm1b* was only downregulated in control myoblasts. A potential explanation of why some genes were more predictive than others is that some genes, such as *Gls* and *Ppm1b*, were identified by the proteomic study, but were validated by mRNA expression. As is described in the discussion of the previous chapter (Section 3.4.1), there is often a low correlation between proteomic and transcriptomic results. Overall, harmine treatment had a success rate of 60% in C2C12, NSC-34, SMA patient myoblasts and control myoblasts of changing the expression of validation genes in the opposite direction.

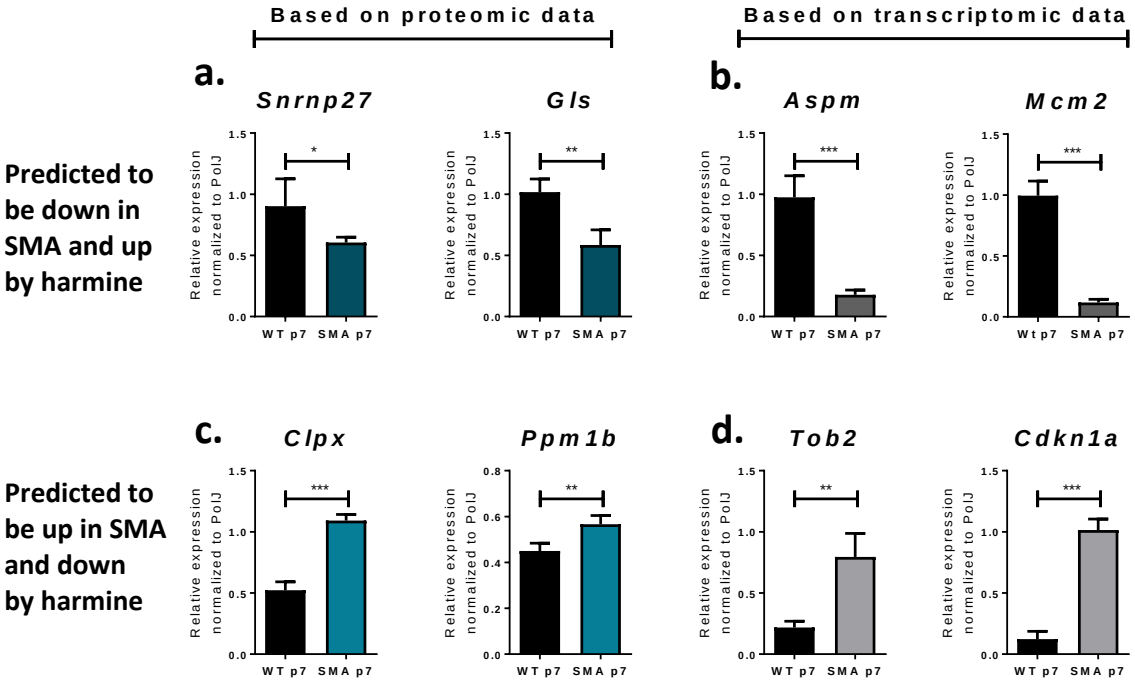


Figure 4.5. Validation by qPCR of proteomic and transcriptomic data comparing symptomatic P7 SMA muscle with age-matched WT controls. a. Based on proteomic data, *Snrnp27* and *Gl*s were validated to be significantly downregulated in SMA. **b.** Based on transcriptomic data, *Aspm* and *Mcm2* were validated to be significantly downregulated in SMA. **c.** Based on proteomic data, *Clpx* and *Ppm1b* were validated to be significantly upregulated in SMA. **d.** Based on transcriptomic data, *Tob2* and *Cdkn1a* were validated to be significantly upregulated in SMA. Data represents mean ± standard deviation, $n = 3$ for all groups and statistical analyses were executed using Student's *t* tests, * $p < 0.05$, ** $p < 0.01$, *** $p < 0.001$.

Table 4.4. Summary of *in vitro* studies investigating effects of harmine on various cell types. **'**Significant' in this table means a significant change in mRNA expression in the CMap predicted direction after harmine treatment. All cell types were treated for 48 hours with 25, 35 and 50 µM levels of harmine.

	Downregulated in SMA and up-regulated by harmine treatment				**Upregulated in SMA and down-regulated by harmine treatment**			
	Snrnp27	***Gls***	***Aspm***	***Mcm2***	***Clpx***	***Ppm1b***	***Cdkn1a***	***Tob2***
C2C12	Significant	Ns	Significant	Significant	Significant	Ns	Ns	Significant
NSC-34	Significant	Significant	Significant	Significant	Ns	Ns	Significant	Ns
Patient myoblast	Significant	Ns	Ns	Ns	Significant	Ns	Ns	Significant
Control myoblast	Significant	Ns	Significant	Ns	Significant	Significant	Significant	Significant

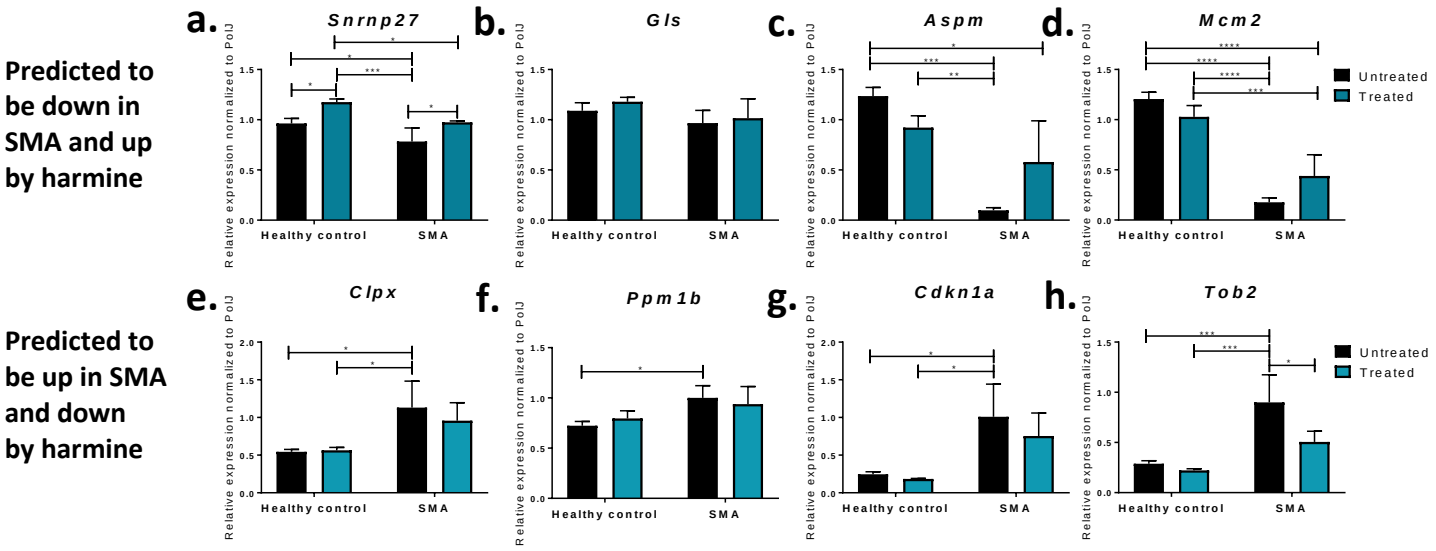


Figure 4.6. mRNA expression levels of validation genes of harmine treated and untreated SMA mice and healthy control TA muscle. a.–d. mRNA expression after treatment validation genes predicted to be upregulated by harmine treatment. **e.–f.** mRNA expression after treatment of validation genes predicted to be downregulated by harmine treatment. Data represents mean ± standard deviation, *n* = 3 or *n* = 4 per group, two-way ANOVA, Bonferroni, * $p < 0.05$, ** $p < 0.01$, *** $p < 0.001$, **** and $p < 0.0001$.

Next, we evaluated the effects of harmine treatment on reference genes in the *triceps* of SMA mice (*Smn*$^{-/-}$;*SMN2*$^{+/-}$) and healthy littermate controls (*Smn*$^{+/-}$;*SMN2*$^{+/-}$). Animals received from birth onwards daily oral harmine, 10 mg/kg. The *triceps* were harvested at P7 and mRNA expression of validation genes are displayed in Figure 4.6. Harmine treatment significantly upregulated *Snrnp27* and significantly downregulated *Tob2* in SMA skeletal muscle. A trend in the proposed direction was seen in *Aspm*, *Mcm2*, *Clpx* and *Cdkn1a*. Harmine treatment did not have a visible effect on *Gls* and *Ppm1b* in SMA skeletal muscle (Figure 4.6), reflecting the *in vitro* results, in which harmine treatment in *Gls* and *Ppm1b* were the least impacted (Table 4.4).

4.3.5 Harmine treatment increases SMN mRNA expression but not SMN protein expression

The goal of this study is to find a treatment that can be used in combination with SMN restoration therapy to alleviate skeletal muscle pathology in SMA. The main contributor in SMA to DEG in proteomic and transcriptomic studies is SMN. Therefore, it is not surprising that some compounds identified by CMap in this study such as the HDAC inhibitors trichostatin A [95], target *SMN* expression. To test effects of harmine on *Smn* gene expression, we treated C2C12 and NSC-34 cells for 48 hours with 25, 35 and 50 µM concentrations of harmine. As these cell lines are murine, they don't have the *SMN2* gene. 25 and 35 µM harmine treatment resulted in a significant upregulation of *Smn* in C2C12 cells (Figure 4.7a) and in NSC-34 cells at all tested concentrations (25, 35 and 50 µM) (Figure 4.7b). Harmine treatment (35 and 50 µM) in patient myoblasts resulted in a significant increase of full-length *SMN* (Figure 4.7c), while total *SMN* levels remained unchanged (Figure 4.7d). Furthermore, harmine treatment also resulted *in vivo* in an upregulation of full-length *SMN* transcript in treated *Smn*$^{-/-}$;*SMN2*$^{+/-}$ *triceps* muscle after daily 10 mg/kg harmine administration (Figure 4.7e) but did not change total *SMN* levels (Figure 4.7f). However, no upregulation of the SMN protein was found in harmine treated C2C12, NSC-34, patient myoblast (Western blot data not shown) and SMA mouse *triceps* (Figure 4.7g). As is explained in Chapter 3, Section 3.4.1, there could be multiple methodological and biological factors causing this disparity between mRNA expression and protein expression. Since there was no increase in SMN protein after treatment, we can conclude that harmine is most likely not an SMN restoration therapy.

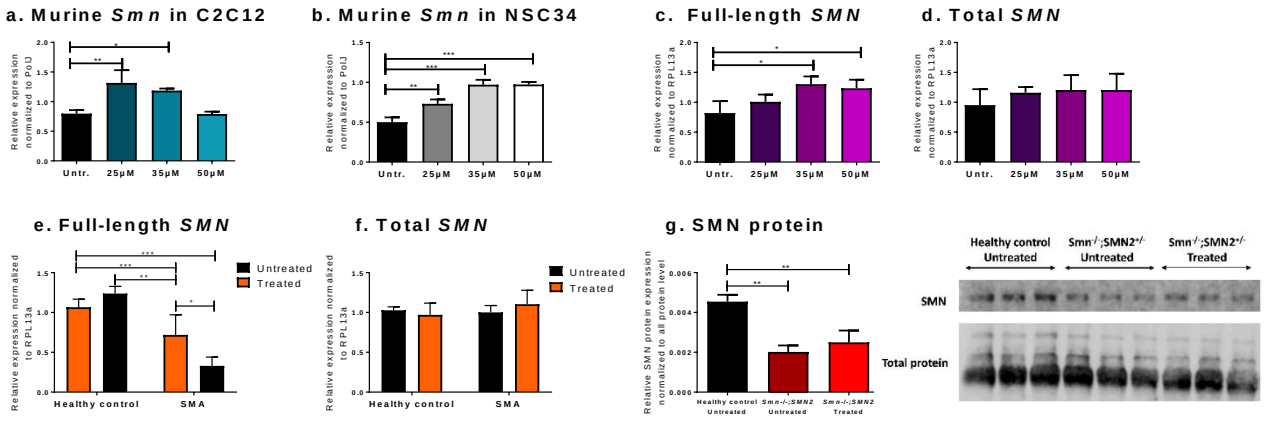


Figure 4.7. Effects of harmine treatment on *Smn* and *SMN* transcripts. Cells were treated with 25, 35 or 50 µM harmine concentrations for 48 hours after which *Smn*/full-length *SMN*/total *SMN* mRNA levels were measured. **a.** *Smn* mRNA expression levels in C2C12 cells, **b.** *Smn* expression levels in NSC-34 cells, **c.** Full-length *SMN* mRNA expression in patient myoblasts, **d.** Total *SMN* mRNA expression levels in patient myoblasts. For **a.–d.** values were calculated using a one-way ANOVA and data represent mean ± standard deviation, *n* = 3. **e.** Full-length *SMN* mRNA expression levels from daily 10 mg/kg harmine treated P7 *Smn*$^{-/-}$;*SMN2*$^{+/-}$ mice and healthy littermates compared to untreated animals. **f.** total *SMN* mRNA expression levels from daily 10 mg/kg harmine treated P7 *Smn*$^{-/-}$;*SMN2*$^{+/-}$ mice and healthy littermates compared to untreated animals. For **e.–f.** values were calculated using a two-way ANOVA and represent mean ± standard deviation, *n* = 3–4. **g.** SMN protein expression levels from daily 10 mg/kg harmine treated P7 *Smn*$^{-/-}$;*SMN2*$^{+/-}$ mice compared to untreated P7 *Smn*$^{-/-}$;*SMN2*$^{+/-}$ mice and untreated healthy littermates. SMN protein levels were normalized using total protein count and values were calculated using a one-way ANOVA and data represent mean ± standard deviation, *n* = 3. For all graphs * $p < 0.05$, ** $p < 0.01$ and *** $p < 0.001$, ****.

4.3.6 Harmine treatment improves disease phenotype and survival

To study the effects of harmine treatment on SMA disease progression, we used the severe *Smn*$^{-/-}$;*SMN2*$^{+/-}$ and the moderate *Smn*$^{2B/-}$ SMA mouse model and compared the pups to healthy littermates and untreated animals. Pups were treated daily from postnatal day 0 onwards with a 10 mg/kg dose of harmine dissolved in saline. Survival was recorded until the humane end point was reached. Untreated *Smn*$^{-/-}$;*SMN2*$^{+/-}$ had a median survival of 9.5 days (8–12 days) while harmine treatment significantly increased survival to a median of 12 days (Figure 4.8a). Untreated *Smn*$^{2B/-}$ mice

had a median survival of 20 days (Figure 4.8d). Harmine-treated *Smn*$^{2B/-}$ were doing remarkably better than untreated mice at this age. However, they started trembling around day 21 and therefore had to be culled due to the occurrence of adverse tremors. Nevertheless, survival was significantly slightly increased to a median of 21 days. Recent studies have not reported tremors in harmine-treated mice, however, these animals mice were treated for less than a week [449,458,472]. However, older studies in which higher doses of harmine were used (such as 15 mg/kg or 40 mg/kg) reported some short-term trembling for up to one hour after treatment [473–475]. To circumvent the tremors, we opted for every 3 days treatment of *Smn*$^{2B/-}$ mice and observed further significant weight and survival improvement, and the mice are at date of submitting of this thesis alive (P40, Figure 4.8d and e).

Since losing weight is part of SMA disease progression in both the severe and moderate mouse models and improved weight typically reflects improved health, we also investigated if harmine treatment had an effect on overall weight. Harmine treated *Smn*$^{-/-}$;*SMN2*$^{+/-}$ and *Smn*$^{2B/-}$ SMA mice were significantly heavier than untreated animals, from P7 (*Smn*$^{-/-}$;*SMN2*$^{+/-}$, Figure 4.8b) and day P16 (*Smn*$^{2B/-}$ Figure 4.8e) until their respectively humane endpoints. Overall, our results demonstrate that daily harmine treatment improves weight and survival.

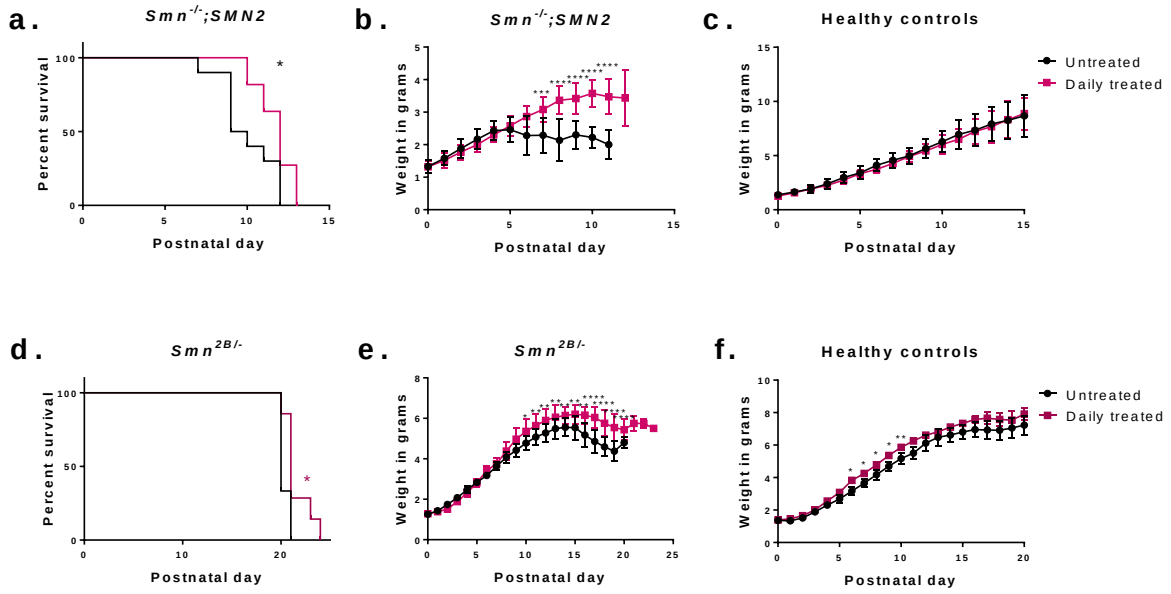


Figure 4.8. Effects of daily oral 10 mg/kg treatment on weight and survival in severe and moderate SMA mice. a. Survival curve for *Smn*$^{-/-}$;*SMN2*$^{+/-}$ untreated (*n* = 10) and treated (*n* = 11) pups. Harmine treatment significantly increased survival (from median 9.5 days to 12 days, $p < 0.05$, log-ran Mantel-Cox test). **b.** Weights of untreated (*n* = 10) and treated (*n* = 11) severe SMA *Smn*$^{-/-}$;*SMN2*$^{+/-}$ pups plotted as mean ± standard deviation. Harmine treated pups weighed significantly more than *Smn*$^{-/-}$;*SMN2*$^{+/-}$ untreated pups starting from P7 (one-way ANOVA). **c.** Healthy littermates did not show any significant weight differences between treated and untreated animals (one-way ANOVA). **d.** Survival curve for *Smn*$^{2B/-}$ untreated (*n* = 9) and treated (*n* = 7) pups. Harmine treatment significantly increased survival (from median 20 days to 21 days, $p < 0.05$, log-ran Mantel-Cox test). **e.** Weights of untreated (*n* = 9) and treated (*n* = 7) moderate SMA *Smn*$^{2B/-}$ pups plotted as mean ± standard deviation. Harmine treated pups weighed significantly more than untreated *Smn*$^{2B/-}$ pups (one-way ANOVA). **e.** Harmine treated healthy littermates demonstrated a slight increase of weight between day 6–10 compared to untreated pups (one-way ANOVA). For all graphs * $p < 0.05$, ** $p < 0.01$ and *** $p < 0.001$, **** $p < 0.0001$.

4.3.7 Harmine treatment increases myofiber size in the severe SMA mouse model

We investigated the effect of harmine on the muscle fiber size of the TA of P7 mice. The muscle fibers of *Smn*$^{-/-}$;*SMN2*$^{+/-}$ mice were significantly smaller than their healthy control littermates (Figure 4.9a and 4.8b, $p < 0.0001$). Harmine treatment had no significant effect on myofiber size in healthy controls,

however, *Smn*$^{-/-}$;*SMN2*$^{+/-}$ mice that were administered harmine displayed a significant increase in muscle fiber size (Figure 4.9a–c, $p < 0.0001$).

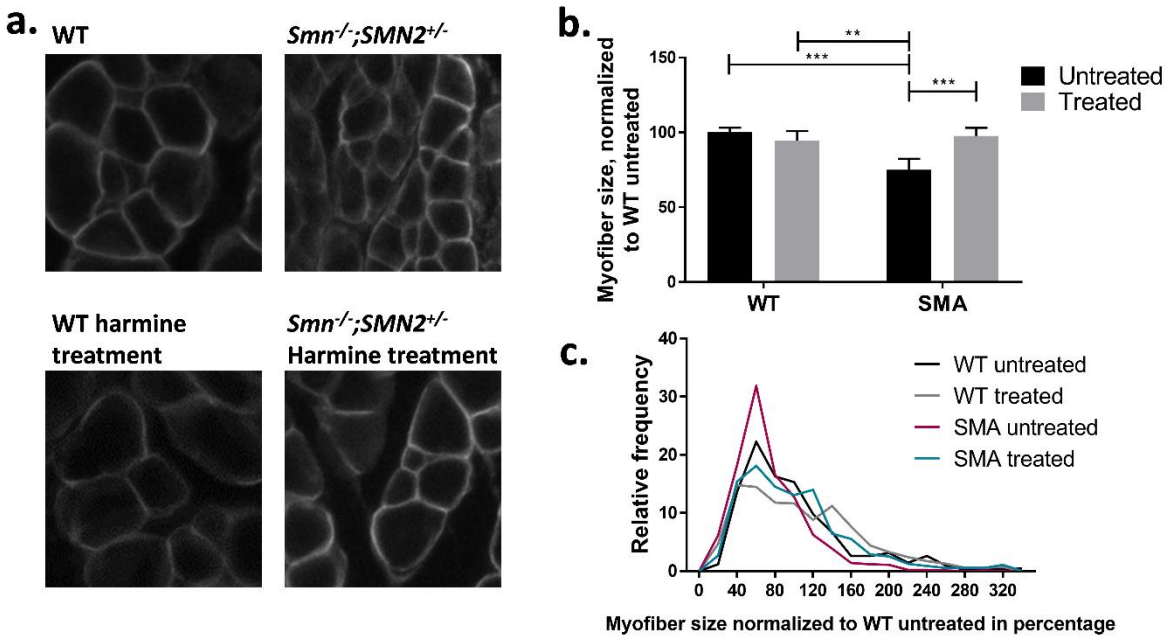


Figure 4.9. Treatment of *Smn*$^{-/-}$;*SMN2*$^{+/-}$ mice with harmine (10 mg/kg) increases fiber diameter in *tibialis anterior* muscle. The different age-matched groups analyzed were: untreated healthy control littermates ($n = 4$), untreated *Smn*$^{-/-}$;*SMN2*$^{+/-}$ mice ($n = 4$), harmine treated healthy control littermates ($n = 3$) and harmine treated *Smn*$^{-/-}$;*SMN2*$^{+/-}$ mice ($n = 4$). **a.** Representative images showing a laminin staining of muscle fibers within a designated area of the TA muscle. **b.** Quantification of the cross-sectional area of TA muscle fibers, average per muscle of multiple counts throughout the muscle. Untreated *Smn*$^{-/-}$;*SMN2*$^{+/-}$ mice have significantly smaller muscle fibers than their healthy control littermates $p < 0.001$. Administration of harmine significantly increased the muscle fiber size of *Smn*$^{-/-}$;*SMN2*$^{+/-}$ mice $p < 0.0001$. **c.** Harmine treatment caused a shift of myofiber size in treated *Smn*$^{-/-}$;*SMN2*$^{+/-}$.

4.3.8 Harmine displays neuroprotective properties in the CNS of severe SMA mice

We next studied neuroprotective properties of harmine in the CNS of *Smn*$^{-/-}$;*SMN2*$^{+/-}$ mice. Previous research with harmine has shown that it increases glutamate transporter 1 (GLT-1), which has neuroprotective effects. Therefore, we tested whether harmine increases protein levels of GLT-1 in

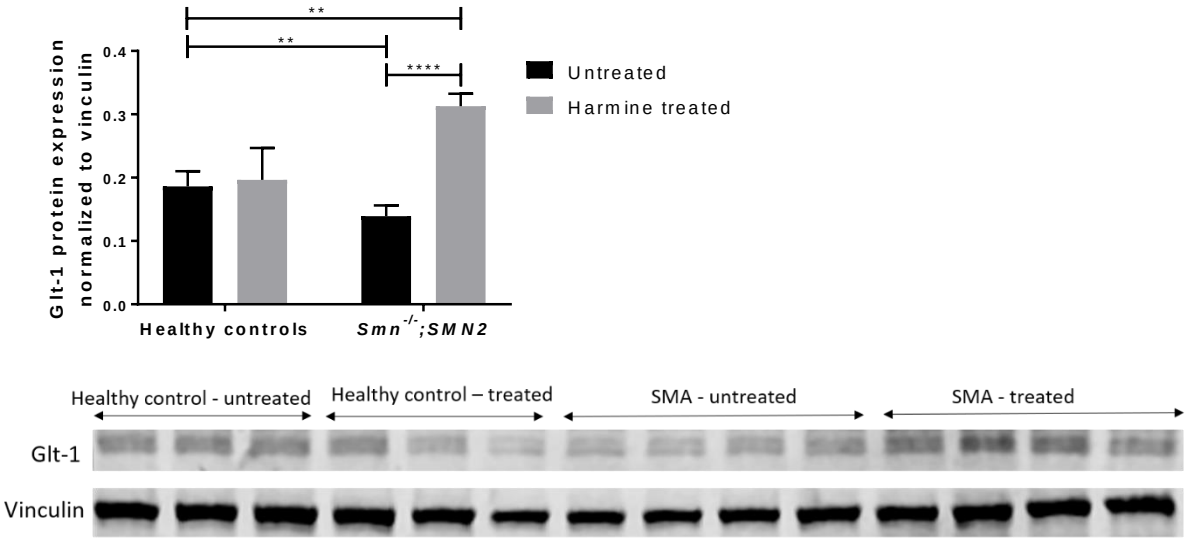


Figure 4.10. Harmine increases GLT-1 expression *in vivo* in *Smn*$^{-/-}$;*SMN2*$^{+/-}$ mice. GLT-1 western blot analysis of spinal cord tissues collected from harmine (10mg/kg; daily) and untreated *Smn*$^{-/-}$;*SMN2*$^{+/-}$ mice and healthy controls. Data represents mean ± standard deviation, n = 3 or 4 for all groups and statistical analyses were executed using a two-way ANOVA, Bonferroni, ** $p < 0.01$, **** $p < 0.0001$.

Smn$^{-/-}$;*SMN2*$^{+/-}$ mice. *Smn*$^{-/-}$;*SMN2*$^{+/-}$ mice and healthy littermates were daily treated from birth onwards with a 10 mg/kg subcutaneous harmine injection. After 7 days, animals were sacrificed, and the spinal cord was harvested and analyzed by Western blot. After normalization to vinculin, we observed that untreated *Smn*$^{-/-}$;*SMN2*$^{+/-}$ mice have significantly lower levels of GLT-1 protein than healthy controls ($p < 0.01$) in the spinal cord (Figure 4.10). Harmine treatment significantly increased GLT-1 protein expression ($p < 0.0001$) in the spinal cord from *Smn*$^{-/-}$;*SMN2*$^{+/-}$ mice.

We next investigated the effects of harmine treatment on motor neuron viability within the ventral horn area of the lumbar spinal cord in P7 mice. Animals were daily treated with a 10 mg/kg dose of harmine from birth onwards. Untreated *Smn*$^{-/-}$;*SMN2*$^{+/-}$ mice had significant fewer motor neurons than untreated healthy littermates (Figure 4.11b, $p < 0.0001$). Harmine treatment significantly increased the number of motor neurons in *Smn*$^{-/-}$;*SMN2*$^{+/-}$ mice (Figure 4.11b, $p < 0.001$). Together, these results demonstrate that harmine has neuroprotective properties in the CNS of severe SMA mice and rescues motor neuron loss.

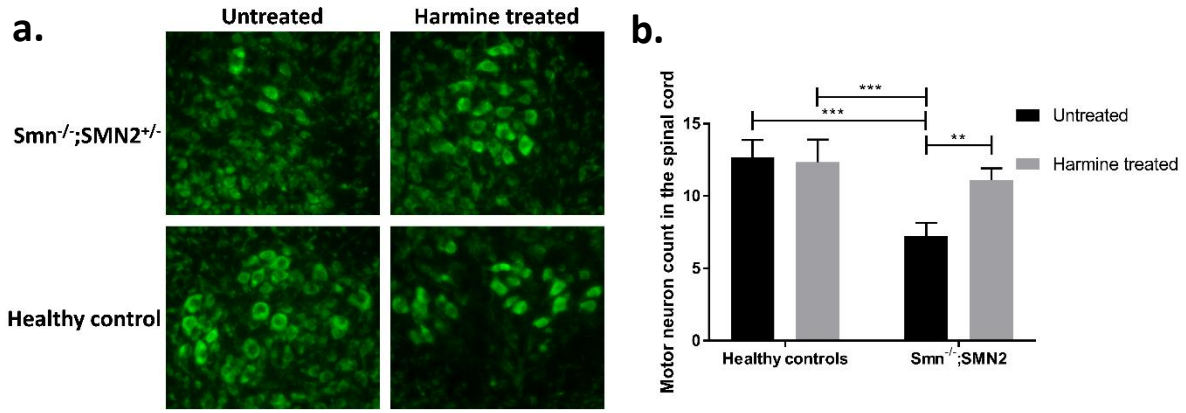


Figure 4.11. Treatment of harmine (10 mg/kg) results in rescue of motor neuron death in *Smn$^{-/-}$;SMN2$^{+/-}$* mice. The different age-matched groups analyzed were: untreated healthy control littermates (n = 3), untreated *Smn$^{-/-}$;SMN2$^{+/-}$* mice (n = 5), harmine treated healthy control littermates (n = 4) and harmine treated *Smn$^{-/-}$;SMN2$^{+/-}$* mice (n = 4). **a.** Representative images showing a Nissl staining of motor neuron cell bodies within the ventral horn area of the lumbar spinal cord. **b.** Quantification of the number of motor neuron cell bodies, average per mouse of multiple counts throughout the spinal cord of P7 *Smn$^{-/-}$;SMN2$^{+/-}$* mice and healthy controls shows a significant decrease in untreated *Smn$^{-/-}$;SMN2$^{+/-}$* mice vs. healthy littermates ($p < 0.001$) and a significant increase of the number of motor neuron cell bodies of harmine treated *Smn$^{-/-}$;SMN2$^{+/-}$* mice compared to untreated *Smn$^{-/-}$;SMN2$^{+/-}$* mice ($p < 0.01$). Data represents mean ± standard deviation and statistical analyses were executed using a two-way ANOVA, Bonferroni.

4.3.9 Pathway analysis after RNA sequencing reveals full rescue of 20% of dysregulated genes in the severe SMA mouse model after harmine treatment

To examine the effects of harmine in SMA muscle, we performed RNA-seq on TA of untreated and harmine-treated *Smn$^{-/-}$;SMN2$^{+/-}$* and WT mice. Harmine-treated *Smn$^{-/-}$;SMN2$^{+/-}$* and WT mice received daily orally administered harmine (10 mg/kg). RNA was extracted from 7-day old TAs. Using RNA-seq, we identified 15.523 protein coding genes across all samples.

As demonstrated in Table 4.5, 5183 genes were differently expressed between untreated SMA mice vs. WT mice. We first wanted to investigate the rescue of harmine treatment in SMA mice, comparing harmine treated *Smn$^{-/-}$;SMN2$^{+/-}$* mice to untreated WT mice. The number of genes dysregulated

between harmine treated SMA mice and untreated WT mice was 4144, meaning that 1038 genes, according to this method, were fully rescued after treatment. We next wanted to examine if harmine treatment had positive effects on dysregulated genes in SMA but did not fully rescue. As is illustrated in Figure 4.12a, 547 genes were partly rescued, but were still not at the same level as WT. Further, we investigated any possible side-effects. Harmine treatment had a far larger effect in SMA mice (harmine-treated SMA compared to untreated SMA, DEG 1426) than in WT mice (harmine-treated WT compared to untreated WT DEG 88, Table 4.5) and from these 88 DEG, 74 genes were differently expressed in the SMA disease condition, meaning that harmine had side effects on only 14 genes not dysregulated in SMA (10 + 4, Figure 4.12b).

The molecular functions of the genes rescued by harmine treatment in SMA skeletal muscle can be found in Figure 4.13, which shows the gene ontology and distinguishes fully rescued (1038) and partly rescued (574, Figure 4.12) genes. Harmine treatment impacted various muscle functions such as glucose metabolism and oxidation-reduction. Clustering of the 500 most dysregulated genes (all significant) in SMA compared to WT is visualized in Figure 4.14a. Interestingly, genes that cluster together are normally dysregulated in the same way in this study (either up or down). In Figure 4.14b are the effects of Harmine illustrated on DEG genes.

The network pathway analysis confirms that main processes in SMA muscle have been restored by harmine treatment; however, 75% of genes are still dysregulated after harmine treatment in SMA mice. Therefore, we can see an improvement but not a complete reversed effect of harmine on SMA.

Table 4.5. Differential gene expression analysis based on DESeq2 showing DEG between various groups of harmine treated and untreated SMA and WT skeletal muscle.

Comparisons	Differently expressed genes
SMA vs. WT	5183
SMA harmine tr vs. WT	4144
SMA harmine tr vs. SMA	1426
WT harmine tr vs. WT	88

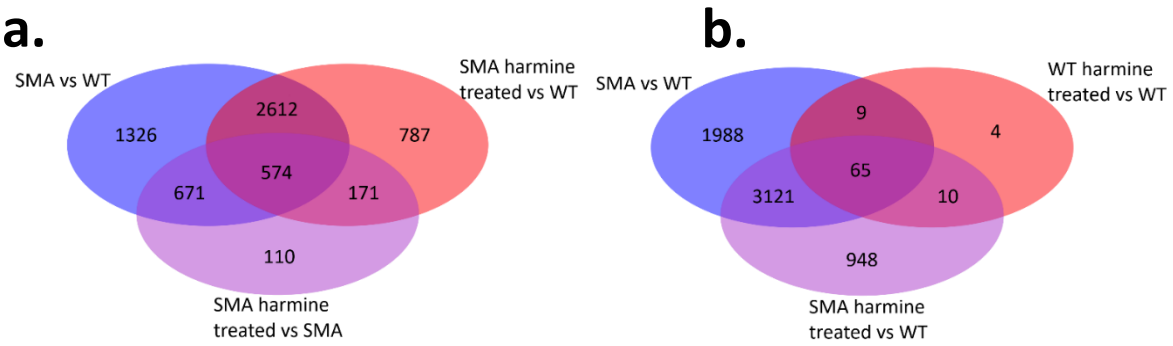


Figure 4.12. Differential gene expression analysis based on the negative binomial distribution (DESeq2). a. Demonstrating overlap of DEG between disease state and treatment, showing rescue of harmine treatment and number of DEG unchanged after treatment. **b.** Illustrating side effects of harmine in treated WT.

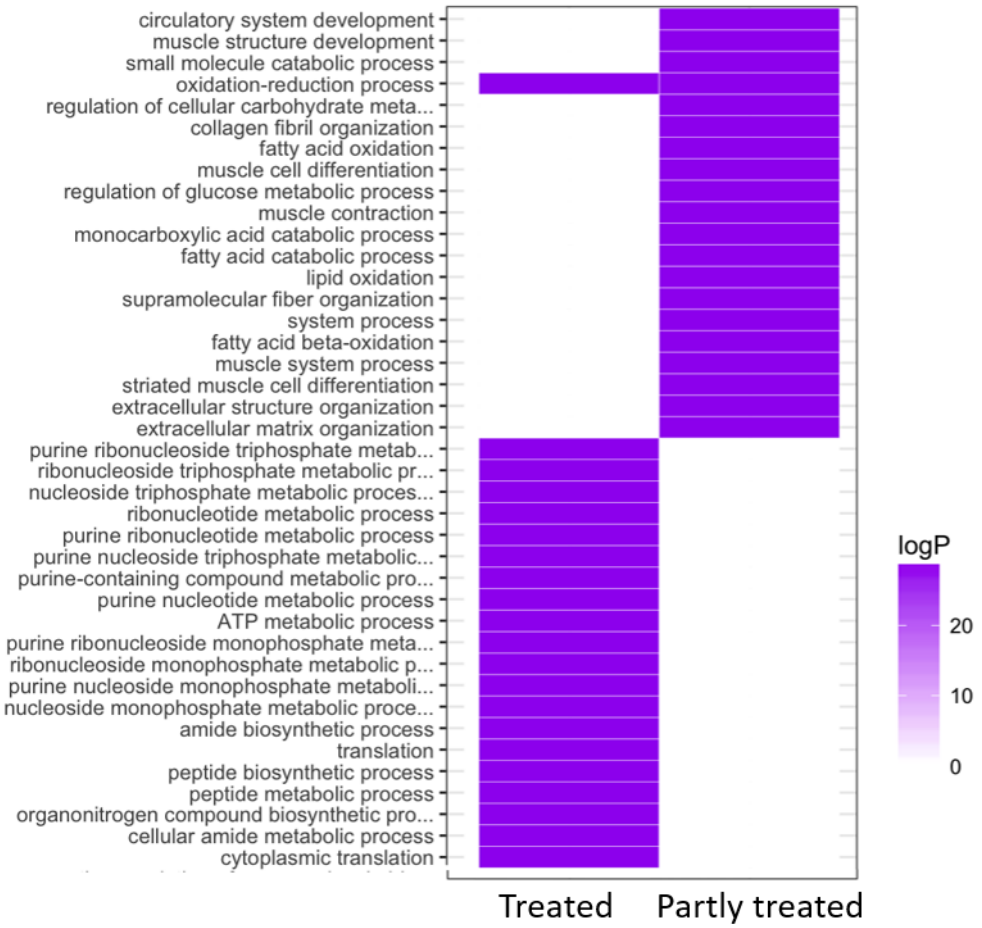


Figure 4.13. Gene Ontology (GO)/Molecular function for genes fully rescued (Table 4.5: 1038 genes) and partly rescued (Figure 4.12a: 574 genes) by harmine treatment in skeletal muscle.

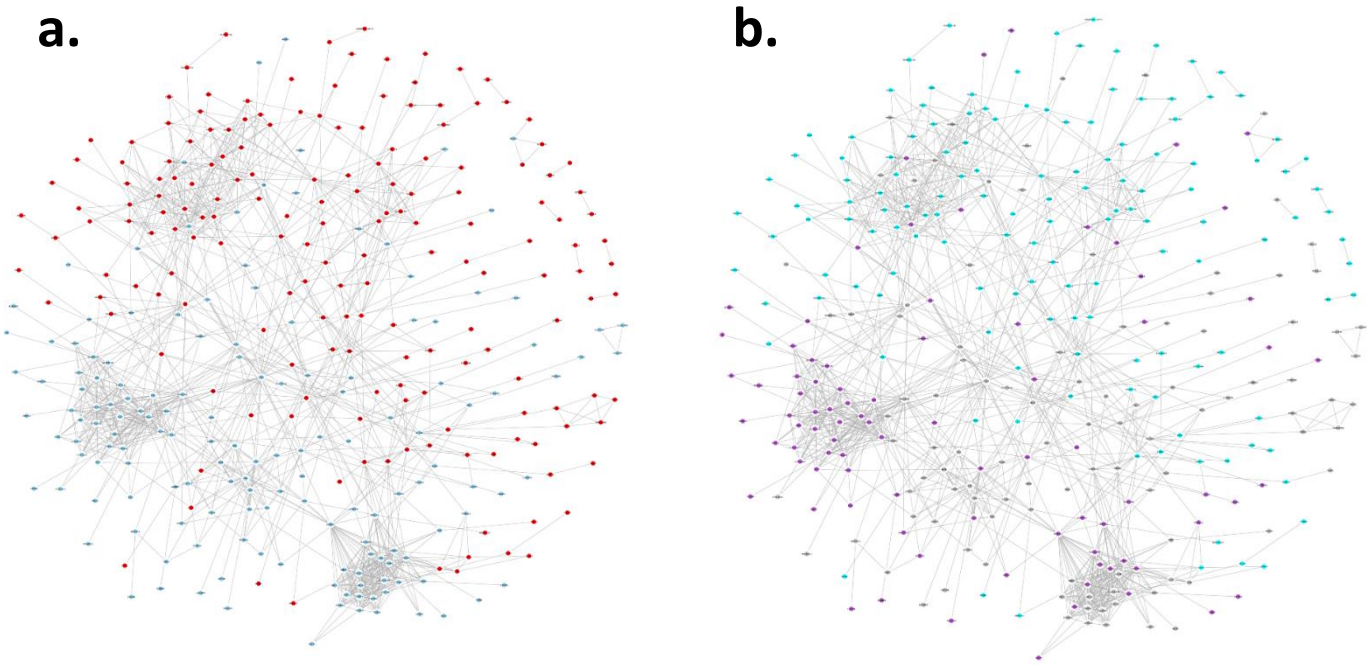


Figure 4.14. Network pathway analysis using a Phenotypic-Linkage Network. a. Clustering of DE genes (SMA vs. WT, top best 500 genes). Genes are colored by disease: red nodes = upregulated in SMA, light blue nodes = downregulated in SMA. **b.** Genes are colored by harmine effect: purple nodes: upregulated after harmine treatment, cyan nodes: downregulated after harmine treatment, grey: unchanged.

4.4 Discussion

SMN restoration therapy is the main treatment for SMA and is particularly successful in early-diagnosed patients. However, it is not a cure and patients will most likely have a less severe version of SMA after SMN restoration therapy. Furthermore, the treatment is suboptimal for later-in-life diagnosed patients as there is a limited therapeutic window (Chapter 1, Section 1.4.9). Therefore we aim in this study to identify treatments that will alleviate skeletal muscle pathology in SMA, that can be used in combination with SMN restoration therapies. We identified the repositioning strategy CMap as a tool to detect numerous potential therapies based on proteomic and transcriptomic data for the treatment of skeletal muscle pathology in SMA.

4.4.1 Capability of CMap analysis to find therapeutic options for SMA

The purpose of CMap is to identify associations between gene expression profiles for a disease and a drug treatment states, by linking gene expression patterns associated with the disease state with corresponding patterns derived from drug-treated cell lines. Although this is a straight-forward approach, there are some critical points to keep in mind while using CMap's predictive value for identifying new treatments. First, CMap analysis relies on signature genes in a disease condition that can be reversed by compounds that have opposite signature genes. The parameters for signature genes can be influenced by population size, the cell line being studied, disease severity or differential gene expression methods, creating a test-set bias [476]. Second, CMap analysis ignores gene interactions and pathways by which the genes are regulated and only uses gene expression signatures [477]. Third, CMap ignores gene function, thereby possibly finding compounds that reverse gene dysregulations that eventually do not play a major role in the disease pathology and ignoring genes with a particular function that are important. It is also important to be aware of possible side effects of the compounds proposed by CMap. Many of the compounds that were predicted to have positive effects on SMA muscle were chemotherapies. This therapeutic approach is not feasible in SMA, considering the weak condition many patients are in and the many side effects these treatments present.

To overcome these problems, we decided to not only do CMap analyses, but also gene ontology analyses to investigate biological processes rescued by harmine treatment (discussed further in Section 4.4.4 and 4.4.5). Furthermore, we validated our selected compound, harmine, by validating reference genes (Section 4.4.2). Another validation of the CMap method is the identification of therapies already considered for the treatment of SMA such as Salbutamol [437], alsterpaullone [83], trichostatin A [95], Valproic acid [318–322], Vorinostat [327,328] and sodium phenylbutyrate [325].

These compounds have all proven to increase full-length SMN, but also demonstrate other beneficial effects in SMA patients such as neuroprotection and muscle strengthening. Salbutamol (known in the US as albuterol) , a β2-adrenoceptor agonist (β2-agonist), has been FDA approved for asthma and has been evaluated in studies with different muscle disorders, such as facio-scapulo-humeral muscular dystrophy [478] or congenital myopathies [437,479]. Salbutamol is also used as doping in athletes because it increases peripheral muscle contractility, improves force recovery after a localized endurance exercise and it reduces fatigability [480]. In SMA, salbutamol treatment has proven to increase full-length *SMN2* transcripts in patient fibroblasts and to improve muscle strength in SMA patients [437,481]. HDAC inhibitors trichostatin A [95], Valproic acid [318–322], Vorinostat [327,328,482] and sodium phenylbutyrate [325] not only correct *SMN2* splicing, but also demonstrate neuroprotective properties. Alsterpaullone is a small molecule that increase full-length SMN in patient fibroblast [83] and has neuroprotective functions by inhibiting glycogen synthase kinase (GSK-3β), which is involved in regulating protein stability [483]. It is unclear if these compounds were ranked so high in the CMap analyses because of their effect on full-length SMN or because of their effect on pathways involving neuroprotection and muscle strength, although it is likely that it was based on a combination of these two. These findings underscore the capability of CMap to identify relevant therapeutic options for the treatment of SMA.

4.4.2 Harmine

Based on the CMap analysis we chose to study harmine further as our proof of concept that CMap analyses can be used to find treatments for SMA. Harmine had large negative CMap scores, meaning

it was predicted to have a large opposite effect on the disease signature of SMA. Also, other compounds closely related to harmine, originating from the same plant Peganum Harmala had large negative scores.

To validate the effects of CMap, we first investigated eight genes and proteins that were according to the CMap analysis dysregulated in SMA vs. WT, then we studied the effects of harmine treatment on these genes *in vitro* and *in vivo*. Some of our validation genes were unchanged after harmine treatment, both *in vivo* and *vitro*. This is not surprising, as CMap is based on certain instances, meaning four cell lines are used in CMap, which are treated with different doses of the compounds. These compounds may have a distinct effect on a particular gene in one cell line than the other or even *in vivo*. Overall, we found that all our validation genes were dysregulated in SMA and ~60% could be rescued by harmine treatment.

Since harmine was identified by CMap analyses as a potential treatment for skeletal muscle in SMA, a special interest in this chapter is the effect of harmine on skeletal muscle. Although harmine has been investigated in the atrial muscle [484], any direct effects of harmine on skeletal muscle pathology have yet to be explored. However, harmine treatment in a mouse model for myotonic dystrophy type 1 (DM1), a long-term genetic muscular disorder, corrected splicing of mis spliced DM1 genes, TNNT2 and INSR, in skeletal muscle [470]. Harmine treatment *in vitro* in DM1 and WT human myoblasts resulted in similar alternative splicing of these genes [470]. In our study, we found upregulation of full-length *SMN*, but not total *SMN*, implying that harmine treatment possibly had an effect on alternative splicing of *SMN2*. Another finding in our study is that harmine treatment increased myofiber size in our severe SMA mouse model. Histology demonstrated that harmine treatment did not restore percentages of fibers with internalized nuclei in DM1 mice skeletal muscle, which might have been due to the short treatment duration of only 14–16 h [470]. Also, myopathy in DM1 is different than in SMA and we investigated myofiber size, whereas the DM1 study investigated internalized nuclei. One of the main reasons why harmine was chosen to study further is because of its neuroprotective effects, since the

main pathology in SMA is motor neuron pathology. Various studies show neuroprotective properties of harmine after brain damage caused by MPTP and MPP+ treatment, as harmine treatment attenuated the induced mitochondrial damage and inhibited dopamine-induced mitochondrial damage and PC12 cell death [485,486]. The researchers of these studies propose that the effects of harmine in these studies are mediated through a scavenging action on reactive oxygen species (ROS) and inhibition of monoamine oxidase and thiol oxidation [486]. Harmine also ameliorated functional impairment and neuronal death after traumatic brain injury by controlled cortical impact in rats [457]. Harmine treatment in this study attenuated cerebral edema and improved learning and memory. Furthermore, expression levels of interleukin 1β and tumor necrosis factor α was reduced, thereby constricting apoptotic neuronal death in the hippocampus. Harmine treatment in rats with traumatic brain injury increased the protein expression of GLT-1 [457]. Glutamate is an excitatory amino acid neurotransmitter in the CNS and upregulation of glutamate is associated with neuronal cell death in acute brain trauma and neurodegenerative diseases. Increase of glutamate transporters such as GLT-1, is protective *in vitro* and delays neurotoxicity *in vivo* in these conditions. This has also been proven in ALS [469]. Indeed, a study in ALS and WT mouse models showed that harmine treatment increased GLT-1 protein and glutamate transporter activity *in vivo* [458]. Mice were treated from P90 until P100 with either a 10mg/kg or 30mg/kg dose of harmine twice per day via an intraperitoneal injection and no tremors were reported. A study in an ALS rat model showed a decrease in neuronal death and upregulation of GLT-1 after brain injury when animals were directly after injury once treated with a 30mg/kg dose of harmine [456] and no tremors were reported. Reduced glutamate transporter activity throughout the CNS is also demonstrated in SMA patients [487]. We confirmed this reduced glutamate transporter activity in spinal cord tissue from the severe SMA mouse model. We further found that harmine treatment significantly increased GLT-1 protein expression and reduced motor neuron death in severe SMA mice.

Momentarily, the only approved treatment for SMA is Spinraza, which needs to be delivered by a lumbar puncture. This administration technique is invasive and less-than-ideal for SMA patients as it

presents side effects. Also, SMA patients are often very weak and suffer from scoliosis, which makes it technically more challenging to perform a lumbar puncture [488]. Therefore, it is crucial that any medication used in combination therapy with SMN restoration can be delivered in a non-invasive way. The fact that harmine exerts CNS effects, can penetrate the blood-brain barrier and has neuroprotective properties [456–458,485,486], makes it an interesting therapeutic option for SMA, as SMA is characterized by motor neuron death. In this study, we treated mice by oral gavage, which exerted effects on a molecular and histological level, both in the CNS (measured by GLT-1 expression and motor neuron count) and in skeletal muscle.

Despite the positive effects harmine showed in both severe and moderate SMA mouse models, harmine is not suited for therapeutic application itself. Indeed, we had to terminate treatment in the moderate mouse model because of the occurrence of tremors after three weeks of daily treatment. Another known pharmacologic effects of harmine is hallucinogenesis [439]. Toxicity and side effects are issues that require medicinal chemistry optimization. However, in our research we found only 88 genes that were dysregulated between WT untreated and WT harmine-treated mice and only 14 DEG that were dysregulated between WT untreated and WT harmine-treated mice but not in SMA mice. Further research is necessary to entangle the exact influence of these genes to generate a chemical version of harmine that does not exert side-effects.

In conclusion, our data indicate a rescue of muscle pathology in the severe SMA mouse model and an induction of GLT-1 expression by harmine treatment which resulted in protection of motor neurons and increased lifespan.

4.4.3 Effects of harmine on SMN expression

In this study, we used CMap analyses to find SMN-independent pharmacological compounds. We nevertheless decided to investigate the effects of harmine on SMN expression for two reasons: 1. As harmine treatment had an effect on mis-splicing in myotonic dystrophy type 1, we were interested if

harmine treatment would also correct *SMN2* splicing [470]. 2. CMap analysis is based on the genetic signature of a disease. The main dysregulated gene and protein in SMA is SMN, therefore, CMap is likely to predict compounds that are also upregulating SMN.

We investigated the effects of harmine on SMN expression in various cell lines. As the two murine cell lines we used did not have *SMN2*, we investigated murine *Smn*. However, murine *Smn* mRNA expression was upregulated in a dose-dependent manner after harmine treatment. Harmine treatment in patient myoblasts significantly increased full-length *SMN*, but not total *SMN*. Harmine treatment in the *Smn*$^{-/-}$;*SMN2*$^{+/-}$ mice, which have the human *SMN2* gene, also showed upregulation of full-length *SMN*, and not total *SMN* in skeletal muscle. However, no increase of SMN protein was found after harmine treatment in skeletal muscle. Therefore, the positive effects of harmine on weight, survival and skeletal muscle morphology must most likely be because of effects of harmine on other genes and proteins.

4.4.4 Pathway analysis demonstrates pathways rescued by harmine treatment

Harmine treatment had positive effects on weight, survival and myofiber size in SMA mice. Since these effects were not likely caused by an increase of SMN (as SMN protein did not increase), we investigated the effects of harmine treatment on SMA by a pathway analysis using RNA sequencing on treated *Smn*$^{-/-}$;*SMN2*$^{+/-}$ skeletal muscle. We found that ~20% of genes that were differently expressed between untreated *Smn*$^{-/-}$;*SMN2*$^{+/-}$ and WT mice were rescued in harmine-treated *Smn*$^{-/-}$;*SMN2*$^{+/-}$ mice vs. WT mice and ~10% of differently expressed genes were partly rescued. The network pathway analysis confirms that main processes of SMA have been treated by harmine treatment. As is discussed in Chapter 1, Section 1.1.4.1, oxidative stress is one of the disease modifiers in SMA and is found in *Smn*$^{-/-}$;*SMN2*$^{+/-}$ mice [203] and in SMA Type 1 patient fibroblasts [489]. One of the processes dysregulated in SMA that was fully rescued after harmine treatment is oxidation-reduction (redox). Whereas oxidative stress refers to elevated intracellular levels of reactive oxygen species (ROS) that cause damage to lipids, proteins and DNA, redox processes refer to low levels of ROS and

are critical for cell viability, activation, proliferation and organ function [490,491]. Many of the other rescued processes are involved in metabolism. As discussed in Chapter 1, Section 1.3.4.2 and Chapter 5, glucose metabolism is affected in SMA [263–266,271], potentially because skeletal muscle is the largest insulin-sensitive tissue in the body and is involved in glucose utilization [270]. Another biological process that is disturbed in SMA and rescued by harmine treatment is translation. A recent study identified SMN-dependent translation defects that are cell autonomous in *Smn*$^{-/-}$;*SMN2*$^{+/-}$ mice [385]. However, not all genes and pathways were rescued after harmine treated SMA mice compared to WT mice. Therefore, we can see an improvement but not a complete reversal effect of harmine on SMA DEG in skeletal muscle.

4.4.5 The effect of harmine treatment on skeletal muscle in SMA

Our study demonstrated various positive effects of harmine treatment on skeletal muscle in SMA. Harmine treatment increased overall health in both the severe *Smn*$^{-/-}$;*SMN2*$^{+/-}$ and moderate *Smn*$^{2B/-}$ mice SMA mouse models. Harmine treatment also enlarged myofiber size in *Smn*$^{-/-}$;*SMN2*$^{+/-}$ mice. As to be expected as our analysis was in muscle, the pathway GO analysis demonstrated that harmine had many positive effects on muscle related processes, such as muscle structure development, muscle contraction, muscle system process and muscle cell differentiation. As discussed in Chapter 1 Section 1.3.3, skeletal muscle is severely affected in SMA and abnormal myogenic processes have been reported in young SMA patients [236]. Problems with proper muscle contractions and muscle weakness have been reported in various mouse models [395,492] and are associated with a delay in the transition from neonatal to adult isoforms of proteins important for proper muscle contractions, such as sodium channels and ryanodine receptors [395]. Harmine treatment improved DEG involved in muscle contractions. Furthermore, muscle differentiation was partly rescued after harmine treatment. Previous research has shown that reduced levels of Smn lead to a profound disruption in the expression of myogenic genes and differentiation is dysregulated in different SMA models [145,492] . This

work highlights the capability of CMap analyses to find treatments for skeletal muscle pathology in SMA.

4.4.6 Conclusion and future directions

Instead of focusing on a particular pathway or gene, in this project we proposed a non-biased approach in which pharmacological compounds are selected, based purely on their effects on genes in human cells, using CMap analyses. CMap analyses of skeletal muscle proteomic and transcriptomic datasets uncovered numerous potential treatments for SMA, including treatments already tested in clinical and preclinical studies. Proof-of-concept assessment of harmine shows promising effects *in vivo* and *in vitro*. Harmine treatment increased weight and survival in severely affected SMA mice and rescued myofiber size in skeletal muscle.

While harmine was our proof-of-concept that CMap analyses can be used to find treatment for SMA that can be used in combination with SMN restoration therapy, we have generated an extensive list of drugs that can similarly be evaluated alone or in combination with SMN therapies. This could potentially open up new therapeutic opportunities for future studies.

5. Results III

Defining a role for the TWEAK/Fn14 pathway in muscle pathology in SMA

5.1 Introduction

Although motor neurons are the primary target in SMA, as described in Chapter 1, skeletal muscle is also pathologically affected in SMA. Some of the core muscle pathologies in SMA are denervation induced muscle atrophy caused by motor neuron death [189] as well as intrinsic muscle pathologies starting before denervation such as abnormalities in myogenesis [236] and metabolic dysfunction [263–266]. Metabolism is closely related to muscle health as skeletal muscle is the largest insulin-sensitive tissue in the body and is involved in glucose utilization [270]. In order to search for muscle-specific treatments, a better understanding is necessary about muscle physiopathology in SMA. Tumor necrosis factor-like weak inducer of apoptosis (TWEAK) and its main signaling receptor, the TNF receptor superfamily member fibroblast growth factor inducible 14 (Fn14) [493], play a crucial role in shaping responses to both acute and chronic injury and disease in muscle and is also involved in regulating glucose metabolism [494,495]. The TWEAK/Fn14 pathway has been implicated in ALS muscle pathology [496]. As ALS shows similarities to SMA, such as denervation-induced muscle atrophy [497] and SMA is also typified by intrinsic muscle pathology and metabolic dysfunction, we decided to investigate the potential contributions of TWEAK and Fn14 to muscle pathology in SMA.

TWEAK is fairly ubiquitously expressed and is synthesized as a Type II transmembrane protein but can also be cleaved by proteolytic processing and secreted as a soluble cytokine [498]. Cells can co-express both transmembrane and soluble forms of TWEAK [499]. TWEAK signaling activates the canonical and non-canonical nuclear factor kappa-light-chain-enhancer of activated B cells (NF-κB) pathway [500] (Figure 5.1). The transmembrane TWEAK protein mainly activates the canonical NF-κB pathway,

whereas both TWEAK variants activate the non-canonical NF-κB pathway [501]. Five proteins, RelA (p65), RelB, c-Rel, p105/p50 (NF-κB1) and p100/52 (NF-κB2) form the NF-κB transcription factor family in mammals. They bind to each other to create distinct homo- and heterodimeric complexes that are transcriptionally active [502]. The canonical pathway is activated by extracellular stimuli such as inflammatory cytokines. In this pathway, the IKK complex protein IKKβ phosphorylates IκBα and triggers IκBα polyubiquitination and degradation, thereby allowing NF-κB dimers RelA /p50) to translocate to the nucleus and regulate gene expression. In the non-canonical pathway, the kinase NIK phosphorylates IKKα. IKKα then phosphorylates p100, causing p100 ubiquitination and partial proteasomal degradation, which generates p52. Next, RelB/p52 heterodimers translocate to the nucleus and regulate gene expression [503]. Notably, only pathologically high levels of TWEAK will activate the canonical NF-κB pathway. This will promote myoblast proliferation and inhibit myogenesis, which is especially necessary during the early phases of muscle repair and regeneration that require expansion of number of myoblasts [504,505]. Lower physiological concentrations are unable to activate the canonical NF-κB pathway; they will however, activate the non-canonical pathway. The function of the non-canonical pathway is to promote myogenesis by increasing fusion of myoblasts [500].

Fn14 is a transmembrane protein that is dormant or present in low levels in normal healthy muscle [506]. Atrophic conditions such as denervation stimulate the expression of Fn14 through an increase of Mitogen-activated protein kinase (MAPK), activator protein 1 (AP1) and specificity protein 1 (SP1) transcription factors, leading to the activation of the TWEAK/Fn14 pathway and eventually causing skeletal muscle atrophy [507]. The main role of the TWEAK/Fn14 pathway is shaping tissue responses to disease and injury through the induction of cellular responses, such as pro-angiogenic and pro-inflammatory responses, the regulation of migration and differentiation, and fate of survival and progenitor cells [494,508,509]. In order to do so, TWEAK/Fn14 triggers activation of various downstream signaling pathways.

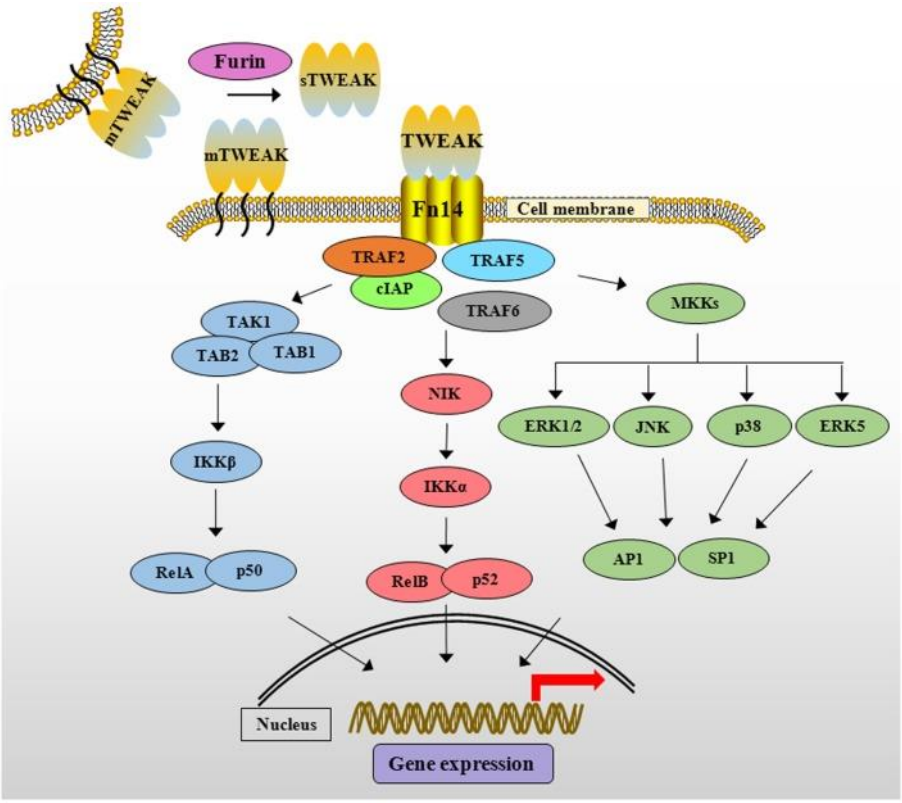


Figure 5.1. The TWEAK/Fn14 signaling cascade. TWEAK cytokine is initially synthesized as membrane-anchored protein (mTWEAK). mTWEAK is then cleaved by furin into soluble form of TWEAK (sTWEAK). Binding of trimeric mTWEAK or sTWEAK to Fn14 receptor leads to the recruitment of cellular inhibitors of apoptosis (cIAPs) and various TNF receptor-associated factors (TRAFs) resulting in the activation of multiple downstream signaling cascades. TWEAK stimulates canonical NF-κB pathway through activation of transforming growth factor β-activated kinase 1 (TAK1) and IKKβ and phosphorylation and degradation of IκB protein. TWEAK activates non-canonical NF-κB pathway through activation of NIK and IKKα leading to proteolytic processing of p100 protein into p52. TWEAK-mediated signaling also causes the activation of various mitogen-activated protein kinase kinases (MKKs), which phosphorylate extracellular signal-regulating kinase (ERK) 1/2, ERK5, c-Jun N-terminal kinase (JNK), and p38 resulting in the activation of downstream transcription factors such as AP1 and SP1. Figure and text adopted from Sato, S., Ogura, Y. & Kumar, A. (2014). *Front. Immunol.* 5, 18.

Various downstream effectors of the TWEAK/Fn14 pathway have shown to play a role in metabolism. TWEAK has a repressive effect on peroxisome proliferator-activated receptor-gamma coactivator 1α (PGC-1α) [494,495,507,510]. PGC-1α plays a major role in the regulation of mitochondrial content, skeletal muscle fiber composition and oxidative metabolism in physiological and pathophysiological conditions

[511–513]. TWEAK represses the expression of PGC-1α in denervated skeletal muscle of mice and overexpression of PGC-1α is able to rescue TWEAK-induced atrophy in myotubes [507]. Recent evidence suggests that PGC-1α may play a role in preserving skeletal muscle mass and mitochondrial content in atrophic states [494,507]. Therefore it is relevant to investigate PGC-1α signaling cascades in SMA, as SMA is also characterized by mitochondrial dysfunction in skeletal muscle (Section 1.3.3). PGC-1α regulates skeletal muscle fiber composition through regulation of the activity of myocyte enhancer factor-2 (MEF2) transcription factors, which are a family of muscle-enriched nuclear factors that are indispensable for muscle differentiation and development [514]. Further evidence of the role of the TWEAK/Fn14 pathway in metabolism is the recent demonstration that transgenic mice specifically overexpressing *Tweak* in skeletal muscle display metabolic abnormalities, including aberrant expression of glucose transporter 4 (Glut4), myogenic transcription factor 2D (Mef2D), hexokinase II (HKII) and Krüppel-like factor 15 (Klf15) [495]. In Figure 5.2, we propose a model for the interactions of TWEAK/Fn14 with downstream effectors based on these studies. Recent research conducted by our group demonstrates a downregulation of Klf15 in SMA mice and pharmacological upregulation of its expression improved disease phenotypes in SMA mice [271]. PGC-1α influences Glut4 expression [515], the major mediator of glucose transport in skeletal muscle by regulating Mef2D. Mef2D and KLF15 bind the promoter of Glut4 and promote its transcription [516], and HKII catalyzes the first phosphorylation step of glycolysis [517]. Glut4 expression is intensely regulated in skeletal muscle so that its level determines whole-body glucose disposal in response to insulin. Glut4 expression is also repressed by denervation [518] and is regulated by innervation [519]. Different studies in mice overexpressing Glut4 specifically in skeletal muscle have demonstrated an improvement in whole-body insulin action, more rapid glucose clearance from the blood and improved glucose homeostasis [520–526]. As abnormalities in glucose metabolism, fatty acid metabolism and pancreatic development are found in SMA (Chapter 1, Section 1.3.4.2) and multiple studies report on the coexistence of diabetes mellitus and diabetic ketoacidosis in SMA patients [264,527,528] we decided to further investigate the TWEAK and Fn14 and metabolic effectors in SMA.

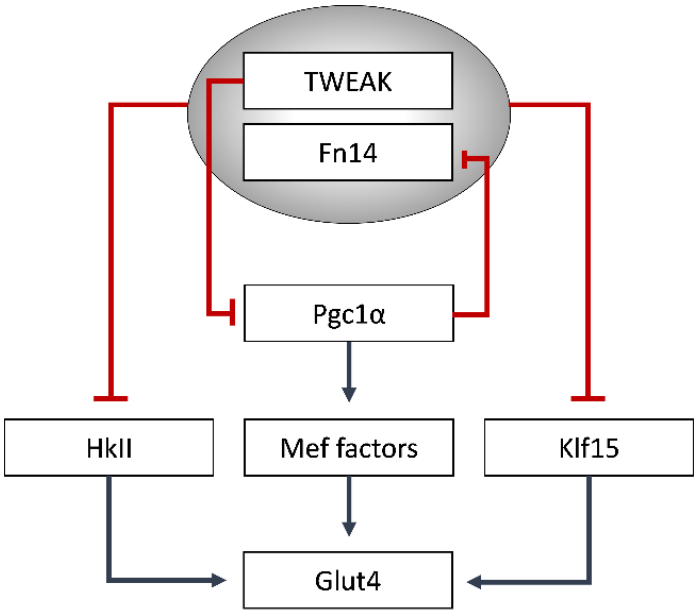


Figure 5.2. Proposed mechanisms of dysregulation of the TWEAK/Fn14 pathway in skeletal muscle leading to muscle pathology and metabolic dysfunction in SMA. Red lines represent repressing effects and blue lines represent promoting effects.

It is presently acknowledged that skeletal muscle atrophy and metabolic defects typify SMA pathogenesis and can be affected by factors other than motor neuron death. While metabolic perturbations have been documented in SMA, the role of muscle as a metabolic tissue in SMA is not fully understood. Further, skeletal atrophy in SMA is often explained by denervation. Considering the complexity of skeletal muscle atrophy, a better understanding of molecular pathways that regulate skeletal muscle atrophy and metabolism in SMA is needed. Much research has been conducted on the role of the TWEAK/Fn14 pathway in damaged muscle, including in denervation-induced atrophy in ALS [496]; however, this pathway has yet to be investigated in the context of SMA. The overall aim of this project is to define the potential role of the TWEAK and Fn14 pathway in SMA pathology and investigate possible connections between TWEAK, Fn14 and SMN.

Hypothesis

Aberrant expression of the TWEAK/Fn14 pathway in SMA muscle promotes and exacerbates muscle atrophy and modulation of this pathway may ameliorate disease pathology.

Objectives

1. Characterize the expression profile of the TWEAK/Fn14 pathway and its downstream effectors in SMA mouse and patient muscle.
2. Investigate if dysregulation of the TWEAK/Fn14 pathway is dependent on denervation, muscle atrophy, developmental stage and/or the presence of *SMN*.
3. Define the role of the TWEAK/Fn14 signaling cascade during myoblast differentiation.
4. Determine the therapeutic potential for modulating the TWEAK/Fn14 pathway as a muscle specific pathway.
5. Investigate similarities of dysregulation in glucose metabolism as well as myopathy and myogenesis pathways between SMA *Smn*$^{-/-}$;*SMN2*$^{+/-}$, *Fn14*$^{-/-}$ and *TWEAK*$^{-/-}$ mouse skeletal muscle.

5.2 Materials and methods

5.2.1 Animals and animal procedures

Evaluation of the TWEAK/Fn14 pathway was executed in *triceps brachii*, *gastrocnemius*, *tibialis anterior* and *quadriceps femoris* of *Smn*$^{-/-}$;*SMN2*$^{+/-}$ and Smn$^{2B/-}$ SMA mouse models. Wild-type mice (FVB/N [366] and C57BL/6J [367]) were used as controls. The skeletal muscles were harvested at various timepoints throughout the disease: birth, pre-symptomatic, symptomatic, late-symptomatic and end-stage (Table 5.2). Mouse Fc-TWEAK, a fusion protein with the murine IgG2a Fc region, and Ig isotope control were kindly provided by Dr. Linda Burkly (Biogen) [369]. Effects of Fc-TWEAK treatment on weight and survival were tested in *Smn*$^{-/-}$;*SMN2*$^{+/-}$ and Smn$^{2B/-}$ SMA mouse models. Heterozygous littermates (*Smn*$^{+/-}$;*SMN2*$^{+/-}$ and *Smn*$^{2B/+}$) were used as healthy controls. Mice were weighed and monitored daily and culled upon reaching their defined humane endpoint. Fc-TWEAK was administered in *Smn*$^{+/-}$;*SMN2*$^{+/-}$ mice by subcutaneous injections using a sterile 0.1 cc insulin syringe at various doses (7.9 µg, 15.8 µg or 31.6 µg) and at a volume of 20 µl every four days. Dose 15.8 µg was further investigated, treating *Smn*$^{-/-}$;*SMN2*$^{+/-}$ mice daily or every other day. *Smn*$^{2B/-}$ mice were treated every four days with a 15.8 µg dose of Fc-TWEAK.

To investigate molecular and histological changes after Fc-TWEAK treatment, *Smn*$^{-/-}$;*SMN2*$^{+/-}$ mice and healthy littermates were subcutaneously injected every day with a 15.8 µg dose of Fc-TWEAK and skeletal muscles were harvested at P7. To investigate molecular and histological changes after Fc-TWEAK treatment, Smn$^{2B/-}$ mice and healthy littermates were subcutaneously injected every 4 days with a 15.8 µg dose of Fc-TWEAK and skeletal muscles were harvested at P15. To reduce the total number of mice used, the fast-twitch *tibialis anterior* and *triceps* muscles from the same mice were used interchangeably for respective molecular and histological analyses.

Smn$^{-/-}$;*SMN2*$^{+/-}$, *TWEAK*$^{-/-}$ knockout [369] and *Fn14*$^{-/-}$ knockout mouse [368] skeletal muscle were used to investigate similarities of dysregulation in glucose metabolism as well as myopathy and myogenesis pathways in P7 skeletal muscle.

5.2.2 Nerve crush

For nerve crush, four P7 WT FVB/N [366] mice were anesthetized with 2% isoflurane/oxygen, then one of their lateral thighs was shaved and a 1 cm incision in the skin was made over the lateral femur. The muscle layers were split with blunt scissors and the sciatic nerve localized and crushed with tweezers for 15 seconds. The skin incision was closed with surgical glue and animals allowed to recover on a warming blanket. Ipsilateral and contralateral TAs were harvested at p14 and fixated in 4% PFA for 24 hours for histological analyses or snap frozen for molecular analyses.

5.2.3 Cardiotoxin

Cardiotoxin γ (Cytotoxin I, Latoxan, L8102, Portes les Valence) was dissolved in 0.9% saline and injected at a concentration of 10 µM in a 4 µl/g per total mouse weight into the left *tibialis anterior* muscle of WT FVB/N [366] mice at P10. The right TA was injected with the same volume of 0.9% saline. During the injection mice were anesthetized with 2% isoflurane/oxygen and all injections were done using a sterile 0.3 cc insulin syringe. TAs were harvested after 3 and 6 days and fixated in 4% PFA for 24 hours for histological analysis. The procedure was then repeated, and TAs were harvested 6 days after injection and snap frozen to investigate molecular changes.

5.2.4 Human skeletal muscle

SMA Type 1 patient and control human *Iliopsoas* and *diaphragms* were collected at autopsy following parental informed consent approved by the Johns Hopkins Medicine Institutional Review Board. Some control human tissues were obtained from the NICHD Brain and Tissue Bank for Developmental Disorders at the University of Maryland, Baltimore, MD. As can be seen in Table 5.1, the age of the

Type 1 SMA patients ranged between 7 weeks and 8 months and the age of the control human tissues ranged between 1.5 weeks and 36 months.

Table 5.1. Age of patients/control humans when skeletal muscles were collected.

	Age in months	Cause of death	Tissue
Control 1	0.3	Unknown	*Iliopsoas*, *diaphragm*
Control 2	0.3	Meconium aspiration	*Iliopsoas*, *diaphragm*
Control 3	19	Unknown	*Iliopsoas*, *diaphragm*
Control 4	36	Transverse Myelitis	*Iliopsoas*, *diaphragm*
Control 5	3.9	Asphyxia by suffocation	*Diaphragm*
Control 6	4	Complications of prematurity	*Iliopsoas*
SMA 1	1.75	SMA Type 1	*Iliopsoas*, *diaphragm*
SMA 2	2.5	SMA Type 1	*Iliopsoas*, *diaphragm*
SMA 3	4	SMA Type 1	*Iliopsoas*, *diaphragm*
SMA 4	8	SMA Type 1	*Iliopsoas*, *diaphragm*
SMA 5	16	SMA Type 1	*Iliopsoas*, *diaphragm*

5.2.5 Small interfering RNA

C2C12 cells were seeded onto 12 well plates at a 50% confluency and cultured overnight in 2 mL of DMEM. Cells were washed with PBS prior to siRNA transfection. For siRNA transfections, 100 pmol of each siRNA (*Tweak*, *Fn14*, *Smn*) (Invitrogen) in a complex with 10 µl of Lipofectamine RNAi/MAX (Invitrogen) dissolved in OptiMEM solution (Gibco) were incubated in C2C12 cells for three hours. The transfection mix was then substituted with either DMEM with 10% FBS/1% Penicillin/Streptomycin or a differentiation medium mix existing of DMEM supplemented with 2% horse serum (Gibco), 1% Penicillin/Streptomycin for either 1, 3 or 7 days until cells were harvested for RNA extraction.

5.2.6 PCR array

RNA from *triceps* and *quadriceps* of *Smn*$^{-/-}$;*SMN2*$^{+/-}$, *TWEAK* knockout, *Fn14* knockout, and WT mice (FVB/N and C57BL/6J) was extracted using the RNeasy® Microarray Tissue Kit. cDNA was made using the RT^2 First Strand Kit. qPCRs were performed using RT² Profiler™ PCR Array Mouse Skeletal Muscle: Myogenesis & Myopathy Mouse (PAMM-099Z, SABiosciences) and RT² Profiler™ PCR Array Mouse Glucose Metabolism (PAMM-006Z SABiosciences). The data were analyzed with RT Profiler PCR Array Data Analysis (version 3.5) and mRNA expression was normalized to the two most stably expressed genes between all samples. We used the publicly available database STRING (version 10.5) for network and enrichment analysis of differently expressed genes [529]. The minimum required interaction score was set at 0.4, medium confidence.

5.3 Results

5.3.1 Dysregulation of the TWEAK/Fn14 pathway expression in SMA

We investigated the expression of the TWEAK/Fn14 pathway in the *Smn$^{-/-}$;SMN2$^{+/-}$* and *Smn$^{2B/-}$* mouse models and in SMA Type 1 patient skeletal muscle.

As mentioned in Section 1.3.3, not all skeletal muscles are equally affected in SMA patients [169,241,242]. A study showed that skeletal muscles have different vulnerabilities to NMJ denervation, with the *triceps brachii* muscle being the most vulnerable, followed by the *gastrocnemius* following, TA and the *quadriceps femoris* [169]. Therefore, we assessed expression of the TWEAK/Fn14 pathway in these skeletal muscles individually in the *Smn$^{-/-}$;SMN2$^{+/-}$* mouse model. Muscles were harvested from *Smn$^{-/-}$;SMN2$^{+/-}$* and WT mice at several timepoints during disease progression as explained in Table 5.2. For *Smn$^{2B/-}$* mice we investigated the TA only. We investigated skeletal muscle from SMA Type 1 patients, the severely affected muscle *iliopsoas*, and the relatively spared *diaphragm* and compared expression to age-matched controls.

Table 5.2. Skeletal muscles were harvested from *Smn$^{-/-}$;SMN2$^{+/-}$* and *Smn$^{2B/-}$* mice at various timepoints during disease progression.

Timepoint	*Smn$^{-/-}$;SMN2$^{+/-}$*	*Smn$^{2B/-}$*
Birth	P0	P0
Pre-symptomatic	P2	P2
Symptomatic	P5	P4
Late-symptomatic	P7	P11
End-stage	P10	P19

We first investigated parvalbumin in the individual muscles. Parvalbumin is a high affinity Ca(2+)-binding protein found in skeletal muscle and has been shown to decrease in denervated muscle [530,531] as well as in symptomatic skeletal muscle from SMA patients and *Smn$^{-/-}$;SMN2$^{+/-}$* mice [532]. We therefore used parvalbumin as a muscle atrophy marker. As is demonstrated in Figure 5.3,

parvalbumin mRNA expression is significantly downregulated in *Smn*$^{-/-}$;*SMN2*$^{+/-}$ mice in the *triceps* and *gastrocnemius* starting at a pre-symptomatic stage and in the TA and *quadriceps* starting from a symptomatic stage (Figure 5.3a–d). *Parvalbumin* was also downregulated in the TA from *Smn*$^{2B/-}$ mice starting at a symptomatic stage (Figure 5.3e).

In SMA Type 1 patient skeletal muscle, we found no dysregulation of *parvalbumin* in spared *diaphragm* tissue (Figure 5.3f), but we found a significant upregulation of *parvalbumin* in the vulnerable *iliopsoas* (Figure 5.3g). This upregulation, rather than downregulation, of *parvalbumin* was surprising, as a previous study observed downregulation of parvalbumin in SMA patient skeletal muscle. In that study, however, a different muscle (*quadriceps*) was investigated and they were from less severely affected Type 2 and 3 SMA patients, which might explain the differential expression. Indeed, there are different hypertrophy levels in different skeletal muscles from SMA Type 1 patients [239]. The upregulation of *parvalbumin* in our study might be due to high hypertrophy levels in the muscle, as parvalbumin acts on the calcineurin-dependent pathway, which plays a major role in hypertrophy [533]. These results underline the findings that not all skeletal muscles are equally affected in SMA [169,241,242] (Section 1.3.3) and that vulnerability is most likely linked to neuromuscular junction denervation [169].

We next investigated the Tweak/Fn14 pathway in skeletal muscle from the *Smn*$^{-/-}$;*SMN2*$^{+/-}$ SMA mouse model and compared the expression to age-matched WT controls at different timepoints (Table 5.2). As demonstrated in Figure 5.4a, there is a downregulation of *Tweak* in *triceps*, TA and *gastrocnemius* starting at a pre-symptomatic stage and continuing until end-stage. However, there are no differences in *Tweak* levels between *Smn*$^{-/-}$;*SMN2*$^{+/-}$ *quadriceps* compared to WT *quadriceps*. This is in accordance with the notion that *quadriceps* are relatively invulnerable muscles in SMA [169]. As demonstrated in Figure 5.4b, *Smn*$^{-/-}$;*SMN2*$^{+/-}$ mice are born with lower levels of *Fn14* compared to WT mice. *Fn14* in *Smn*$^{-/-}$;*SMN2*$^{+/-}$ mice is increased at P2 in *triceps*, which might be due to overcompensation; however,

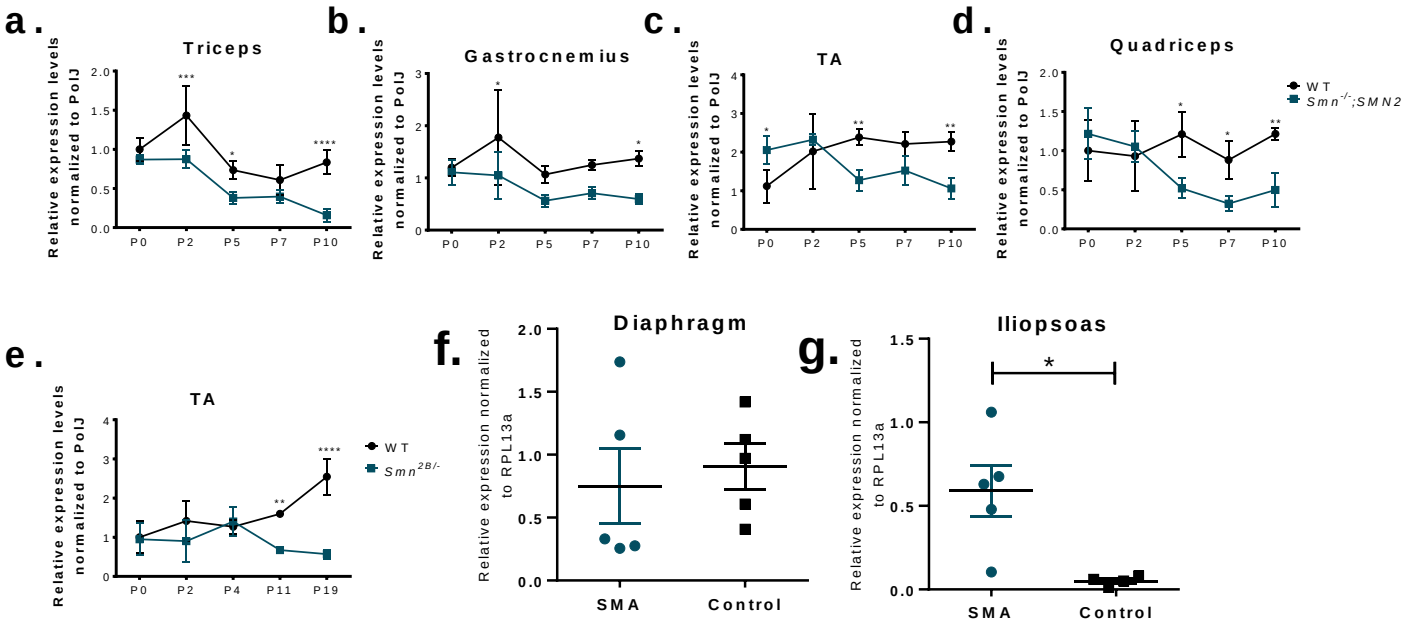


Figure 5.3. *Parvalbumin* mRNA expression in vulnerable and resistant skeletal muscle in SMA. *Parvalbumin* expression during different stages of SMA disease progression in *Smn*$^{-/-}$;*SMN2*$^{+/-}$ mice compared to WT mice in **a.** *triceps*, **b.** *gastrocnemius*, **c.** TA, **d.** *quadriceps* (from most vulnerable to most resistant muscle). Two-way ANOVA, *post hoc*: Bonferroni. **e.** *Parvalbumin* expression during different stages of SMA disease progression in the TA of moderate *Smn*$^{2B/-}$ mice compared to WT mice. Two-way ANOVA, *post hoc*: Bonferroni. **f.** No difference in *parvalbumin* expression between SMA Type 1 patient tissues and age-matched control tissues in the *diaphragm*. Student's *t* tests, not significant. **g.** A significant upregulation of *parvalbumin* in SMA Type 1 *iliopsoas* tissues compared to age-matched control tissues. Student's *t* tests. * $p < 0.05$, * $p < 0.05$, ** $p < 0.01$, *** $p < 0.001$, **** $p < 0.0001$.

Fn14 becomes severely downregulated after P2 and P5 when compared to *Fn14* expression in WT mice. This downregulation of *Tweak* is interesting as atrophic conditions normally stimulate Tweak expression [494,507]. mRNA levels of *Tweak* and *Fn14* were evaluated as we could not find working antibodies to measure Tweak and Fn14 protein quantity.

We further investigated metabolic and muscle effectors that are regulated by the TWEAK/Fn14 pathway. *Pgc-1α* in Figure 5.4c shows an opposite pattern to *Tweak*, whereby when *Tweak* decreases, there is an increase of *Pgc-1α* expression. This is expected because, as is explained in Figure 5.2, TWEAK has a repressing effect on PGC-1α [507] and when this repression is reduced because of lower

TWEAK levels, PGC-1α expression increases. This negative correlation is also illustrated in Figure 5.5, where the differences between *Tweak* and PGC-1α expression between *Smn*$^{-/-}$;*SMN2*$^{+/-}$ and WT mice are plotted against each other.

Figures 5.5a and b show a strong negative correlation between difference of *Pgc-1α* expression in *Smn*$^{-/-}$;*SMN2*$^{+/-}$ vs. WT mice and *Tweak* or *Fn14* expression in *Smn*$^{-/-}$;*SMN2*$^{+/-}$ vs. WT mice. This is in accordance with research from the Kumar group [510] , which shows that PGC-1α can inhibit upregulation of Fn14. Figure 5.4d demonstrates the dysregulation of *Mef2d* in *Smn*$^{-/-}$;*SMN2*$^{+/-}$ mice, which is to be expected since Pgc-1α regulates expression of Mef2. These dysregulations start for most skeletal muscle tested in this study roughly around P5, when also *PGC-1α* expression is upregulated. We see similar movement of *KLF15* (Figure 5.4f) and *HKII* (Figure 5.4g), which are both repressed by *Tweak*. At a symptomatic timepoint, there is an increase of both *KLF15* and *HKII* in most skeletal muscle following the significant decrease of *Tweak*. In accordance to the findings that Glut4 expression is transcriptionally promoted by transcription factors Mef2d [516] and Klf15, and influenced by HKII [517], we found *Glut4* to be upregulated at a symptomatic timepoint in *Smn*$^{-/-}$;*SMN2*$^{+/-}$ mice compared to WT mice (Figure 5.4e).

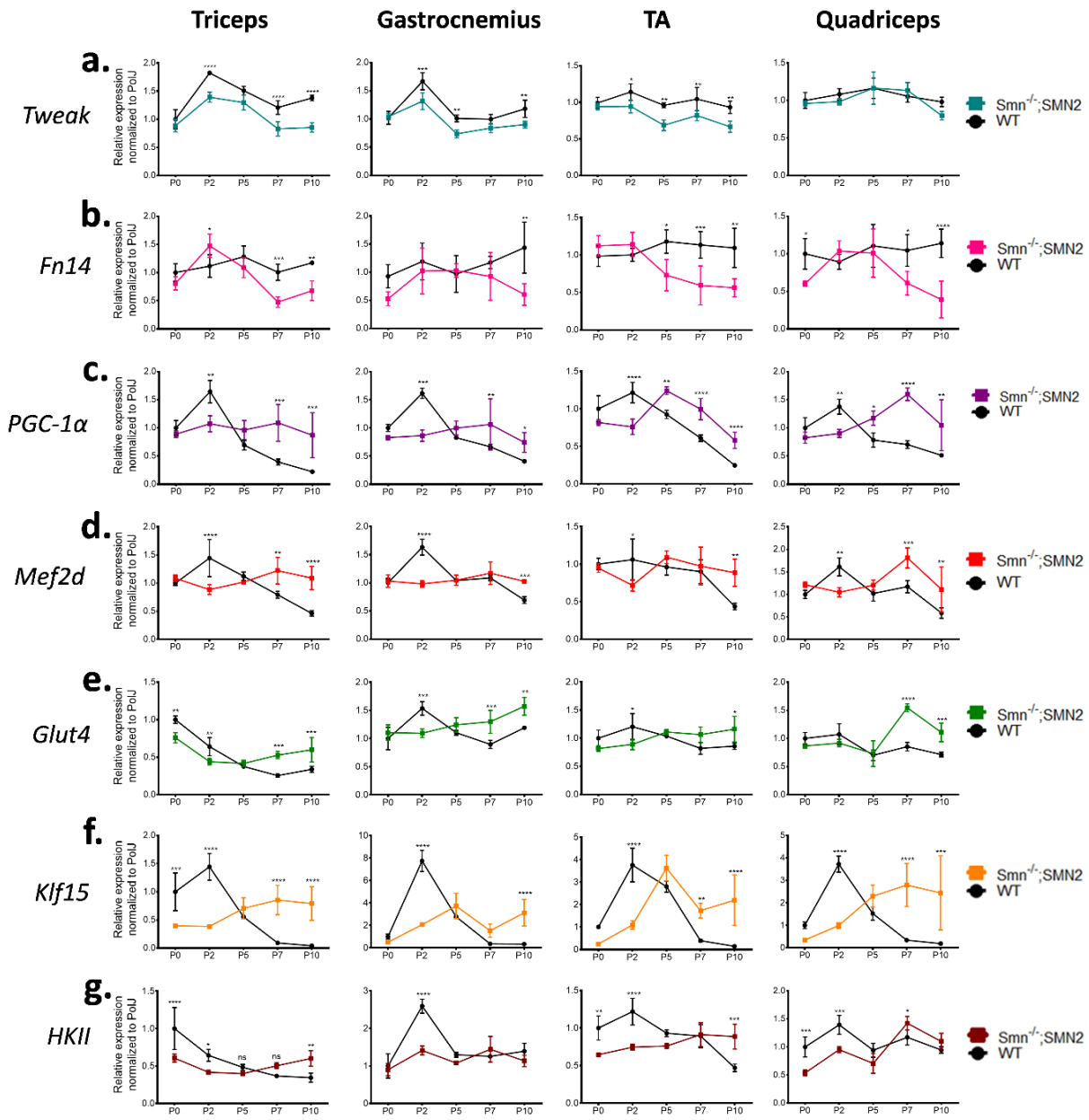


Figure 5.4. Aberrant mRNA expression of the TWEAK/Fn14 pathway in *Smn$^{-/-}$;SMN2* mice. mRNA expression of **a.** *Tweak*, **b.** *Fn14*, **c.** *Pgc-1α*, **d.** *Mef2d*, **e.** *Glut4*, **f.** *Klf15*, **g.** *HKII* in skeletal muscle of *Smn$^{-/-}$;SMN2* mice compared to WT mice. qPCR analyses for five different timepoints: at birth (P0), pre-symptomatic (P2), early-symptomatic (P5), late-symptomatic (P7), end-stage (p10). This was tested in four different muscle: *quadriceps*, *triceps*, TA, *gastrocnemius*. Two-way ANOVA, *post hoc*: Bonferroni, * $p < 0.05$, ** $p < 0.01$, *** $p < 0.001$, **** $p < 0.0001$.

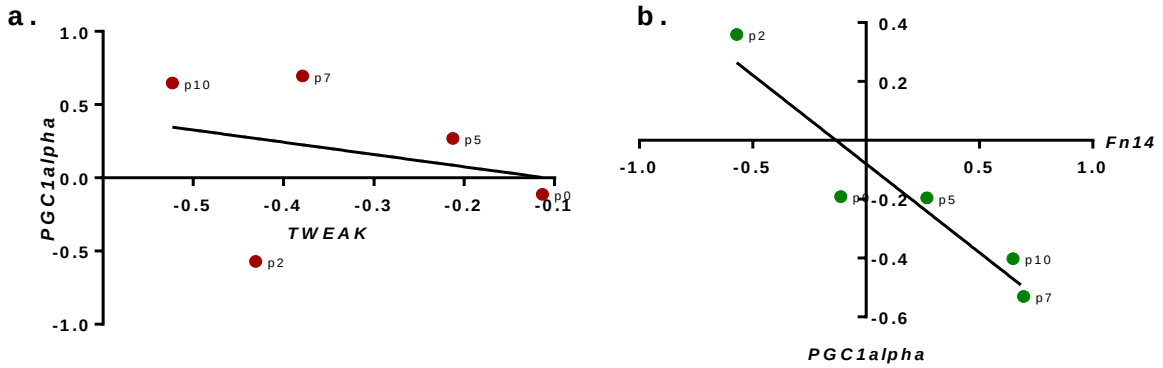


Figure 5.5. Effects of Tweak and Fn14 on Pgc-1α expression displayed in correlation. a. Correlation between *Tweak* (*X*-axis) and *Pgc-1α* (*Y*-axis), measured by differences of *Smn*$^{-/-}$*;SMN2* towards WT mice at 5 different timepoints in *triceps* (R^2 = 0.06816, not significant, without outlier P2 R^2 = 0.8303). **b.** The correlation between *Pgc-1α* (*Y*-axis) and *Fn14* (*X*-axis) measured by differences of *Smn*$^{-/-}$*;SMN2* towards WT mice at 5 different timepoints in *triceps* is significant (R^2 = 0.894, $p < 0.05$).

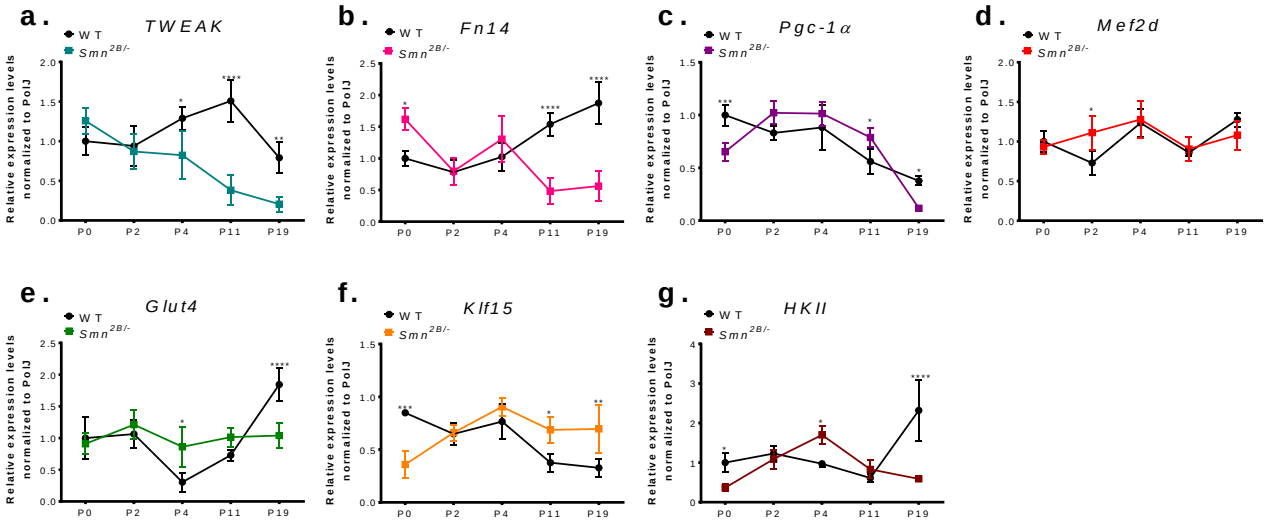


Figure 5.6. Aberrant mRNA expression of the TWEAK/Fn14 pathway in *Smn*$^{2B/-}$ mice. mRNA expression of **a.** *Tweak*, **b.** *Fn14*, **c.** *Pgc-1α*, **d.** *Mef2d*, **e.** *Glut4*, **f.** *Klf15*, **g.** *HKII* in the TA of *Smn*$^{2B/-}$ mice compared to WT mice. qPCR analyses for five different timepoints: at birth (P0), pre-symptomatic (P2), early-symptomatic (P4), late-symptomatic (P11), end-stage (P19). Two-way ANOVA, *post hoc*: Bonferroni, * $p < 0.05$, ** $p < 0.01$, *** $p < 0.001$, **** $p < 0.0001$.

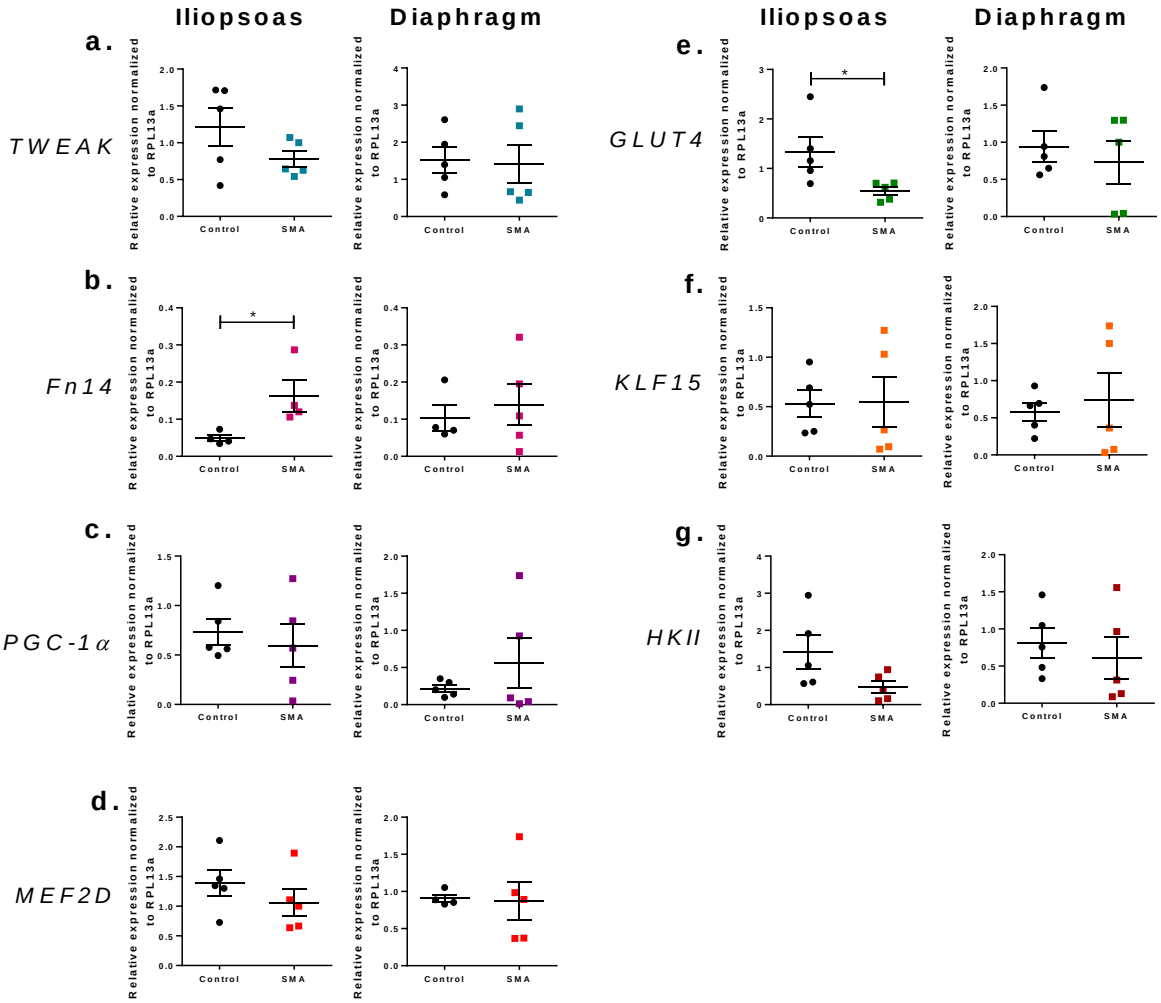


Figure 5.7. mRNA expression of the TWEAK/Fn14 pathway in SMA Type 1 skeletal muscle. mRNA expression of **a.** *Tweak*, **b.** *Fn14* (*Iliopsoas* $p < 0.05$), **c.** *Pgc-1α*, **d.** *Mef2d,* **e.** *Glut4* (*Iliopsoas* $p < 0.05$), **f.** *Klf15*, **g.** *HKII* (*Iliopsoas* $p = 0.08$), in resistant *diaphragm* and vulnerable *iliopsoas* skeletal muscle of SMA Type 1 patients and age-matched controls in the *diaphragm*. Student's *t* tests, $p < 0.05$.

In order to confirm the results found in the severe *Smn*$^{-/-}$;*SMN2*$^{+/-}$ mouse model regarding aberrant TWEAK/Fn14 pathway expression in symptomatic SMA mice, we repeated the experiment in the TA of moderate *Smn*$^{2B/-}$ SMA mouse model. Mice in this model start to exhibit symptoms after P4 and normally have a lifespan of 18–20 days. We found very similar effects in this model compared to the severe SMA mouse model. As is demonstrated by Figure 5.6a and b, both *TWEAK* and *Fn14* were significantly less expressed compared to age-matched WT controls from a symptomatic timepoint onwards. Comparable to what was seen in *Smn*$^{-/-}$;*SMN2*$^{+/-}$ mice, *Pgc-1α*, *Glut4*, *Klf15* and *HKII* (Figure

5.6c,e–g) were significantly upregulated at a symptomatic and/or late-symptomatic timepoint; however, *Pgc-1α*, *Glut4* and *HKII* became significantly downregulated, compared to WT mice, at the end-stage.

We also verified the dysregulation of the TWEAK/Fn14 pathway in SMA Type 1 patients. We compared the expression of the TWEAK/Fn14 pathway in the *iliopsoas*, a severely affected muscle, and the *diaphragm*, a relatively spared muscle, in Type 1 SMA patients and compared these to mRNA expression in age-matched controls. We did not see any differential expression from the TWEAK/Fn14 pathway in the *diaphragm* of Type 1 patients, demonstrating again that this muscle is relatively spared during SMA progression (Figure 5.3f, normal *parvalbumin* levels). As is demonstrated in Figure 5.7, the TWEAK/Fn14 pathway is dysregulated in SMA Type 1 patient affected *Iliopsoas*. It shows a different dysregulation of the TWEAK/Fn14 pathway than the severe (Figure 5.4) and moderate (Figure 5.6) SMA mouse models. *TWEAK* levels are comparable in SMA Type 1 patient and age-matched control skeletal muscle. *Fn14* is significantly upregulated in SMA Type 1 vulnerable *Iliopsoas* muscle (Figure 5.7b), but significantly downregulated in both the SMA mouse models at a symptomatic stage (Figure 5.4b and Figure 5.6b). *Glut4* is significantly downregulated and *HKII* shows a trend towards downregulation in SMA Type 1 vulnerable *Iliopsoas* muscle (Figure 5.7e,g), but significantly upregulated in both the SMA mouse models at a symptomatic stage (Figure 5.4e,g and Figure 5.6e,g). Although this dysregulation in TWEAK/Fn14 pathway occurs in different directions in SMA Type 1 patient and SMA mouse models, they all follow the model proposed in Figure 5.2. TWEAK/Fn14 have a repressive effect on HKII and Glut4, so when Fn14 is upregulated, HKII and Glut4 are downregulated. There are a few factors that could have played a role in the different dysregulation between SMA Type 1 patient skeletal muscle and the severe and moderate SMA mouse models skeletal tissue. The results in these experiments originated from different species (human vs. mouse), different skeletal muscle (*Iliopsoas* and *diaphragm* vs. *triceps*, *gastrocnemius*, TA and *quadriceps*) and possibly different timepoints (postmortem vs. timepoints prior to death). Also, as is shown in Figure 5.3g, *parvalbumin*

was upregulated in SMA Type 1 *Iliopsoas* muscle, in contrast to the downregulation of *parvalbumin* seen in both SMA mouse models (Figure 5.3a–e).

In summary, these findings in SMA Type 1 vulnerable skeletal muscle and in the severe and moderate SMA mouse models suggest that the TWEAK/Fn14 pathway is dysregulated in SMA muscle and also support the model proposed in Figure 5.2, which is based on previous research that TWEAK/Fn14 has a repressive effect on PGC-1α, Mef2d, Klf15, HKII and Glut4 and that PGC-1α has in return a repressive effect on Fn14.

5.3.2 Altered NF-κB activity in severe SMA mice

Since TWEAK levels regulate the canonical and non-canonical NF-κB pathways in skeletal muscle [77], we next investigated if these were also dysregulated in SMA skeletal muscle. We found no difference in activity of the canonical NF-κB pathway in pre-symptomatic P2 *Smn*$^{-/-}$;*SMN2*$^{+/-}$ TAs compared to WT TAs (Figure 5.8a), which is not surprising, as *TWEAK* is not dysregulated at birth in P2 *Smn*$^{-/-}$;*SMN2*$^{+/-}$ TAs compared to WT TAs (Figure 5.4a). However, at P7, there is a significant decreased activity of the canonical NF-κB pathway in symptomatic *Smn*$^{-/-}$;*SMN2*$^{+/-}$ mice compared to WT mice (Figure 5.8b), measured in the TA, which could be due to low *Tweak* levels in *Smn*$^{-/-}$;*SMN2*$^{+/-}$ mice (Figure 5.4a) [500]. Next, we investigated if these low levels of *Tweak* in *Smn*$^{-/-}$;*SMN2*$^{+/-}$ mice influence the non-canonical NF-κB pathway activity. As we could not find functioning antibodies to measure non-canonical NF-κB pathway protein activity, we evaluated mRNA expression levels of NF-κB – inducing kinase, a critical kinase of the non-canonical NF-κB activation pathway [534]. Indeed, we found that mRNA expression levels of NF-κB – inducing kinase are significantly increased in P7 *Smn*$^{-/-}$;*SMN2*$^{+/-}$ TAs compared to age-matched WT control TAs (Figure 5.8c). The NF-κB activity dysregulation that we found in our study may play a major role in SMA skeletal muscle pathology as these pathways normally regulate myoblast proliferation and myogenesis [500,504,505].

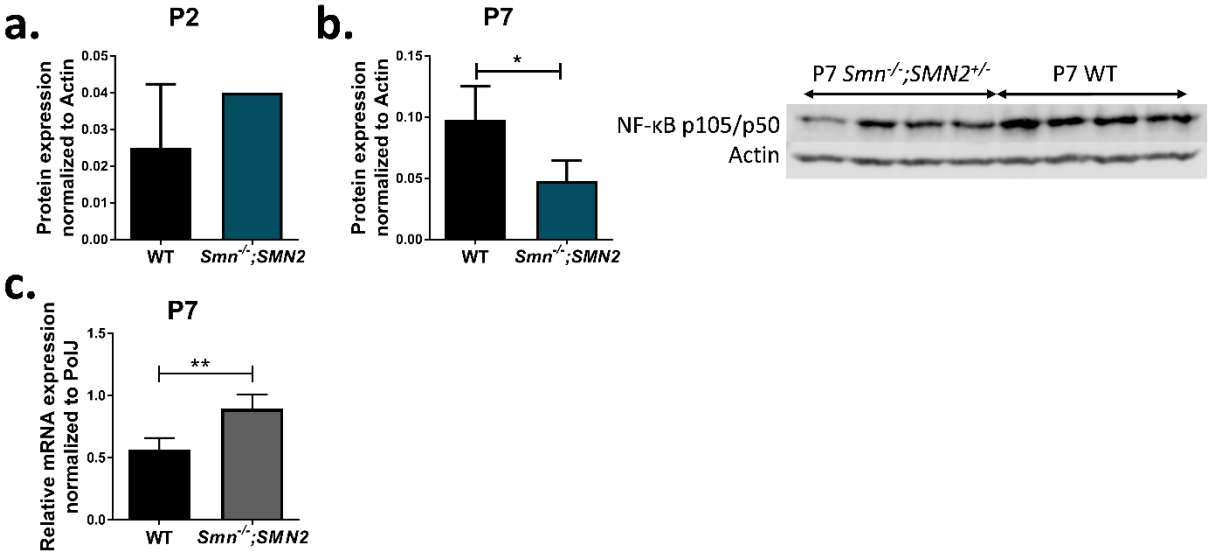


Figure 5.8. The canonical and non-canonical NF-κB pathways are dysregulated in TA of symptomatic P7 *Smn$^{-/-}$;SMN2$^{+/-}$* mice. a. No significant difference in protein expression of the canonical NF-κB protein between pre-symptomatic P2 *Smn$^{-/-}$;SMN2$^{+/-}$* skeletal muscle and age-matched WT skeletal muscle. Graph values indicate the expression of NF-κB p105/p50 vs. actin (loading control). **b.** The canonical NF-κB pathway is downregulated in late-symptomatic P7 *Smn$^{-/-}$;SMN2$^{+/-}$* skeletal muscle compared to age-matched WT skeletal muscle. Representative Western blot for NF-κB p105/p50 and actin (loading control). Graph values indicate the expression of NF-κB p105/p50 vs. actin. Student's *t* tests $p < 0.05$. **c.** NF-κB inducing kinase mRNA expression, a critical kinase of the non-canonical NF-κB activation pathway, is significantly increased in late-symptomatic P7 *Smn$^{-/-}$;SMN2$^{+/-}$* TAs compared to age-matched WT TAs. Student's *t* tests $p < 0.01$.

5.3.3 Dysregulation of the TWEAK/Fn14 pathway is not denervation dependent

As SMA is characterized by denervation due to motor neuron death, we determined if the dysregulation of the Tweak/Fn14 pathway in SMA is denervation-dependent. We performed nerve crush experiments in which the sciatic nerves of WT mice were crushed at P7 and the muscle harvested at P14 [535]. We chose these early timepoints as the SMA models we used in this study have a maximum lifespan of 12 days (*Smn$^{-/-}$;SMN2$^{+/-}$*) and 20 days (Smn$^{2B/-}$). H&E staining was used to visualize the muscle. The myofibers in ipsilateral muscle showed a significant decrease in myofiber size compared

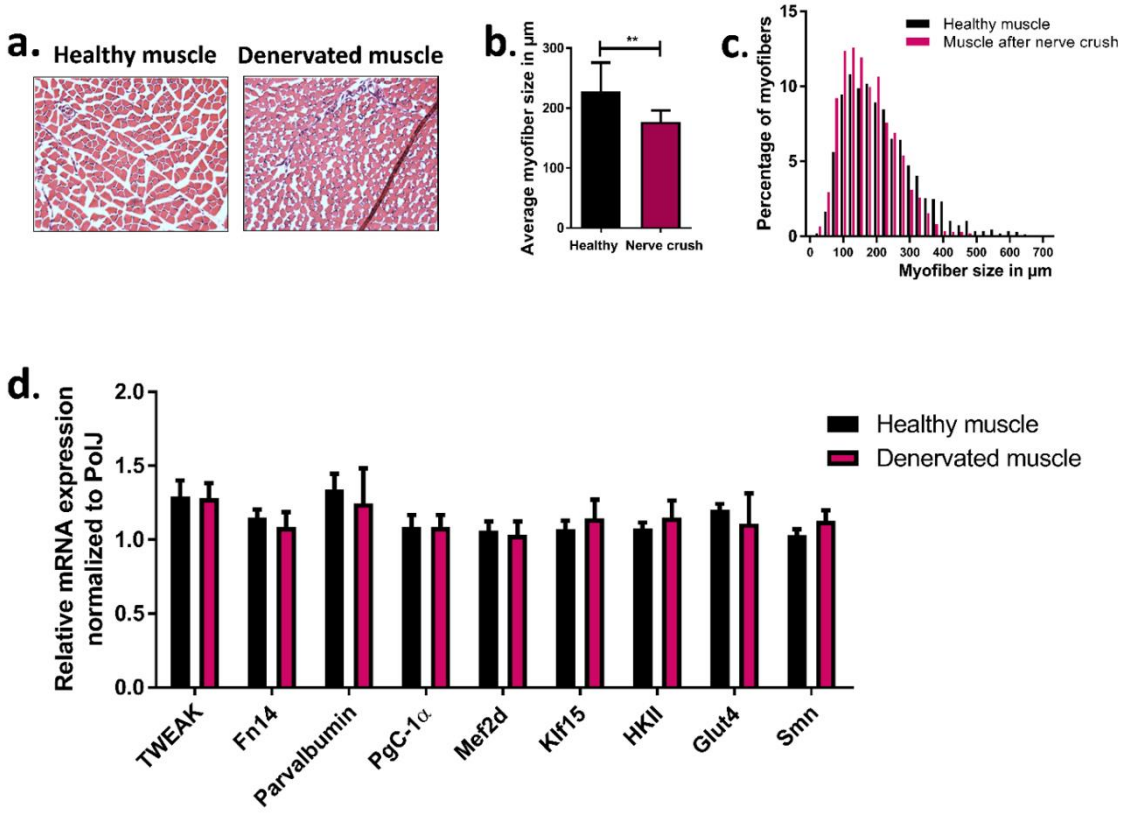


Figure 5.9. Hematoxylin-eosin staining and cross-sectional area analyses of TA muscle fibers after nerve crush. a. Healthy control muscle at the contralateral side of nerve cut shows normal myofiber size and patterns and muscle after nerve cut at ipsilateral side shows smaller myofiber size and atrophy pattern. **b.** Bar diagrams display a significant difference in average myofiber size of healthy muscle and muscle after nerve crush. Student's *t* tests, $p < 0.01$. **c.** Size distribution of percentage of myofibers in µm per group. **d.** mRNA expression of *Tweak*, *Fn14* and downstream effectors of the pathway show no significant difference between nerve crush muscle and healthy control muscle. There was also no difference in *parvalbumin* expression between denervated and healthy muscle. Student's *t* tests, not significant.

to the muscle in the healthy contralateral leg (Figure 5.9a–c). This makes this muscle a suitable control for measuring if the dysregulation of the Tweak/Fn14 pathway and downstream effectors is denervation-dependent or if it is caused by SMA specific variables. Figure 5.10 shows no significant difference in TWEAK/Fn14 pathway expression between nerve crush muscle and healthy muscle. Despite the strong atrophy after denervation, as is demonstrated in Figure 5.9a–c, *parvalbumin* mRNA expression was not significantly downregulated in denervated muscle in this study, as was expected

based on previous studies [530,531]. Overall, these results suggest that the dysregulation of this pathway in SMA is not denervation dependent.

5.3.4 Cardiotoxin-induced myofiber necrosis activates the TWEAK/Fn14 cascade

As the dysregulation of the TWEAK/Fn14 pathway is most likely not denervation dependent (Figure 5.9), we next investigated if impairing muscle integrity and causing myofiber necrosis using cardiotoxin affects expression of the TWEAK/Fn14 pathway. We performed cardiotoxin experiments in P10 WT pups in order to compare results to our SMA mouse models, which have a maximum lifespan of 12 days (*Smn*$^{-/-}$;*SMN2*$^{+/-}$) and 20 days (Smn$^{2B/-}$). The cardiotoxin was injected at a concentration of 10 µM in a 4 µl/g total mouse weight into the left *tibialis anterior* muscle and the right TA was injected with a same volume of 0.9% saline. TAs were harvested after 3 and 6 days so as to investigate the timepoint with the highest degeneration levels [536]. Analysis of the centrally located nuclei/fiber ratio shows, in Figure 5.10a and b, a significantly increased percentage of centrally located nuclei after 6 days following cardiotoxin treatment, but not after 3 days, suggesting regeneration levels are higher after 6 days than after 3. Next, we investigated mRNA expression of the TWEAK/Fn14 pathway 6 days after cardiotoxin induced myofiber injury. Atrophy marker *parvalbumin* was significantly downregulated in cardiotoxin treated TA compared to saline treated TA. *Fn14* expression was significantly increased after cardiotoxin injury, which is in accordance with previous research showing that atrophy conditions activate Fn14 [507]. *Pgc-1α*, *HKII* and *Klf15* expression were significantly downregulated, as is also to be expected, considering the high levels of Fn14. Interestingly, Smn expression was increased in injured muscle. This could be explained by studies showing that there is a requirement for SMN during fiber regeneration [234]. The dysregulations of the TWEAK/Fn14 pathway that we found in this experiment are similar to the dysregulation of the TWEAK/Fn14 pathway that we found in in SMA Type 1 *iliopsoas* muscle (Figure 5.7), in which *Fn14* was upregulated and *Glut4* and *HKII* were downregulated. These muscles were likely hypertrophied as parvalbumin levels were elevated (Figure

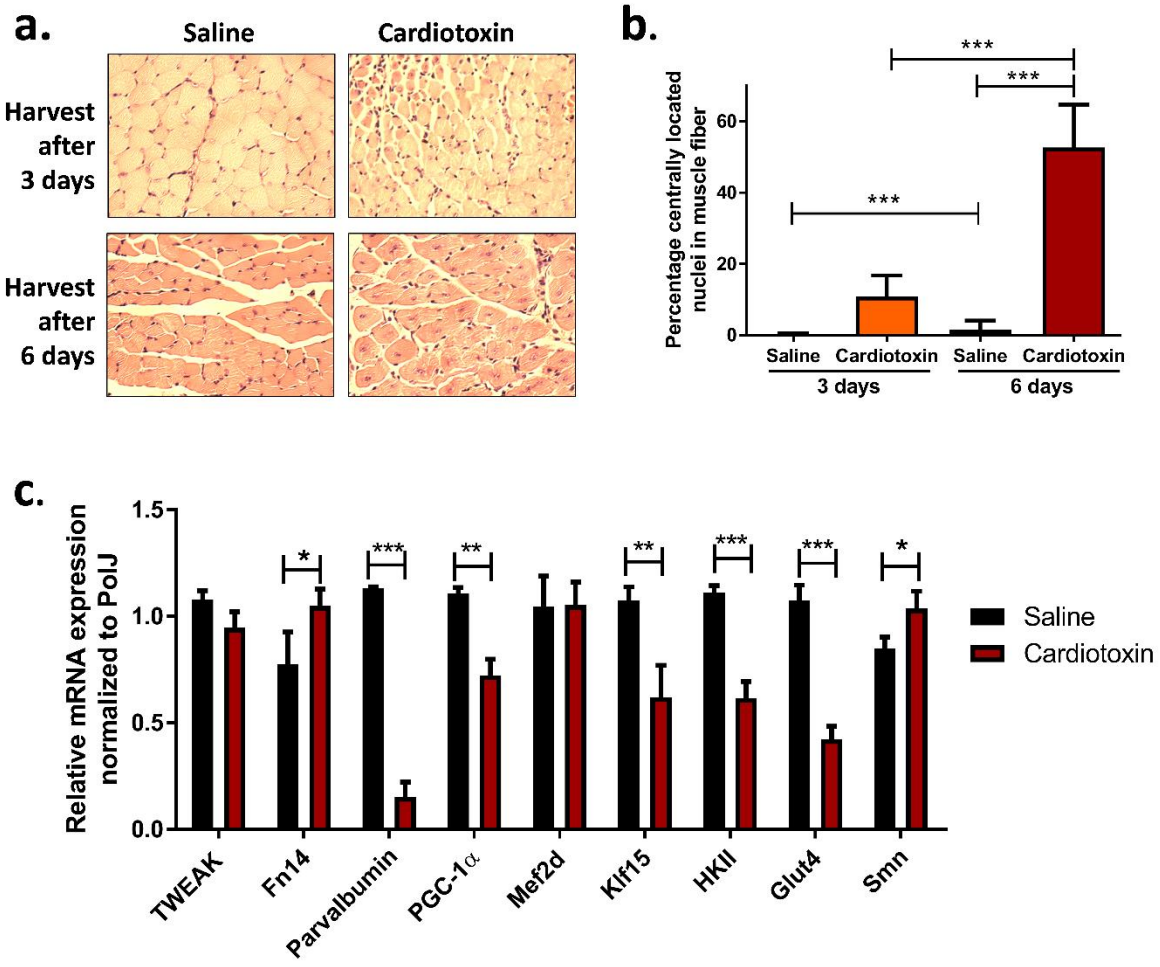


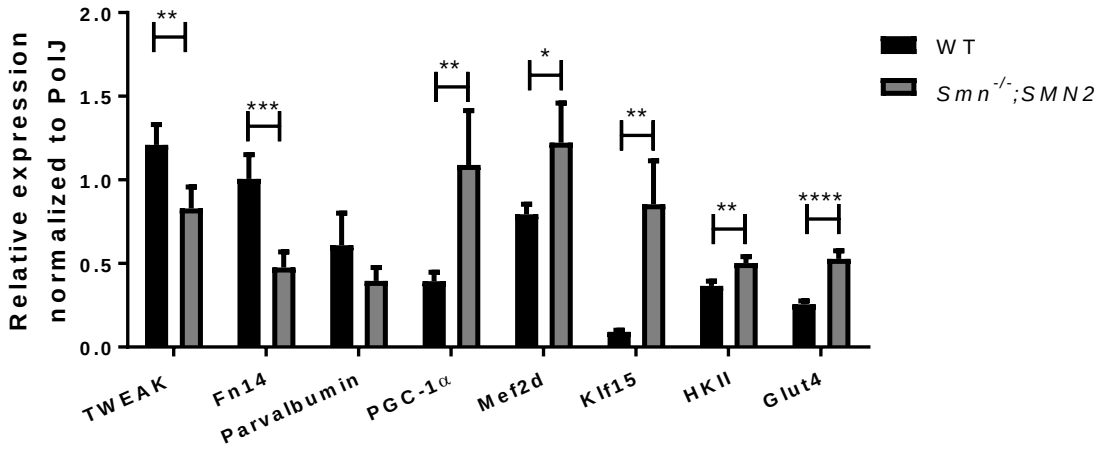
Figure 5.10. Cardiotoxin and saline treatment of *tibialis anterior* muscle in 10-day-old mice. a. Representative hematoxylin-and-eosin (H&E) stains of TA shows centrally located nuclei 6 days after cardiotoxin treatment, but not after 3 days and also not in saline treated TA. **b.** Analysis of the centrally located nuclei/fiber ratio shows a significant rise in percentage of centrally located nuclei after 6 days following cardiotoxin treatment, but not after 3 days, suggesting degeneration levels is higher after 6 days than 3 days. 20x magnification; *n* = 3 mice per group; a one-way ANOVA was used for analyses. **c.** mRNA expression of TWEAK/Fn14 pathway showing a significant increase in *Fn14* and significant decrease in *Pgc-1α*, *Klf15*, *HKII* and *Glut4*. Atrophy marker *parvalbumin* was significantly decreased in cardiotoxin-treated TA tissue. Student's *t* tests, * $p < 0.05$, ** $p < 0.01$, *** $p < 0.001$.

5.3f), which could explain the similarities of results, as hypertrophy and regeneration (in this experiment caused by cardiotoxin injury) are closely linked [537]. Together, these results demonstrate that TWEAK/Fn14 dysregulation is likely partly dependent on intrinsic myopathy as the pathway was dysregulated in cardiotoxin damaged muscle.

5.3.5 Relationship between Smn, Tweak and Fn14 *in vivo*

To further understand the relationship between TWEAK, Fn14 and Smn in skeletal muscle, we compared mRNA levels of the TWEAK/Fn14 pathway in the skeletal muscle of *Smn$^{-/-}$;SMN2$^{+/-}$*, *Fn14$^{-/-}$*, *TWEAK$^{-/-}$* and WT mice. As is demonstrated in Section 5.3.2, the TWEAK/Fn14 pathway is severely dysregulated in *Smn$^{-/-}$;SMN2$^{+/-}$* at P7 in *triceps* (also shown in Figure 5.11a). P7 mice lacking *Tweak* (*TWEAK$^{-/-}$*) demonstrated a significant increase of *Fn14*, while *Klf15* was significantly downregulated in *triceps* (Figure 5.11b) and *Fn14* knockout mice (*Fn14$^{-/-}$*) demonstrated an upregulation of *Pgc-1α* (Figure 5.11c) Atrophy marker *parvalbumin* was unchanged in P7 *triceps* in *Fn14$^{-/-}$* and *TWEAK$^{-/-}$*, which was to be expected, as *TWEAK$^{-/-}$* mice show no overt structural differences in skeletal muscle in the first three months after birth [538] and *Fn14$^{-/-}$* mice do not express a muscle phenotype at all [539]. *Smn* expression levels were significantly decreased in *TWEAK$^{-/-}$* mice (Figure 5.11b). This suggests a connection between SMN and the TWEAK/Fn14 pathway in SMA.

a.



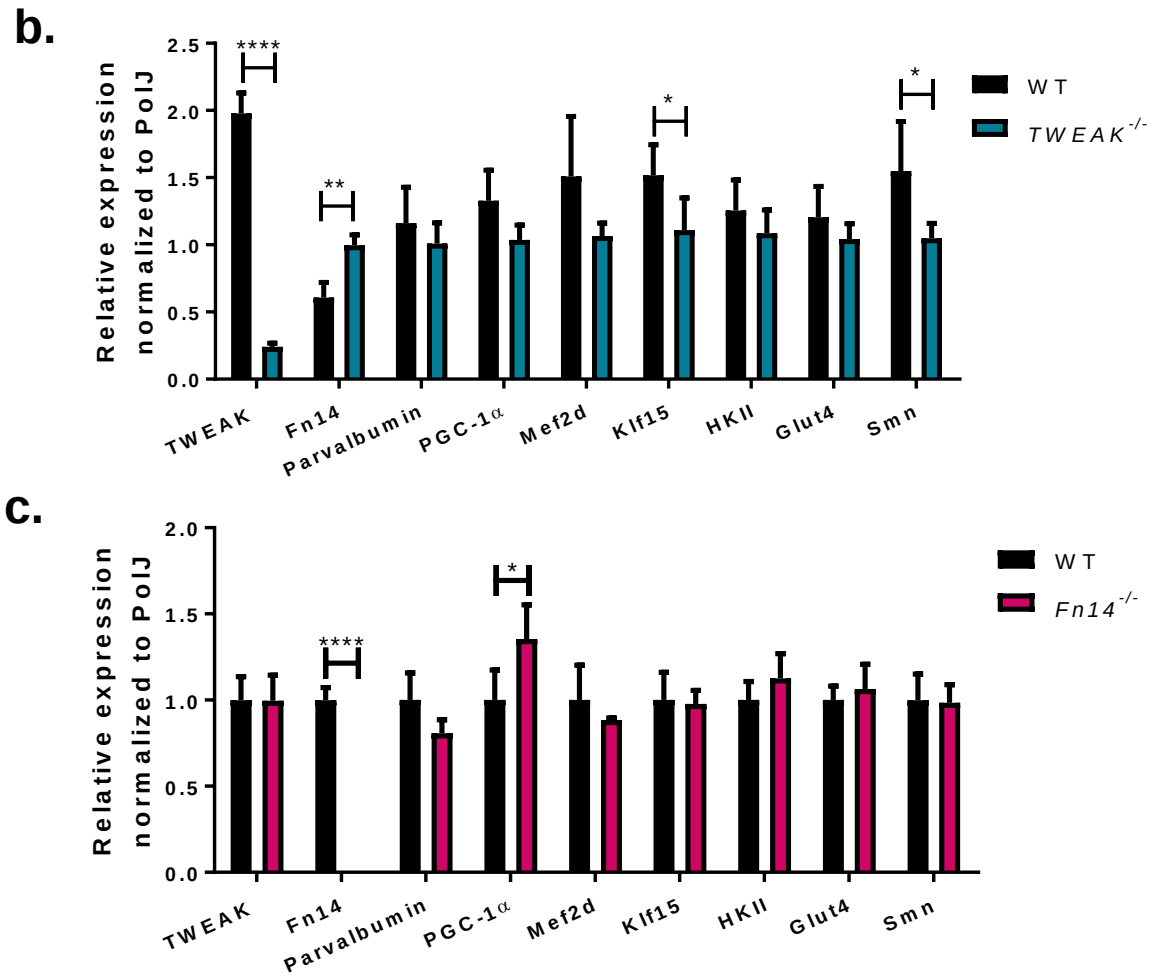


Figure 5.11. TWEAK/Fn14 pathway mRNA expression in *Smn*$^{-/-}$;*SMN2*$^{+/-}$, *Fn14*$^{-/-}$ and *TWEAK*$^{-/-}$ mouse skeletal muscle. a. mRNA expression of TWEAK/Fn14 pathway and atrophy marker *parvalbumin* in P7 late-symptomatic *Smn*$^{-/-}$;*SMN2* mice compared to age-matched WT controls. **b.** mRNA expression of TWEAK/Fn14 pathway and atrophy marker *parvalbumin* in P7 *TWEAK*$^{-/-}$ mice compared to age-matched WT controls. **c.** mRNA expression of TWEAK/Fn14 pathway and atrophy marker *parvalbumin* in P7 *Fn14*$^{-/-}$ mice compared to age-matched WT controls. Student's *t* tests, * $p < 0.05$, ** $p < 0.01$, *** $p < 0.001$, $n = 4$ per group.

5.3.6 Smn depletion presents a role behind muscle pathology in SMA via the TWEAK/Fn14 pathway during myogenic differentiation

We next wanted to assess the influence of Smn, Tweak and Fn14 depletion on the expression of metabolic downstream effectors of the TWEAK/Fn14 pathway during myogenic differentiation. We first evaluated the expression pattern of the TWEAK/Fn14 pathway during myoblast differentiation in

untreated C2C12 myoblasts. As is shown in Figure 5.12a, induction of differentiation in untreated C2C12 resulted in an upregulation of *Tweak* mRNA expression halfway during differentiation while *Fn14* mRNA expression decreased during differentiation. Further, Figures 5.12 f, g, h reveal an increase of *Glut4*, *Klf15* and *HKII* during differentiation. These results imply an involvement of the TWEAK/Fn14 pathway in myogenic differentiation.

Further, we performed knockdown experiments using siRNA transfection in C2C12s to define the role of the TWEAK/Fn14 signaling cascade during myoblast differentiation and the relationship between Smn, Tweak and Fn14. siRNA-mediated knockdown of *Tweak* resulted in a significant downregulation of *Fn14* (Figure 5.12a), whereas siRNA-mediated knockdown of *Fn14* did not have any effects on *Tweak* expression during myoblast differentiation (Figure 5.12b). Both knockdown of *Tweak* and knockdown of *Fn14* resulted in an upregulation of *Pgc-1α* (Figure 5.12d) and Mef2d (Figure 5.12e), and *Klf15* (Figure 5.12g) was upregulated in knocked down Fn14 C2C12 cells, as was to be expected from the model proposed in Figure 5.2. siRNA-mediated knockdown of *Tweak* resulted in a downregulation from HKII and Glut4 during myogenic differentiation. This is an interesting result, as the Kumar group proposes a repressive effect of TWEAK on HKII and Glut4 based on a study showing that TWEAK represses the mRNA levels of *HKII* in cultured myotubes and mice overexpressing *Tweak* show downregulated levels of *HKII* in skeletal muscle [540]. As *Tweak* was knocked down in C2C12, we expected to see an upregulation, instead of a downregulation, of both *HKII* and *Glut4* (Figure 5.12h, f).

As SMN depletion is the major player in SMA, we also investigated the role of SMN in the TWEAK/Fn14 pathway to entangle the relationships between SMN, TWEAK and Fn14 in muscle pathology in SMA. Intriguingly, both *Tweak* and *Fn14* knockdown resulted in elevated *Smn* levels in fully differentiated C2C12 cells (Figure 5.12a,b). As can be seen in Figure 5.12c, siRNA-mediated knockdown of *Smn* resulted in a downregulation of both *Tweak* and *Fn14*, an upregulation of *Pgc-1α* and a

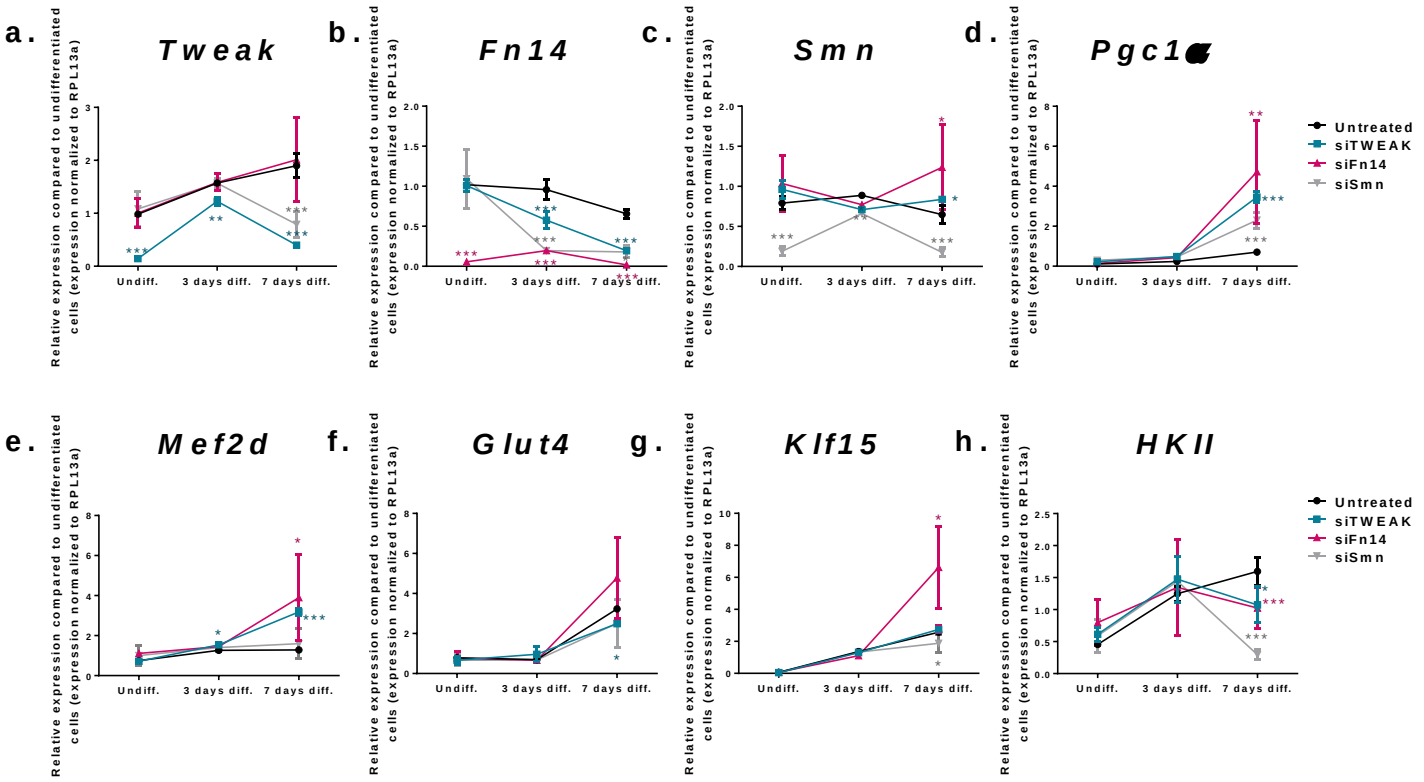


Figure 5.12. siRNA mediated knockdown of *Tweak*, *Fn14* and *Smn* in C2C12 cells during differentiation. mRNA expression levels of *Tweak*, *Fn14* and downstream effectors at three timepoints during differentiation (undifferentiated, 3 days and 7 days after differentiation) after siRNA mediated knockdown compared to untreated cells. **a.** *Tweak*, **b.** *Fn14*, **c.** *Smn,* **d.** *Pgc-1α*, **e.** *Mef2d,* **f.** *Glut4*, **g.** *Klf15*, **h.** *HKII*. Two-way ANOVA, * $p < 0.05$, ** $p < 0.01$, *** $p < 0.001$, **** $p < 0.0001$.

downregulation of *Klf15* and *HKII* during myogenic differentiation. *Mef2d* and *Glut4* expression remained unchanged, compared to untreated myoblasts. Figure 5.13 gives an overview of all the interactions we found in this experiment between Smn, Tweak, Fn14 and downstream effectors after siRNA-mediated knockdown or Smn, Tweak and Fn14. These results suggest that aberrant expression of the TWEAK/Fn14 pathway in SMA is not just a reaction to muscle atrophy and further pathology, but that SMN depletion potentially presents a driving role behind muscle pathology in SMA via the TWEAK/Fn14 pathway.

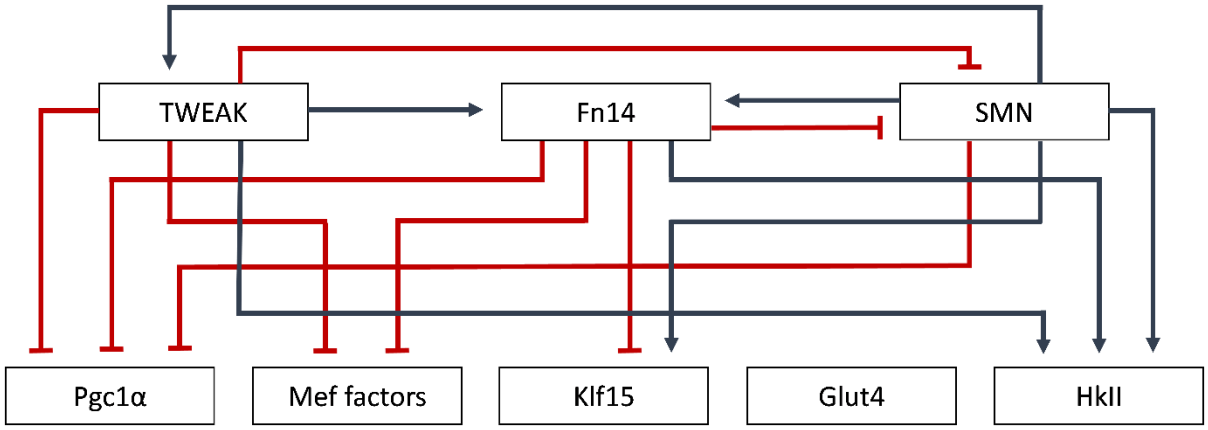


Figure 5.13. Overview of effects of siRNA mediated knockdown of *Tweak*, *Fn14* and *Smn* in C2C12 cells during differentiation. Red lines represent repressing effects and blue lines represent promoting effects.

5.3.7 Overlap between dysregulation of myopathy and myogenesis genes in *Smn*$^{-/-}$;*SMN2*$^{+/-}$, *Fn14*$^{-/-}$ and *TWEAK*$^{-/-}$ mice

In our *in vitro* work, we identify possible interactions between the genes, whereby one affects the expression of the others. As Smn, Tweak and Fn14 play roles in muscle pathology, we wanted to further decipher the precise contribution of each gene to the muscle pathologies observed in SMA muscle. For this purpose, we used commercially available mouse myopathy and myogenesis qPCR arrays (SABiosciences), which look at a subset of 84 genes known to display and/or regulate myopathy and myogenesis. We executed this experiment in two different muscle that represent a vulnerable (*triceps*) and resistant state (*quadriceps*).

We observed a large number of dysregulated myopathy and myogenesis genes in *triceps* of *Smn*$^{-/-}$;*SMN2*$^{+/-}$ mice (almost 80%, Table 5.3), and to a lesser extent in the same muscle from *Fn14*$^{-/-}$ (35%) and *TWEAK*$^{-/-}$ (35%) mice. In the more resistant *quadriceps*, 60% of myopathy and myogenesis genes were dysregulated in *Smn*$^{-/-}$;*SMN2*$^{+/-}$ mice and in *Fn14*$^{-/-}$ mice 25% and *TWEAK*$^{-/-}$ almost 30%. A total of 11 genes (13%) were aberrantly expressed in the same direction in all three mouse models tested compared to age-matched WT controls, in P7 *triceps* (10 genes) and/or

quadriceps (5 genes, Figure 5.14a,b, Table 5.4). We used the publicly available database STRING (version 10.5) [529] for network and enrichment analysis of these differently expressed genes. As could be seen in Figure 5.14c, there were no known protein–protein interactions between any of the dysregulated genes and Smn, Fn14 or TWEAK. In the center of Figure 5.14c, MyoD1, Pax7 and Myf6 are the connections, which were dysregulated in all three groups. Pax7 is an absolute requirement for satellite cell function in skeletal muscle. Satellite cells are precursors to skeletal muscle cells [541]. A study in *Pax7*$^{-/-}$ mice showed cell-cycle arrest of satellite cells and myoblasts, and dysregulation of myogenic regulatory factors in skeletal muscle [542]. siRNA-mediated knockdown of *Pax7* in cultured myoblasts or satellite cells results in growth arrest [543,544]. In our study, we found Pax7 mRNA expression levels to be significantly reduced in *Smn*$^{-/-}$*;SMN2*$^{+/-}$, *Fn14*$^{-/-}$ and *TWEAK*$^{-/-}$ mice. This reduction in Pax7 might contribute to skeletal muscle pathology in SMA. MyoD and Myf6 are fundamental regulators of skeletal muscle and are normally upregulated after skeletal muscle injury [541]. Titin was downregulated in the *quadriceps* of all three mouse models. Titin has not been implicated in SMA before but plays major roles in muscle contraction and force production, which are muscle functions affected in SMA patients [545]. Titin mutations have been reported to cause a range of skeletal muscle diseases and phenotypes (reviewed in [546]). Myogenesis and myopathy genes were in all three mouse models dysregulated in our study, showing a shared pattern of aberrant expression of myogenic regulatory factors in SMA and the TWEAK/Fn14 pathway. In conclusion, individually and together, Smn, Tweak and Fn14 depletion impact important myogenic regulators. This common depletion could exacerbate muscle pathology, which may explain the severe muscle pathology found in the moderate and severe SMA mouse models, as both models showed a decrease of, next to SMN, Tweak and Fn14.

Table 5.3. Number of dysregulated genes compared to WT mice, p < 0.05.

Myogenesis and myopathy	*Triceps*	*Quadriceps*
Total genes	84	84
Dysregulated in *Smn*$^{-/-}$;*SMN2*$^{+/-}$	66	51
Dysregulated in *Fn14*$^{-/-}$	29	21
Dysregulated in *TWEAK*$^{-/-}$	30	24

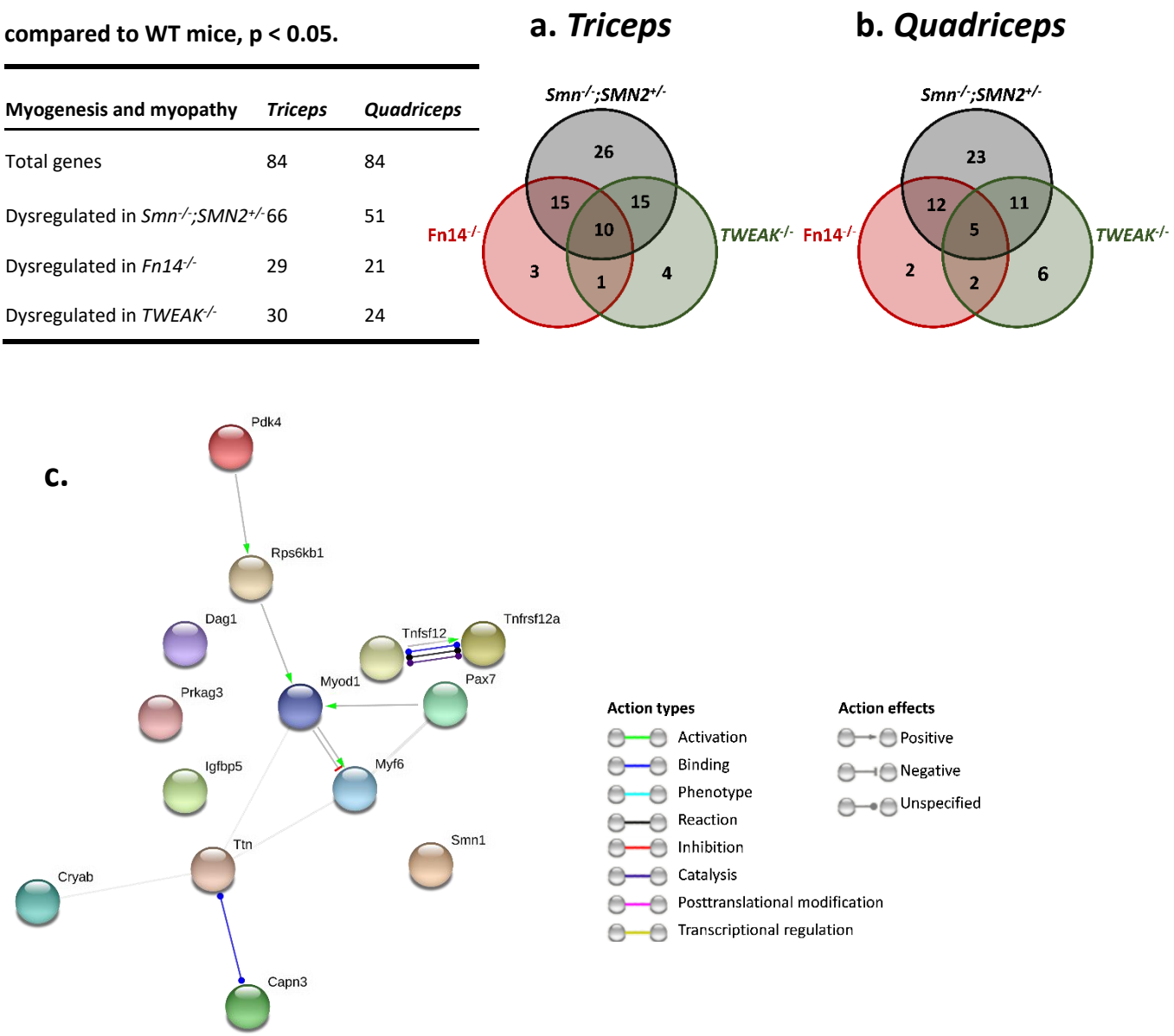


Figure 5.14. Overlap between dysregulated genes involved in myogenesis and myopathy, in P7 *Smn*$^{-/-}$;*SMN2*$^{+/-}$, *Fn14*$^{-/-}$ and *TWEAK*$^{-/-}$ mice. a. Overlap of genes dysregulated in all three mouse models in the same direction (either up or downregulated) compared to WT age-matched controls in *triceps*, $p < 0.05$. **b.** Overlap of genes dysregulated in all three mouse models in the same direction (either up or downregulated) compared to WT age-matched controls in *quadriceps*, $p < 0.05$. **c.** Network and enrichment analysis of the overlap of significantly dysregulated genes in all three groups (*Smn*$^{-/-}$;*SMN2*$^{+/-}$, *Fn14*$^{-/-}$ and *TWEAK*$^{-/-}$ mice) in *triceps* and/or *quadriceps* using STRING software. Smn (Smn1), TWEAK (Tnfsf12) and Fn14 (Tnfrsf12a) are included in the analysis. Corresponding protein nodes in the network are highlighted in color. The connection color and shape between proteins

represent protein–protein associations (in legend under 'Action types') and whether the association is positive, negative or unspecified (in legend under 'Action effects').

Table 5.4. Myogenesis and myopathy genes significantly dysregulated in the same direction in P7 *Smn$^{-/-}$;SMN2$^{+/-}$*, *Fn14$^{-/-}$* and *TWEAK$^{-/-}$* mouse *triceps* and *quadriceps*, when compared to P7 WT *triceps* and *quadriceps*. Significant change (up or down regulated in all three mouse models, compared to WT control).

Gene	*Triceps*	*Quadriceps*
Calpain3 (Capn3)	Up	Up
Crystallin Alpha B (Cryab)	Up	—
Dystroglycan 1 (Dag1)	Down	Down
Insulin Like Growth Factor Binding Protein 5 (Igfbp5)	Down	—
Myogenic Factor 6 (Myf6)	Up	—
Myogenic Differentiation 1 (Myod1)	Up	—
Paired Box 7 (Pax7)	Down	—
Protein Kinase AMP-Activated Non-Catalytic Subunit Gamma 3 (Prkag3)	Down	Down
Pyruvate Dehydrogenase Kinase 4 (Pdk4)	Up	—
Ribosomal Protein S6 Kinase B1 (Rps6kb1)	Down	Down
Titin (Ttn)	—	Down

5.3.8 Overlap between dysregulation of glucose metabolism pathways in *Smn$^{-/-}$;SMN2$^{+/-}$*, *Fn14$^{-/-}$* and *TWEAK$^{-/-}$* mice

As discussed in Chapter 1, Section 1.3.4.2, diabetes and alterations in glucose metabolism have been reported in SMA Type 1, 2 and 3 patients [263–266]. The most common metabolic defect in SMA patients is alterations in fatty acid [265,266]. Metabolic defects have also been demonstrated in SMA mouse models [263,268,269]. However, the role of skeletal muscle as a metabolic tissue in SMA is not fully understood. As the TWEAK/Fn14 pathway is also involved in metabolism, we decided to further investigate the role of Tweak, Fn14 and Smn in glucose metabolism using qPCR arrays which look at a subset of 84 genes known to display and/or regulate glucose metabolism. Similar to the experiments

described in the previous section, we investigated mRNA expression of P7 *triceps* and *quadriceps* from *Smn$^{-/-}$;SMN2$^{+/-}$*, *Fn14$^{-/-}$* and *TWEAK$^{-/-}$* mice.

About 70% of glucose metabolism genes were dysregulated in both *triceps* and *quadriceps* from *Smn$^{-/-}$;SMN2$^{+/-}$* mice (57 and 55 genes from 84 in total tested by qPCR array, Table 5.5), providing further evidence that glucose metabolism is indeed dysregulated in SMA muscle. In *Fn14$^{-/-}$* mice, 37% of genes in *triceps* and 49% of genes in *quadriceps* were dysregulated and in *TWEAK$^{-/-}$* mice, 29% of genes and 32% of genes in *quadriceps* were dysregulated, further indicating a role for both TWEAK and Fn14 in glucose metabolism.

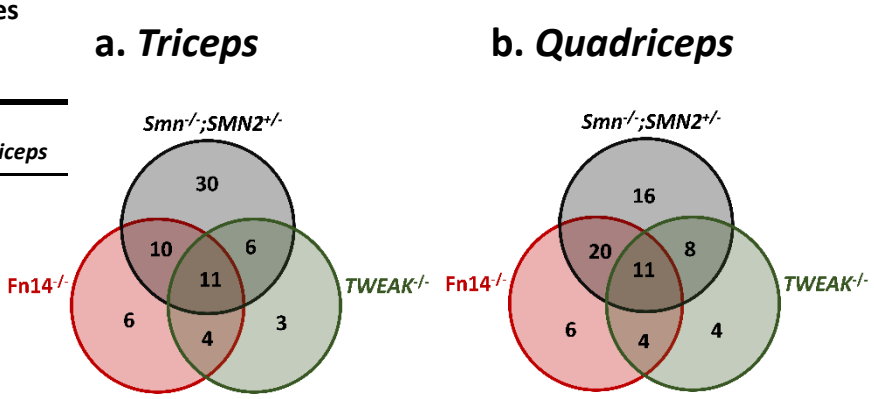
Interestingly, the number of dysregulated glucose metabolism genes were similar in *triceps* and *quadriceps* in *Smn$^{-/-}$;SMN2$^{+/-}$*, while there were more myogenesis and myopathy genes dysregulated in *triceps* than in *quadriceps* in *Smn$^{-/-}$;SMN2$^{+/-}$* (previous section). This could be explained by the notion that the different resistances of skeletal muscle to SMA muscle pathology are based on the vulnerability of certain skeletal muscles to neuromuscular junction denervation [169]. Denervation in skeletal muscle has possibly a greater effect on myogenesis and myopathy than on glucose metabolism.

A total of 17 genes were aberrantly regulated in the same direction in all three mouse models, in *triceps* (11 genes) and/or *quadriceps* (11 genes, Figure 5.15a,b, Table 5.6). Network and enrichment analysis using STRING (version 10.5) [529] revealed that there are no known protein–protein interactions between any of the dysregulated genes and Smn, Fn14 or TWEAK.

Most dysregulated glucose metabolism genes showing overlap between *Smn$^{-/-}$;SMN2$^{+/-}$*, *Fn14$^{-/-}$* and *TWEAK$^{-/-}$* mice were downregulated, which suggests that many metabolic processes are decreased in SMA which is connected to the downregulation of Tweak and Fn14 found in our SMA mouse models. Overall, these results show a close connection between SMA and the TWEAK/Fn14 pathway in dysregulation of glucose metabolism.

Table 5.5. Number of dysregulated genes compared to WT.

Glucose metabolism	*Triceps*	*Quadriceps*
Total genes	84	84
Dysregulated in *Smn*$^{-/-}$;*SMN2*$^{+/-}$	57	55
Dysregulated in *Fn14*$^{-/-}$	31	41
Dysregulated in *TWEAK*$^{-/-}$	24	27



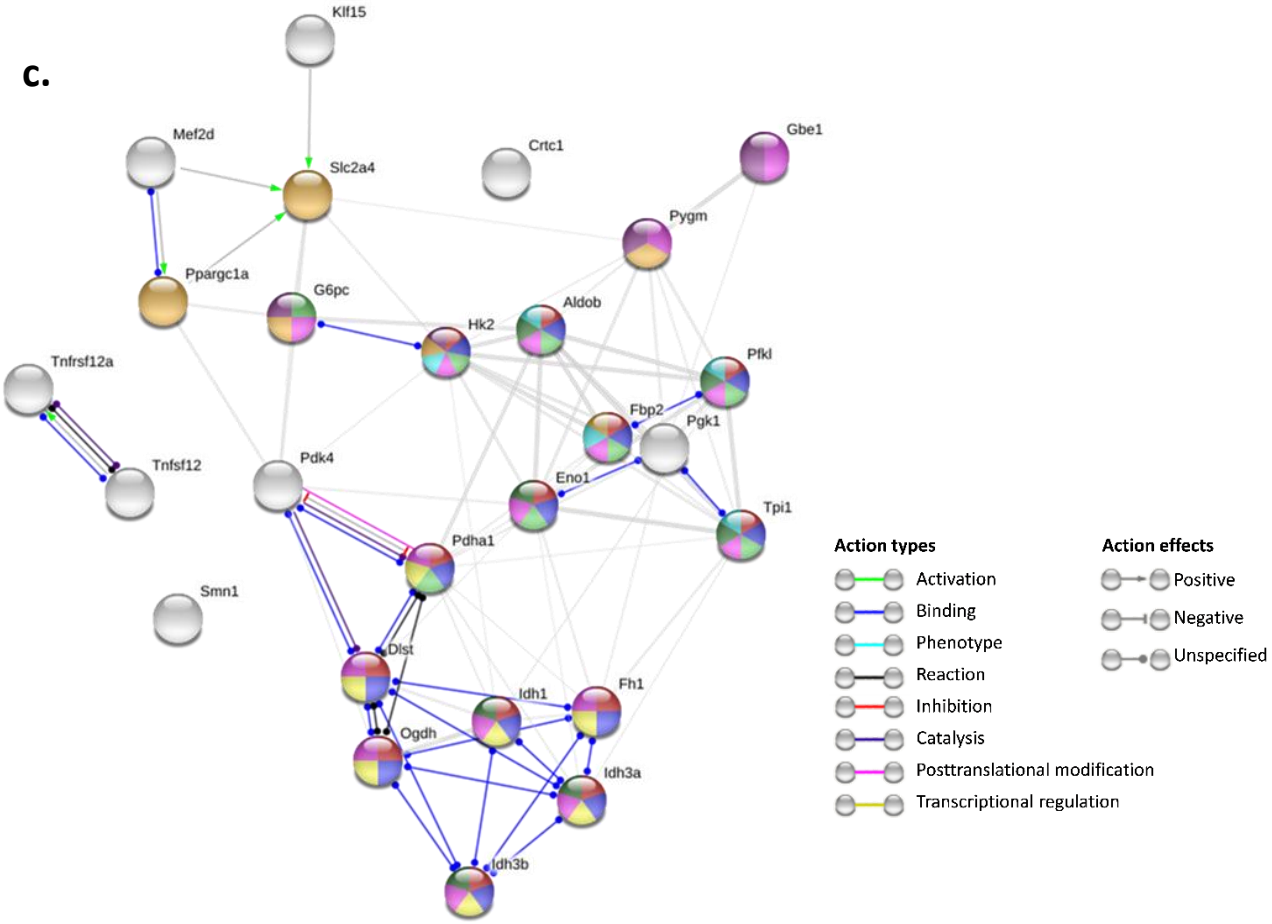


Figure 5.15. Overlap between dysregulated genes involved in glucose metabolism in P7 *Smn*$^{-/-}$;*SMN2*$^{+/-}$, *Fn14*$^{-/-}$ and *TWEAK*$^{-/-}$ mice. a. Overlap of genes dysregulated in all three mouse models in the same direction (either up or downregulated) compared to WT age-matched controls in *triceps*, $p < 0.05$. **b.** Overlap of genes dysregulated in all three mouse models in the same direction (either up or downregulated) compared to WT age-matched controls in *quadriceps*, $p < 0.05$. **c.** Network and enrichment analysis of the overlap of significantly dysregulated genes in all three groups

(*Smn*$^{-/-}$;*SMN2*$^{+/-}$, *Fn14*$^{-/-}$ and *TWEAK*$^{-/-}$ mice) in *triceps* and/or *quadriceps* using STRING software (version 10.5). Smn (Smn1), TWEAK (Tnfsf12), Fn14 (Tnfrsf12a), HKII (Hk2), Glut4 (Slc2a4), Pgc1α (Ppargc1a), Klf15, Mef2d are included in the analysis. Corresponding protein KEGG pathways with the six lowest FDRs highlighted in color (for different colors per KEGG pathway, see Table 5.7). The connection color and shape between proteins represent protein–protein associations (in legend under 'Action types') and if the association is positive, negative or unspecified (in legend under 'Action effects').

Table 5.6. Glucose metabolism genes significantly dysregulated in the same direction in P7 *Smn*$^{-/-}$;*SMN2*$^{+/-}$, *Fn14*$^{-/-}$ and *TWEAK*$^{-/-}$ mice *triceps* and *quadriceps*, when compared to P7 WT *triceps* and *quadriceps*. Significant change (up or down regulated in all three mouse models, compared to WT control).

Gene	*Triceps*	*Quadriceps*
Aldolase, Fructose-Bisphosphate B (Aldob)	Down	—
1,4-Alpha-Glucan Branching Enzyme 1 (Gbe1)	—	Down
Dihydrolipoamide S-Succinyltransferase (Dlst)	Down	Down
Enolase 1 (Eno1)	Down	Down
Filamin B (Fh1)	Down	—
Fructose-Bisphosphatase 2 (Fbp2)	Up	—
Glucose-6-Phosphatase Catalytic Subunit (G6pc)	Down	—
Glycogen Phosphorylase Muscle Associated (Pygm)	—	Down
Isocitrate Dehydrogenase (NADP(+)) 1, Cytosolic (Idh1)	Down	—
Isocitrate Dehydrogenase 3 (NAD(+)) Alpha (Idh3a)	Down	Down
Isocitrate Dehydrogenase 3 (NAD(+)) Beta (Idh3b)	—	Down
Oxoglutarate Dehydrogenase (Ogdh)	Down	Down
Phosphofructokinase, Liver Type (Pfkl)	—	Down
Pyruvate Dehydrogenase E1 Alpha 1 Subunit (Pdha1)	—	Down
Pyruvate Dehydrogenase Kinase 4 (Pdk4)	Up	Up
Phosphoglycerate Kinase 1 (Pgk1)	Down	—
Triosephosphate Isomerase 1 (Tpi1)	—	Down

Table 5.7. KEGG pathways of glucose metabolism genes. Genes are significantly dysregulated in the same direction in P7 *Smn*$^{-/-}$;*SMN2*$^{+/-}$, *Fn14*$^{-/-}$ and *TWEAK*$^{-/-}$ mice *triceps* and *quadriceps*, when compared to P7 WT *triceps* and *quadriceps*.

Pathway ID		Pathway description	Count in gene set	False discovery rate (FDR)
01200		Carbon metabolism	13	7.62e-22
01120		Microbial metabolism in diverse environments	13	1.87e-19
00010		Glycolysis/Gluconeogenesis	8	2.09e-13
00020		Citrate cycle (TCA cycle)	7	2.09e-13
01100		Metabolic pathways	16	7.65e-13
01230		Biosynthesis of amino acids	7	8.75e-11
00051		Fructose and mannose metabolism	5	1.7e-08
04910		Insulin signaling pathway	6	3.09e-07
00500		Starch and sucrose metabolism	4	8.58e-06
04152		AMPK signaling pathway	5	8.58e-06
01210		2-Oxocarboxylic acid metabolism	3	2.79e-05
00030		Pentose phosphate pathway	3	0.000126
04066		HIF-1 signaling pathway	4	0.000141
00052		Galactose metabolism	3	0.000145
04920		Adipocytokine signaling pathway	3	0.00138
00620		Pyruvate metabolism	2	0.0177
04973		Carbohydrate digestion and absorption	2	0.0177
04930		Type II diabetes mellitus	2	0.0227
00310		Lysine degradation	2	0.0233

In Table 5.7 are the Kyoto Encyclopedia of Genes and Genomes (KEGG) pathways displayed of glucose metabolism genes significantly dysregulated in the same direction in P7 *Smn*$^{-/-}$;*SMN2*$^{+/-}$, *Fn14*$^{-/-}$ and *TWEAK*$^{-/-}$ mice *triceps* and *quadriceps* and the downstream effectors of the TWEAK/Fn14 pathway studied in this project (Pgc-1α, Mef2d, Glut4, Klf15, and HKII) with an FDR < 0.05. This analysis shows that many aspects of glucose metabolism, such as insulin signaling, glycolysis are dysregulated, both in Smn depleted mice and in Tweak and Fn14 depleted mice, demonstrating a shared role for the SMN

and the TWEAK/Fn14 in metabolism , which might act in SMA synergistically and lead to the metabolic disturbances found in SMA patients and in SMA mouse models.

5.3.9 Modulating TWEAK levels by Fc-TWEAK treatment improves phenotype of moderate SMA mouse model

As both SMA models used in this study show a significant decrease of *Tweak* expression during disease progression, we asked whether TWEAK upregulation could have therapeutic potential for improving muscle pathology in SMA. For this purpose, we injected *Smn$^{-/-}$;SMN2$^{+/-}$* mice subcutaneously with different doses of Fc-TWEAK every 4 days, starting from birth (doses: 7.9 µg, 15.8 µg, 23.7 µg and 31.6 µg). Survival was recorded until the humane end point was reached.

Smn$^{-/-}$;SMN2$^{+/-}$ mice treated with Fc-TWEAK at 15.8 µg demonstrated a trend of weight gain compared to the untreated group (Figure 5.16.a) but did not show a change in survival (Figure 5.16.b). Based on the weight gain, we decided to continue with the 15.8 µg Fc-TWEAK dose. Fc-TWEAK treatment had no effect on weight or survival in healthy littermates (Figure 5.16.c,d). *Smn$^{-/-}$;SMN2$^{+/-}$* mice have a small therapeutic window, as they die at a very young age (median lifespan 11 days), giving less opportunity for the treatment to show beneficial effects. We therefore repeated Fc-TWEAK treatment in the intermediate *Smn$^{2B/-}$* mouse model, which has median lifespan of 21 days. Mice were treated every 4 days with a 15.8 µg dose of Fc-TWEAK or isotype-matched Ig control via the subcutaneous route. Ig control treatment in *Smn$^{2B/-}$* mice resulted in weight gain, but had no effect on survival. Fc-TWEAK treatment significantly increased weight gain compared to untreated animals from P12 onwards. Untreated *Smn$^{2B/-}$* mice start to lose weight around P14, as Figure 5.16e shows, whereas Fc-TWEAK treated *Smn$^{2B/-}$ mice* maintain weight from P14 until P24, at which age they start to gain weight on a daily basis. Fc-TWEAK treatment significantly increased lifespan of *Smn$^{2B/-}$* mice to a median survival of 33 days vs. 21 days in untreated animals (Figure 5.16f).

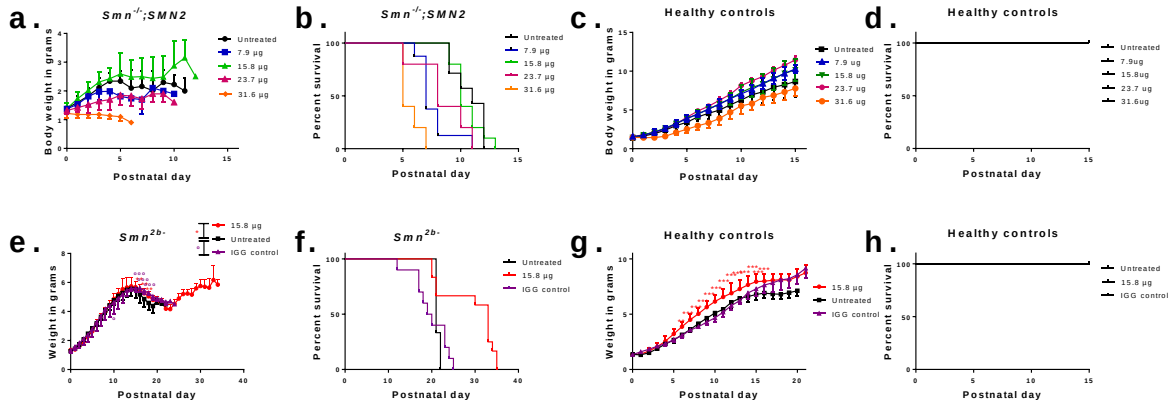


Figure 5.16. Fc-TWEAK treatment improves disease phenotypes in severe and moderate SMA mice.

a. Weight curves of *Smn*$^{-/-}$;*SMN2*$^{+/-}$ mice treated every 4 days with Fc-TWEAK at 7.9 µg, 15.8 µg, 23.7 µg and 31.6 µg vs. untreated *Smn*$^{-/-}$;*SMN2*$^{+/-}$ mice. Non-significant; *n* = 8–10 animals per group. **b.** Survival of *Smn*$^{-/-}$;*SMN2*$^{+/-}$ mice treated every 4 days with FC-TWEAK at 7.9 µg, 15.8 µg, 23.7 µg and 31.6 µg vs. untreated *Smn*$^{-/-}$;*SMN2*$^{+/-}$ mice. Non-significant; *n* = 8–10 animals per group. **c.** Weight curves of healthy control littermate *Smn*$^{+/-}$;*SMN2*$^{+/-}$ mice treated every 4 days with FC-TWEAK at 7.9 µg, 15.8 µg, 23.7 µg and 31.6 µg vs. untreated healthy control mice. Non-significant; *n* = 5–22 animals per group. **d.** Survival of healthy control littermate *Smn*$^{+/-}$;*SMN2*$^{+/-}$ mice treated every 4 days with Fc-TWEAK at 7.9 µg, 15.8 µg, 23.7 µg and 31.6 µg vs. untreated healthy control mice. All healthy controls were alive at the end of the experiment at P15. Non-significant; *n* = 5–22 animals per group. **e.** Weight curves of *Smn*$^{2B/-}$ mice treated every 4 days or daily with Fc-TWEAK or Ig control at 15.8 µg vs. untreated *Smn*$^{2B/-}$ mice. ** $p < 0.01$, *** $p < 0.001$; *n* = 9–12 animals per group. **f.** Survival of *Smn*$^{2B/-}$ mice treated every 4 days with Fc-TWEAK or Ig control at 15.8 µg vs. untreated *Smn*$^{2B/-}$ mice. Median survival of untreated animals 21 days, for Ig control treated 23 and for Fc-TWEAK treated animals significantly elevated to 33 days. Significant difference between Fc-TWEAK treated and untreated mice, $p < 0.05$; *n* = 9–12 animals per group. **g.** Weight curves of healthy control littermate *Smn*$^{2B/+}$ mice treated every 4 days with Fc-TWEAK or Ig control at 15.8 µg vs. untreated healthy controls. Non-significant; *n* = 6–12 animals per group. **h.** Survival of healthy control littermate *Smn*$^{2B/+}$ mice treated every 4 days with Fc-TWEAK or Ig control at 15.8 µg vs. untreated healthy controls. All healthy controls were alive at the end of the experiment at P20. Non-significant; *n* = 6–12 animals per group. The data in all graphs about weight (a, c, e, g) represent mean ± SD and a two-way ANOVA was used for statistical analyses (post-hoc Bonferroni). The data in survival graphs (b, d, f, h) represent Kaplan-Meier curves and a Log-rank (Mantel-Cox) test was used for statistical analyses.

5.3.10 Fc-TWEAK treatment improves muscle phenotype in the severe and moderate SMA mouse models

To evaluate the effects of Fc-TWEAK on the TWEAK/Fn14 pathway, we treated *Smn*$^{-/-}$;*SMN2*$^{+/-}$ mice, *Smn*$^{2B/-}$ mice and healthy littermates with a dose of 15.8 µg of Fc-TWEAK via the subcutaneous route every four days, starting at birth. *Triceps* from *Smn*$^{-/-}$;*SMN2*$^{+/-}$ mice were harvested at P7 and *triceps* from *Smn*$^{2B/-}$ mice at P15, both at a late-symptomatic disease stage. As is shown in Figure 5.17a,b, *Tweak* mRNA levels were unchanged in treated SMA mouse models and healthy controls compared to untreated mice, which is likely caused by the short half-life of soluble Fc-TWEAK *in vivo* [547]. The time between last Fc-TWEAK treatment and harvest was 24 hours in *Smn*$^{-/-}$;*SMN2*$^{+/-}$ mice and 72 hours in *Smn*$^{2B/-}$ mice. *Fn14* mRNA expression showed a trend towards upregulation after Fc-TWEAK treatment in *Smn*$^{2B/-}$ mice, but not in *Smn*$^{-/-}$;*SMN2*$^{+/-}$ mice, which may also potentially be caused by the short half-life of Fc-TWEAK. *Mef2d* and *Klf15* were upregulated in untreated *Smn*$^{-/-}$;*SMN2*$^{+/-}$ mice but were significantly decreased after Fc-TWEAK treatment. The other metabolic factors were unchanged after treatment (Figure 5.17a,b). Since the effects of Fc-TWEAK treatment on the TWEAK/Fn14 pathway were not strongly demonstrated by mRNA levels in *triceps*, but the treatment significantly prolonged lifespan and increased weight in *Smn*$^{2B/-}$ mice and *Smn*$^{-/-}$;*SMN2*$^{+/-}$ mice, we further investigated determinants of muscle health previously involved in SMA muscle pathology [145,532,548]. We investigated the expression of MuRF-1 and atrogin1, which are atrogenes that are upregulated during skeletal muscle atrophy [549] and MyoD and myogenin, which are myogenic regulatory factors that modulate muscle-specific gene expression [541], and compared treated mice with untreated mice. SMA mice treated with Fc-TWEAK showed overall positive effects on the investigated muscle markers. *Parvalbumin* levels showed a trend towards upregulation in treated *Smn*$^{-/-}$;*SMN2*$^{+/-}$ mice (Figure 5.17c). MyoD and myogenin are normally downregulated in SMA but showed here a trend towards increase in both animal models after treatment (Figure 5.17c,d). *Murf1* and *atrogin1* were both upregulated in *Smn*$^{-/-}$;*SMN2*$^{+/-}$ and *Smn*$^{2B/-}$ mice and were downregulated after Fc-TWEAK treatment. As is shown in Figure 5.18a–c, Fc-TWEAK treatment significantly increased myofiber size in

Smn$^{-/-}$;*SMN2*$^{+/-}$ mice TA after daily Fc-TWEAK treatment for 7 days. Both, the downregulation of atrogenes and the increase of myofiber size after treatment shows a modulation of atrophy. Taken together, our molecular and histopathological analyses reveal a myogenic response and an increase of myofiber size, which potentially explains the ameliorated phenotype of Fc-TWEAK treated *Smn*$^{-/-}$;*SMN2* and *Smn*$^{2B/-}$ mice.

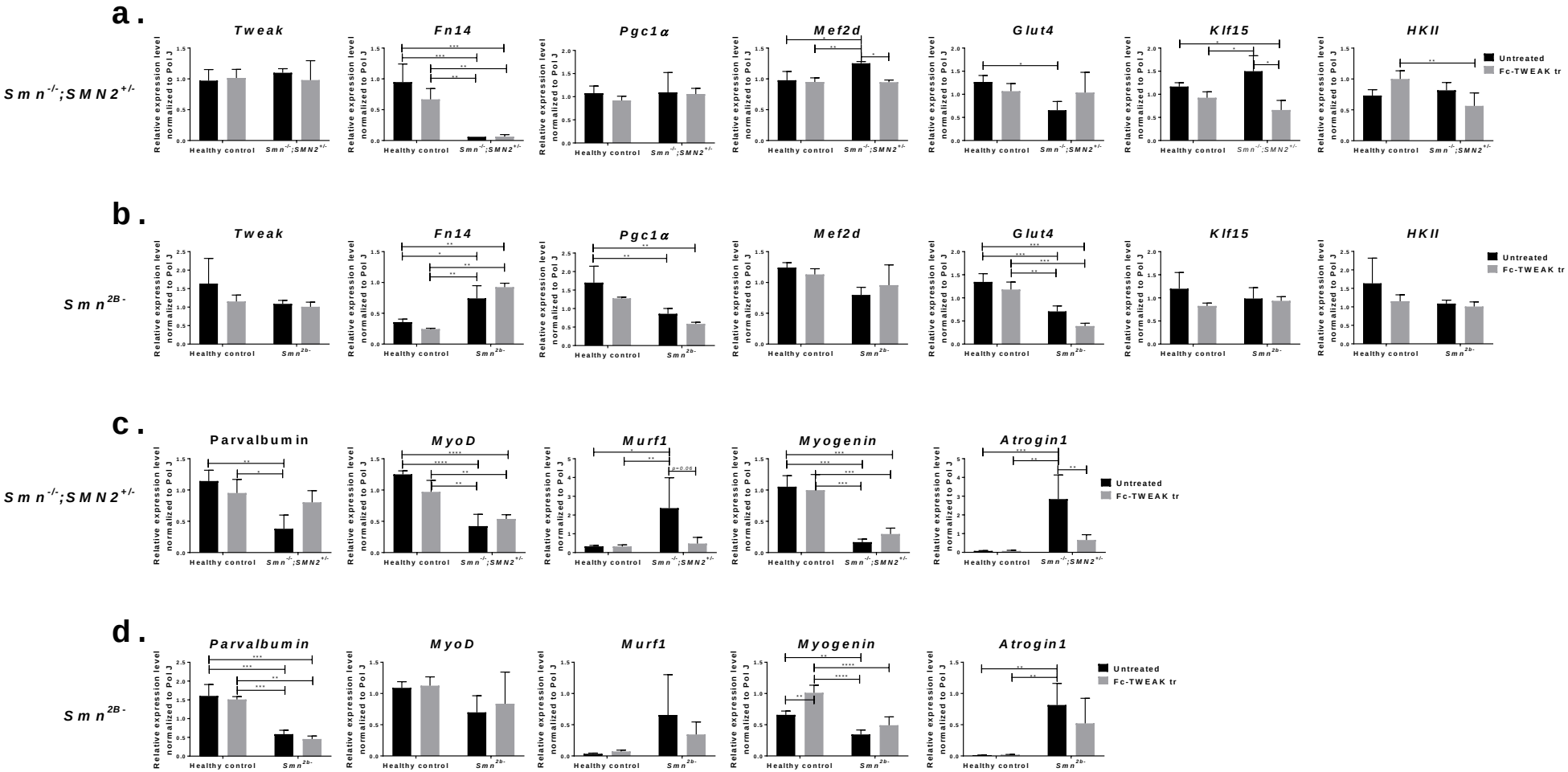


Figure 5.17. mRNA expression of Tweak/Fn14 pathway and muscle markers after Fc-TWEAK treatment in *triceps* from *Smn$^{-/-}$;SMN2$^{+/-}$* and *Smn$^{2B/-}$* mice and healthy littermates, compared to untreated animals. a. qPCR analysis of TWEAK/Fn14 pathway expression in *Smn$^{-/-}$;SMN2$^{+/-}$* mice and healthy littermates treated daily with Fc-TWEAK at 15.8 µg, compared to untreated mice. **b.** qPCR analysis of TWEAK/Fn14 pathway expression in *Smn$^{2B/-}$* mice and

healthy littermates treated every 4 days with Fc-TWEAK at 15.8 µg, compared to untreated mice. **c.** qPCR analysis of muscle health determinants *parvalbumin*, *MyoD, Murf1, myogenin* and *atrogin1* expression in *Smn*$^{-/-}$;*SMN2*$^{+/-}$ mice and healthy littermates treated daily with Fc-TWEAK at 15.8 µg, compared to untreated mice. **d.** qPCR analysis of muscle health determinants parvalbumin, *MyoD, Murf1, myogenin* and *atrogin1* expression in *Smn*$^{2B/-}$ mice and healthy littermates treated every 4 days with Fc-TWEAK at 15.8 µg, compared to untreated mice. **a–d.** Data represent mean ± SD; n = 3–4 animals per group; two-way ANOVA; *p < 0.05, **p < 0.01, ***p < 0.001, ****p < .0001.

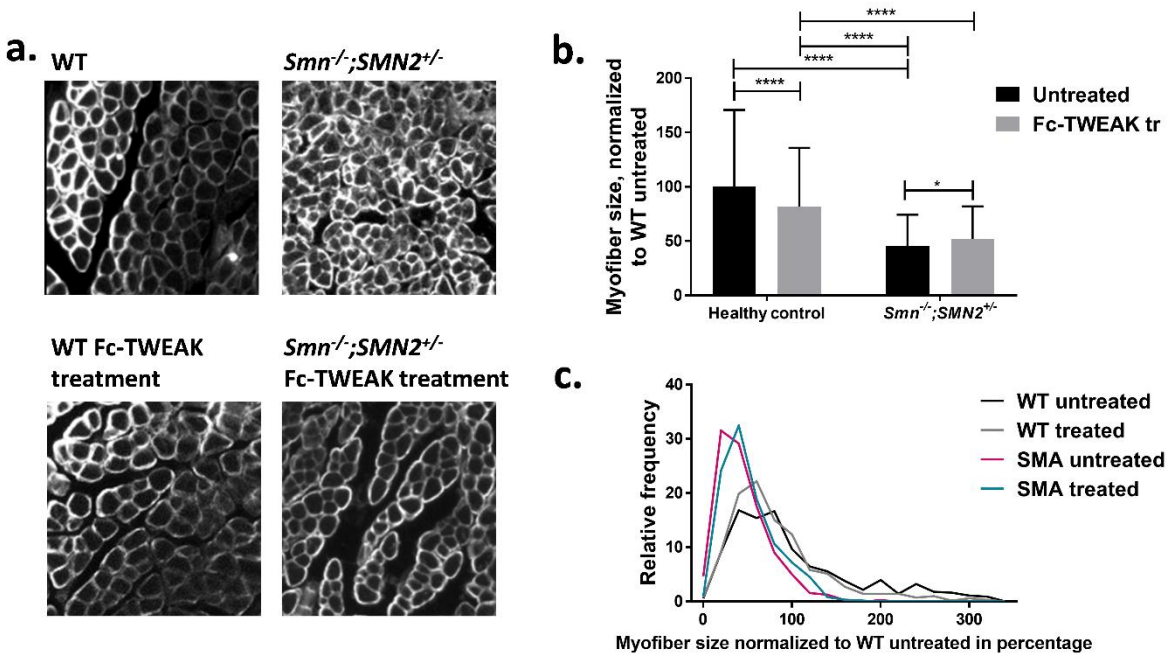


Figure 5.18. Fc-TWEAK treatment in *Smn*$^{-/-}$;*SMN2*$^{+/-}$ mice increases fiber diameter in *tibialis anterior* muscle. The different age-matched groups analyzed were: untreated healthy control littermates, untreated *Smn*$^{-/-}$;*SMN2*$^{+/-}$ mice, Fc-TWEAK treated healthy control littermates and Fc-TWEAK treated *Smn*$^{-/-}$;*SMN2*$^{+/-}$ mice. **a.** Representative images showing a laminin staining of muscle fibers within a designated area of the TA muscle. **b.** Quantification of the cross-sectional area of TA muscle fibers, multiple counts per muscle throughout the muscle. Untreated *Smn*$^{-/-}$;*SMN2*$^{+/-}$ mice have significantly smaller muscle fibers than their healthy control littermates $p < 0.0001$. Administration of Fc-TWEAK significantly increased the muscle fiber size of *Smn*$^{-/-}$;*SMN2*$^{+/-}$ mice $p < 0.05$. Data represent mean ± SD; $n = 3–4$ animals per group; two-way ANOVA. **c.** Fc-TWEAK treatment caused a shift of myofiber size in treated *Smn*$^{-/-}$;*SMN2*$^{+/-}$ mice.

5.4 Discussion

Motor neuron death and muscle pathology are closely linked in SMA, as neuronal dysfunction contributes significantly to muscle atrophy. As is discussed in Chapter 1, Section 1.3.3, there is a plethora of evidence suggesting there are also muscle-intrinsic abnormalities in skeletal muscle in SMA, which could be directly or indirectly caused by SMN deficiency [144,156,235,236,239]. In this study, we addressed the underlying mechanisms of muscle-intrinsic abnormalities leading to muscle pathology in SMA by investigating the role of the TWEAK/Fn14 pathway in muscle atrophy in SMA.

5.4.1 Dysregulation of TWEAK/Fn14 in SMA

We showed that the TWEAK/Fn14 pathway is aberrantly expressed in skeletal muscle during the course of SMA in both SMA mouse models and in SMA Type 1 patients. Contrary to previous studies, which showed how high levels of TWEAK and Fn14 have repressive effects on metabolic factors [495,510,550], we found that low levels of TWEAK and Fn14 are accompanied by higher levels of metabolic factors in SMA mouse models. Interestingly, the dysregulation of the TWEAK/Fn14 pathway in SMA is not denervation dependent, as we found no dysregulation in denervated muscle, but is likely to be dependent on intrinsic myopathy as the pathway was dysregulated in cardiotoxin damaged muscle.

Next, we demonstrated the overlap between TWEAK, Fn14 and SMN dysregulation in muscle pathology and the TWEAK/Fn14 pathway. This is the first study on the role of the TWEAK and Fn14 pathway in SMA and no earlier direct links between TWEAK, Fn14 and SMN have been published as far as we are aware. In our study, we found a dysregulation of the NF-κB pathway in SMA. One of the ways in which TWEAK regulates muscle response to injury is by activating the NF-κB pathway [501]. In accordance with the findings in previous research that only pathological high levels activate the canonical NF-κB pathway, we found this pathway to be downregulated, as TWEAK levels were decreased in SMA mouse muscle. The non-canonical NF-κB pathway however, was upregulated in symptomatic *Smn*$^{-/-}$;*SMN2*$^{+/-}$ skeletal muscle. One of the proposed roles of TWEAK and Fn14 in regulating muscle atrophy is that once TWEAK binds to Fn14, the complex will activate several

signaling proteins, including TRAF6 and IKK [551]. Previous research demonstrated that SMN prevents the activation of TRAF6 and IκB kinase (IKK), thereby negatively regulating NF-κB signaling processes [552]. We also found that siRNA mediated knockdown of *Smn* in C2C12 myoblast cells was followed by dysregulation of components of the TWEAK/Fn14 pathway during differentiation (*Fn14*, *Pgc1α*, *Klf15* and *Glut4*). Surprisingly, siRNA mediated knockdown of *Tweak* and separately of *Fn14* resulted in dysregulation of *Smn* mRNA expression during differentiation in C2C12 cells. We also showed an aberrant expression of the TWEAK/Fn14 pathway in SMA patient myoblast during differentiation. Further evidence for the connection between TWEAK and Fn14 and SMN in muscle pathology in SMA is the high overlap we found of dysregulation of myogenesis and myopathy genes and glucose metabolism genes in *Smn*$^{-/-}$;*SMN2*$^{+/-}$, *Fn14*$^{-/-}$ and *TWEAK*$^{-/-}$ mice. Together, these results suggest that aberrant expression of the TWEAK/Fn14 pathway in SMA is not just a reaction to muscle atrophy and further pathology, but that SMN depletion potentially presents a driving role behind muscle pathology in SMA via the TWEAK/Fn14 pathway.

5.4.2 Unanticipated findings

We initially became interested in the TWEAK/Fn14 pathway in the context of SMA as one of the main symptoms is skeletal muscle atrophy and TWEAK and its main receptor Fn14 play a crucial role in shaping skeletal muscle responses to both acute and chronic injury and disease. Normally, after muscle damage, there is a sharp increase of TWEAK, which will activate and upregulate the normally dormant receptor Fn14. As both the severe and the moderate SMA mouse models we used in this study are characterized by severe muscle atrophy, we expected to find an upregulation of both TWEAK and Fn14; however, both were downregulated in diseased SMA mice (Figure 5.4 and 5.6). There are a few possible explanations for these results. 1. As far as we are aware, this is the only study on the TWEAK/Fn14 pathway executed in neonatal rodents. TWEAK/Fn14 may exert different functionalities in skeletal muscle during development vs. adulthood. Previous research showed that *Tweak* mRNA expression in WT mice is low at 30 days and is increased 150-fold at 90 days in the *gastrocnemius*,

which suggests a time-dependent regulation of Tweak expression [496]. 2. The TWEAK/Fn14 pathway might work in a specific way in SMA and possibly other motor neuron diseases. An ALS study in *SOD1^{G93A}* mice also demonstrated a significant decrease of Tweak levels in the *gastrocnemius* at an early-symptomatic stage at P90 [496], while atrophy is already detected in P30 skeletal muscle (TA) [553]. This suggests there might be a neuromuscular-specific reaction of the TWEAK/Fn14 pathway in skeletal muscle and that the role of TWEAK/Fn14 in skeletal muscle pathology is more nuanced; the pathway is dysregulated, rather than simply upregulated during muscle atrophy. This could be explained by the dual role that TWEAK presents in muscle, as TWEAK signaling can activate the canonical NF-κB signaling pathway, which promotes myoblast proliferation and inhibits myogenesis, but also activate the non-canonical NF-κB pathway, which, in contrast, promotes myogenesis by increasing myoblast fusion [500].

Another surprising result was that the TWEAK/Fn14 pathway was not altered in denervated muscle in our study (Figure 5.9) even though there was decrease of myofiber size and the denervated muscles showed atrophy. A denervation study in 12-week-old WT mice showed a significant 6-fold increase of Fn14 in denervated *gastrocnemius* compared to healthy *gastrocnemius* [538]. This discrepancy in results could be explained by one of the previous points, that our results were found in pups (denervation experiment in Figure 5.9 was conducted in P7 pups), whereas normally denervation experiments are conducted in adult mice [538]. Previous research in young adult mice (P25) showed tibial nerve cut in P17 mice resulted in 89% of neuromuscular junction endplates denervation, whereas in P17 mice this procedure resulted in only 12% denervation [554].

5.4.3 Metabolic perturbations in SMA and connections to the TWEAK/Fn14 pathway

Skeletal muscle is the principal organ for glucose disposal in the body and a reduction of skeletal muscle can cause metabolic abnormalities [270]. In SMA, there is a severe decline of skeletal muscle mass during disease progression. Moreover, alterations in glucose metabolism have been found in SMA Type 1, 2 and 3 patients [263–266] and in various SMA mouse models [263,268,269]. Since both TWEAK and Fn14

were found to be dysregulated in our study, we further investigated metabolic factors that are regulated by TWEAK/Fn14 [495]. As is described in Figure 5.2, previous research has demonstrated the repressive effects of TWEAK and Fn14 metabolic factors on HKII, KLF15 and PGC1α, the latter of which regulates Mef2d expression. KLF15 and Mef2d promote Glut4 expression [516] and HKII catalyzes the first phosphorylation step of glycolysis [517]. It is therefore not surprising that in this study, all of these downstream factors were upregulated in the severe and the moderate SMA mouse model, as both TWEAK and Fn14 were decreased during disease progression (Figure 5.4 and 5.6), confirming the repressive effects of TWEAK/Fn14 on metabolic factors found in previous research [495,510]. Previous studies instead showed that TWEAK and Fn14 were upregulated and, therefore, Glut4 was downregulated, which in turn resulted in metabolic perturbations. This is because low levels of Glut4 result in reduced glucose uptake, which leads to insulin resistance [555], while muscle-specific Glut4 overexpression improves glucose disposal in animal models of insulin resistance [520,523]. About 20% of these genes were also dysregulated in the same direction in *Fn14*$^{-/-}$ and *TWEAK*$^{-/-}$ mice, showing a close connection between SMA and the TWEAK/Fn14 pathway in dysregulation of glucose metabolism. All but one of dysregulated genes were downregulated, suggesting that many metabolic processes are decreased in SMA, which may be connected to the downregulation of Tweak and Fn14 found in our SMA mouse models (Table 5.6).

KEGG analysis over metabolic genes that were dysregulated in P7 *Smn*$^{-/-}$*;SMN2*$^{+/-}$*, Fn14*$^{-/-}$ and *TWEAK*$^{-/-}$ mouse skeletal muscle came up with various pathways involved in glucose metabolism, showing a connection between TWEAK, Fn14 and SMN in SMA. For example, the AMPK signaling pathway, which plays a key role as a master regulator of cellular energy homeostasis, is dysregulated in all three mouse models in this study. A previous study in *SMNΔ7* mice also shows a dysregulation of the AMPK signaling pathway and chronic treatment with the AMPK agonist AICAR prevented skeletal muscle pathology in these mice [556]. Further research shows that TWEAK/Fn14 promotes oxidative stress through AMPK in endothelial cells. AMPK also interacts with PGC-1α, as it phosphorylates PGC-1α protein directly, resulting in the induction of the PGC-1α promoter in skeletal

muscle [557]. Other metabolic pathways that are dysregulated in SMA as well as *Fn14*$^{-/-}$ and *TWEAK*$^{-/-}$ mice are glycolysis and Pyruvate metabolism. Glycolysis pathways convert glucose into pyruvate, and the free energy released in this process is used to form ATP. Research in NSC-34 cells showed a decrease of 26% in ATP after siRNA Smn mediated knockdown. ATP was also decreased in *Smn*$^{-/-}$*;SMN2*$^{+/-}$ mice and in smn morphant zebrafish [558]. These results could explain mitochondrial dysfunction in SMA patients [239].

Overall, this glucose metabolism pathway analysis confirms results from multiple studies about metabolic dysfunction in SMA models and observations of metabolic dysfunction in SMA patients. We also show that metabolic dysfunction in SMA is closely related to the TWEAK/Fn14 pathway.

5.4.4 Differences of TWEAK/Fn14 pathway dysregulation in distinct skeletal muscle demonstrates unequal vulnerabilities in SMA skeletal muscle

As is discussed in Chapter 1, Section 1.3.3. and in the introduction of this chapter, not all skeletal muscles are the same: they can vary in fiber type, function and innervation. In SMA, skeletal muscles are not evenly affected. It has previously been demonstrated that muscle vulnerability in SMA mice is independent of location and fiber type [169]. Thus, in addition to the typically studied *tibialis anterior* and *gastrocnemius* muscles [559], we also assessed *Tweak* and *Fn14* mRNA expression by qPCR in the *triceps brachii* (vulnerable) and *quadriceps femoris* (less-vulnerable) muscles in mice.

SMA skeletal atrophy marker *parvalbumin* was significantly decreased from an earlier timepoint in vulnerable muscle *triceps* and *gastrocnemius* than in the more resistant TA and *quadriceps* in *Smn*$^{-/-}$*;SMN2*$^{+/-}$ mice. Furthermore, *Tweak* expression remained at normal levels in *quadriceps* from *Smn*$^{-/-}$*;SMN2*$^{+/-}$ mice but was significantly downregulated in the more vulnerable muscle. Fn14 and other downstream effectors, however, were dysregulated in all muscles, including *quadriceps*. We found a similar trend In SMA Type 1 patients, in which expressions of parvalbumin and the TWEAK/Fn14 pathway were unchanged in the spared *diaphragm* tissue but dysregulated in the

vulnerable *iliopsoas* tissue. These results show that indeed not all skeletal muscles are equally affected in SMA and that vulnerability is linked to neuromuscular junction denervation [169].

We also found that 20% more genes were dysregulated in *Smn$^{-/-}$;SMN2$^{+/-}$* mice in the vulnerable *triceps* than in the less-vulnerable *quadriceps* (qPCR Array Myogenesis and Myopathy). Surprisingly, we found no difference in number of glucose metabolism genes dysregulated between SMA *triceps* and *quadriceps* (qPCR Array Glucose Metabolism). Denervation in skeletal muscle in SMA possibly has a more prominent effect on myogenesis and myopathy than on glucose metabolism.

5.4.5 Modulation of the pathway – treatment options

As both SMA mouse models in this study were characterized by decreased *Tweak* expression during disease progression, we decided to investigate the effects of TWEAK supplementation on weight, lifespan, TWEAK/Fn14 pathway expression and muscle health. Fc-TWEAK treatment resulted in a significant increase in the lifespan and weight of *Smn$^{2B/-}$* mice and a trend towards weight gain in *Smn$^{-/-}$;SMN2$^{+/-}$* mice. However, TWEAK mRNA levels were not notably changed after Fc-TWEAK treatment, which was likely caused by the short half-life of soluble Fc-TWEAK *in vivo* [547]. Fn14 mRNA expression showed a trend towards an increase after Fc-TWEAK treatment and *Klf15* and *Mef2d* were significantly decreased in treated animals. Although TWEAK/Fn14 expression was not completely rescued after Fc-TWEAK treatment, the treatment did have positive effects in muscle. Dysregulated skeletal health muscle markers were partly rescued and myofiber size was increased after Fc-TWEAK treatment. These results, taken together, could potentially explain the ameliorated phenotype of Fc-TWEAK treated *Smn$^{-/-}$;SMN2* and *Smn$^{2B/-}$* mice.

5.4.6 Conclusion and future directions

One of the limitations of this research were the potential off-target effects of Fc-TWEAK. The TWEAK/Fn14 pathway is involved in many other conditions, such as tumor development and metastasis [560,561], heart-related diseases [562], kidney injury [563], cerebral ischemia [564,565] and autoimmune

diseases [566,567]. Indeed, we found that daily treatment of Fc-TWEAK resulted in early death in healthy control mice, which was likely caused by cardiac problems after Fc-TWEAK treatment [562]. In order to use the TWEAK/Fn14 pathway as a muscle-specific combinatorial therapy in SMA, the therapy should be skeletal muscle specific, which for example could be achieved through muscle-specific AAV therapy [568]. Furthermore, additional research is necessary to investigate the TWEAK/Fn14 pathway in different skeletal muscle from patients with different Types of SMA at different timepoints during disease progression in order to optimize the muscle benefits of TWEAK/Fn14 modulation therapy.

The TWEAK/Fn14 axis appears to be an important regulator of myopathy and glucose metabolism perturbations in SMA. Here we demonstrate an aberrant expression of the TWEAK/Fn14 pathway in SMA muscle during disease progression, which may contribute to muscle and even whole-body metabolic perturbations and which is not denervation dependent. Through pharmacological interventions that target TWEAK/Fn14 pathway signaling, we were able to significantly improve SMA disease phenotypes in two distinct SMA mouse models.

6. Discussion

6.1 Overview of results

This thesis is centered on muscle pathology in SMA and the development of muscle-specific treatments that could ultimately be used next to SMN restoration therapy. We have taken both an unbiased approach, in which we searched for treatments based on differently expressed genes and proteins using CMap, and a biased approach, in which we investigated TWEAK/Fn14 signaling, an atrophy pathway that had previously been investigated in other conditions but not in SMA.

In the first part of the thesis (Chapter 3 and Chapter 4), we conducted a proteomic and transcriptomic study in SMA mouse skeletal muscle, investigating which pathways are restored and unchanged in muscle after SMN restoration therapy, using Pip6a-PMO, in order to identify new and effective muscle-specific treatments. Our studies revealed that all genes and almost all proteins were rescued after SMN restoration therapy and further allowed us to identify which GO pathways were also recovered. These were undoubtedly excellent results, yet it remained clear that SMN restoration in itself is not a cure and was not sufficient to address all of the symptoms of the disease. Therefore, further investigation of other therapeutic avenues was necessary to find a treatment that could be used in combination with SMN restoration therapies to potentially provide a longer-lasting and more effective treatment strategy for SMA. This study has generated a great deal of proteomic and transcriptomic data comparing not only symptomatic SMA mice to Pip6a-PMO treated SMA mice and WT mice, but also data comparing untreated pre-symptomatic mice to untreated symptomatic mice, which allows us to see the evolution of pathological pathways over time between the SMA and WT muscle. This data generated in our study presented us with the opportunity to systematically analyze the proteomic and transcriptomic data to identify novel non-SMN pathological pathways and related pharmacological compounds using Connectivity Map (CMap) analysis [425]. It also provided us with the opportunity to test whether using CMap would be effective in finding new treatments for SMA.

CMap is a bioinformatics tool and drug repurposing strategy that shows functional connections between drugs and gene expression signatures of diseases [425], which we used to build six sets of expression signatures, three based on proteomic data and three on transcriptomic data. Out of the compounds identified by CMap, five drugs already considered for treatment of SMA in preclinical and clinical studies were highly ranked (namely salbutamol [437], alsterpaullone [83], trichostatin A [95], Valproic acid [318–322], Vorinostat [327,328] and sodium phenylbutyrate [325]), which underscores the capability of CMap to identify relevant therapeutic options for the treatment of SMA.

Another compound that was highly ranked in CMap analysis but never assessed in the context of SMA was harmine. Harmine has various therapeutic effects [440] and is, amongst other properties, neuroprotective [456–459]. One of these neuroprotective pathways is glutamate transportation [456,458]. The glutamate transporter GLT-1, for example, is upregulated in harmine treated ALS mice [469]. We also found that harmine treatment had shown positive effects in studies on the muscular dystrophy disease myotonic dystrophy type 1 (DM1) [470]. Like ALS, SMA is characterized by motor neuron death, and, like DM1, muscle pathology and as such would benefit from neuromuscular protection. Therefore, we decided to validate our combined ‘omics and drug repositioning strategy with harmine.

This thesis shows harmine treatment in the severe and moderate SMA mouse models resulted in significant rescue of disease phenotypes such as weight and survival. It further increased skeletal myofiber size and was demonstrated to be neuroprotective, as we found an upregulation of GLT-1 and a decrease in motor neuron death. A pathway analysis after RNA-seq demonstrated that 20% of dysregulated genes were fully restored after harmine treatment and 10% were partly rescued. Various pathways normally dysregulated in SMA, such as muscle contraction, oxidation-reduction, and metabolic pathways were restored by harmine treatment.

In addition to demonstrating the benefits of CMap for the discovery of treatments for SMA that can be used in combination with SMN restoration therapy, such as harmine, we also generated an

extensive list of drugs that can similarly be evaluated, alone or in combination with SMN therapies. This could potentially open new therapeutic opportunities for future studies.

The second part of the thesis (Chapter 5) took a biased approach, investigating the TWEAK and Fn14 pathway, which has been ascribed a critical role in the regulation of denervation-induced muscle atrophy as well as in muscle proliferation, differentiation and metabolism. Since neurodegeneration, muscle atrophy and metabolic perturbations typify SMA, we investigated the expression profile of Tweak and Fn14 in SMA muscle and found significantly decreased levels during disease progression in the severe *Smn*$^{-/-}$;*SMN2*$^{+/-}$ and intermediate *Smn*$^{2B/-}$ SMA mouse models and a dysregulation of Fn14 in Type 1 SMA patient skeletal muscle. Furthermore, in the same muscles, we demonstrated an abnormal expression of PGC1α, Mef2D, KLF15, HKII and Glut4, molecular effectors critical for muscle health and function and known to be regulated by the TWEAK/Fn14 pathway. Interestingly, the aberrant expression of the TWEAK/Fn14 pathway in SMA is not denervation-dependent, as we found no dysregulation in denervated muscle in WT mice but is likely to be dependent on intrinsic myopathy due to the dysregulation of the pathway in the cardiotoxin damaged muscle of WT mice. Using murine C2C12 myoblast cells and human fibroblast-derived myoblasts, we have confirmed a regulated expression of Tweak, Fn14, PGC-1α, Glut4 and Mef2D during differentiation, which is dysregulated in SMA myoblasts.

The downregulation of TWEAK that we found in the severe SMA mouse model was accompanied by the dysregulation of both the canonical and non-canonical NF-κB pathways. We found the canonical NF-κB pathway to be downregulated in the skeletal muscle of the severe SMA mouse model, which is in accordance with the findings of previous research that only pathologically high levels of TWEAK activate this pathway. The non-canonical NF-κB pathway, however, was upregulated in skeletal muscle of the severe SMA mouse muscle. This dysregulation related to the TWEAK/Fn14 pathway is possibly of considerable importance to skeletal muscle pathology in SMA because these pathways normally regulate myoblast proliferation and myogenesis [500,504,505].

This led us to investigate whether SMN depletion plays a role in the dysregulation of the TWEAK/Fn14 pathway. Our investigations demonstrate that aberrant expression of the TWEAK/Fn14 pathway in SMA is partly caused by SMN depletion, and we can therefore conclude that SMN depletion potentially performs a critical role in muscle pathology in SMA via the TWEAK/Fn14 pathway, thereby also influencing metabolic downstream effectors of TWEAK and Fn14.

We also have provided support of previous findings that skeletal muscle is not equally vulnerable to SMA pathology [169]. Dysregulation of the TWEAK/Fn14 pathway and muscle atrophy marker parvalbumin were more advanced in the *triceps*, *gastrocnemius*, and *iliopsoas*, more vulnerable muscles, than in the *quadriceps* and *diaphragm*, more resistant muscles. Using qPCR arrays to further investigate the functions of SMN, TWEAK and Fn14 in myopathy and myogenesis, we found a greater number of genes dysregulated in the more vulnerable *triceps* muscle tissue of SMA mice than in the more resistant *quadriceps* muscle. Notably, the number of dysregulated glucose metabolism genes were similar in the *triceps* and *quadriceps* muscle of SMA mice. This could be explained by the notion that the different resistances of skeletal muscle to SMA muscle pathology are based on the vulnerability of certain skeletal muscles to neuromuscular junction denervation [169], therefore concluding that denervation in skeletal muscle possibly has a greater effect on myogenesis and myopathy than on glucose metabolism.

Ultimately, this project on the dysregulation of the TWEAK/Fn14 pathway in SMA has not only scientific value, but also translational value, as we found that that modulating TWEAK levels by the administration of Fc-TWEAK treatment improved disease phenotypes and lifespan in the moderate SMA mouse model as well as muscular phenotype in the severe and moderate SMA mouse models.

6.2 Application to other fields

6.2.1 Connectivity map analysis

A considerable portion of this thesis has been dedicated to presenting an efficient way of analyzing extensive proteomic and transcriptomic datasets in order to find new therapeutic strategies for the treatment of SMA. The implications, however, are not only relevant to the field of SMA, but also to research on other human (genetic) diseases. We provide a comprehensive assessment of the CMap technique, validating the results *in vitro* and *in vivo*. As far as we are aware, this is the only study currently using RNA-seq for an elaborate pathway analysis to validate a CMap generated result. Many therapies for SMA are focused on only the *SMN1* and *SMN2* genes. A monogenic approach is not necessarily useful for other genetic conditions because they are often characterized by multiple genetic or protein dysregulations. In this study, we used an SMN-independent approach and demonstrated that, using CMap, treatments can be found that can restore disease pathology and multiple pathways by rescuing hundreds of genes through the simple application of one drug.

6.2.2 TWEAK/Fn14 pathway

The project on the TWEAK/Fn14 pathway in SMA described in this thesis is also valuable for other, non-SMA-related fields. This is the first study, as far as we are aware, that investigates this atrophy pathway in pups. We demonstrate the effects of denervation and muscle injury by cardiotoxin on the TWEAK/Fn14 pathway in young animals who are still going through development. Furthermore, using the glucose metabolism qPCR arrays, we confirmed and extrapolated on the findings of previous studies [495,510] showing a link between TWEAK/Fn14 and glucose metabolism using TWEAK and Fn14 knockout mice and comparing them to WT mice.

6.3 SMA research: the way forward

Lately, the rapid progression of new therapies for SMA approved or on the verge of approval has changed the scientific landscape of SMA research. These developments are crucial for the field; however, SMA is not cured and many questions at the level of basic and clinical research remain to be answered and each success is followed by new questions. Future research in SMA should address perfecting SMN restoration therapy, investigate combinatorial treatments and research therapeutic possibilities for patients who are not responding to SMN restoration [569] or have missed the SMN restoration therapeutic window [234].

Although clinical trials for Spinraza and scAAV9-*SMN1* have shown impressive motor function and survival improvements, many treated infants still lag behind in their paths towards normal development. Furthermore, it is not known whether there would be a ceiling for potential motor function improvement [570]. Further research, therefore, is necessary, including on the ability of motor neurons in different disease states to take up SMN restoration therapy and produce more SMN protein.

A consistent challenge in the SMN restoration therapy field is the difficulty in studying the distribution and durability of SMN restoration in humans, as motor neurons in the spinal cord are the main targets and cannot be sampled during life. Currently, the only way to investigate is by examining autopsy tissues from treated SMA patients who have passed away. It is rather fortunate, but nonetheless a constraint, that not many such studies yet exist. Analysis of autopsy tissue from 3 SMA Type 1 patients exposed to nusinersen (Spinraza) showed drug uptake into motor neurons throughout the spinal cord and neurons, as well as other cell types in the brainstem and other regions of the brain and increased *SMN2* mRNA exon 7 inclusion and SMN protein concentrations in the spinal cord [291]. Nevertheless, further study would be necessary to investigate its efficacy in terms of the relationship between SMN levels in different tissues, especially since Spinraza treated SMA patients showed less improvement in breathing and swallowing functions than in motor functions [571].

The only therapy for SMA currently approved, Spinraza, is only delivered in the CNS; however, as discussed in Chapter 1, other tissues and organs are affected in SMA. Preclinical research has shown that ICV combined with systemic subcutaneous ASO treatment was much more effective than ICV administration alone in *Smn*$^{-/-}$;*SMN2*$^{+/-}$ mice, extending the median lifespan by 25-fold [243]. This suggests a synergistic benefit to body-wide SMN restoration and needs to be further addressed.

Presently, Spinraza is administered to patients 3 times per year, continuing treatment throughout the patient's lifetime; however, the exact effects of SMN restoration over time require further investigation. SMN requirements are highest during development [234] and preclinical research has shown that only early SMN restoration resulted in near-normal development in treated *Smn*$^{-/-}$;*SMN2*$^{+/-}$ mice [143]. This is less of a problem for scAAV9-SMN treatment, notably; as this is a gene replacement therapy and motor neurons do not regenerate. Furthermore, clinical trials on SMN restoration have started only recently, so there is little information today on the long-term prognosis for treated patients. It is possible that the disease course of treated patients will resemble the disease course of less severe SMA Types, but it may instead show a different course.

Despite the incredible results from SMN restoration therapy, many issues remained to be addressed in order to optimize treatment.

6.4 Importance of considering heterogeneity among SMA patients in the investigation of therapeutic avenues

One area of SMA research urgently needing further investigation is the heterogeneity among SMA patients and the varying severities of disease pathology. As described in Chapter 1, there are 5 Types of SMA. All are caused by the same genetic defect, SMN depletion, often leading to all of them being therapeutically approached largely the same way. This, however, is not entirely appropriate. Older patients, for example, have different pathologies and therapeutic needs than younger patients. For example, Type 1 SMA patients are inclined to be underweight [572], whereas more mildly affected Type

2 and 3 patients tend to be overweight [573,574]. Severely affected SMA patients might also develop pathologies that older/milder patients will never experience, such as declining respiratory muscle function [575], and vice-versa: untreated severe patients might pass away before developing pathologies that are characteristic in older/milder affected patients, such as slowly losing the ability to walk [576]. Therefore, distinct treatment approaches are in order for different patients.

As most SMA patients are severely affected and categorized as Type 1 and 2 [11,12], the majority of therapies that have been developed are focused on treating this group. This is one of the reasons behind the great emphasis on SMN-restoration therapy: it is currently the most effective treatment for Type 1 and Type 2 patients. The majority of clinical trials involving nusinersen/Spinraza treatment were in patients ranging from newborns to a maximum of 12 years of age (e.g. ENDEAR [569], NURTURE [362], CHERISH [577]). Moreover, Avexis-101 (scAAV9-*SMN1*) therapy is only evaluated in Type 1 [314] (STR1VE [245]) and Type 2 (STRONG [578]) patients. The main reason to target severe patients, arguably, is that they might be assumed to have the greatest clinical need, and one advantage of treating them is that it requires a shorter time to demonstrate meaningful clinical outcomes.

Nevertheless, there is a great need for future research focused on therapies that are specifically targeted to older/less affected patients. This is for multiple reasons. First, older patients may benefit less from SMN restoration, as SMN is mainly required during development [234,365], and SMN restoration therapy might therefore not have a substantial clinical effect in adult patients. Second, the later the treatment takes place, the more extensive the irreversible motor neuron damage and therefore, the less effective the SMN restoration treatment. This, however, is not an argument for refraining to give SMN restoration therapy to older patients, because SMN plays different roles in many cell types and tissues (e.g. [203,237,269]) and SMN restoration treatment might still be advantageous in treating peripheral pathology in SMA, even after motor neuron death. Third, the underlying cellular events behind clinical responses are likely to be different between various patient groups. The greater progress in treated infants is due to the reversal of impaired development, whereas more modest

improvements in older treated patients might be mediated by remodeling events, such as improvement of neuromuscular junction transmission or recovery of motor neurons that are in a dysfunctional pre-degenerative state [570]. Fourth, as Type 1 and Type 2 patients will live longer after SMN restoration therapy, we may easily foresee a growth in patients with a more chronic and less-severe form of SMA.

The first step in investigating the therapeutic needs of older and less severely affected patients is conducting further natural histories of disease studies on Type 3 and 4 patients, as currently most are focused on Type 1 and Type 2 [11,579–582]. These studies should not only address motor neuron and denervation dependent skeletal muscle pathology, but also intrinsic muscle pathology, metabolism, and other peripheral pathologies. A next step would be to investigate and treat these pathologies in the more mildly affected SMA (mouse) models. Most SMA research has been executed in the severe *SMNΔ7* and *Smn*$^{-/-}$;*SMN2*$^{+/-}$ mouse models and cellular and other animal models in which SMN was completely or almost completely knocked out. In this thesis, we made a concerted attempt to do this by not only investigating muscle atrophy and the effects of treatment in the severe SMA mouse model, but also the same in the moderate SMA mouse model. Additionally, many pharmacological studies in SMA are begun in pre-symptomatic SMA mice; however, many patients are diagnosed after disease onset. It would therefore be beneficial to also study treatments in symptomatic mice and investigate if pathology can be restored and dysregulated pathways can be rescued.

In summary, the field of SMA research is biased towards the most severely affected SMA patients. Although tremendous progress has been made on the treatment of severe SMA patients, this unfortunately does not automatically translate into progress for less severely affected Type 3 and 4 SMA patients who exhibit a more chronic course of the disease. Insight into disease progression in older patients will enable a more optimal therapeutic development by taking patient-specific pathology into account, which will lead to longer lasting and more effective treatments for a larger patient population.

6.5 Differences in dysregulation of muscle-related pathways in SMA compared to other muscle conditions

Recently, advances have been made in the muscle combinatorial research field, in which muscle strategies for the treatment of SMA have entered clinical trials. In most cases, these muscle treatments have been evaluated for other muscle-related diseases. This is a most welcome development; however, we must bear in mind that muscle pathology differs in distinct diseases and should be first investigated thoroughly in SMA before expecting positive results in SMA patients.

One of the muscle strategies for SMA currently being tested in clinical trials is myostatin inhibition [351], which has been evaluated in various clinical trials. Different methods of inhibition have been tested in healthy individuals [583], older individuals who have had recent falls or have low muscle strength and power [584] and in individuals with Duchenne [585] or Becker [586] muscular dystrophy. Nevertheless, as described in Chapter 1, Section 1.4.8, myostatin inhibition demonstrated mixed results in SMA mouse models in preclinical studies [346–348]. Moreover, a study of serum from SMA patients (aged 8.9–12.9 years, disease Type unknown) showed that SMA patients already exhibit decreased myostatin expression [350] compared to healthy individuals, raising the question whether inhibition of something already registering as low in SMA patients would be beneficial as a treatment.

We encountered similar circumstances in the current thesis. Reports on chronic muscle atrophy or injury-induced atrophy showed an increase of the TWEAK/Fn14 pathway in skeletal muscle. We therefore expected to see an increase of this pathway in the severe and moderate SMA mouse models, but we instead found a significant decrease during disease progression in both mouse models. These examples emphasize the need for proper investigation of muscle pathology as well as gene and protein dysregulation in muscle in SMA before bringing a therapy into the clinic.

6.6 Concluding remarks

It took 100 years to find the gene causing SMA after the disease was first described by Guido Werdnig and Johann Hoffmann. Following this, it took an additional 21 years to develop a treatment for this devastating disease. SMN restoration trials have met with their most success when conducted using pre-symptomatic treated SMA patients. This raised the awareness of the importance of genetic screening for newborns [587,588]. However, the search for SMA treatments is not over: recent developments have not presented a cure and are not applicable to all patients. Combining SMN restoration therapies with pharmacological strategies is a more effective way of treating aspects of the disease in which SMN restoration therapies fall short. Skeletal muscle therapies are fertile ground for combinatorial strategies, but in order to produce working treatments, better understanding of muscle pathology and the role of SMN depletion in SMA is necessary. To this end, this thesis has sought to contribute to a better understanding of the biology of muscle pathology in SMA and the TWEAK/Fn14 pathway. It also presents and validates CMap as a method for searching extensive 'omics data sets to identify drugs that can restore aberrant pathways in SMA. Our proof-of-concept assessment of harmine demonstrated a rescue of hundreds of genes and multiple pathways as well as benefits to muscle and motor neuron pathology and increases in the lifespans in SMA mice. In the end, it is hoped that the work in this thesis is able to contribute towards the establishment of a muscle treatment for SMA that can be used in combination with SMN restoration therapy and ultimately produce longer-lasting and more effective results for those affected by SMA.

References

1. Ben-Shachar, S., Orr-Urtreger, A., Bardugo, E., Shomrat, R. & Yaron, Y. Large-scale population screening for spinal muscular atrophy: Clinical implications. *Genet. Med.* **13,** 110–114 (2011).

2. Miniño, A. M., Xu, J. & Kochanek, K. D. National Vital Statistics Reports, Volume 59, Number 2, (December 9, 2010). (2008).

3. Wadman, R. I., Vrancken, A. F. J. E., van den Berg, L. H. & van der Pol, W. L. Dysfunction of the neuromuscular junction in spinal muscular atrophy types 2 and 3. *Neurology* **79,** 2050–5 (2012).

4. Crawford, T. O. & Pardo, C. A. The neurobiology of childhood spinal muscular atrophy. *Neurobiol. Dis.* **3,** 97–110 (1996).

5. Werdnig, G. Zwei frühinfantile hereditäre Fälle von progressiver Muskelatrophie unter dem Bilde der Dystrophie, aber anf neurotischer Grundlage. *Arch. Psychiatr. Nervenkr.* **22,** 437–480 (1891).

6. Hoffmann, J. Ueber chronische spinale Muskelatrophie im Kindesalter, auf familiärer Basis. *Dtsch. Z. Nervenheilkd.* **3,** 427–470 (1893).

7. Meijboom, K. E., Wood, M. J. A. & McClorey, G. Splice-Switching Therapy for Spinal Muscular Atrophy. *Genes (Basel).* **8,** 161 (2017).

8. Grotto, S. *et al.* Type 0 Spinal Muscular Atrophy: Further Delineation of Prenatal and Postnatal Features in 16 Patients. *J. Neuromuscul. Dis.* **3,** 487–495 (2016).

9. Dubowitz, V. Very severe spinal muscular atrophy (SMA type 0): an expanding clinical phenotype. *Eur. J. Paediatr. Neurol.* **3,** 49–51 (1999).

10. Macleod, M. J., Taylor, J. E., Lunt, P. W., Mathew, C. G. & Robb, S. A. Prenatal onset spinal muscular atrophy. *Eur. J. Paediatr. Neurol.* **3,** 65–72 (1999).

11. Gregoretti, C. *et al.* Survival of patients with spinal muscular atrophy type 1. *Pediatrics* **131,** e1509-14 (2013).

12. Feldkötter, M., Schwarzer, V., Wirth, R., Wienker, T. F. & Wirth, B. Quantitative analyses of SMN1 and SMN2 based on real-time lightCycler PCR: fast and highly reliable carrier testing and prediction of severity of spinal muscular atrophy. *Am. J. Hum. Genet.* **70,** 358–68 (2002).

13. Khirani, S. *et al.* Longitudinal course of lung function and respiratory muscle strength in spinal muscular atrophy type 2 and 3. *Eur. J. Paediatr. Neurol.* **17,** 552–560 (2013).

14. Katayama, M. *et al.* Long-term stabilization of respiratory conditions in patients with spinal muscular atrophy type 2 by continuous positive airway pressure: a report of two cases. *Kobe J. Med. Sci.* **57,** E98-105 (2011).

15. Mailman, M. D. *et al.* Molecular analysis of spinal muscular atrophy and modification of the phenotype by SMN2. *Genet. Med.* **4,** 20–26 (2002).

16. Wirth, B. *et al.* Mildly affected patients with spinal muscular atrophy are partially protected by an increased SMN2 copy number. *Hum. Genet.* **119,** 422–428 (2006).

17. Melki, J. *et al.* Gene for chronic proximal spinal muscular atrophies maps to chromosome 5q. *Nature* **344,** 767–768 (1990).

18. Gilliam, T. C. *et al.* Genetic homogeneity between acute and chronic forms of spinal muscular atrophy. *Nature* **345,** 823–825 (1990).

19. Lefebvre, S. *et al.* Identification and Characterization of a Spinal Muscular Atrophy-Determining Gene. *Cell* **80,** 155–65 (1995).

20. Rochette, C. F., Gilbert, N. & Simard, L. R. SMN gene duplication and the emergence of the SMN2 gene occurred in distinct hominids: SMN2 is unique to Homo sapiens. *Hum. Genet.* **108,** 255–66 (2001).

21. Lorson, C. L., Hahnen, E., Androphy, E. J. & Wirth, B. A single nucleotide in the SMN gene regulates splicing and is responsible for spinal muscular atrophy. *Proc. Natl. Acad. Sci.* **96,** 6307–6311 (1999).

22. Monani, U. R. A single nucleotide difference that alters splicing patterns distinguishes the SMA gene SMN1 from the copy gene SMN2. *Hum. Mol. Genet.* **8,** 1177–1183 (1999).

23. Chang, H.-C., Hung, W.-C., Chuang, Y.-J. & Jong, Y.-J. Degradation of survival motor neuron (SMN) protein is mediated via the ubiquitin/proteasome pathway. *Neurochem. Int.* **45,** 1107–1112 (2004).

24. Schrank, B. *et al.* Inactivation of the survival motor neuron gene, a candidate gene for human spinal muscular atrophy, leads to massive cell death in early mouse embryos. *Proc. Natl. Acad. Sci. U. S. A.* **94,** 9920–5 (1997).

25. Monani, U. R. *et al.* A single nucleotide difference that alters splicing patterns distinguishes the SMA gene SMN1 from the copy gene SMN2. *Hum. Mol. Genet.* **8,** 1177–1183 (1999).

26. Jodelka, F. M., Ebert, A. D., Duelli, D. M. & Hastings, M. L. A feedback loop regulates splicing of the spinal muscular atrophy-modifying gene, SMN2. *Hum. Mol. Genet.* **19,** 4906–17 (2010).

27. Staropoli, J. F. *et al.* Rescue of gene-expression changes in an induced mouse model of spinal muscular atrophy by an antisense oligonucleotide that promotes inclusion of SMN2 exon 7. *Genomics* **105,** 220–228 (2015).

28. Lefebvre, S. *et al.* Identification and characterization of a spinal muscular atrophy-determining gene. *Cell* **80,** 155–65 (1995).

29. Bürglen, L. *et al.* SMN gene deletion in variant of infantile spinal muscular atrophy. *Lancet* **346,** 316–317 (1995).

30. Wirth, B. An update of the mutation spectrum of the survival motor neuron gene (SMN1) in autosomal recessive spinal muscular atrophy (SMA). *Hum. Mutat.* **15,** 228–37 (2000).

31. Wirth, B. *et al.* De Novo Rearrangements Found in 2% of Index Patients with Spinal Muscular Atrophy: Mutational Mechanisms, Parental Origin, Mutation Rate, and Implications for Genetic Counseling. *Am. J. Hum. Genet.* **61,** 1102–1111 (1997).

32. Campbell, L., Potter, A., Ignatius, J., Dubowitz, V. & Davies, K. Genomic Variation and Gene Conversion in Spinal Muscular Atrophy: Implications for Disease Process and Clinical Phenotype. *Am. J. Hum. Genet* **61,** 40–50 (1997).

33. Sugarman, E. A. *et al.* Pan-ethnic carrier screening and prenatal diagnosis for spinal muscular atrophy: clinical laboratory analysis of >72 400 specimens. *Eur. J. Hum. Genet.* **20,** 27–32 (2012).

34. Shawky, R. M. & El-Sayed, N. S. Clinico-epidemiologic characteristics of spinal muscular atrophy among Egyptians. *Egypt. J. Med. Hum. Genet.* **12,** 25–30 (2011).

35. Lyahyai, J., Sbiti, A., Barkat, A., Ratbi, I. & Sefiani, A. Spinal Muscular Atrophy Carrier Frequency and Estimated Prevalence of the Disease in Moroccan Newborns. *Genet. Test. Mol. Biomarkers* **16,** 215–218 (2012).

36. Verhaart, I. E. C. *et al.* Prevalence, incidence and carrier frequency of 5q-linked spinal muscular atrophy - a literature review. *Orphanet J. Rare Dis.* **12,** 124 (2017).

37. Sangaré, M. *et al.* Genetics of low spinal muscular atrophy carrier frequency in sub-Saharan Africa. *Ann. Neurol.* **75,** 525–532 (2014).

38. Chong, J. X. *et al.* A common spinal muscular atrophy deletion mutation is present on a single founder haplotype in the US Hutterites. *Eur. J. Hum. Genet.* **19,** 1045–1051 (2011).

39. Basel-Vanagaite, L. *et al.* Genetic Carrier Screening for Spinal Muscular Atrophy and Spinal Muscular Atrophy with Respiratory Distress 1 in an Isolated Population in Israel.

40. Prior, T. W., Swoboda, K. J., Scott, H. D. & Hejmanowski, A. Q. Homozygous SMN1 deletions in unaffected family members and modification of the phenotype by SMN2. *Am. J. Med. Genet. A* **130A,** 307–10 (2004).

41. Cobben, J. M. *et al.* Deletions of the survival motor neuron gene in unaffected siblings of patients with spinal muscular atrophy. *Am. J. Hum. Genet.* **57,** 805–8 (1995).

42. Wang, C. H. *et al.* Characterization of survival motor neuron (SMNT) gene deletions in asymptomatic carriers of spinal muscular atrophy. *Hum. Mol. Genet.* **5,** 359–65 (1996).

43. Liu, Q. & Dreyfuss, G. A novel nuclear structure containing the survival of motor neurons protein. *EMBO J.* **15,** 3555–65 (1996).

44. Wahl, M. C., Will, C. L. & Lührmann, R. The Spliceosome: Design Principles of a Dynamic RNP Machine. *Cell* **136,** 701–718 (2009).

45. Liu, Q., Fischer, U., Wang, F. & Dreyfuss, G. The spinal muscular atrophy disease gene product, SMN, and its associated protein SIP1 are in a complex with spliceosomal snRNP proteins. *Cell* **90,** 1013–21 (1997).

46. Fischer, U., Liu, Q. & Dreyfuss, G. The SMN-SIP1 complex has an essential role in spliceosomal snRNP biogenesis. *Cell* **90,** 1023–9 (1997).

47. Pellizzoni, L., Yong, J. & Dreyfuss, G. Essential role for the SMN complex in the specificity of snRNP assembly. *Science* **298,** 1775–9 (2002).

48. Zhang, Z. *et al.* SMN Deficiency Causes Tissue-Specific Perturbations in the Repertoire of snRNAs and Widespread Defects in Splicing. *Cell* **133,** 585–600 (2008).

49. Bäumer, D. *et al.* Alternative splicing events are a late feature of pathology in a mouse model of spinal muscular atrophy. *PLoS Genet.* **5,** e1000773 (2009).

50. Olaso, R. *et al.* Activation of RNA metabolism-related genes in mouse but not human tissues deficient in SMN. *Physiol. Genomics* **24,** 97–104 (2006).

51. Campion, Y., Neel, H., Gostan, T., Soret, J. & Bordonné, R. Specific splicing defects in S. pombe carrying a degron allele of the Survival of Motor Neuron gene. *EMBO J.* **29,** 1817–1829 (2010).

52. Lotti, F. *et al.* An SMN-Dependent U12 Splicing Event Essential for Motor Circuit Function. *Cell* **151,** 440–454 (2012).

53. Jangi, M. *et al.* SMN deficiency in severe models of spinal muscular atrophy causes widespread intron retention and DNA damage. *Proc. Natl. Acad. Sci.* **114,** E2347–E2356 (2017).

54. McWhorter, M. L., Boon, K., Horan, E. S., Burghes, A. H. M. & Beattie, C. E. The SMN binding protein gemin2 is not involved in motor axon outgrowth. *Dev. Neurobiol.* **68,** 182–194 (2008).

55. Tucker, K. E. *et al.* Residual Cajal bodies in coilin knockout mice fail to recruit Sm snRNPs and SMN, the spinal muscular atrophy gene product. *J. Cell Biol.* **154,** 293–307 (2001).

56. Hebert, M. D., Szymczyk, P. W., Shpargel, K. B. & Matera, A. G. Coilin forms the bridge between Cajal bodies and SMN, the spinal muscular atrophy protein. *Genes Dev.* **15,** 2720–9 (2001).

57. Sanchez, G. *et al.* A novel role for CARM1 in promoting nonsense-mediated mRNA decay: potential implications for spinal muscular atrophy. *Nucleic Acids Res.* **44,** 2661–2676 (2016).

58. Pellizzoni, L., Baccon, J., Charroux, B. & Dreyfuss, G. The survival of motor neurons (SMN) protein interacts with the snoRNP proteins fibrillarin and GAR1. *Curr. Biol.* **11,** 1079–88 (2001).

59. Jones, K. W. *et al.* Direct interaction of the spinal muscular atrophy disease protein SMN with the small nucleolar RNA-associated protein fibrillarin. *J. Biol. Chem.* **276,** 38645–51 (2001).

60. Tisdale, S. *et al.* SMN is essential for the biogenesis of U7 small nuclear ribonucleoprotein and 3'-end formation of histone mRNAs. *Cell Rep.* **5,** 1187–95 (2013).

61. Pillai, R. S. *et al.* Unique Sm core structure of U7 snRNPs: assembly by a specialized SMN complex and the role of a new component, Lsm11, in histone RNA processing. *Genes Dev.* **17,** 2321–2333 (2003).

62. Thompson, L. W. *et al.* Neurochondrin interacts with the SMN protein suggesting a novel mechanism for spinal muscular atrophy pathology. *J. Cell Sci.* **131,** jcs211482 (2018).

63. Piazzon, N. *et al.* Implication of the SMN complex in the biogenesis and steady state level of the Signal Recognition Particle. *Nucleic Acids Res.* **41,** 1255–1272 (2013).

64. Bachand, F., Boisvert, F.-M., Côté, J., Richard, S. & Autexier, C. The product of the survival of motor neuron (SMN) gene is a human telomerase-associated protein. *Mol. Biol. Cell* **13,** 3192–202 (2002).

65. Poole, A. R. & Hebert, M. D. SMN and coilin negatively regulate dyskerin association with telomerase RNA. *Biol. Open* **5,** 726–735 (2016).

66. Lorson, C. L. *et al.* SMN oligomerization defect correlates with spinal muscular atrophy severity. *Nat. Genet.* **19,** 63–66 (1998).

67. Cho, S. *et al.* hnRNP M facilitates exon 7 inclusion of SMN2 pre-mRNA in spinal muscular atrophy by targeting an enhancer on exon 7. *Biochim. Biophys. Acta - Gene Regul. Mech.* **1839,** 306–315 (2014).

68. Singh, N. N. K., Singh, N. N. K., Androphy, E. J. & Singh, R. N. Splicing of a critical exon of human Survival Motor Neuron is regulated by a unique silencer element located in the last intron. *Mol. Cell. Biol.* **26,** 1333–46 (2006).

69. Singh, N. N., Lee, B. M. & Singh, R. N. Splicing regulation in spinal muscular atrophy by an RNA

structure formed by long-distance interactions. *Ann. N. Y. Acad. Sci.* **1341,** 176–187 (2015).

70. Pedrotti, S. *et al.* The splicing regulator Sam68 binds to a novel exonic splicing silencer and functions in SMN2 alternative splicing in spinal muscular atrophy. *EMBO J.* **29,** 1235–1247 (2010).

71. Qu, Y. *et al.* A rare variant (c.863G>T) in exon 7 of SMN1 disrupts mRNA splicing and is responsible for spinal muscular atrophy. *Eur. J. Hum. Genet.* **24,** 864–870 (2016).

72. Helmken, C. *et al.* Evidence for a modifying pathway in SMA discordant families: reduced SMN level decreases the amount of its interacting partners and Htra2-beta1. *Hum. Genet.* **114,** 11–21 (2003).

73. Prior, T. W. *et al.* A positive modifier of spinal muscular atrophy in the SMN2 gene. *Am. J. Hum. Genet.* **85,** 408–13 (2009).

74. Fan, L. & Simard, L. R. Survival motor neuron (SMN) protein: role in neurite outgrowth and neuromuscular maturation during neuronal differentiation and development. *Hum. Mol. Genet.* **11,** 1605–14 (2002).

75. Gabanella, F., Carissimi, C., Usiello, A. & Pellizzoni, L. The activity of the spinal muscular atrophy protein is regulated during development and cellular differentiation. *Hum. Mol. Genet.* **14,** 3629–3642 (2005).

76. Baron-Delage, S., Abadie, A., Echaniz-Laguna, A., Melki, J. & Beretta, L. Interferons and IRF-1 induce expression of the survival motor neuron (SMN) genes. *Mol. Med.* **6,** 957–68 (2000).

77. Majumder, S. *et al.* Identification of a Novel Cyclic AMP-response Element (CRE-II) and the Role of CREB-1 in the cAMP-induced Expression of the Survival Motor Neuron (*SMN*) Gene. *J. Biol. Chem.* **279,** 14803–14811 (2004).

78. Ting, C.-H., Lin, C.-W., Wen, S.-L., Hsieh-Li, H.-M. & Li, H. Stat5 constitutive activation rescues defects in spinal muscular atrophy. *Hum. Mol. Genet.* **16,** 499–514 (2007).

79. Farooq, F. *et al.* Prolactin increases SMN expression and survival in a mouse model of severe spinal muscular atrophy via the STAT5 pathway. *J. Clin. Invest.* **121,** 3042–3050 (2011).

80. Lunke, S. & El-Osta, A. The emerging role of epigenetic modifications and chromatin remodeling in spinal muscular atrophy. *J. Neurochem.* **109,** 1557–1569 (2009).

81. Farooq, F., Balabanian, S., Liu, X., Holcik, M. & MacKenzie, A. p38 Mitogen-activated protein kinase stabilizes SMN mRNA through RNA binding protein HuR. *Hum. Mol. Genet.* **18,** 4035–4045 (2009).

82. Workman, E., Veith, A. & Battle, D. J. U1A regulates 3’ processing of the survival motor neuron mRNA. *J. Biol. Chem.* **289,** 3703–12 (2014).

83. Makhortova, N. R. *et al.* A screen for regulators of survival of motor neuron protein levels. *Nat. Chem. Biol.* **7,** 544–552 (2011).

84. Chen, P. C. *et al.* Identification of a Maleimide-Based Glycogen Synthase Kinase-3 (GSK-3) Inhibitor, BIP-135, that Prolongs the Median Survival Time of Δ7 SMA KO Mouse Model of Spinal Muscular Atrophy. *ACS Chem. Neurosci.* **3,** 5–11 (2012).

85. Burnett, B. G. *et al.* Regulation of SMN Protein Stability. *Mol. Cell. Biol.* **29,** 1107–1115 (2009).

86. Grimmler, M. *et al.* Phosphorylation regulates the activity of the SMN complex during assembly of spliceosomal U snRNPs. *EMBO Rep.* **6,** 70–76 (2005).

87. Garbes, L. *et al.* VPA response in SMA is suppressed by the fatty acid translocase CD36. *Hum. Mol. Genet.* **22,** 398–407 (2013).

88. Kwon, D. Y., Motley, W. W., Fischbeck, K. H. & Burnett, B. G. Increasing expression and decreasing degradation of SMN ameliorate the spinal muscular atrophy phenotype in mice. *Hum. Mol. Genet.* **20,** 3667–3677 (2011).

89. Balak, C. D. *et al.* Functional characterizations of rare UBA1 variants in X-linked Spinal Muscular Atrophy. *F1000Research* **6,** 1636 (2017).

90. Wishart, T. M. *et al.* Dysregulation of ubiquitin homeostasis and β-catenin signaling promote spinal muscular atrophy. *J. Clin. Invest.* **124,** 1821–1834 (2014).

91. Aghamaleky Sarvestany, A. *et al.* Label-free quantitative proteomic profiling identifies disruption of ubiquitin homeostasis as a key driver of schwann cell defects in spinal muscular atrophy. *J. Proteome Res.* **13,** 4546–57 (2014).

92. Powis, R. A. *et al.* Systemic restoration of UBA1 ameliorates disease in spinal muscular atrophy. *JCI Insight* **1,** 1634–1644 (2016).

93. Bebee, T. W., Dominguez, C. E., Samadzadeh-Tarighat, S., Akehurst, K. L. & Chandler, D. S. Hypoxia is a modifier of SMN2 splicing and disease severity in a severe SMA mouse model. *Hum. Mol. Genet.* **21,** 4301–4313 (2012).

94. Sahashi, K. *et al.* TSUNAMI: an antisense method to phenocopy splicing-associated diseases in animals. *Genes Dev.* **26,** 1874–1884 (2012).

95. Narver, H. L. *et al.* Sustained improvement of spinal muscular atrophy mice treated with trichostatin a plus nutrition. *Ann. Neurol.* **64,** 465–470 (2008).

96. Butchbach, M. E. R. *et al.* Effect of diet on the survival and phenotype of a mouse model for spinal muscular atrophy. *Biochem. Biophys. Res. Commun.* **391,** 835–40 (2010).

97. Lemoine, T. J. *et al.* Spinal muscular atrophy type 1: are proactive respiratory interventions associated with longer survival? *Pediatr. Crit. Care Med.* **13,** e161-5 (2012).

98. Seo, J. *et al.* Oxidative Stress Triggers Body-Wide Skipping of Multiple Exons of the Spinal Muscular Atrophy Gene. *PLoS One* **11,** e0154390 (2016).

99. Kapitein, L. C. & Hoogenraad, C. C. Building the Neuronal Microtubule Cytoskeleton. *Neuron* **87,** 492–506 (2015).

100. Xiao, Q., Hu, X., Wei, Z. & Tam, K. Y. Cytoskeleton Molecular Motors: Structures and Their Functions in Neuron. *Int. J. Biol. Sci.* **12,** 1083–92 (2016).

101. Oprea, G. E. *et al.* Plastin 3 is a protective modifier of autosomal recessive spinal muscular atrophy. *Science* **320,** 524–7 (2008).

102. Stratigopoulos, G. *et al.* Association of Plastin 3 Expression With Disease Severity in Spinal Muscular Atrophy Only in Postpubertal Females. *Arch. Neurol.* **67,** 1252–6 (2010).

103. Yanyan, C. *et al.* Correlation of PLS3 expression with disease severity in children with spinal muscular atrophy. *J. Hum. Genet.* **59,** 24–27 (2014).

104. Lyon, A. N. *et al.* Calcium binding is essential for plastin 3 function in Smn-deficient motoneurons. *Hum. Mol. Genet.* **23,** 1990–2004 (2014).

105. Kaifer, K. A. *et al.* Plastin-3 extends survival and reduces severity in mouse models of spinal muscular atrophy. *JCI Insight* **2,** e89970 (2017).

106. Hosseinibarkooie, S. *et al.* The Power of Human Protective Modifiers: PLS3 and CORO1C Unravel Impaired Endocytosis in Spinal Muscular Atrophy and Rescue SMA Phenotype. *Am. J. Hum. Genet.* **99,** 647–665 (2016).

107. Bowerman, M., Shafey, D. & Kothary, R. Smn depletion alters profilin II expression and leads to upregulation of the RhoA/ROCK pathway and defects in neuronal integrity. *J. Mol. Neurosci.* **32,** 120–31 (2007).

108. Bowerman, M. *et al.* SMN, profilin IIa and plastin 3: A link between the deregulation of actin dynamics and SMA pathogenesis. *Mol. Cell. Neurosci.* **42,** 66–74 (2009).

109. Nölle, A. *et al.* The spinal muscular atrophy disease protein SMN is linked to the rho-kinase pathway via profilin. *Hum. Mol. Genet.* **20,** 4865–4878 (2011).

110. Stankiewicz, T. R. & Linseman, D. A. Rho family GTPases: key players in neuronal development, neuronal survival, and neurodegeneration. *Front. Cell. Neurosci.* **8,** 314 (2014).

111. Bowerman, M., Beauvais, A., Anderson, C. L. & Kothary, R. Rho-kinase inactivation prolongs survival of an intermediate SMA mouse model. *Hum. Mol. Genet.* **19,** 1468–1478 (2010).

112. Bowerman, M., Murray, L. M., Boyer, J. G., Anderson, C. L. & Kothary, R. Fasudil improves survival and promotes skeletal muscle development in a mouse model of spinal muscular atrophy. *BMC Med.* **10,** 24 (2012).

113. Mooren, O. L., Galletta, B. J. & Cooper, J. A. Roles for Actin Assembly in Endocytosis. *Annu. Rev. Biochem.* **81,** 661–686 (2012).

114. Liu, X.-A., Rizzo, V. & Puthanveettil, S. V. Pathologies of axonal transport in neurodegenerative diseases. doi:10.2478/s13380-012-0044-7

115. Kong, L. *et al.* Impaired Synaptic Vesicle Release and Immaturity of Neuromuscular Junctions in Spinal Muscular Atrophy Mice. *J. Neurosci.* **29,** 842–851 (2009).

116. Torres-Benito, L., Neher, M. F., Cano, R., Ruiz, R. & Tabares, L. SMN Requirement for Synaptic Vesicle, Active Zone and Microtubule Postnatal Organization in Motor Nerve Terminals. *PLoS One* **6,** e26164 (2011).

117. Ruiz, R., Casanas, J. J., Torres-Benito, L., Cano, R. & Tabares, L. Altered Intracellular Ca2+ Homeostasis in Nerve Terminals of Severe Spinal Muscular Atrophy Mice. *J. Neurosci.* **30,** 849–857 (2010).

118. Custer, S. K. & Androphy, E. J. Autophagy dysregulation in cell culture and animals models of spinal muscular atrophy. *Mol. Cell. Neurosci.* **61,** 133–140 (2014).

119. Garcera, A., Bahi, N., Periyakaruppiah, A., Arumugam, S. & Soler, R. M. Survival motor neuron protein reduction deregulates autophagy in spinal cord motoneurons in vitro. *Cell Death Dis.* **4,** e686–e686 (2013).

120. Riessland, M. *et al.* Neurocalcin Delta Suppression Protects against Spinal Muscular Atrophy in Humans and across Species by Restoring Impaired Endocytosis. *Am. J. Hum. Genet.* **100,** 297–

315 (2017).

121. Monani, U. R. *et al.* The human centromeric survival motor neuron gene (SMN2) rescues embryonic lethality in Smn(-/-) mice and results in a mouse with spinal muscular atrophy. *Hum. Mol. Genet.* **9,** 333–9 (2000).

122. Hsieh-Li, H. M. *et al.* A mouse model for spinal muscular atrophy. *Nat. Genet.* **24,** 66–70 (2000).

123. Takahashi, K. *et al.* Induction of Pluripotent Stem Cells from Adult Human Fibroblasts by Defined Factors. *Cell* **131,** 861–872 (2007).

124. Thomson, J. A. *et al.* Embryonic stem cell lines derived from human blastocysts. *Science* **282,** 1145–7 (1998).

125. Wang, Z.-B., Zhang, X. & Li, X.-J. Recapitulation of spinal motor neuron-specific disease phenotypes in a human cell model of spinal muscular atrophy. *Cell Res.* **23,** 378–393 (2013).

126. Ebert, A. D. *et al.* Induced pluripotent stem cells from a spinal muscular atrophy patient. *Nature* **457,** 277–280 (2009).

127. Zhou, M. *et al.* Seamless Genetic Conversion of *SMN2* to *SMN1* via CRISPR/Cpf1 and Single-Stranded Oligodeoxynucleotides in Spinal Muscular Atrophy Patient-Specific Induced Pluripotent Stem Cells. *Hum. Gene Ther.* hum.2017.255 (2018). doi:10.1089/hum.2017.255

128. Ramirez, A. *et al.* Investigation of New Morpholino Oligomers to Increase Survival Motor Neuron Protein Levels in Spinal Muscular Atrophy. *Int. J. Mol. Sci.* **19,** 167 (2018).

129. Feng, M. *et al.* Restoration of SMN expression in mesenchymal stem cells derived from gene-targeted patient-specific iPSCs. *J. Mol. Histol.* **49,** 27–37 (2018).

130. Ando, S. *et al.* Edaravone is a candidate agent for spinal muscular atrophy: In vitro analysis using a human induced pluripotent stem cells-derived disease model. *Eur. J. Pharmacol.* **814,** 161–168 (2017).

131. Wen, H.-L. L. *et al.* Stathmin, a microtubule-destabilizing protein, is dysregulated in spinal muscular atrophy. *Hum. Mol. Genet.* **19,** 1766–1778 (2010).

132. Acsadi, G., Li, X., Murphy, K. J., Swoboda, K. J. & Parker, G. C. Alpha-synuclein loss in spinal muscular atrophy. *J. Mol. Neurosci.* **43,** 275–83 (2011).

133. Trülzsch, B., Garnett, C., Davies, K. & Wood, M. Knockdown of SMN by RNA interference induces apoptosis in differentiated P19 neural stem cells. *Brain Res.* **1183,** 1–9 (2007).

134. Trülzsch, B., Davies, K. & Wood, M. Survival of motor neuron gene downregulation by RNAi: towards a cell culture model of spinal muscular atrophy. *Mol. Brain Res.* **120,** 145–150 (2004).

135. Kashima, T., Rao, N. & Manley, J. L. An intronic element contributes to splicing repression in spinal muscular atrophy. *Proc. Natl. Acad. Sci. U. S. A.* **104,** 3426–31 (2007).

136. Dal Mas, A., Rogalska, M. E., Bussani, E. & Pagani, F. Improvement of SMN2 Pre-mRNA Processing Mediated by Exon-Specific U1 Small Nuclear RNA. *Am. J. Hum. Genet.* **96,** 93–103 (2015).

137. Woll, M. G. *et al.* Discovery and Optimization of Small Molecule Splicing Modifiers of Survival Motor Neuron 2 as a Treatment for Spinal Muscular Atrophy. (2016). doi:10.1021/ACS.JMEDCHEM.6B00460

138. Madocsai, C., Lim, S. R., Geib, T., Lam, B. J. & Hertel, K. J. Correction of SMN2 Pre-mRNA splicing by antisense U7 small nuclear RNAs. *Mol. Ther.* **12,** 1013–1022 (2005).

139. Doktor, T. K. *et al.* RNA-sequencing of a mouse-model of spinal muscular atrophy reveals tissue-wide changes in splicing of U12-dependent introns. **45,** 395–416 (2017).

140. Fuller, H. R. *et al.* Spinal Muscular Atrophy Patient iPSC-Derived Motor Neurons Have Reduced Expression of Proteins Important in Neuronal Development. *Front. Cell. Neurosci.* **9,** 506 (2016).

141. Tajik-Ahmadabad, B., Polyzos, A., Separovic, F. & Shabanpoor, F. Amphiphilic lipopeptide significantly enhances uptake of charge-neutral splice switching morpholino oligonucleotide in spinal muscular atrophy patient-derived fibroblasts. *Int. J. Pharm.* **532,** 21–28 (2017).

142. Farrelly-Rosch, A., Lau, C. L., Patil, N., Turner, B. J. & Shabanpoor, F. Combination of valproic acid and morpholino splice-switching oligonucleotide produces improved outcomes in spinal muscular atrophy patient-derived fibroblasts. *Neurochem. Int.* **108,** 213–221 (2017).

143. Hammond, S. M. *et al.* Systemic peptide-mediated oligonucleotide therapy improves long-term survival in spinal muscular atrophy. *Proc. Natl. Acad. Sci.* **113,** 10962–10967 (2016).

144. Shafey, D., Côté, P. D. & Kothary, R. Hypomorphic Smn knockdown C2C12 myoblasts reveal intrinsic defects in myoblast fusion and myotube morphology. *Exp. Cell Res.* **311,** 49–61 (2005).

145. Boyer, J. G. *et al.* Myogenic program dysregulation is contributory to disease pathogenesis in spinal muscular atrophy. *Hum. Mol. Genet.* **23,** 4249–59 (2014).

146. Arnold, A.-S. *et al.* Reduced expression of nicotinic AChRs in myotubes from spinal muscular atrophy I patients. *Lab. Investig.* **84,** 1271–1278 (2004).

147. Goldstein, B. Sydney Brenner on the Genetics of Caenorhabditis elegans. *Genetics* **204,** 1–2 (2016).

148. Boulin, T. & Hobert, O. From genes to function: the C. elegans genetic toolbox. *Wiley Interdiscip. Rev. Dev. Biol.* **1,** 114–37 (2012).

149. Miguel-Aliaga, I. *et al.* The Caenorhabditis Elegans Orthologue of the Human Gene Responsible for Spinal Muscular Atrophy Is a Maternal Product Critical for Germline Maturation and Embryonic Viability. *Hum. Mol. Genet.* **8,** 2133–2143 (1999).

150. Briese, M. *et al.* Deletion of smn-1, the Caenorhabditis elegans ortholog of the spinal muscular atrophy gene, results in locomotor dysfunction and reduced lifespan. *Hum. Mol. Genet.* **18,** 97–104 (2008).

151. Sleigh, J. N. *et al.* A novel Caenorhabditis elegans allele, smn-1(cb131), mimicking a mild form of spinal muscular atrophy, provides a convenient drug screening platform highlighting new and pre-approved compounds. *Hum. Mol. Genet.* **20,** 245–260 (2011).

152. Stephenson, R. & Metcalfe, N. Drosophila melanogaster: a fly through its history and current use. *J. R. Coll. Physicians Edinb.* **43,** 70–75 (2013).

153. Miguel-Aliaga, I., Chan, Y. B., Davies, K. E. & van den Heuvel, M. Disruption of SMN function by ectopic expression of the human SMN gene in Drosophila. *FEBS Lett.* **486,** 99–102 (2000).

154. Chan, Y. B. *et al.* Neuromuscular defects in a Drosophila survival motor neuron gene mutant. *Hum. Mol. Genet.* **12,** 1367–1376 (2003).

155. Fernandes, J. J. & Keshishian, H. Development of the Adult Neuromuscular System. *Int. Rev. Neurobiol.* **43,** 221–239 (1999).

156. Rajendra, T. K. *et al.* A Drosophila melanogaster model of spinal muscular atrophy reveals a function for SMN in striated muscle. *J. Cell Biol.* **176,** 831–41 (2007).

157. Shpargel, K. B., Praveen, K., Rajendra, T. K. & Matera, A. G. Gemin3 is an essential gene required for larval motor function and pupation in Drosophila. *Mol. Biol. Cell* **20,** 90–101 (2009).

158. Praveen, K., Wen, Y. & Matera, A. G. A Drosophila Model of Spinal Muscular Atrophy Uncouples snRNP Biogenesis Functions of Survival Motor Neuron from Locomotion and Viability Defects. *Cell Rep.* **1,** 624–631 (2012).

159. Grunwald, D. J. & Eisen, J. S. Headwaters of the zebrafish — emergence of a new model vertebrate. *Nat. Rev. Genet.* **3,** 717–724 (2002).

160. Ciura, S. *et al.* Loss of function of C9orf72 causes motor deficits in a zebrafish model of Amyotrophic Lateral Sclerosis. *Ann. Neurol.* n/a-n/a (2013). doi:10.1002/ana.23946

161. Ramesh, T. *et al.* A genetic model of amyotrophic lateral sclerosis in zebrafish displays phenotypic hallmarks of motoneuron disease. *Dis. Model. Mech.* **3,** 652–62 (2010).

162. McWhorter, M. L., Monani, U. R., Burghes, A. H. M. & Beattie, C. E. Knockdown of the survival motor neuron (Smn) protein in zebrafish causes defects in motor axon outgrowth and pathfinding. *J. Cell Biol.* **162,** 919–31 (2003).

163. Hwang, W. Y. *et al.* Efficient genome editing in zebrafish using a CRISPR-Cas system. *Nat. Biotechnol.* **31,** 227–229 (2013).

164. Huang, P. *et al.* Heritable gene targeting in zebrafish using customized TALENs. *Nat. Biotechnol.* **29,** 699–700 (2011).

165. Boon, K.-L. *et al.* Zebrafish survival motor neuron mutants exhibit presynaptic neuromuscular junction defects. *Hum. Mol. Genet.* **18,** 3615–3625 (2009).

166. Hao, L. T., Burghes, A. H. & Beattie, C. E. Generation and Characterization of a genetic zebrafish model of SMA carrying the human SMN2 gene. *Mol. Neurodegener.* **6,** 24 (2011).

167. Le, T. T. *et al.* SMNΔ7, the major product of the centromeric survival motor neuron (SMN2) gene, extends survival in mice with spinal muscular atrophy and associates with full-length SMN. *Hum. Mol. Genet.* **14,** 845–857 (2005).

168. Mentis, G. Z. *et al.* Early functional impairment of sensory-motor connectivity in a mouse model of spinal muscular atrophy. *Neuron* **69,** (2011).

169. Ling, K. K. Y., Gibbs, R. M., Feng, Z. & Ko, C.-P. C.-P. Severe neuromuscular denervation of clinically relevant muscles in a mouse model of spinal muscular atrophy. *Hum. Mol. Genet.* **21,** 185–95 (2012).

170. Gogliotti, R. G., Hammond, S. M., Lutz, C. & Didonato, C. J. Molecular and phenotypic reassessment of an infrequently used mouse model for spinal muscular atrophy. *Biochem. Biophys. Res. Commun.* **391,** 517–522 (2010).

171. DiDonato, C. J. *et al.* Regulation of murine survival motor neuron (Smn) protein levels by modifying Smn exon 7 splicing. *Hum. Mol. Genet.* **10,** 2727–36 (2001).

172. Hammond, S. M. *et al.* Mouse survival motor neuron alleles that mimic SMN2 splicing and are inducible rescue embryonic lethality early in development but not late. *PLoS One* **5,** e15887 (2010).

173. Bowerman, M., Murray, L. M., Beauvais, A., Pinheiro, B. & Kothary, R. A critical smn threshold in mice dictates onset of an intermediate spinal muscular atrophy phenotype associated with a distinct neuromuscular junction pathology. *Neuromuscul. Disord.* **22,** 263–276 (2012).

174. Monani, U. R. *et al.* A transgene carrying an A2G missense mutation in the SMN gene modulates phenotypic severity in mice with severe (type I) spinal muscular atrophy. *J. Cell Biol.* **160,** 41–52 (2003).

175. Gladman, J. T. *et al.* A humanized Smn gene containing the SMN2 nucleotide alteration in exon 7 mimics SMN2 splicing and the SMA disease phenotype. *Hum. Mol. Genet.* **19,** 4239–4252 (2010).

176. Eshraghi, M., McFall, E., Gibeault, S. & Kothary, R. Effect of genetic background on the phenotype of the Smn2B/- mouse model of spinal muscular atrophy. *Hum. Mol. Genet.* **25,** 4494–4506 (2016).

177. Liu, C. Strategies for designing transgenic DNA constructs. *Methods Mol. Biol.* **1027,** 183–201 (2013).

178. McGovern, V. L. *et al.* SMN expression is required in motor neurons to rescue electrophysiological deficits in the SMNΔ7 mouse model of SMA. *Hum. Mol. Genet.* **24,** 5524–5541 (2015).

179. Park, G.-H., Maeno-Hikichi, Y., Awano, T., Landmesser, L. T. & Monani, U. R. Reduced Survival of Motor Neuron (SMN) Protein in Motor Neuronal Progenitors Functions Cell Autonomously to Cause Spinal Muscular Atrophy in Model Mice Expressing the Human Centromeric (SMN2) Gene. *J. Neurosci.* **30,** 12005–12019 (2010).

180. Cifuentes-Diaz, C. *et al.* Deletion of murine SMN exon 7 directed to skeletal muscle leads to severe muscular dystrophy. *J. Cell Biol.* **152,** 1107–14 (2001).

181. Vitte, J. M. *et al.* Deletion of Murine Smn Exon 7 Directed to Liver Leads to Severe Defect of Liver Development Associated with Iron Overload. *Am. J. Pathol.* **165,** 1731–1741 (2004).

182. Bebee, T. W., Gladman, J. T. & Chandler, D. S. Generation of a tamoxifen inducible SMN mouse for temporal SMN replacement. *genesis* **49,** 927–934 (2011).

183. Duque, S. I. *et al.* A large animal model of spinal muscular atrophy and correction of phenotype. *Ann. Neurol.* **77,** 399–414 (2015).

184. Doktor, T. K. *et al.* Absence of an intron splicing silencer in porcine Smn1 intron 7 confers immunity to the exon skipping mutation in human SMN2. *PLoS One* **9,** e98841 (2014).

185. Hinderer, C. *et al.* Severe Toxicity in Nonhuman Primates and Piglets Following High-Dose Intravenous Administration of an Adeno-Associated Virus Vector Expressing Human SMN. *Hum. Gene Ther.* **29,** 285–298 (2018).

186. Meyer, K. *et al.* Improving single injection CSF delivery of AAV9-mediated gene therapy for SMA: a dose-response study in mice and nonhuman primates. **23,** (2015).

187. Paton, D. M. Nusinersen: antisense oligonucleotide to increase SMN protein production in

spinal muscular atrophy. *Drugs of Today* **53,** 327 (2017).

188. Workman, E., Kolb, S. J. & Battle, D. J. Spliceosomal small nuclear ribonucleoprotein biogenesis defects and motor neuron selectivity in spinal muscular atrophy. *Brain Res.* **1462,** 93–9 (2012).

189. Swoboda, K. J. *et al.* Natural history of denervation in SMA: relation to age, SMN2 copy number, and function. *Ann. Neurol.* **57,** 704–12 (2005).

190. Thomson, S. R. *et al.* Morphological Characteristics of Motor Neurons Do Not Determine Their Relative Susceptibility to Degeneration in a Mouse Model of Severe Spinal Muscular Atrophy. *PLoS One* **7,** e52605 (2012).

191. Murray, L. M., Beauvais, A., Gibeault, S., Courtney, N. L. & Kothary, R. Transcriptional profiling of differentially vulnerable motor neurons at pre-symptomatic stage in the Smn (2b/-) mouse model of spinal muscular atrophy. *Acta Neuropathol. Commun.* **3,** 55 (2015).

192. Rodriguez-Muela, N. *et al.* Single-Cell Analysis of SMN Reveals Its Broader Role in Neuromuscular Disease. *Cell Rep.* **18,** 1484–1498 (2017).

193. Onodera, O. *et al.* Minor splicing pathway is not minor any more: Implications for the pathogenesis of motor neuron diseases. *Neuropathology* **34,** 99–107 (2014).

194. Gabanella, F. *et al.* Ribonucleoprotein assembly defects correlate with spinal muscular atrophy severity and preferentially affect a subset of spliceosomal snRNPs. *PLoS One* **2,** e921 (2007).

195. Highley, J. R. *et al.* Loss of nuclear TDP-43 in amyotrophic lateral sclerosis (ALS) causes altered expression of splicing machinery and widespread dysregulation of RNA splicing in motor neurones. *Neuropathol. Appl. Neurobiol.* **40,** 670–685 (2014).

196. Zhang, Z. *et al.* Dysregulation of synaptogenesis genes antecedes motor neuron pathology in spinal muscular atrophy. *Proc. Natl. Acad. Sci. U. S. A.* **110,** 19348–53 (2013).

197. Zong, Y. & Jin, R. Structural mechanisms of the agrin-LRP4-MuSK signaling pathway in neuromuscular junction differentiation. *Cell. Mol. Life Sci.* **70,** 3077–88 (2013).

198. See, K. *et al.* SMN deficiency alters Nrxn2 expression and splicing in zebrafish and mouse models of spinal muscular atrophy. *Hum. Mol. Genet.* **23,** 1754–1770 (2014).

199. Zhang, W. *et al.* Extracellular Domains of -Neurexins Participate in Regulating Synaptic Transmission by Selectively Affecting N- and P/Q-Type Ca2+ Channels. *J. Neurosci.* **25,** 4330–4342 (2005).

200. Missler, M. *et al.* α-Neurexins couple Ca2+ channels to synaptic vesicle exocytosis. *Nature* **423,** 939–948 (2003).

201. Acsadi, G. *et al.* Mitochondrial Dysfunction in a Neural Cell Model of Spinal Muscular Atrophy. doi:10.1002/jnr.22106

202. Xu, C.-C., Denton, K. R., Wang, Z.-B., Zhang, X. & Li, X.-J. Abnormal mitochondrial transport and morphology as early pathological changes in human models of spinal muscular atrophy. *Dis. Model. Mech.* **9,** 39–49 (2016).

203. Miller, N., Shi, H., Zelikovich, A. S. & Ma, Y.-C. Motor neuron mitochondrial dysfunction in spinal muscular atrophy. *Hum. Mol. Genet.* **25,** 3395–3406 (2016).

204. Zhang, H. L. *et al.* Active transport of the survival motor neuron protein and the role of exon-7

in cytoplasmic localization. *J. Neurosci.* **23,** 6627–37 (2003).

205. Fallini, C. *et al.* The Survival of Motor Neuron (SMN) Protein Interacts with the mRNA-Binding Protein HuD and Regulates Localization of Poly(A) mRNA in Primary Motor Neuron Axons. *J. Neurosci.* **31,** 3914–3925 (2011).

206. Carrel, T. L. *et al.* Survival motor neuron function in motor axons is independent of functions required for small nuclear ribonucleoprotein biogenesis. *J. Neurosci.* **26,** 11014–22 (2006).

207. Zhang, H. *et al.* Multiprotein Complexes of the Survival of Motor Neuron Protein SMN with Gemins Traffic to Neuronal Processes and Growth Cones of Motor Neurons. *J. Neurosci.* **26,** 8622–8632 (2006).

208. Dombert, B., Sivadasan, R., Simon, C. M., Jablonka, S. & Sendtner, M. Presynaptic Localization of Smn and hnRNP R in Axon Terminals of Embryonic and Postnatal Mouse Motoneurons. *PLoS One* **9,** e110846 (2014).

209. Akten, B. *et al.* Interaction of survival of motor neuron (SMN) and HuD proteins with mRNA cpg15 rescues motor neuron axonal deficits. *Proc. Natl. Acad. Sci.* **108,** 10337–10342 (2011).

210. Rossoll, W. *et al.* Specific interaction of Smn, the spinal muscular atrophy determining gene product, with hnRNP-R and gry-rbp/hnRNP-Q: a role for Smn in RNA processing in motor axons? *Hum. Mol. Genet.* **11,** 93–105 (2002).

211. Saal, L., Briese, M., Kneitz, S., Glinka, M. & Sendtner, M. Subcellular transcriptome alterations in a cell culture model of spinal muscular atrophy point to widespread defects in axonal growth and presynaptic differentiation. **20,** (2014).

212. Rage, F. *et al.* Genome-wide identification of mRNAs associated with the protein SMN whose depletion decreases their axonal localization. *RNA* **19,** 1755–1766 (2013).

213. Fallini, C., Donlin-Asp, P. G., Rouanet, J. P., Bassell, G. J. & Rossoll, W. Deficiency of the Survival of Motor Neuron Protein Impairs mRNA Localization and Local Translation in the Growth Cone of Motor Neurons. *J. Neurosci.* **36,** 3811–3820 (2016).

214. Kye, M. J. *et al.* SMN regulates axonal local translation via miR-183/mTOR pathway. *Hum. Mol. Genet.* **23,** 6318–31 (2014).

215. Wertz, M. H. *et al.* Cell-type-specific miR-431 dysregulation in a motor neuron model of spinal muscular atrophy. *Hum. Mol. Genet.* **25,** 2168–2181 (2016).

216. Maragakis, N. J. & Rothstein, J. D. Mechanisms of Disease: astrocytes in neurodegenerative disease. *Nat. Clin. Pract. Neurol.* **2,** 679–689 (2006).

217. McGivern, J. V *et al.* Spinal muscular atrophy astrocytes exhibit abnormal calcium regulation and reduced growth factor production. *Glia* **61,** 1418–1428 (2013).

218. Zhou, C., Feng, Z. & Ko, C.-P. Defects in Motoneuron–Astrocyte Interactions in Spinal Muscular Atrophy. *J. Neurosci.* **36,** 2543–2553 (2016).

219. Chung, W.-S., Allen, N. J. & Eroglu, C. Astrocytes Control Synapse Formation, Function, and Elimination. *Cold Spring Harb. Perspect. Biol.* **7,** a020370 (2015).

220. Rindt, H. *et al.* Astrocytes influence the severity of spinal muscular atrophy. *Hum. Mol. Genet.* **24,** 4094–102 (2015).

221. Hunter, G., Aghamaleky Sarvestany, A., Roche, S. L., Symes, R. C. & Gillingwater, T. H. SMN-dependent intrinsic defects in Schwann cells in mouse models of spinal muscular atrophy. *Hum. Mol. Genet.* **23,** 2235–2250 (2014).

222. Hunter, G. *et al.* Restoration of SMN in Schwann cells reverses myelination defects and improves neuromuscular function in spinal muscular atrophy. *Hum. Mol. Genet.* **25,** ddw141 (2016).

223. Jablonka, S. *et al.* Distinct and overlapping alterations in motor and sensory neurons in a mouse model of spinal muscular atrophy. *Hum. Mol. Genet.* **15,** 511–518 (2006).

224. Henderson, C. E. *et al.* Extracts of muscle biopsies from patients with spinal muscular atrophies inhibit neurite outgrowth from spinal neurons. *Neurology* **37,** 1361–4 (1987).

225. Gavrilina, T. O. *et al.* Neuronal SMN expression corrects spinal muscular atrophy in severe SMA mice while muscle-specific SMN expression has no phenotypic effect. *Hum. Mol. Genet.* **17,** 1063–75 (2008).

226. Martinez, T. L. *et al.* Survival Motor Neuron Protein in Motor Neurons Determines Synaptic Integrity in Spinal Muscular Atrophy. *J. Neurosci.* **32,** 8703–8715 (2012).

227. Valsecchi, V., Boido, M., De Amicis, E., Piras, A. & Vercelli, A. Expression of Muscle-Specific MiRNA 206 in the Progression of Disease in a Murine SMA Model. *PLoS One* **10,** e0128560 (2015).

228. Kariya, S. *et al.* Reduced SMN protein impairs maturation of the neuromuscular junctions in mouse models of spinal muscular atrophy. *Hum. Mol. Genet.* **17,** 2552–69 (2008).

229. Murray, L. M. *et al.* Selective vulnerability of motor neurons and dissociation of pre- and post-synaptic pathology at the neuromuscular junction in mouse models of spinal muscular atrophy. *Hum. Mol. Genet.* **17,** 949–962 (2008).

230. Cifuentes-Diaz, C. *et al.* Neurofilament accumulation at the motor endplate and lack of axonal sprouting in a spinal muscular atrophy mouse model. *Hum. Mol. Genet.* **11,** 1439–47 (2002).

231. Dale, J. M. *et al.* The spinal muscular atrophy mouse model, SMAΔ7, displays altered axonal transport without global neurofilament alterations. *Acta Neuropathol.* **122,** 331–341 (2011).

232. Torres-Benito, L., Ruiz, R. & Tabares, L. Synaptic defects in spinal muscular atrophy animal models. *Dev. Neurobiol.* **72,** 126–133 (2012).

233. McGovern, V. L., Gavrilina, T. O., Beattie, C. E. & Burghes, A. H. M. Embryonic motor axon development in the severe SMA mouse. *Hum. Mol. Genet.* **17,** 2900–2909 (2008).

234. Kariya, S. *et al.* Requirement of enhanced Survival Motoneuron protein imposed during neuromuscular junction maturation. *J. Clin. Invest.* **124,** 785–800 (2014).

235. Martínez-Hernández, R. *et al.* The developmental pattern of myotubes in spinal muscular atrophy indicates prenatal delay of muscle maturation. *J. Neuropathol. Exp. Neurol.* **68,** 474–81 (2009).

236. Martínez-Hernández, R., Bernal, S., Alias, L. & Tizzano, E. F. Abnormalities in Early Markers of Muscle Involvement Support a Delay in Myogenesis in Spinal Muscular Atrophy. *J. Neuropathol. Exp. Neurol.* **73,** 559–567 (2014).

237. Nicole, S. *et al.* Intact satellite cells lead to remarkable protection against Smn gene defect in

differentiated skeletal muscle. *J. Cell Biol.* **161,** 571–82 (2003).

238. Hayhurst, M., Wagner, A. K., Cerletti, M., Wagers, A. J. & Rubin, L. L. A cell-autonomous defect in skeletal muscle satellite cells expressing low levels of survival of motor neuron protein. *Dev. Biol.* **368,** 323–34 (2012).

239. Ripolone, M. *et al.* Impaired Muscle Mitochondrial Biogenesis and Myogenesis in Spinal Muscular Atrophy. *JAMA Neurol.* **72,** 666–75 (2015).

240. Romanello, V. *et al.* Mitochondrial fission and remodelling contributes to muscle atrophy. *EMBO J.* **29,** 1774–1785 (2010).

241. Deymeer, F., Serdaroglu, P., Parman, Y. & Poda, M. Natural history of SMA IIIb: muscle strength decreases in a predictable sequence and magnitude. *Neurology* **71,** 644–9 (2008).

242. Wadman, R. I. *et al.* Muscle strength and motor function throughout life in a cross-sectional cohort of 180 patients with spinal muscular atrophy types 1c-4. *Eur. J. Neurol.* **25,** 512–518 (2018).

243. Hua, Y. *et al.* Peripheral SMN restoration is essential for long-term rescue of a severe spinal muscular atrophy mouse model. *Nature* **478,** 123–6 (2011).

244. Møller, P. *et al.* Spinal muscular atrophy type I combined with atrial septal defect in three sibs. *Clin. Genet.* **38,** 81–3 (1990).

245. Vaidla, E. *et al.* Neonatal Spinal Muscular Atrophy Type 1 With Bone Fractures and Heart Defect. *J. Child Neurol.* **22,** 67–70 (2007).

246. Rudnik-Schoneborn, S. *et al.* Congenital heart disease is a feature of severe infantile spinal muscular atrophy. *J. Med. Genet.* **45,** 635–638 (2008).

247. El-Matary, W., Kotagiri, S., Cameron, D. & Peart, I. Spinal muscle atrophy type 1 (Werdnig-Hoffman disease) with complex cardiac malformation. *Eur. J. Pediatr.* **163,** 331–332 (2004).

248. Cook, A. L., Curzon, C. L. & Milazzo, A. S. An infant with hypoplastic left heart syndrome and spinal muscular atrophy. *Cardiol. Young* **16,** 78 (2006).

249. Menke, L. A. *et al.* Congenital heart defects in spinal muscular atrophy type I: A clinical report of two siblings and a review of the literature. *Am. J. Med. Genet. Part A* **146A,** 740–744 (2008).

250. Falsaperla, R. *et al.* Electrocardiographic Evaluation in Patients With Spinal Muscular Atrophy: A Case-Control Study. *J. Child Neurol.* **33,** 487–492 (2018).

251. ROOS, M. *et al.* Malignant Ventricular Arrhythmia in a Case of Adult Onset of Spinal Muscular Atrophy (Kugelberg-Welander Disease). *J. Cardiovasc. Electrophysiol.* **20,** 342–344 (2009).

252. Ceroni, M., Grandi, A., Poloni, M. & Venco, A. Association of cardiomyopathy with Kugelberg-Welander disease. *Ital. J. Neurol. Sci.* **3,** 143–7 (1982).

253. Tanaka, H., Uemura, N., Toyama, Y., Kudo, A. & Ohkatsu, Y. Cardiac involvement in the Kugelbert-Welander syndrome. *Am. J. Cardiol.* **38,** 528–32 (1976).

254. Rudnik-Schöneborn, S. *et al.* Digital necroses and vascular thrombosis in severe spinal muscular atrophy. *Muscle Nerve* **42,** 144–147 (2010).

255. Bach, J. R. Medical Considerations of Long-Term Survival of Werdnig???Hoffmann Disease. *Am.*

J. Phys. Med. Rehabil. **86,** 349–355 (2007).

256. Schreml, J. *et al.* Severe SMA mice show organ impairment that cannot be rescued by therapy with the HDACi JNJ-26481585. *Eur. J. Hum. Genet.* **21,** 643–52 (2013).

257. Maxwell, G. K., Szunyogova, E., Shorrock, H. K., Gillingwater, T. H. & Parson, S. H. Developmental and degenerative cardiac defects in the Taiwanese mouse model of severe spinal muscular atrophy. *J. Anat.* **232,** 965–978 (2018).

258. Bevan, A. K. *et al.* Early heart failure in the SMNDelta7 model of spinal muscular atrophy and correction by postnatal scAAV9-SMN delivery. **19,** (2010).

259. Shababi, M. *et al.* Cardiac defects contribute to the pathology of spinal muscular atrophy models. *Hum. Mol. Genet.* **19,** 4059–4071 (2010).

260. Shababi, M. *et al.* Partial restoration of cardio-vascular defects in a rescued severe model of spinal muscular atrophy. *J. Mol. Cell. Cardiol.* **52,** 1074–1082 (2012).

261. Biondi, O. *et al.* Physical exercise reduces cardiac defects in type 2 spinal muscular atrophy-like mice. *J. Physiol.* **590,** 5907–5925 (2012).

262. Heier, C. R. & DiDonato, C. J. ECG in neonate mice with spinal muscular atrophy allows assessment of drug efficacy. *Front. Biosci. (Elite Ed).* **7,** 107–16 (2015).

263. Bowerman, M. *et al.* Glucose metabolism and pancreatic defects in spinal muscular atrophy. *Ann. Neurol.* **72,** 256–268 (2012).

264. Lamarca, N. H. *et al.* Diabetic Ketoacidosis in an Adult Patient With Spinal Muscular Atrophy Type II: Further Evidence of Extraneural Pathology Due to Survival Motor Neuron 1 Mutation? doi:10.1177/0883073812460096

265. Tein, I. *et al.* Fatty acid oxidation abnormalities in childhood-onset spinal muscular atrophy: primary or secondary defect(s)? *Pediatr. Neurol.* **12,** 21–30 (1995).

266. Crawford, T. O., Sladky, J. T., Hurko, O., Besner-Johnston, A. & Kelley, R. I. Abnormal fatty acid metabolism in childhood spinal muscular atrophy. *Ann. Neurol.* **45,** 337–43 (1999).

267. Kim, T. W., Jeong, J.-H. & Hong, S.-C. The Impact of Sleep and Circadian Disturbance on Hormones and Metabolism. *Int. J. Endocrinol.* **2015,** 1–9 (2015).

268. Walter, L. M. *et al.* Light modulation ameliorates expression of circadian genes and disease progression in spinal muscular atrophy mice. *Hum. Mol. Genet.* (2018). doi:10.1093/hmg/ddy249

269. Bowerman, M. *et al.* Defects in pancreatic development and glucose metabolism in SMN-depleted mice independent of canonical spinal muscular atrophy neuromuscular pathology. *Hum. Mol. Genet.* **23,** 3432–3444 (2014).

270. Stump, C. S., Henriksen, E. J., Wei, Y. & Sowers, J. R. The metabolic syndrome: Role of skeletal muscle metabolism. *Ann. Med.* **38,** 389–402 (2006).

271. Walter, L. M. *et al.* Interventions Targeting Glucocorticoid-Krüppel-like Factor 15-Branched-Chain Amino Acid Signaling Improve Disease Phenotypes in Spinal Muscular Atrophy Mice. *EBioMedicine* **31,** 226–242 (2018).

272. Haldar, S. M. *et al.* Kruppel-like factor 15 regulates skeletal muscle lipid flux and exercise

adaptation. doi:10.1073/pnas.1121060109

273. Frayn, K. N., Arner, P. & Yki-Järvinen, H. Fatty acid metabolism in adipose tissue, muscle and liver in health and disease. *Essays Biochem.* **42,** 89–103 (2006).

274. Kelley, R. I. & Sladky, J. T. Dicarboxylic aciduria in an infant with spinal muscular atrophy. *Ann. Neurol.* **20,** 734–736 (1986).

275. Szunyogova, E. *et al.* Survival Motor Neuron (SMN) protein is required for normal mouse liver development. *Sci. Rep.* **6,** 34635 (2016).

276. Coovert, D. *et al.* The survival motor neuron protein in spinal muscular atrophy. *Hum. Mol. Genet.* **6,** 1205–1214 (1997).

277. Mendell, J. R. *et al.* Eteplirsen for the treatment of Duchenne muscular dystrophy. *Ann. Neurol.* **74,** 637–47 (2013).

278. Lim, S. R. & Hertel, K. J. Modulation of survival motor neuron pre-mRNA splicing by inhibition of alternative 3' splice site pairing. *J. Biol. Chem.* **276,** 45476–83 (2001).

279. Hua, Y., Vickers, T. A., Okunola, H. L., Bennett, C. F. & Krainer, A. R. Antisense masking of an hnRNP A1/A2 intronic splicing silencer corrects SMN2 splicing in transgenic mice. *Am. J. Hum. Genet.* **82,** 834–48 (2008).

280. Williams, J. H. *et al.* Oligonucleotide-Mediated Survival of Motor Neuron Protein Expression in CNS Improves Phenotype in a Mouse Model of Spinal Muscular Atrophy. *J. Neurosci.* **29,** 7633–7638 (2009).

281. Porensky, P. N. *et al.* A single administration of morpholino antisense oligomer rescues spinal muscular atrophy in mouse. *Hum. Mol. Genet.* **21,** 1625–38 (2012).

282. Zhou, H. *et al.* A novel morpholino oligomer targeting ISS-N1 improves rescue of severe spinal muscular atrophy transgenic mice. *Hum. Gene Ther.* **24,** 331–42 (2013).

283. Hua, Y. *et al.* Antisense correction of SMN2 splicing in the CNS rescues necrosis in a type III SMA mouse model. *Genes Dev.* **24,** 1634–1644 (2010).

284. Passini, M. A. *et al.* Antisense oligonucleotides delivered to the mouse CNS ameliorate symptoms of severe spinal muscular atrophy. *Sci. Transl. Med.* **3,** 72ra18 (2011).

285. Rigo, F. *et al.* Pharmacology of a central nervous system delivered 2'-O-methoxyethyl-modified survival of motor neuron splicing oligonucleotide in mice and nonhuman primates. *J. Pharmacol. Exp. Ther.* **350,** 46–55 (2014).

286. Hua, Y., Vickers, T. A., Baker, B. F., Bennett, C. F. & Krainer, A. R. Enhancement of SMN2 Exon 7 Inclusion by Antisense Oligonucleotides Targeting the Exon. *PLoS Biol.* **5,** e73 (2007).

287. Skordis, L. A., Dunckley, M. G., Yue, B., Eperon, I. C. & Muntoni, F. Bifunctional antisense oligonucleotides provide a trans-acting splicing enhancer that stimulates SMN2 gene expression in patient fibroblasts. *Proc. Natl. Acad. Sci. U. S. A.* **100,** 4114–9 (2003).

288. Osman, E. Y., Yen, P.-F. & Lorson, C. L. Bifunctional RNAs Targeting the Intronic Splicing Silencer N1 Increase SMN Levels and Reduce Disease Severity in an Animal Model of Spinal Muscular Atrophy. *Mol. Ther.* **20,** 119–126 (2012).

289. d'Ydewalle, C. *et al.* The Antisense Transcript SMN-AS1 Regulates SMN Expression and Is a

Novel Therapeutic Target for Spinal Muscular Atrophy. *Neuron* **93,** 66–79 (2017).

290. Chiriboga, C. A. *et al.* Results from a phase 1 study of nusinersen (ISIS-SMN $_{Rx}$) in children with spinal muscular atrophy. *Neurology* **86,** 890–897 (2016).

291. Finkel, R. S. *et al.* Treatment of infantile-onset spinal muscular atrophy with nusinersen: a phase 2, open-label, dose-escalation study. *Lancet* **388,** 3017–3026 (2016).

292. Darras, B. *et al.* G.O.18: Results of a phase 2 study of ISIS-SMNRx in children with spinal muscular atrophy. *Neuromuscul. Disord.* **24,** (2014).

293. Biogen and Ionis Pharmaceuticals Announce SPINRAZA (nusinersen) Meets Primary Endpoint at Interim Analysis of Phase 3 CHERISH Study in Later-Onset Spinal Muscular Atrophy | Business Wire. (2016). Available at: https://www.businesswire.com/news/home/20161107005392/en/Biogen-Ionis-Pharmaceuticals-Announce-SPINRAZA-nusinersen-Meets. (Accessed: 16th July 2018)

294. Kegel, M. Achievements, hopes and limits of SMA treatment: Interview with Spinraza researcher and CureSMA. Available at: https://smanewstoday.com/2017/11/01/sma-treatment-achievements-hopes-limits-interview-with-spinraza-researcher-cure-sma/. (Accessed: 2nd October 2018)

295. Hoy, S. M. Nusinersen: First Global Approval. *Drugs* **77,** 473–479 (2017).

296. Derossi, D., Joliot, A. H., Chassaing, G. & Prochiantz, A. The third helix of the Antennapedia homeodomain translocates through biological membranes. *J. Biol. Chem.* **269,** 10444–50 (1994).

297. A. El Andaloussi, S., M. Hammond, S., Mager, I. & J.A. Wood, M. Use of Cell-Penetrating-Peptides in Oligonucleotide Splice Switching Therapy. *Curr. Gene Ther.* **12,** 161–178 (2012).

298. Lebleu, B. *et al.* Cell penetrating peptide conjugates of steric block oligonucleotides. *Adv. Drug Deliv. Rev.* **60,** 517–529 (2008).

299. Turner, J. J., Arzumanov, A. A. & Gait, M. J. Synthesis, cellular uptake and HIV-1 Tat-dependent trans-activation inhibition activity of oligonucleotide analogues disulphide-conjugated to cell-penetrating peptides. *Nucleic Acids Res.* **33,** 27–42 (2005).

300. Kang, S. H., Cho, M. J. & Kole, R. Up-regulation of luciferase gene expression with antisense oligonucleotides: implications and applications in functional assay development. *Biochemistry* **37,** 6235–9 (1998).

301. Jearawiriyapaisarn, N. *et al.* Sustained dystrophin expression induced by peptide-conjugated morpholino oligomers in the muscles of mdx mice. *Mol. Ther.* **16,** 1624–9 (2008).

302. Maier, M. A. *et al.* Evaluation of basic amphipathic peptides for cellular delivery of antisense peptide nucleic acids. *J. Med. Chem.* **49,** 2534–42 (2006).

303. Andaloussi, S. E. L. *et al.* Design of a peptide-based vector, PepFect6, for efficient delivery of siRNA in cell culture and systemically in vivo. *Nucleic Acids Res.* **39,** 3972–87 (2011).

304. Yin, H. *et al.* Pip5 transduction peptides direct high efficiency oligonucleotide-mediated dystrophin exon skipping in heart and phenotypic correction in mdx mice. *Mol. Ther.* **19,** 1295–303 (2011).

305. Du, L. *et al.* Arginine-rich cell-penetrating peptide dramatically enhances AMO-mediated ATM

aberrant splicing correction and enables delivery to brain and cerebellum. *Hum. Mol. Genet.* **20,** 3151–60 (2011).

306. Caillé, I. *et al.* Soluble form of amyloid precursor protein regulates proliferation of progenitors in the adult subventricular zone. *Development* **131,** 2173–81 (2004).

307. Re, F. *et al.* Functionalization of liposomes with ApoE-derived peptides at different density affects cellular uptake and drug transport across a blood-brain barrier model. *Nanomedicine* **7,** 551–9 (2011).

308. Zhou, H. *et al.* Repeated low doses of morpholino antisense oligomer: an intermediate mouse model of spinal muscular atrophy to explore the window of therapeutic response. *Hum. Mol. Genet.* **24,** 6265–77 (2015).

309. Anderton, R., Meloni, B., Mastaglia, F. & Boulos, S. Investigation of a recombinant SMN protein delivery system to treat spinal muscular atrophy. *Transl. Neurosci.* **5,** 8–16 (2014).

310. Azzouz, M. *et al.* Lentivector-mediated SMN replacement in a mouse model of spinal muscular atrophy. *J. Clin. Invest.* **114,** 1726–31 (2004).

311. Passini, M. A. *et al.* Translational Fidelity of Intrathecal Delivery of Self-Complementary AAV9–Survival Motor Neuron 1 for Spinal Muscular Atrophy. *Hum. Gene Ther.* **25,** 619–630 (2014).

312. Foust, K. D. *et al.* Rescue of the spinal muscular atrophy phenotype in a mouse model by early postnatal delivery of SMN. *Nat. Biotechnol.* **28,** 271–4 (2010).

313. AveXis: A Clinical-stage Gene Therapy Biotech Company. Available at: https://avexis.com/. (Accessed: 24th December 2016)

314. Mendell, J. R. *et al.* Single-Dose Gene-Replacement Therapy for Spinal Muscular Atrophy. *N. Engl. J. Med.* **377,** 1713–1722 (2017).

315. First SMA Infant Dosed in Phase 3 Trial of AVXS-101, AveXis Announces. Available at: https://smanewstoday.com/2018/04/27/first-sma-patient-dosed-phase-3-trial-avxs-101-avexis/. (Accessed: 1st August 2018)

316. Brichta, L. *et al.* Valproic acid increases the SMN2 protein level: a well-known drug as a potential therapy for spinal muscular atrophy. *Hum. Mol. Genet.* **12,** 2481–9 (2003).

317. Sumner, C. J. *et al.* Valproic acid increases SMN levels in spinal muscular atrophy patient cells. *Ann. Neurol.* **54,** 647–654 (2003).

318. Swoboda, K. J. *et al.* Phase II Open Label Study of Valproic Acid in Spinal Muscular Atrophy. *PLoS One* **4,** e5268 (2009).

319. Weihl, C. C., Connolly, A. M. & Pestronk, A. Valproate may improve strength and function in patients with type III/IV spinal muscle atrophy. *Neurology* **67,** 500–1 (2006).

320. Swoboda, K. J. *et al.* SMA CARNI-VAL trial part I: double-blind, randomized, placebo-controlled trial of L-carnitine and valproic acid in spinal muscular atrophy. *PLoS One* **5,** e12140 (2010).

321. Kissel, J. T. *et al.* SMA CARNIVAL TRIAL PART II: a prospective, single-armed trial of L-carnitine and valproic acid in ambulatory children with spinal muscular atrophy. *PLoS One* **6,** e21296 (2011).

322. Kissel, J. T. *et al.* SMA valiant trial: A prospective, double-blind, placebo-controlled trial of

valproic acid in ambulatory adults with spinal muscular atrophy. *Muscle Nerve* **49,** 187–192 (2014).

323. Pruss, R. M. *et al.* Drug discovery and development for spinal muscular atrophy: lessons from screening approaches and future challenges for clinical development. *Future Med. Chem.* **2,** 1429–40 (2010).

324. Asconapé, J. J., Penry, J. K., Dreifuss, F. E., Riela, A. & Mirza, W. Valproate-associated pancreatitis. *Epilepsia* **34,** 177–83

325. Mercuri, E. *et al.* Pilot trial of phenylbutyrate in spinal muscular atrophy. *Neuromuscul. Disord.* **14,** 130–5 (2004).

326. Iannitti, T. & Palmieri, B. Clinical and experimental applications of sodium phenylbutyrate. *Drugs R. D.* **11,** 227–49 (2011).

327. Riessland, M. *et al.* SAHA ameliorates the SMA phenotype in two mouse models for spinal muscular atrophy. *Hum. Mol. Genet.* **19,** 1492–1506 (2010).

328. Hahnen, E. *et al.* In vitro and ex vivo evaluation of second-generation histone deacetylase inhibitors for the treatment of spinal muscular atrophy. *J. Neurochem.* **98,** 193–202 (2006).

329. Sunyach, C. *et al.* Olesoxime delays muscle denervation, astrogliosis, microglial activation and motoneuron death in an ALS mouse model. *Neuropharmacology* **62,** 2346–2353 (2012).

330. Bordet, T. *et al.* Identification and Characterization of Cholest-4-en-3-one, Oxime (TRO19622), a Novel Drug Candidate for Amyotrophic Lateral Sclerosis. *J. Pharmacol. Exp. Ther.* **322,** 709–720 (2007).

331. Roche Stops Work on Potential SMA Therapy Olesoxime After Disappointing Results in Phase 2 Trial. Available at: https://smanewstoday.com/2018/06/06/roche-stops-development-of-sma-therapy-olesoxime-after-disappointing-trial-results/. (Accessed: 2nd October 2018)

332. Rothstein, J. D. *et al.* β-Lactam antibiotics offer neuroprotection by increasing glutamate transporter expression. *Nature* **433,** 73–77 (2005).

333. Cudkowicz, M. E. *et al.* Safety and efficacy of ceftriaxone for amyotrophic lateral sclerosis: a multi-stage, randomised, double-blind, placebo-controlled trial. *Lancet. Neurol.* **13,** 1083–1091 (2014).

334. Nizzardo, M. *et al.* Beta-lactam antibiotic offers neuroprotection in a spinal muscular atrophy model by multiple mechanisms. *Ann. Neurosci.* **18,** 156–7 (2011).

335. Russman, B. S., Iannaccone, S. T. & Samaha, F. J. A Phase 1 Trial of Riluzole in Spinal Muscular Atrophy. *Arch. Neurol.* **60,** 1601 (2003).

336. López-González, R., Kunckles, P. & Velasco, I. Transient Recovery in a Rat Model of Familial Amyotrophic Lateral Sclerosis after Transplantation of Motor Neurons Derived from Mouse Embryonic Stem Cells. *Cell Transplant.* **18,** 1171–1181 (2009).

337. Rossi, S. L. *et al.* Histological and Functional Benefit Following Transplantation of Motor Neuron Progenitors to the Injured Rat Spinal Cord. *PLoS One* **5,** e11852 (2010).

338. Lu, P., Jones, L. L., Snyder, E. Y. & Tuszynski, M. H. Neural stem cells constitutively secrete neurotrophic factors and promote extensive host axonal growth after spinal cord injury. *Exp. Neurol.* **181,** 115–29 (2003).

339. Corti, S. *et al.* Neural stem cell transplantation can ameliorate the phenotype of a mouse model of spinal muscular atrophy. *J. Clin. Invest.* **118,** 3316–3330 (2008).

340. Corti, S. *et al.* Embryonic stem cell-derived neural stem cells improve spinal muscular atrophy phenotype in mice. *Brain* **133,** 465–481 (2010).

341. Villanova, M. & Bach, J. R. Allogeneic Mesenchymal Stem Cell Therapy Outcomes for Three Patients with Spinal Muscular Atrophy Type 1. *Am. J. Phys. Med. Rehabil.* **94,** 410–415 (2015).

342. Carrozzi, M. *et al.* Stem cells in severe infantile spinal muscular atrophy (SMA1). *Neuromuscul. Disord.* **22,** 1032–1034 (2012).

343. McPherron, A. C., Lawler, A. M. & Lee, S.-J. Regulation of skeletal muscle mass in mice by a new TGF-p superfamily member. *Nature* **387,** 83–90 (1997).

344. Schuelke, M. *et al.* Myostatin Mutation Associated with Gross Muscle Hypertrophy in a Child. *N. Engl. J. Med.* **350,** 2682–2688 (2004).

345. Rose, F. F., Mattis, V. B., Rindt, H. & Lorson, C. L. Delivery of recombinant follistatin lessens disease severity in a mouse model of spinal muscular atrophy. *Hum. Mol. Genet.* **18,** 997–1005 (2009).

346. Sumner, C. J. *et al.* Inhibition of myostatin does not ameliorate disease features of severe spinal muscular atrophy mice. *Hum. Mol. Genet.* **18,** 3145–3152 (2009).

347. Rindt, H. *et al.* Transgenic inactivation of murine myostatin does not decrease the severity of disease in a model of Spinal Muscular Atrophy. *Neuromuscul. Disord.* **22,** 277–285 (2012).

348. Liu, M., Hammers, D. W., Barton, E. R. & Sweeney, H. L. Activin Receptor Type IIB Inhibition Improves Muscle Phenotype and Function in a Mouse Model of Spinal Muscular Atrophy. *PLoS One* **11,** e0166803 (2016).

349. Feng, Z. *et al.* Pharmacologically induced mouse model of adult spinal muscular atrophy to evaluate effectiveness of therapeutics after disease onset. *Hum. Mol. Genet.* **25,** 964–975 (2016).

350. Mariot, V. *et al.* Myostatin inhibition for neuromuscular disorders: defining the good candidate. *Neuromuscul. Disord.* **27,** S8 (2017).

351. Phase 1 Trial of Potential SMA Therapy, SRK-015, Completes 1st Dosing, Scholar Rock Reports. Available at: https://smanewstoday.com/2018/06/04/scholar-rocks-phase-1-trial-of-sma-therapy-srk-015-completes-dosing-first-group/. (Accessed: 5th August 2018)

352. Hwee, D. T. *et al.* The Small-Molecule Fast Skeletal Troponin Activator, CK-2127107, Improves Exercise Tolerance in a Rat Model of Heart Failure. *J. Pharmacol. Exp. Ther.* **353,** 159–168 (2015).

353. Andrews, J. A. *et al.* CK-2127107 amplifies skeletal muscle response to nerve activation in humans. *Muscle Nerve* **57,** 729–734 (2018).

354. A Study of CK-2127107 in Patients With Spinal Muscular Atrophy - Full Text View - ClinicalTrials.gov. Available at: https://clinicaltrials.gov/ct2/show/NCT02644668. (Accessed: 6th August 2018)

355. Bowerman, M., Beauvais, A., Anderson, C. L. & Kothary, R. Rho-kinase inactivation prolongs survival of an intermediate SMA mouse model. *Hum. Mol. Genet.* **19,** 1468–1478 (2010).

356. Hadwen, J. *et al.* VPAC2 receptor agonist BAY 55-9837 increases SMN protein levels and moderates disease phenotype in severe spinal muscular atrophy mouse models. *Orphanet J. Rare Dis.* **9,** 4 (2014).

357. Kolb, S. J. *et al.* Natural history of infantile-onset spinal muscular atrophy. *Ann. Neurol.* **82,** 883–891 (2017).

358. Finkel, R. S. *et al.* Observational study of spinal muscular atrophy type I and implications for clinical trials. *Neurology* **83,** 810–7 (2014).

359. Simic, G. *et al.* Ultrastructural Analysis and TUNEL Demonstrate Motor Neuron Apoptosis in Werdnig-Hoffmann Disease. *J. Neuropathol. Exp. Neurol.* **59,** 398–407 (2000).

360. Soler-Botija, C., Ferrer, I., Gich, I., Baiget, M. & Tizzano, E. F. Neuronal death is enhanced and begins during foetal development in type I spinal muscular atrophy spinal cord. *Brain* **125,** 1624–1634 (2002).

361. Govoni, A., Gagliardi, D., Comi, G. P. & Corti, S. Time Is Motor Neuron: Therapeutic Window and Its Correlation with Pathogenetic Mechanisms in Spinal Muscular Atrophy. *Mol. Neurobiol.* **55,** 6307–6318 (2018).

362. Chiriboga, C. A. Nusinersen for the treatment of spinal muscular atrophy. *Expert Rev. Neurother.* **17,** 955–962 (2017).

363. Kraszewski, J. N. *et al.* Pilot study of population-based newborn screening for spinal muscular atrophy in New York state. *Genet. Med.* **20,** 608–613 (2018).

364. Calcedo, R. *et al.* Adeno-associated virus antibody profiles in newborns, children, and adolescents. *Clin. Vaccine Immunol.* **18,** 1586–8 (2011).

365. Hao, L. T. *et al.* Temporal requirement for SMN in motoneuron development. *Hum. Mol. Genet.* **22,** 2612–2625 (2013).

366. Taketo, M. *et al.* FVB/N: an inbred mouse strain preferable for transgenic analyses. *Proc. Natl. Acad. Sci. U. S. A.* **88,** 2065–9 (1991).

367. Mekada, K. *et al.* Genetic differences among C57BL/6 substrains. *Exp. Anim.* **58,** 141–9 (2009).

368. Xia, Y. *et al.* Deficiency of fibroblast growth factor-inducible 14 (Fn14) preserves the filtration barrier and ameliorates lupus nephritis. *J. Am. Soc. Nephrol.* **26,** 1053–70 (2015).

369. Campbell, S. *et al.* Proinflammatory effects of TWEAK/Fn14 interactions in glomerular mesangial cells. *J. Immunol.* **176,** 1889–98 (2006).

370. Schindelin, J. *et al.* Fiji: an open-source platform for biological-image analysis. *Nat. Methods* **9,** 676–682 (2012).

371. Radonić, A. *et al.* Guideline to reference gene selection for quantitative real-time PCR. *Biochem. Biophys. Res. Commun.* **313,** 856–62 (2004).

372. YAFFE, D. & SAXEL, O. Serial passaging and differentiation of myogenic cells isolated from dystrophic mouse muscle. *Nature* **270,** 725–727 (1977).

373. Cashman, N. R. *et al.* Neuroblastoma × spinal cord (NSC) hybrid cell lines resemble developing motor neurons. *Dev. Dyn.* **194,** 209–221 (1992).

374. Sumner, C. J., Paushkin, S. & Ko, C. *Spinal muscular atrophy : disease mechanisms and therapy*.

375. Zhang, R. *et al.* Structure of a Key Intermediate of the SMN Complex Reveals Gemin2's Crucial Function in snRNP Assembly. *Cell* **146,** 384–395 (2011).

376. So, B. R. *et al.* A U1 snRNP–specific assembly pathway reveals the SMN complex as a versatile hub for RNP exchange. *Nat. Struct. Mol. Biol.* **23,** 225–230 (2016).

377. Li, D. K., Tisdale, S., Lotti, F. & Pellizzoni, L. SMN control of RNP assembly: from post-transcriptional gene regulation to motor neuron disease. *Semin. Cell Dev. Biol.* **32,** 22–9 (2014).

378. Young, P. J. *et al.* A Direct Interaction between the Survival Motor Neuron Protein and p53 and Its Relationship to Spinal Muscular Atrophy. *J. Biol. Chem.* **277,** 2852–2859 (2002).

379. Strasswimmer, J. *et al.* Identification of survival motor neuron as a transcriptional activator-binding protein. *Hum. Mol. Genet.* **8,** 1219–26 (1999).

380. Fayzullina, S. & Martin, L. J. DNA Damage Response and DNA Repair in Skeletal Myocytes From a Mouse Model of Spinal Muscular Atrophy. *J. Neuropathol. Exp. Neurol.* **75,** 889–902 (2016).

381. Sanchez, G. *et al.* A novel function for the survival motoneuron protein as a translational regulator. *Hum. Mol. Genet.* **22,** 668–684 (2013).

382. Zou, T. *et al.* SMN Deficiency Reduces Cellular Ability to Form Stress Granules, Sensitizing Cells to Stress. *Cell. Mol. Neurobiol.* **31,** 541–550 (2011).

383. Gabanella, F. *et al.* SMN affects membrane remodelling and anchoring of the protein synthesis machinery. *J. Cell Sci.* **129,** 804–816 (2016).

384. Huo, Q. *et al.* Splicing changes in SMA mouse motoneurons and SMN-depleted neuroblastoma cells: evidence for involvement of splicing regulatory proteins. *RNA Biol.* **11,** 1430–46 (2014).

385. Bernabò, P. *et al.* In Vivo Translatome Profiling in Spinal Muscular Atrophy Reveals a Role for SMN Protein in Ribosome Biology. *Cell Rep.* **21,** 953–965 (2017).

386. Ng, S.-Y. *et al.* Genome-wide RNA-Seq of Human Motor Neurons Implicates Selective ER Stress Activation in Spinal Muscular Atrophy. *Cell Stem Cell* **17,** 569–84 (2015).

387. Maeda, M. *et al.* Transcriptome Profiling of Spinal Muscular Atrophy Motor Neurons Derived from Mouse Embryonic Stem Cells. *PLoS One* **9,** e106818 (2014).

388. Wishart, T. M. *et al.* SMN deficiency disrupts brain development in a mouse model of severe spinal muscular atrophy. *Hum. Mol. Genet.* **19,** 4216–4228 (2010).

389. Wu, C.-Y. *et al.* Proteomic assessment of a cell model of spinal muscular atrophy. *BMC Neurosci.* **12,** 25 (2011).

390. Hsu, S.-H. H. *et al.* Ubiquitin carboxyl-terminal hydrolase L1 (UCHL1) regulates the level of SMN expression through ubiquitination in primary spinal muscular atrophy fibroblasts. *Clin. Chim. Acta* **411,** 1920–1928 (2010).

391. Korhonen, L. & Lindholm, D. The ubiquitin proteasome system in synaptic and axonal degeneration: Figure 1. *J. Cell Biol.* **165,** 27–30 (2004).

392. Mutsaers, C. a, Lamont, D. J., Hunter, G., Wishart, T. M. & Gillingwater, T. H. Label-free proteomics identifies Calreticulin and GRP75/Mortalin as peripherally accessible protein

biomarkers for spinal muscular atrophy. *Genome Med* **5,** 95 (2013).

393. Kobayashi, D. T. *et al.* SMA-MAP: A Plasma Protein Panel for Spinal Muscular Atrophy. *PLoS One* **8,** e60113 (2013).

394. Murdocca, M. *et al.* IPLEX administration improves motor neuron survival and ameliorates motor functions in a severe mouse model of spinal muscular atrophy. *Mol. Med.* **18,** 1076–85 (2012).

395. Boyer, J. G. *et al.* Early onset muscle weakness and disruption of muscle proteins in mouse models of spinal muscular atrophy. *Skelet. Muscle* **3,** 24 (2013).

396. Boido, M. & Vercelli, A. Neuromuscular Junctions as Key Contributors and Therapeutic Targets in Spinal Muscular Atrophy. *Front. Neuroanat.* **10,** 6 (2016).

397. Ghazalpour, A. *et al.* Comparative Analysis of Proteome and Transcriptome Variation in Mouse. *PLoS Genet.* **7,** e1001393 (2011).

398. Yeung, E. S. Genome-wide correlation between mRNA and protein in a single cell. *Angew. Chem. Int. Ed. Engl.* **50,** 583–5 (2011).

399. Pascal, L. E. *et al.* Correlation of mRNA and protein levels: cell type-specific gene expression of cluster designation antigens in the prostate. *BMC Genomics* **9,** 246 (2008).

400. Liu, Y., Beyer, A. & Aebersold, R. On the Dependency of Cellular Protein Levels on mRNA Abundance. *Cell* **165,** 535–50 (2016).

401. Gustafsson, C., Govindarajan, S. & Minshull, J. Codon bias and heterologous protein expression. *Trends Biotechnol.* **22,** 346–353 (2004).

402. Wethmar, K., Smink, J. J. & Leutz, A. Upstream open reading frames: molecular switches in (patho)physiology. *Bioessays* **32,** 885–93 (2010).

403. Ingolia, N. T., Ghaemmaghami, S., Newman, J. R. S. & Weissman, J. S. Genome-Wide Analysis in Vivo of Translation with Nucleotide Resolution Using Ribosome Profiling. *Science (80-.).* **324,** 218–223 (2009).

404. Barrett, L. W., Fletcher, S. & Wilton, S. D. Regulation of eukaryotic gene expression by the untranslated gene regions and other non-coding elements. *Cell. Mol. Life Sci.* **69,** 3613–3634 (2012).

405. Schwanhäusser, B. *et al.* Global quantification of mammalian gene expression control. *Nature* **473,** 337–342 (2011).

406. Tang, Y.-C. & Amon, A. Gene copy-number alterations: a cost-benefit analysis. *Cell* **152,** 394–405 (2013).

407. McRedmond, J. P. *et al.* Integration of Proteomics and Genomics in Platelets. *Mol. Cell. Proteomics* **3,** 133–144 (2004).

408. Delmotte, N. *et al.* An integrated proteomics and transcriptomics reference data set provides new insights into the Bradyrhizobium japonicum bacteroid metabolism in soybean root nodules. *Proteomics* **10,** 1391–1400 (2010).

409. Perco, P. *et al.* Linking transcriptomic and proteomic data on the level of protein interaction networks. *Electrophoresis* **31,** 1780–1789 (2010).

410. Greenbaum, D., Colangelo, C., Williams, K. & Gerstein, M. Comparing protein abundance and mRNA expression levels on a genomic scale. *Genome Biol.* **4,** 117 (2003).

411. Nie, L., Wu, G., Brockman, F. J. & Zhang, W. Integrated analysis of transcriptomic and proteomic data of Desulfovibrio vulgaris: zero-inflated Poisson regression models to predict abundance of undetected proteins. *Bioinformatics* **22,** 1641–1647 (2006).

412. Nie, L., Wu, G. & Zhang, W. Correlation of mRNA Expression and Protein Abundance Affected by Multiple Sequence Features Related to Translational Efficiency in Desulfovibrio vulgaris: A Quantitative Analysis. *Genetics* **174,** 2229–2243 (2006).

413. Haider, S. & Pal, R. Integrated analysis of transcriptomic and proteomic data. *Curr. Genomics* **14,** 91–110 (2013).

414. Le, T. T. *et al.* Temporal requirement for high SMN expression in SMA mice. *Hum. Mol. Genet.* **20,** 3578–91 (2011).

415. Grohmann, K. *et al.* Mutations in the gene encoding immunoglobulin μ-binding protein 2 cause spinal muscular atrophy with respiratory distress type 1. *Nat. Genet.* **29,** 75–77 (2001).

416. Nardo, G. *et al.* Transcriptomic indices of fast and slow disease progression in two mouse models of amyotrophic lateral sclerosis. *Brain* **136,** 3305–3332 (2013).

417. Nardo, G., Trolese, M. C. & Bendotti, C. Major Histocompatibility Complex I Expression by Motor Neurons and Its Implication in Amyotrophic Lateral Sclerosis. *Front. Neurol.* **7,** 89 (2016).

418. Oliveira, A. L. R. *et al.* A role for MHC class I molecules in synaptic plasticity and regeneration of neurons after axotomy. *Proc. Natl. Acad. Sci.* **101,** 17843–17848 (2004).

419. Thams, S. *et al.* Classical Major Histocompatibility Complex Class I Molecules in Motoneurons: New Actors at the Neuromuscular Junction. *J. Neurosci.* **29,** 13503–13515 (2009).

420. Paulsson, K. M. *et al.* Association of tapasin and COPI provides a mechanism for the retrograde transport of major histocompatibility complex (MHC) class I molecules from the Golgi complex to the endoplasmic reticulum. *J. Biol. Chem.* **277,** 18266–71 (2002).

421. Raghuraman, G., Lapinski, P. E. & Raghavan, M. Tapasin interacts with the membrane-spanning domains of both TAP subunits and enhances the structural stability of TAP1 x TAP2 Complexes. *J. Biol. Chem.* **277,** 41786–94 (2002).

422. Verrillo, E. *et al.* Sleep architecture in infants with spinal muscular atrophy type 1. *Sleep Med.* **15,** 1246–1250 (2014).

423. Pera, M. C. *et al.* Sleep disorders in spinal muscular atrophy. *Sleep Med.* **30,** 160–163 (2017).

424. Bersanini, C. *et al.* Nocturnal hypoxaemia and hypercapnia in children with neuromuscular disorders. *Eur. Respir. J.* **39,** 1206–1212 (2012).

425. Lamb, J. *et al. The Connectivity Map: Using Gene-Expression Signatures to Connect Small Molecules, Genes, and Disease*. *Science* **313,** 1929–1935 (2006).

426. Segal, M. R., Xiong, H., Bengtsson, H., Bourgon, R. & Gentleman, R. Querying Genomic Databases: Refining the Connectivity Map. *Stat. Appl. Genet. Mol. Biol.* **11,** (2012).

427. Kunkel, S. D. *et al.* mRNA expression signatures of human skeletal muscle atrophy identify a natural compound that increases muscle mass. *Cell Metab.* **13,** 627–38 (2011).

428. Chang, M., Smith, S., Thorpe, A., Barratt, M. J. & Karim, F. Evaluation of Phenoxybenzamine in the CFA Model of Pain following Gene Expression Studies and Connectivity Mapping. *Mol. Pain* **6,** 1744-8069-6–56 (2010).

429. Brum, A. M. *et al.* Connectivity Map-based discovery of parbendazole reveals targetable human osteogenic pathway. *Proc. Natl. Acad. Sci. U. S. A.* **112,** 12711–6 (2015).

430. Koh, L. W.-H. *et al.* A Distinct Reactive Oxygen Species Profile Confers Chemoresistance in Glioma-Propagating Cells and Associates with Patient Survival Outcome. *Antioxid. Redox Signal.* **19,** 2261–2279 (2013).

431. Wang, G. *et al.* Expression-Based In Silico Screening of Candidate Therapeutic Compounds for Lung Adenocarcinoma. *PLoS One* **6,** e14573 (2011).

432. Beck, A. *et al.* Connectivity map identifies HDAC inhibition as a treatment option of high-risk hepatoblastoma. *Cancer Biol. Ther.* **17,** 1168–1176 (2016).

433. Manzotti, G. *et al.* Monocyte-macrophage differentiation of acute myeloid leukemia cell lines by small molecules identified through interrogation of the Connectivity Map database. *Cell Cycle* **14,** 2578–89 (2015).

434. Zhong, Y. *et al.* Renoprotective Effect of Combined Inhibition of Angiotensin-Converting Enzyme and Histone Deacetylase. *J. Am. Soc. Nephrol.* **24,** 801–811 (2013).

435. Wang, K. *et al.* Systematic drug safety evaluation based on public genomic expression (Connectivity Map) data: Myocardial and infectious adverse reactions as application cases. *Biochem. Biophys. Res. Commun.* **457,** 249–255 (2015).

436. Honti, F., Meader, S. & Webber, C. Unbiased Functional Clustering of Gene Variants with a Phenotypic-Linkage Network. *PLoS Comput. Biol.* **10,** e1003815 (2014).

437. Pane, M. *et al.* Daily salbutamol in young patients with SMA type II. *Neuromuscul. Disord.* **18,** 536–540 (2008).

438. Niroumand, M. C., Farzaei, M. H. & Amin, G. Medicinal properties of Peganum harmala L. in traditional Iranian medicine and modern phytotherapy: a review. *J. Tradit. Chinese Med.* **35,** 104–109 (2015).

439. dos Santos, R. G. & Hallak, J. E. C. Effects of the Natural *β* -Carboline Alkaloid Harmine, a Main Constituent of Ayahuasca, in Memory and in the Hippocampus: A Systematic Literature Review of Preclinical Studies. *J. Psychoactive Drugs* **49,** 1–10 (2017).

440. Moloudizargari, M., Mikaili, P., Aghajanshakeri, S., Asghari, M. H. & Shayegh, J. Pharmacological and therapeutic effects of Peganum harmala and its main alkaloids. *Pharmacogn. Rev.* **7,** 199–212 (2013).

441. BERROUGUI, H. *et al.* Vasorelaxant effects of harmine and harmaline extracted from Peganum harmala L. seed's in isolated rat aorta. *Pharmacol. Res.* **54,** 150–157 (2006).

442. Liu, X. *et al.* Harmine is an inflammatory inhibitor through the suppression of NF-κB signaling. *Biochem. Biophys. Res. Commun.* **489,** 332–338 (2017).

443. Cheng, J. *et al.* In in vivo evaluation of the anti-inflammatory and analgesic activities of compound Muniziqi granule in experimental animal models. *BMC Complement. Altern. Med.* **16,** 20 (2016).

444. Salman, S. *et al.* Short Communication: Evaluation of antimicrobial activities of Harmine, Harmaline, Nicotine and their complexes. *Pak. J. Pharm. Sci.* **29,** 1317–20 (2016).

445. Ahmad, A. *et al.* Study of the in vitro antimicrobial activity of harmine, harmaline and their derivatives. *J. Ethnopharmacol.* **35,** 289–294 (1992).

446. Réus, G. Z. *et al.* Harmine and imipramine promote antioxidant activities in prefrontal cortex and hippocampus. *Oxid. Med. Cell. Longev.* **3,** 325–31 (2010).

447. Moura, D. J., Richter, M. F., Boeira, J. M., Pegas Henriques, J. A. & Saffi, J. Antioxidant properties of -carboline alkaloids are related to their antimutagenic and antigenotoxic activities. *Mutagenesis* **22,** 293–302 (2007).

448. Zhang, X.-F. X.-D. *et al.* Synthesis and mechanisms of action of novel harmine derivatives as potential antitumor agents. *Sci. Rep.* **6,** 33204 (2016).

449. Ruan, S., Jia, F. & Li, J. Potential Antitumor Effect of Harmine in the Treatment of Thyroid Cancer. *Evid. Based. Complement. Alternat. Med.* **2017,** 9402615 (2017).

450. Li, C. *et al.* Anticancer activities of harmine by inducing a pro-death autophagy and apoptosis in human gastric cancer cells. *Phytomedicine* **28,** 10–18 (2017).

451. Fortunato, J. J. *et al.* Acute harmine administration induces antidepressive-like effects and increases BDNF levels in the rat hippocampus. *Prog. Neuro-Psychopharmacology Biol. Psychiatry* **33,** 1425–1430 (2009).

452. Fortunato, J. J. *et al.* Chronic administration of harmine elicits antidepressant-like effects and increases BDNF levels in rat hippocampus. *J. Neural Transm.* **117,** 1131–1137 (2010).

453. Liu, F. *et al.* Harmine produces antidepressant-like effects via restoration of astrocytic functions. *Prog. Neuro-Psychopharmacology Biol. Psychiatry* **79,** 258–267 (2017).

454. Owaisat, S., Raffa, R. B. & Rawls, S. M. In vivo comparison of harmine efficacy against psychostimulants: Preferential inhibition of the cocaine response through a glutamatergic mechanism. *Neurosci. Lett.* **525,** 12–16 (2012).

455. Fortunato, J. J. *et al.* Effects of β-carboline harmine on behavioral and physiological parameters observed in the chronic mild stress model: Further evidence of antidepressant properties. *Brain Res. Bull.* **81,** 491–496 (2010).

456. Sun, P., Zhang, S., Li, Y. & Wang, L. Harmine mediated neuroprotection via evaluation of glutamate transporter 1 in a rat model of global cerebral ischemia. *Neurosci. Lett.* **583,** 32–36 (2014).

457. Zhong, Z., Tao, Y. & Yang, H. Treatment with harmine ameliorates functional impairment and neuronal death following traumatic brain injury. *Mol. Med. Rep.* **12,** 7985–91 (2015).

458. Li, Y. *et al.* Harmine, a natural beta-carboline alkaloid, upregulates astroglial glutamate transporter expression. *Neuropharmacology* **60,** 1168–75 (2011).

459. Biradar, S. M., Joshi, H. & Tarak, K. C. Cerebroprotective effect of isolated harmine alkaloids extracts of seeds of Peganum harmala L. on sodium nitrite-induced hypoxia and ethanol-induced neurodegeneration in young mice. *Pakistan J. Biol. Sci. PJBS* **16,** 1687–97 (2013).

460. Kim, H., Sablin, S. O. & Ramsay, R. R. Inhibition of Monoamine Oxidase A by β-Carboline Derivatives. *Arch. Biochem. Biophys.* **337,** 137–142 (1997).

461. Schwarz, M. J., Houghton, P. J., Rose, S., Jenner, P. & Lees, A. D. Activities of extract and constituents of Banisteriopsis caapi relevant to parkinsonism. *Pharmacol. Biochem. Behav.* **75,** 627–33 (2003).

462. Samoylenko, V. *et al.* Banisteriopsis caapi, a unique combination of MAO inhibitory and antioxidative constituents for the activities relevant to neurodegenerative disorders and Parkinson's disease. *J. Ethnopharmacol.* **127,** 357–367 (2010).

463. Brierley, D. I. & Davidson, C. Harmine augments electrically evoked dopamine efflux in the nucleus accumbens shell. *J. Psychopharmacol.* **27,** 98–108 (2013).

464. Glennon, R. A. *et al.* Binding of beta-carbolines and related agents at serotonin (5-HT(2) and 5-HT(1A)), dopamine (D(2)) and benzodiazepine receptors. *Drug Alcohol Depend.* **60,** 121–32 (2000).

465. Grella, B., Teitler, M., Smith, C., Herrick-Davis, K. & Glennon, R. A. Binding of beta-carbolines at 5-HT(2) serotonin receptors. *Bioorg. Med. Chem. Lett.* **13,** 4421–5 (2003).

466. Husbands, S. M. *et al.* beta-carboline binding to imidazoline receptors. *Drug Alcohol Depend.* **64,** 203–8 (2001).

467. Frost, D. *et al.* β-carboline compounds, including harmine, inhibit DYRK1A and tau phosphorylation at multiple Alzheimer's disease-related sites. *PLoS One* **6,** e19264 (2011).

468. Chaurasiya, N. D., Shukla, S. & Tekwani, B. L. A Combined In Vitro Assay for Evaluation of Neurotrophic Activity and Cytotoxicity. *SLAS Discov. Adv. Life Sci. R&D* **22,** 667–675 (2017).

469. Foran, E. & Trotti, D. Glutamate transporters and the excitotoxic path to motor neuron degeneration in amyotrophic lateral sclerosis. *Antioxid. Redox Signal.* **11,** 1587–602 (2009).

470. Herrendorff, R. *et al.* Identification of Plant-derived Alkaloids with Therapeutic Potential for Myotonic Dystrophy Type I. *J. Biol. Chem.* **291,** 17165–77 (2016).

471. Ruggiu, M. *et al.* A role for SMN exon 7 splicing in the selective vulnerability of motor neurons in spinal muscular atrophy. *Mol. Cell. Biol.* **32,** 126–38 (2012).

472. Liu, W.-Z. *et al.* Harmine enhances GABAergic transmission onto basoamygdala projection neurons in mice. *Brain Res. Bull.* **137,** 294–300 (2018).

473. Coates, G. H. & Cox, B. Harmine tremor after brain monoamine oxidase inhibition in the mouse. *Eur. J. Pharmacol.* **18,** 284–6 (1972).

474. AHMED, A. & TAYLOR, N. R. The analysis of drug-induced tremor in mice. *Br. J. Pharmacol. Chemother.* **14,** 350–4 (1959).

475. Kulkarni, S. K. & Kaul, P. N. Modification by levo-propranolol of tremors induced by harmine in mice. *Experientia* **35,** 1627–1628 (1979).

476. Patil, P., Bachant-Winner, P.-O., Haibe-Kains, B. & Leek, J. T. Test set bias affects reproducibility of gene signatures. *Bioinformatics* **31,** 2318–23 (2015).

477. Chibon, F. Cancer gene expression signatures – The rise and fall? *Eur. J. Cancer* **49,** 2000–2009 (2013).

478. Payan, C. A. *et al.* Periodic Salbutamol in Facioscapulohumeral Muscular Dystrophy: A Randomized Controlled Trial. *Arch. Phys. Med. Rehabil.* **90,** 1094–1101 (2009).

479. Messina, S. *et al.* Pilot Trial of Salbutamol in Central Core and Multi-Minicore Diseases. *Neuropediatrics* **35,** 262–266 (2004).

480. DECORTE, N. *et al.* Effect of Salbutamol on Neuromuscular Function in Endurance Athletes. *Med. Sci. Sport. Exerc.* **45,** 1925–1932 (2013).

481. Kinali, M. *et al.* Pilot trial of albuterol in spinal muscular atrophy. *Neurol. , 59 609 - 610.* (2002).

482. Shukla, S., Shariat-Madar, Z., Walker, L. A. & Tekwani, B. L. Mechanism for neurotropic action of vorinostat, a pan histone deacetylase inhibitor. *Mol. Cell. Neurosci.* **77,** 11–20 (2016).

483. Morales-García, J. A. *et al.* Glycogen synthase kinase-3 inhibitors as potent therapeutic agents for the treatment of Parkinson disease. *ACS Chem. Neurosci.* **4,** 350–60 (2013).

484. Carpentier, R. G. Effects of harmine on transmembrane potentials of guinea-pig atrial muscle. *Br. J. Pharmacol.* **69,** 561–4 (1980).

485. Kim, D. H., Jang, Y. Y., Han, E. S. & Lee, C. S. Protective effect of harmaline and harmalol against dopamine- and 6-hydroxydopamine-induced oxidative damage of brain mitochondria and synaptosomes, and viability loss of PC12 cells. *Eur. J. Neurosci.* **13,** 1861–72 (2001).

486. Lee, C. S. *et al.* Protective effect of harmalol and harmaline on MPTP neurotoxicity in the mouse and dopamine-induced damage of brain mitochondria and PC12 cells. *J. Neurochem.* **75,** 521–31 (2000).

487. Hayashi, M. *et al.* Oxidative stress and disturbed glutamate transport in spinal muscular atrophy. *Brain Dev.* **24,** 770–5 (2002).

488. Haché, M. *et al.* Intrathecal Injections in Children With Spinal Muscular Atrophy: Nusinersen Clinical Trial Experience. *J. Child Neurol.* **31,** 899–906 (2016).

489. Köstel, A. S., Bora-Tatar, G. & Erdem-Yurter, H. Spinal muscular atrophy: An oxidative stress response counteracted with curcumin. *Biomed. Aging Pathol.* **2,** 61–66 (2012).

490. Schieber, M. & Chandel, N. S. ROS function in redox signaling and oxidative stress. *Curr. Biol.* **24,** R453-62 (2014).

491. Birben, E., Sahiner, U. M., Sackesen, C., Erzurum, S. & Kalayci, O. Oxidative stress and antioxidant defense. *World Allergy Organ. J.* **5,** 9–19 (2012).

492. Lee, Y. Il, Mikesh, M., Smith, I., Rimer, M. & Thompson, W. Muscles in a mouse model of spinal muscular atrophy show profound defects in neuromuscular development even in the absence of failure in neuromuscular transmission or loss of motor neurons. *Dev. Biol.* **356,** 432–44 (2011).

493. Wiley, S. R. & Winkles, J. A. TWEAK, a member of the TNF superfamily, is a multifunctional cytokine that binds the TweakR/Fn14 receptor. *Cytokine Growth Factor Rev.* **14,** 241–9

494. Tajrishi, M. M., Zheng, T. S., Burkly, L. C. & Kumar, A. The TWEAK-Fn14 pathway: a potent regulator of skeletal muscle biology in health and disease. *Cytokine Growth Factor Rev.* **25,** 215–25 (2014).

495. Sato, S., Ogura, Y., Tajrishi, M. M. & Kumar, A. Elevated levels of TWEAK in skeletal muscle promote visceral obesity, insulin resistance, and metabolic dysfunction. *FASEB J.* **29,** 988–1002 (2015).

496. Bowerman, M. *et al.* Tweak regulates astrogliosis, microgliosis and skeletal muscle atrophy in a mouse model of amyotrophic lateral sclerosis. *Hum. Mol. Genet.* **24,** ddv094- (2015).

497. Muller, F. L. *et al.* Denervation-induced skeletal muscle atrophy is associated with increased mitochondrial ROS production. *Am. J. Physiol. Integr. Comp. Physiol.* **293,** R1159–R1168 (2007).

498. Carmona Arana, J. A. *et al.* TNF Receptor-Associated Factor 1 is a Major Target of Soluble TWEAK. *Front. Immunol.* **5,** 63 (2014).

499. Kawakita, T. *et al.* Functional expression of TWEAK in human colonic adenocarcinoma cells. *Int. J. Oncol.* **26,** 87–93 (2005).

500. Enwere, E. K., Lacasse, E. C., Adam, N. J. & Korneluk, R. G. Role of the TWEAK-Fn14-cIAP1-NF-κB Signaling Axis in the Regulation of Myogenesis and Muscle Homeostasis. *Front. Immunol.* **5,** 34 (2014).

501. Roos, C. *et al.* Soluble and transmembrane TNF-like weak inducer of apoptosis differentially activate the classical and noncanonical NF-kappa B pathway. *J. Immunol.* **185,** 1593–605 (2010).

502. Oeckinghaus, A. & Ghosh, S. The NF-kappaB family of transcription factors and its regulation. *Cold Spring Harb. Perspect. Biol.* **1,** a000034 (2009).

503. Armstrong, C. L., Galisteo, R., Brown, S. A. N. & Winkles, J. A. TWEAK activation of the non-canonical NF-κB signaling pathway differentially regulates melanoma and prostate cancer cell invasion. *Oncotarget* **7,** 81474–81492 (2016).

504. Tidball, J. G. & Villalta, S. A. Regulatory interactions between muscle and the immune system during muscle regeneration. *Am. J. Physiol. Regul. Integr. Comp. Physiol.* **298,** R1173-87 (2010).

505. Merritt, E. K. *et al.* Increased expression of atrogenes and TWEAK family members after severe burn injury in nonburned human skeletal muscle. *J. Burn Care Res.* **34,** e297-304

506. Meighan-Mantha, R. L. *et al.* The mitogen-inducible Fn14 gene encodes a type I transmembrane protein that modulates fibroblast adhesion and migration. *J. Biol. Chem.* **274,** 33166–76 (1999).

507. Sato, S., Ogura, Y. & Kumar, A. TWEAK/Fn14 Signaling Axis Mediates Skeletal Muscle Atrophy and Metabolic Dysfunction. *Front. Immunol.* **5,** 18 (2014).

508. Burkly, L. C., Michaelson, J. S. & Zheng, T. S. TWEAK/Fn14 pathway: an immunological switch for shaping tissue responses. *Immunol. Rev.* **244,** 99–114 (2011).

509. Winkles, J. A. The TWEAK-Fn14 cytokine-receptor axis: discovery, biology and therapeutic targeting. *Nat. Rev. Drug Discov.* **7,** 411–25 (2008).

510. Hindi, S. M. *et al.* Regulatory circuitry of TWEAK-Fn14 system and PGC-1α in skeletal muscle atrophy program. *FASEB J.* **28,** 1398–411 (2014).

511. Finck, B. N. & Kelly, D. P. PGC-1 coactivators: inducible regulators of energy metabolism in health and disease. *J. Clin. Invest.* **116,** 615–622 (2006).

512. Uldry, M. *et al.* Complementary action of the PGC-1 coactivators in mitochondrial biogenesis and brown fat differentiation. *Cell Metab.* **3,** 333–341 (2006).

513. Arany, Z. PGC-1 coactivators and skeletal muscle adaptations in health and disease. *Curr. Opin.*

Genet. Dev. **18,** 426–434 (2008).

514. Naya, F. J. & Olson, E. MEF2: a transcriptional target for signaling pathways controlling skeletal muscle growth and differentiation. *Curr. Opin. Cell Biol.* **11,** 683–8 (1999).

515. Leick, L. *et al.* PGC-1α is required for AICAR-induced expression of GLUT4 and mitochondrial proteins in mouse skeletal muscle. *Am. J. Physiol. - Endocrinol. Metab.* **299,** 567–573 (2010).

516. Zorzano, A., Palacin, M. & Guma, A. Mechanisms regulating GLUT4 glucose transporter expression and glucose transport in skeletal muscle. *Acta Physiol. Scand.* **183,** 43–58 (2005).

517. Roberts, D. J. & Miyamoto, S. Hexokinase II integrates energy metabolism and cellular protection: Akting on mitochondria and TORCing to autophagy. *Cell Death Differ.* **22,** 248–57 (2015).

518. Jensen, E. B. *et al.* Regulation of GLUT4 expression in denervated skeletal muscle. *Am. J. Physiol. Regul. Integr. Comp. Physiol.* **296,** R1820-8 (2009).

519. Moreno, H. *et al.* Differential Regulation of the Muscle-specific GLUT4 Enhancer in Regenerating and Adult Skeletal Muscle. *J. Biol. Chem.* **278,** 40557–40564 (2003).

520. Atkinson, B. J., Griesel, B. A., King, C. D., Josey, M. A. & Olson, A. L. Moderate GLUT4 Overexpression Improves Insulin Sensitivity and Fasting Triglyceridemia in High-Fat Diet-Fed Transgenic Mice. *Diabetes* **62,** 2249–2258 (2013).

521. Brozinick, J. T. *et al.* GLUT4 overexpression in db/db mice dose-dependently ameliorates diabetes but is not a lifelong cure. *Diabetes* **50,** 593–600 (2001).

522. Ikemoto, S. *et al.* High fat diet-induced hyperglycemia: prevention by low level expression of a glucose transporter (GLUT4) minigene in transgenic mice. *Proc. Natl. Acad. Sci. U. S. A.* **92,** 3096–9 (1995).

523. Leturque, A., Loizeau, M., Vaulont, S., Salminen, M. & Girard, J. Improvement of insulin action in diabetic transgenic mice selectively overexpressing GLUT4 in skeletal muscle. *Diabetes* **45,** 23–7 (1996).

524. Ren, J. M. *et al.* Overexpression of Glut4 protein in muscle increases basal and insulin-stimulated whole body glucose disposal in conscious mice. *J. Clin. Invest.* **95,** 429–432 (1995).

525. Treadway, J. L. *et al.* Enhanced peripheral glucose utilization in transgenic mice expressing the human GLUT4 gene. *J. Biol. Chem.* **269,** 29956–61 (1994).

526. Tsao, T. S., Burcelin, R., Katz, E. B., Huang, L. & Charron, M. J. Enhanced insulin action due to targeted GLUT4 overexpression exclusively in muscle. *Diabetes* **45,** 28–36 (1996).

527. Mishra, V. N. *et al.* A clinical and genetic study of spinal muscular atrophy. *Electromyogr. Clin. Neurophysiol.* **44,** 307–12

528. Borkowska, A. *et al.* Coexistence of type 1 diabetes mellitus and spinal muscular atrophy in an 8-year-old girl: a case report. *Acta Biochim. Pol.* **62,** 167–8 (2015).

529. Szklarczyk, D. *et al.* The STRING database in 2017: quality-controlled protein–protein association networks, made broadly accessible. *Nucleic Acids Res.* **45,** D362–D368 (2017).

530. Olive, M. & Ferrer, I. Parvalbumin immunohistochemistry in denervated skeletal muscle. *Neuropathol. Appl. Neurobiol.* **20,** 495–500 (1994).

531. Müntener, M., Berchtold, M. W. & Heizmann, C. W. Parvalbumin in cross-reinnervated and denervated muscles. *Muscle Nerve* **8,** 132–137 (1985).

532. Mutsaers, C. A. *et al.* Reversible molecular pathology of skeletal muscle in spinal muscular atrophy. *Hum. Mol. Genet.* **20,** 4334–44 (2011).

533. Musarò, A., McCullagh, K. J. A., Naya, F. J., Olson, E. N. & Rosenthal, N. IGF-1 induces skeletal myocyte hypertrophy through calcineurin in association with GATA-2 and NF-ATc1. *Nature* **400,** 581–585 (1999).

534. Li, Y. *et al.* Identification of a cell protein (FIP-3) as a modulator of NF- B activity and as a target of an adenovirus inhibitor of tumor necrosis factor -induced apoptosis. *Proc. Natl. Acad. Sci.* **96,** 1042–1047 (1999).

535. Magill, C. K. *et al.* Reinnervation of the tibialis anterior following sciatic nerve crush injury: a confocal microscopic study in transgenic mice. *Exp. Neurol.* **207,** 64–74 (2007).

536. Yan, Z. *et al.* Highly coordinated gene regulation in mouse skeletal muscle regeneration. *J. Biol. Chem.* **278,** 8826–36 (2003).

537. Zanou, N. & Gailly, P. Skeletal muscle hypertrophy and regeneration: interplay between the myogenic regulatory factors (MRFs) and insulin-like growth factors (IGFs) pathways. *Cell. Mol. Life Sci.* **70,** 4117–4130 (2013).

538. Mittal, A. *et al.* The TWEAK-Fn14 system is a critical regulator of denervation-induced skeletal muscle atrophy in mice. *J. Cell Biol.* **188,** 833–49 (2010).

539. Girgenrath, M. *et al.* TWEAK, via its receptor Fn14, is a novel regulator of mesenchymal progenitor cells and skeletal muscle regeneration. *EMBO J.* **25,** 5826–39 (2006).

540. Shuichi Sato, Y. O. M. M. T. A. K., Sato, S., Ogura, Y., Tajrishi, M. M. & Kumar, A. Elevated levels of TWEAK in skeletal muscle promote visceral obesity, insulin resistance, and metabolic dysfunction. *FASEB J.* **29,** 988–1002 (2015).

541. Yin, H., Price, F. & Rudnicki, M. A. Satellite Cells and the Muscle Stem Cell Niche. *Physiol. Rev.* **93,** 23–67 (2013).

542. von Maltzahn, J., Jones, A. E., Parks, R. J. & Rudnicki, M. A. Pax7 is critical for the normal function of satellite cells in adult skeletal muscle. *Proc. Natl. Acad. Sci. U. S. A.* **110,** 16474–9 (2013).

543. McKinnell, I. W. *et al.* Pax7 activates myogenic genes by recruitment of a histone methyltransferase complex. *Nat. Cell Biol.* **10,** 77–84 (2008).

544. Kawabe, Y., Wang, Y. X., McKinnell, I. W., Bedford, M. T. & Rudnicki, M. A. Carm1 Regulates Pax7 Transcriptional Activity through MLL1/2 Recruitment during Asymmetric Satellite Stem Cell Divisions. *Cell Stem Cell* **11,** 333–345 (2012).

545. Werlauff, U., Vissing, J. & Steffensen, B. F. Change in muscle strength over time in spinal muscular atrophy types II and III. A long-term follow-up study. *Neuromuscul. Disord.* **22,** 1069–1074 (2012).

546. Savarese, M., Sarparanta, J., Vihola, A., Udd, B. & Hackman, P. Increasing Role of Titin Mutations in Neuromuscular Disorders. *J. Neuromuscul. Dis.* **3,** 293–308 (2016).

547. Wajant, H. The TWEAK-Fn14 system as a potential drug target. *Br. J. Pharmacol.* **170,** 748–64

(2013).

548. Bricceno, K. V. *et al.* Survival motor neuron protein deficiency impairs myotube formation by altering myogenic gene expression and focal adhesion dynamics. *Hum. Mol. Genet.* **23,** 4745–4757 (2014).

549. Bodine, S. C. *et al.* Identification of ubiquitin ligases required for skeletal muscle atrophy. *Science* **294,** 1704–8 (2001).

550. Liu, H. *et al.* TWEAK/Fn14 promotes oxidative stress through AMPK/PGC-1α/MnSOD signaling pathway in endothelial cells. *Mol. Med. Rep.* **17,** 1998–2004 (2017).

551. Kumar, A., Bhatnagar, S. & Paul, P. K. TWEAK and TRAF6 regulate skeletal muscle atrophy. *Curr. Opin. Clin. Nutr. Metab. Care* **15,** 233–9 (2012).

552. Kim, E. K. & Choi, E.-J. SMN1 functions as a novel inhibitor for TRAF6-mediated NF-κB signaling. *Biochim. Biophys. Acta - Mol. Cell Res.* **1864,** 760–770 (2017).

553. Dobrowolny, G. *et al.* Skeletal Muscle Is a Primary Target of SOD1G93A-Mediated Toxicity. *Cell Metab.* **8,** 425–436 (2008).

554. Murray, L. M., Comley, L. H., Gillingwater, T. H. & Parson, S. H. The response of neuromuscular junctions to injury is developmentally regulated. *FASEB J.* **25,** 1306–1313 (2011).

555. Zisman, A. *et al.* Targeted disruption of the glucose transporter 4 selectively in muscle causes insulin resistance and glucose intolerance. *Nat. Med.* **6,** 924–928 (2000).

556. Cerveró, C. *et al.* Chronic Treatment with the AMPK Agonist AICAR Prevents Skeletal Muscle Pathology but Fails to Improve Clinical Outcome in a Mouse Model of Severe Spinal Muscular Atrophy. *Neurotherapeutics* **13,** 198–216 (2016).

557. Irrcher, I., Ljubicic, V., Kirwan, A. F. & Hood, D. A. AMP-Activated Protein Kinase-Regulated Activation of the PGC-1α Promoter in Skeletal Muscle Cells. *PLoS One* **3,** e3614 (2008).

558. Boyd, P. J. *et al.* Bioenergetic status modulates motor neuron vulnerability and pathogenesis in a zebrafish model of spinal muscular atrophy. *PLOS Genet.* **13,** e1006744 (2017).

559. Boyer, J. G., Ferrier, A. & Kothary, R. More than a bystander: the contributions of intrinsic skeletal muscle defects in motor neuron diseases. *Front. Physiol.* **4,** 356 (2013).

560. Willis, A. L. *et al.* The Fibroblast Growth Factor-Inducible 14 Receptor Is Highly Expressed in HER2-Positive Breast Tumors and Regulates Breast Cancer Cell Invasive Capacity. *Mol. Cancer Res.* **6,** 725–734 (2008).

561. Huang, M. *et al.* Overexpression of Fn14 promotes androgen-independent prostate cancer progression through MMP-9 and correlates with poor treatment outcome. *Carcinogenesis* **32,** 1589–1596 (2011).

562. Jain, M. *et al.* A Novel Role for Tumor Necrosis Factor-Like Weak Inducer of Apoptosis (TWEAK) in the Development of Cardiac Dysfunction and Failure. *Circulation* **119,** 2058–2068 (2009).

563. Sanz, A. B. *et al.* Out of the TWEAKlight: Elucidating the Role of Fn14 and TWEAK in Acute Kidney Injury. *Semin. Nephrol.* **36,** 189–198 (2016).

564. Inta, I. *et al.* Induction of the cytokine TWEAK and its receptor Fn14 in ischemic stroke. *J. Neurol. Sci.* **275,** 117–120 (2008).

565. Haile, W. B. *et al.* Tumor necrosis factor-like weak inducer of apoptosis and fibroblast growth factor-inducible 14 mediate cerebral ischemia-induced poly(ADP-ribose) polymerase-1 activation and neuronal death. *Neuroscience* **171,** 1256–1264 (2010).

566. Yamana, J. *et al.* Inhibition of TNF-induced IL-6 by the TWEAK-Fn14 interaction in rheumatoid arthritis fibroblast like synoviocytes. *Cell. Immunol.* **272,** 293–298 (2012).

567. El-shehaby, A. *et al.* Correlations of Urinary Biomarkers, TNF-Like Weak Inducer of Apoptosis (TWEAK), Osteoprotegerin (OPG), Monocyte Chemoattractant Protein-1 (MCP-1), and IL-8 with Lupus Nephritis. *J. Clin. Immunol.* **31,** 848–856 (2011).

568. Wang, D., Zhong, L., Nahid, M. A. & Gao, G. The potential of adeno-associated viral vectors for gene delivery to muscle tissue. *Expert Opin. Drug Deliv.* **11,** 345–364 (2014).

569. Finkel, R. S. *et al.* Nusinersen versus Sham Control in Infantile-Onset Spinal Muscular Atrophy. *N. Engl. J. Med.* **377,** 1723–1732 (2017).

570. Sumner, C. J. & Crawford, T. O. Two breakthrough gene-targeted treatments for spinal muscular atrophy: challenges remain. *J. Clin. Invest.* **128,** 3219–3227 (2018).

571. Gidaro, T. & Servais, L. Nusinersen treatment of spinal muscular atrophy: current knowledge and existing gaps. *Dev. Med. Child Neurol.* (2018). doi:10.1111/dmcn.14027

572. Poruk, K. E. *et al.* Observational study of caloric and nutrient intake, bone density, and body composition in infants and children with spinal muscular atrophy type I. *Neuromuscul. Disord.* **22,** 966–973 (2012).

573. Sproule, D. M. *et al.* Adiposity is increased among high-functioning, non-ambulatory patients with spinal muscular atrophy. *Neuromuscul. Disord.* **20,** 448–452 (2010).

574. Sproule, D. M. *et al.* Increased fat mass and high incidence of overweight despite low body mass index in patients with spinal muscular atrophy. *Neuromuscul. Disord.* **19,** 391–6 (2009).

575. Finkel, R. S., Weiner, D. J., Mayer, O. H., McDonough, J. M. & Panitch, H. B. Respiratory muscle function in infants with spinal muscular atrophy type I. *Pediatr. Pulmonol.* **49,** 1234–1242 (2014).

576. Mazzone, E. *et al.* Six minute walk test in type III spinal muscular atrophy: A 12month longitudinal study. *Neuromuscul. Disord.* **23,** 624–628 (2013).

577. Mercuri, E. *et al.* Nusinersen versus Sham Control in Later-Onset Spinal Muscular Atrophy. *N. Engl. J. Med.* **378,** 625–635 (2018).

578. Study of Intrathecal Administration of AVXS-101 for Spinal Muscular Atrophy (STRONG). (2018).

579. Davis, R. H. *et al.* Nutritional Practices at a Glance. *J. Child Neurol.* **29,** 1467–1472 (2014).

580. Martínez-Hernández, R. *et al.* Synaptic defects in type I spinal muscular atrophy in human development. *J. Pathol.* **229,** 49–61 (2013).

581. Harding, B. N. *et al.* Spectrum of Neuropathophysiology in Spinal Muscular Atrophy Type I. *J. Neuropathol. Exp. Neurol.* **74,** 15–24 (2015).

582. Gormley, M. C. Respiratory Management of Spinal Muscular Atrophy Type 2. *J. Neurosci. Nurs.* **46,** E33–E41 (2014).

583. Attie, K. M. *et al.* A single ascending-dose study of muscle regulator ace-031 in healthy volunteers. *Muscle Nerve* **47,** 416–423 (2013).

584. Becker, C. *et al.* Myostatin antibody (LY2495655) in older weak fallers: a proof-of-concept, randomised, phase 2 trial. *Lancet Diabetes Endocrinol.* **3,** 948–957 (2015).

585. Campbell, C. *et al.* Myostatin inhibitor ACE-031 treatment of ambulatory boys with Duchenne muscular dystrophy: Results of a randomized, placebo-controlled clinical trial. *Muscle Nerve* **55,** 458–464 (2017).

586. Mendell, J. R. *et al.* A Phase 1/2a Follistatin Gene Therapy Trial for Becker Muscular Dystrophy. *Mol. Ther.* **23,** 192–201 (2015).

587. Boardman, F. K., Sadler, C. & Young, P. J. Newborn genetic screening for spinal muscular atrophy in the UK: The views of the general population. *Mol. Genet. Genomic Med.* **6,** 99 (2018).

588. SMA added to U.S. list of disorders for newborn screening. Available at: https://smanewstoday.com/2018/07/16/sma-added-to-us-list-of-diseases-recommended-for-newborn-screening/. (Accessed: 4th October 2018)

Supplementary data

Supplementary Table 1. CMap analysis of transcriptomic data per instance, based on the expression signature of untreated P7 *Smn*$^{-/-}$;*SMN2*$^{+/-}$ vs. age-matched WT controls.

Rank	Batch	CMap name	Dose	Cell	Score	Up	Down	Id
6100	641	Monocrotaline	12 µM	HL60	-1	-0.14	0.2	1757
6099	618	Salbutamol	17 µM	HL60	-0.991	-0.069	0.268	2344
6098	614	Disulfiram	13 µM	HL60	-0.937	-0.099	0.219	1369
6097	695	Indoprofen	14 µM	MCF7	-0.911	-0.12	0.19	4832
6096	676	Zardaverine	15 µM	MCF7	-0.901	-0.138	0.169	7347
6095	688	Oxamniquine	14 µM	PC3	-0.9	-0.074	0.233	4006
6094	641	Harmine	16 µM	HL60	-0.897	-0.155	0.15	1758
6093	611	Guanabenz	14 µM	PC3	-0.896	-0.135	0.17	1961
6092	612	Hydrochlorothiazide	13 µM	HL60	-0.894	-0.064	0.24	1987
6091	611	Aciclovir	18 µM	PC3	-0.883	-0.127	0.174	1960
6090	714	Phenylpropanolamine	21 µM	PC3	-0.879	-0.072	0.227	6699
6089	631	Carisoprodol	15 µM	HL60	-0.876	-0.082	0.216	1314
6088	1055	SB-203580	1 µM	MCF7	-0.868	-0.105	0.19	6899
6087	658	Nafcillin	9 µM	HL60	-0.848	-0.101	0.188	2983
6086	745	Cytisine	21 µM	MCF7	-0.841	-0.114	0.172	6217
6085	1067	Colforsin	500 nM	PC3	-0.839	-0.125	0.16	7059
6084	730	Pilocarpine	15 µM	MCF7	-0.826	-0.098	0.184	5341
6083	640	Harmol	16 µM	HL60	-0.818	-0.129	0.149	1750
6082	665	Loracarbef	11 µM	HL60	-0.814	-0.128	0.149	2970
6081	614	Neomycin	4 µM	HL60	-0.812	-0.098	0.179	1383
6080	746	Hexylcaine	13 µM	MCF7	-0.802	-0.076	0.197	6244
6079	1075	PHA-00846566E	10 µM	PC3	-0.8	-0.119	0.153	7086
6078	641	Noscapine	10 µM	HL60	-0.796	-0.086	0.185	1753
6077	741	Fenspiride	13 µM	MCF7	-0.783	-0.143	0.123	6001
6076	709	Acebutolol	11 µM	PC3	-0.782	-0.141	0.125	6631

Supplementary Table 2. CMap analysis of transcriptomic data per instance, based on the expression signature of untreated P7 *Smn*$^{-/-}$;*SMN2*$^{+/-}$ vs. Pip6a-PMO treatment.

Rank	Batch	CMap name	Dose	Cell	Score	Up	Down	Id
1	650	Troglitazone	10 µM	HL60	1	0.13	-0.175	2692
2	641	Harmine	16 µM	HL60	0.99	0.156	-0.146	1758
3	648	Sulfamethizole	15 µM	HL60	0.975	0.136	-0.161	2536
4	665	Netilmicin	3 µM	HL60	0.93	0.148	-0.136	2963
5	1075	PHA-00846566E	10 µM	PC3	0.909	0.139	-0.138	7086
6	640	Harmol	16 µM	HL60	0.906	0.189	-0.087	1750
7	623	Zaprinast	15 µM	HL60	0.887	0.17	-0.1	1611
8	676	Zardaverine	15 µM	MCF7	0.88	0.126	-0.143	7347
9	1055	SB-203580	1 µM	MCF7	0.876	0.134	-0.134	6899
10	622	Vinpocetine	11 µM	HL60	0.875	0.147	-0.12	1557
11	21	Genistein	1 µM	MCF7	0.866	0.158	-0.106	268
12	614	Disulfiram	13 µM	HL60	0.856	0.151	-0.11	1369
13	628	Benzonatate	7 µM	PC3	0.832	0.129	-0.125	1801
14	618	Mebendazole	14 µM	HL60	0.832	0.191	-0.063	2338
15	661	Enilconazole	13 µM	HL60	0.824	0.112	-0.14	3139
16	741	Lymecycline	7 µM	MCF7	0.824	0.087	-0.164	5994
17	714	Debrisoquine	9 µM	PC3	0.822	0.167	-0.083	6688
18	618	Dilazep	6 µM	HL60	0.814	0.112	-0.137	2333
19	691	Tiaprofenic acid	15 µM	MCF7	0.807	0.098	-0.148	4171
20	611	Guanabenz	14 µM	PC3	0.807	0.1	-0.146	1961
21	1067	Alsterpaullone	10 µM	PC3	0.804	0.077	-0.168	7056
22	645	Methylbenzethonium chloride	9 µM	HL60	0.803	0.132	-0.113	2190
23	642	Prilocaine	16 µM	MCF7	0.798	0.155	-0.089	2314
24	644	Cinchonine	14 µM	HL60	0.797	0.166	-0.077	2133
25	602	Genistein	10 µM	HL60	0.795	0.163	-0.08	1176

Supplementary Table 3. CMap analysis of transcriptomic data per instance, based on the overlap between the expression signature of untreated P7 *Smn$^{-/-}$;SMN2$^{+/-}$* vs. Pip6a-PMO treatment and the expression signature of untreated P7 *Smn$^{-/-}$;SMN2$^{+/-}$* vs. age-matched WT controls.

Rank	Batch	CMap name	Dose	Cell	Score	Up	Down	Id
6100	614	Disulfiram	13 µM	HL60	-1	-0.147	0.254	1369
6099	648	Sulfamethizole	15 µM	HL60	-0.921	-0.197	0.173	2536
6098	623	Zaprinast	15 µM	HL60	-0.92	-0.089	0.28	1611
6097	641	Harmine	16 µM	HL60	-0.919	-0.159	0.209	1758
6096	688	Oxamniquine	14 µM	PC3	-0.906	-0.101	0.262	4006
6095	1055	SB-203580	1 µM	MCF7	-0.893	-0.154	0.204	6899
6094	644	Cinchonine	14 µM	HL60	-0.886	-0.101	0.253	2133
6093	749	Ciprofibrate	14 µM	HL60	-0.885	-0.154	0.201	6138
6092	665	Cyclic adenosine monophosphate	12 µM	HL60	-0.883	-0.08	0.274	2969
6091	618	Salbutamol	17 µM	HL60	-0.873	-0.046	0.304	2344
6090	665	Netilmicin	3 µM	HL60	-0.865	-0.127	0.219	2963
6089	715	Ioversol	5 µM	PC3	-0.863	-0.197	0.148	6726
6088	618	Mebendazole	14 µM	HL60	-0.862	-0.081	0.264	2338
6087	676	Zardaverine	15 µM	MCF7	-0.859	-0.174	0.17	7347
6086	631	Carisoprodol	15 µM	HL60	-0.857	-0.123	0.221	1314
6085	702	Deferoxamine	6 µM	PC3	-0.855	-0.179	0.164	4317
6084	602	Genistein	10 µM	HL60	-0.854	-0.091	0.251	1176
6083	1075	PHA-00846566E	10 µM	PC3	-0.853	-0.183	0.159	7086
6082	612	Hydrochlorothiazide	13 µM	HL60	-0.852	-0.077	0.265	1987
6081	640	Harmol	16 µM	HL60	-0.851	-0.104	0.237	1750
6080	613	Guanabenz	14 µM	HL60	-0.845	-0.103	0.235	2045
6079	21	Genistein	1 µM	MCF7	-0.842	-0.099	0.238	268
6078	612	4-hydroxyphenazone	20 µM	HL60	-0.838	-0.159	0.176	1997
6075	641	Monocrotaline	12 µM	HL60	-0.834	-0.116	0.218	1757
6076	644	Prestwick-682	6 µM	HL60	-0.834	-0.11	0.225	2164

Supplementary Table 4. CMap analysis of transcriptomic data per perturbagen, based on the expression signature of untreated P7 *Smn*$^{-/-}$;*SMN2*$^{+/-}$ vs. age-matched WT controls.

Rank	CMap name	Mean	N	Enrichment	P	Specificity	Percent non-null
21	Terazosin	-0.609	4	-0.912	0.0001	0	100
49	5252917	-0.592	2	-0.945	0.00658	0.0121	100
41	Nystatin	-0.499	3	-0.874	0.00403	0.0072	100
70	Hydrocortisone	-0.479	3	-0.791	0.01841	0.0263	66
59	Hydrochlorothiazide	-0.442	5	-0.646	0.01354	0.0057	60
40	Carbimazole	-0.44	3	-0.876	0.00385	0.0069	100
85	Meprylcaine	-0.431	4	-0.662	0.02932	0.0121	75
94	Clorsulon	-0.392	4	-0.65	0.03527	0.078	75
51	Tetryzoline	-0.377	3	-0.839	0.00837	0	66
57	Captopril	-0.374	5	-0.647	0.01348	0.0423	60
95	Scopolamine	-0.37	4	-0.644	0.03831	0.0544	75
62	Tolazoline	-0.354	5	-0.639	0.0155	0.0195	60
47	Salsolinol	-0.345	3	-0.857	0.00587	0	66
42	Cyclopenthiazide	-0.325	4	-0.785	0.00426	0	50
31	Nifurtimox	-0.304	4	-0.829	0.00159	0.0049	50
78	Ergocalciferol	-0.304	4	-0.679	0.02357	0.0269	50
64	Fluvastatin	-0.302	4	-0.702	0.01643	0.0278	50
97	Theophylline	-0.286	4	-0.638	0.04126	0.0449	75
67	Dimethadione	-0.279	4	-0.7	0.01685	0.0253	50
54	Oxedrine	-0.273	4	-0.737	0.00953	0.0078	50
36	SR-95639A	-0.267	4	-0.81	0.00255	0	50
68	Tolfenamic acid	-0.263	4	-0.698	0.01755	0.0059	50
90	Ampicillin	-0.248	4	-0.659	0.03079	0.0189	50
50	Propantheline bromide	-0.246	4	-0.746	0.00826	0.0057	50
84	Piperine	-0.246	4	-0.665	0.02847	0.0059	50
72	Metrizamide	-0.233	4	-0.688	0.02051	0.0482	50

Supplementary Table 5. CMap analysis of transcriptomic data per perturbagen, based on the expression signature of untreated P7 *Smn*$^{-/-}$;*SMN2*$^{+/-}$ vs. Pip6a-PMO treatment.

Rank	CMap name	Mean	N	Enrichment	P	Specificity	Percent non-null
110	Metamizole sodium	0.25	6	0.521	0.04835	0.123	50
47	Levothyroxine sodium	0.257	4	0.766	0.00575	0.0136	50
82	Pergolide	0.28	4	0.663	0.0294	0.0452	50
107	Nafcillin	0.281	4	0.63	0.04637	0.0296	50
87	Pivmecillinam	0.282	4	0.655	0.03268	0.0305	50
89	Prestwick-1080	0.283	4	0.654	0.03322	0.0226	50
50	Prestwick-857	0.285	4	0.742	0.00855	0.0516	50
58	Nadide	0.3	4	0.714	0.01343	0.0286	50
65	Tranexamic acid	0.321	5	0.639	0.01752	0.1718	60
66	Carbenoxolone	0.325	4	0.693	0.01852	0.0196	50
97	H-7	0.342	4	0.648	0.0365	0.3556	50
112	Prestwick-675	0.371	4	0.626	0.04904	0.1102	75
92	Metrizamide	0.372	4	0.651	0.03489	0.0822	75
34	Metacycline	0.373	4	0.81	0.00247	0.0084	75
22	Rifampicin	0.377	4	0.846	0.0008	0.0058	75
100	Securinine	0.388	4	0.64	0.04088	0.1688	75
94	PHA-00767505E	0.421	4	0.649	0.03599	0.0387	75
45	Tetracaine	0.423	3	0.861	0.00495	0	100
59	Strophanthidin	0.468	4	0.713	0.01377	0.1211	75
75	Arachidonyltrifluoromethane	0.488	2	0.887	0.0263	0.0252	100
70	Harmol	0.492	4	0.685	0.02093	0.0465	75
16	Iproniazid	0.493	5	0.89	0.00006	0	100
14	Terazosin	0.552	4	0.92	0.00004	0	100

Supplementary Table 6. CMap analysis of transcriptomic data per perturbagen, based on the overlap between the expression signature of untreated P7 *Smn*$^{-/-}$;*SMN2*$^{+/-}$ vs. Pip6a-PMO treatment and the expression signature of untreated P7 *Smn*$^{-/-}$;*SMN2*$^{+/-}$ vs. age-matched WT controls.

Rank	CMap name	Mean	N	Enrichment	P	Specificity	Percent non-null
53	5252917	-0.562	2	-0.931	0.01006	0.0422	100
28	Carbimazole	-0.513	3	-0.904	0.00166	0	100
18	Butamben	-0.49	4	-0.867	0.00062	0	75
68	Terazosin	-0.466	4	-0.686	0.02117	0.0896	75
35	Chicago Sky Blue 6B	-0.456	4	-0.792	0.00374	0.0136	75
80	Arachidonyltrifluoromethane	-0.448	2	-0.879	0.02925	0.0588	100
37	Harmalol	-0.43	3	-0.87	0.00433	0	100
24	Loracarbef	-0.421	4	-0.843	0.00107	0	75
75	Hydrochlorothiazide	-0.419	5	-0.608	0.02615	0.0343	60
90	Hydrocortisone	-0.418	3	-0.734	0.0386	0.0461	66
94	Levothyroxine sodium	-0.41	4	-0.638	0.04152	0.0849	75
91	Clorsulon	-0.4	4	-0.643	0.03873	0.0922	75
106	Tetramisole	-0.4	4	-0.626	0.04834	0.0284	75
30	Metrizamide	-0.399	4	-0.823	0.00185	0	75
81	Tropine	-0.388	4	-0.661	0.02966	0	75
52	Trolox C	-0.355	4	-0.736	0.00969	0.0053	75
59	Tranexamic acid	-0.35	5	-0.649	0.01302	0.1946	60
45	Salsolinol	-0.341	3	-0.857	0.00575	0	66
29	Cyclopenthiazide	-0.327	4	-0.826	0.00177	0	50
57	Bicuculline	-0.321	4	-0.726	0.01158	0.0056	50
77	Propidium iodide	-0.311	4	-0.669	0.02688	0	75
61	Ciprofloxacin	-0.309	5	-0.641	0.01516	0.0109	60
102	Meprylcaine	-0.299	4	-0.633	0.04408	0.0121	50
25	Nifurtimox	-0.269	4	-0.84	0.00117	0.0049	50
41	Calcium pantothenate	-0.264	4	-0.774	0.00533	0.0105	50
64	Metamizole sodium	-0.25	6	-0.58	0.01913	0.1737	50
103	Tolfenamic acid	-0.242	4	-0.632	0.0446	0.0412	50
33	Securinine	-0.218	4	-0.803	0.00288	0.038	50
107	Theophylline	-0.212	4	-0.625	0.04894	0.0562	75

Supplementary Table 7. CMap analysis of proteomic data per instance, based on the expression signature of untreated P7 *Smn*$^{-/-}$;*SMN2*$^{+/-}$ vs. age-matched WT controls.

CMap name	Dose	Cell	Score	Up	Down	Instance_id
Alsterpaullone	10 µM	PC3	-1	-0.152	0.113	7078
Camptothecin	11 µM	PC3	-0.944	-0.156	0.094	4541
0175029-0000	10 µM	MCF7	-0.86	-0.122	0.105	4713
Daunorubicin	7 µM	MCF7	-0.842	-0.149	0.074	4983
Doxorubicin	7 µM	MCF7	-0.825	-0.149	0.069	3291
GW-8510	10 µM	MCF7	-0.813	-0.141	0.075	7062
Trichostatin A	1 µM	MCF7	-0.796	-0.08	0.131	873
Troglitazone	10 µM	HL60	-0.79	-0.122	0.087	6191
Famotidine	12 µM	PC3	-0.787	-0.092	0.116	1946
Dihydroergotamine	3 µM	HL60	-0.767	-0.074	0.129	1398
Salbutamol	17 µM	HL60	-0.766	-0.109	0.094	2344
N-acetylmuramic acid	14 µM	MCF7	-0.762	-0.126	0.076	4406
Mitoxantrone	8 µM	PC3	-0.757	-0.136	0.064	6755
Pempidine	13 µM	PC3	-0.756	-0.093	0.107	4307
Flunisolide	9 µM	PC3	-0.752	-0.114	0.085	4303
N6-methyladenosine	14 µM	HL60	-0.743	-0.123	0.074	1271
Moracizine	9 µM	MCF7	-0.732	-0.126	0.068	3520
Fusaric acid	22 µM	HL60	-0.729	-0.131	0.062	1308
Bergenin	12 µM	PC3	-0.728	-0.095	0.098	5870
Valproic acid	1 mM	MCF7	-0.728	-0.094	0.099	989
PHA-00767505E	10 µM	PC3	-0.728	-0.054	0.139	6591

Supplementary Table 8. CMap analysis of proteomic data per instance, based on the expression signature of untreated P7 *Smn*$^{-/-}$;*SMN2*$^{+/-}$ vs. Pip6a-PMO treatment.

CMap name	Score	Instance-id
Acacetin	-1	4324
Estriol	-0.98	7220
Methylprednisolone	-0.956	3183
Etamsylate	-0.952	4576
Alsterpaullone	-0.952	7056
Luteolin	-0.942	3379
Fluorocurarine	-0.94	6083
Dexpanthenol	-0.938	1680
5213008	-0.932	898
Pirenzepine	-0.929	7226
Sulconazole	-0.929	3373
Alsterpaullone	-0.912	7051
Bacampicillin	-0.909	4592
Promazine	-0.905	6028
Tanespimycin	-0.903	5566
Tanespimycin	-0.898	1206
Sc-19220	-0.888	7065
Estradiol	-0.883	6968
Gw-8510	-0.879	7080

Supplementary Table 9. CMap analysis of proteomic data per instance, based on the overlap between the expression signature of untreated P7 *Smn*$^{-/-}$;*SMN2*$^{+/-}$ vs. Pip6a-PMO treatment and the expression signature of untreated P7 *Smn*$^{-/-}$;*SMN2*$^{+/-}$ vs. age-matched WT controls.

CMap name	Dose	Cell	Score	Up	Down	Instance_id
Camptothecin	11 µM	PC3	-1	-0.253	0.135	4541
Irinotecan	100 µM	PC3	-0.94	-0.231	0.133	7535
0175029-0000	10 µM	MCF7	-0.93	-0.187	0.173	4713
Mitoxantrone	8 µM	MCF7	-0.925	-0.222	0.136	3232
Alsterpaullone	10 µM	PC3	-0.912	-0.198	0.155	7078
Irinotecan	100 µM	MCF7	-0.849	-0.215	0.114	7530
Doxorubicin	7 µM	MCF7	-0.823	-0.177	0.142	5671
GW-8510	10 µM	PC3	-0.812	-0.228	0.086	7085
0175029-0000	1 µM	MCF7	-0.811	-0.215	0.099	4716
Daunorubicin	7 µM	MCF7	-0.796	-0.189	0.12	4983
SR-95531	11 µM	HL60	-0.791	-0.167	0.139	1316
Fenbufen	16 µM	HL60	-0.788	-0.173	0.133	2346
GW-8510	10 µM	MCF7	-0.783	-0.184	0.119	7080
Prilocaine	16 µM	HL60	-0.781	-0.134	0.168	2352
Folic acid	9 µM	MCF7	-0.77	-0.148	0.151	7201
Primaquine	9 µM	MCF7	-0.768	-0.209	0.089	3279
Tyrphostin AG-825	25 µM	MCF7	-0.766	-0.183	0.114	1114
Esculin	12 µM	PC3	-0.764	-0.154	0.141	6310
Mycophenolic acid	12 µM	MCF7	-0.753	-0.194	0.098	4137
Cinnarizine	11 µM	MCF7	-0.752	-0.182	0.109	7174

Supplementary Table 10. CMap analysis of proteomic data per perturbagen, based on the expression signature of untreated P7 *Smn*$^{-/-}$;*SMN2*$^{+/-}$ vs. age-matched WT controls.

Rank	CMap name	Mean	N	Enrichment*	P	Specificity	Percent non-null
1	Harmol	-0.786	4	-0.938	0	0.0055	100
2	Irinotecan	-0.789	3	-0.982	0.00002	0.0109	100
3	Withaferin A	0.706	4	0.913	0.00004	0.0526	100
4	Perhexiline	0.597	4	0.909	0.00008	0.0104	100
5	Thioridazine	0.337	20	0.506	0.00008	0.2374	55
6	N6-methyladenosine	0.588	4	0.884	0.00018	0	100
7	Raubasine	0.333	4	0.821	0.00177	0	75
8	5252917	0.694	2	0.967	0.00181	0	100
9	Daunorubicin	-0.402	4	-0.803	0.00294	0.0526	75
10	STOCK1N-35874	-0.625	2	-0.959	0.00364	0.0066	100
11	Trimethylcolchicinic acid	-0.264	4	-0.792	0.00376	0	50
12	Rotenone	0.39	4	0.785	0.0041	0	75
13	Trifluoperazine	0.323	16	0.418	0.00467	0.3702	50
14	Iohexol	0.255	4	0.774	0.00491	0.0114	50
15	Depudecin	0.614	2	0.948	0.00495	0	100
16	Phenindione	-0.279	4	-0.778	0.00503	0.0108	50
17	Clotrimazole	0.511	5	0.704	0.00537	0.0667	80
18	AH-6809	0.623	2	0.945	0.00573	0	100
19	Tribenoside	0.442	4	0.757	0.00666	0.0212	75
20	Fluorometholone	-0.485	4	-0.742	0.00873	0.0253	75

* A negative score indicates that the corresponding perturbagen reversed the expression of the query genes.

Supplementary Table 11. CMap analysis of proteomic data per perturbagen, based on the expression signature of untreated P7 *Smn*$^{-/-}$;*SMN2*$^{+/-}$ vs. Pip6a-PMO treatment.

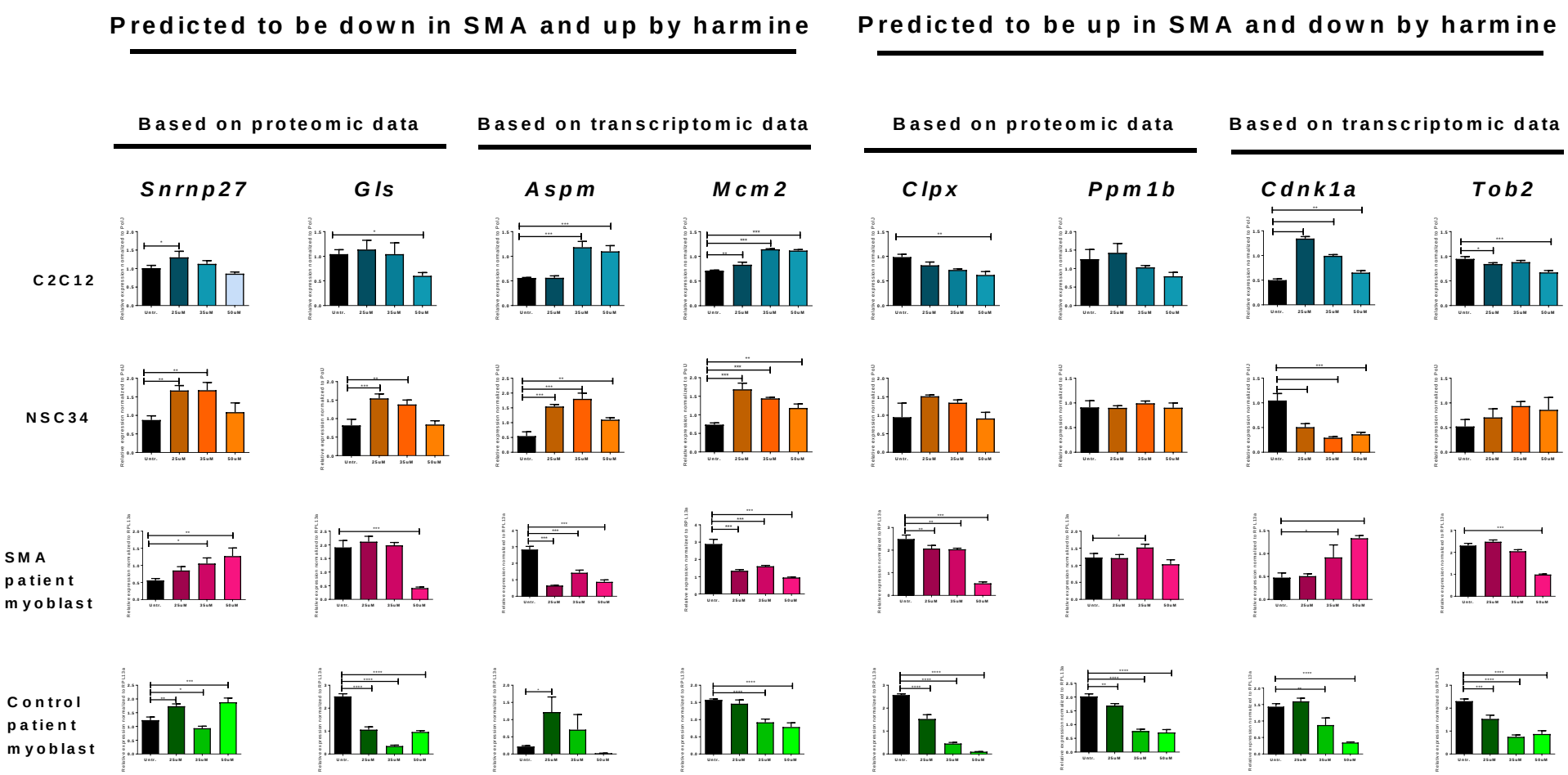
Rank	CMap name	Mean	N	Enrichment*	P	Specificity	Percent non-null
1	Camptothecin	-0.827	3	-0.991	0	0.0455	100
2	Irinotecan	-0.813	3	-0.988	0	0	100
3	H-7	-0.74	4	-0.948	0	0.0833	100
4	0175029-0000	-0.724	6	-0.899	0	0.0211	100
5	Alsterpaullone	-0.862	3	-0.972	0.00008	0.0571	100
6	Doxorubicin	-0.696	3	-0.927	0.00062	0.0827	100
7	Fludroxycortide	-0.572	5	-0.781	0.00088	0.0054	100
8	Clindamycin	-0.505	5	-0.779	0.00096	0	100
9	Staurosporine	-0.561	4	-0.821	0.00193	0	100
10	Nomegestrol	0.533	3	0.896	0.00216	0	100
11	Nocodazole	0.494	6	0.687	0.00242	0.0319	83
12	Memantine	0.407	4	0.796	0.00334	0	75
13	15-delta prostaglandin J2	-0.301	15	-0.443	0.00364	0.1805	66
14	Meticrane	-0.279	5	-0.711	0.00429	0.0293	60
15	Iohexol	0.48	4	0.78	0.00438	0.0114	75
16	Mitoxantrone	-0.628	3	-0.865	0.00497	0.0567	100
17	5252917	0.645	2	0.947	0.00527	0	100
18	Fluorometholone	-0.571	4	-0.767	0.00599	0.019	100
19	Docosahexaenoic acid ethyl ester	-0.655	2	-0.946	0.00644	0.017	100
20	Primaquine	-0.364	4	-0.763	0.00647	0.0278	75

* A negative score indicates that the corresponding perturbagen reversed the expression of the query genes.

Supplementary Table 12. CMap analysis of proteomic data per perturbagen, based on the overlap between the expression signature of untreated P7 *Smn*$^{-/-}$;*SMN2*$^{+/-}$ vs. Pip6a-PMO treatment and the expression signature of untreated P7 *Smn*$^{-/-}$;*SMN2*$^{+/-}$ vs. age-matched WT controls.

Rank	CMap name	Mean	N	Enrichment*	P	Specificity	Percent non-null
1	Alsterpaullone	-0.83	3	-0.997	0	0.0071	100
2	Irinotecan	-0.834	3	-0.995	0	0	100
3	H-7	-0.73	4	-0.968	0	0.0758	100
4	Camptothecin	-0.748	3	-0.966	0.0001	0.0796	100
5	Perhexiline	0.749	4	0.886	0.00018	0.0104	100
6	Methotrexate	-0.287	8	-0.684	0.00032	0.0069	50
7	Thioridazine	0.445	20	0.446	0.00038	0.3744	60
8	Harmol	-0.614	4	-0.879	0.00052	0.0109	100
9	Piperacetazine	0.583	4	0.846	0.0008	0.0057	100
10	0175029-0000	-0.368	6	-0.719	0.00097	0.0634	50
11	16,16-dimethylprostaglandin E2	-0.592	3	-0.914	0.00108	0	100
12	Nocodazole	0.496	6	0.726	0.00109	0.0319	83
13	GW-8510	-0.576	4	-0.837	0.00123	0.1679	75
14	5252917	0.805	2	0.968	0.00173	0	100
15	Iohexol	0.491	4	0.803	0.00286	0	75
16	Cephaeline	0.546	5	0.737	0.00294	0.2808	80
17	Trimethylcolchicinic acid	-0.275	4	-0.792	0.0038	0	50
18	Bendroflumethiazide	-0.302	6	-0.661	0.00417	0.0115	50
19	Isocarboxazid	-0.451	5	-0.713	0.00423	0.007	80
20	Fendiline	0.655	3	0.868	0.00425	0	100

* A negative score indicates that the corresponding perturbagen reversed the expression of the query genes.



Supplementary Figure 1. Various cell lines treated with a 25, 35 of 50 µM harmine for 48 hours. n = 3 per group, one-way ANOVA, Bonferroni, * $p < 0.05$, ** $p < 0.01$, *** $p < 0.001$, **** and $p < 0.0001$. (data relate to Table 4.4).